THE SWEDISH INSTITUTE FOR FOOD AND BIOTECHNOLOGY

ISUD7

The 7th International Symposium on Ultrasonic Doppler Methods for Fluid Mechanics and Fluid Engineering, April 7-9, 2010, Gothenburg,Sweden

Proceedings of the 7th International Symposium on Ultrasonic Doppler Methods for Fluid Mechanics and Fluid Engineering

Chalmers University of Technology, Gothenburg, Sweden
April 7-8, 2010

“Paddan” sight-seeing boat in Gothenburg
Photo: Kjell Holmner

Photo: Jan-Olof Yxell

SIK – The Swedish Institute for Food and Biotechnology

Chalmers University of Technology
Photo: Jan-Olof Yxell

Editors:
J. Wiklund
E. Levenstam Bragd
S. Manneville

Embedded in the 6th Annual European Rheology Conference 2010 (AERC 2010)

Proceedings of the 7th International Symposium on Ultrasonic Doppler Methods for Fluid Mechanics and Fluid Engineering

Chalmers University of Technology, Gothenburg, Sweden
April 7-8, 2010

Scientific Committee:
Dr. V. Bareš, Department of Sanitary and Ecological Engineering, CTU Prague, Czech Republic
Dr. B. Birkhofer, Sika Services AG, Switzerland
Dr. G. De Cesare, Laboratory of Hydraulic Constructions (LCH), Ecole Polytechnique Fédérale de Lausanne (EPFL), Switzerland
Dr. S. Eckert, Forschungszentrum Dresden-Rossendorf (FZD), MHD Department, Dresden, Germany
Dr. S. Fischer, Ubertone, France
Dr. H. Kikura, Research Laboratory for Nuclear Reactors, Tokyo Institute of Technology, Ohokayama, Japan
Prof. Dr. S. Manneville, École Normale Supérieure de Lyon, France
Dr. M. Mori, Tokyo Electric Power Co., Inc. (TEPCO), R&D Center, Yokohama, Japan
Dr. C. Rennie, Department of Civil Engineering, University of Ottawa, Canada
Dr. S.A.K. Jeelani, Food Process Engineering, Swiss Federal Institute of Technology Zurich (ETH), Switzerland
Dr. Y. Tasaka, School of Engineering, Hokkaido University, Sapporo, Japan
Dr. J. Wiklund, SIK-The Swedish Institute for Food and Biotechnology, Gothenburg, Sweden
Prof. Dr. E.J. Windhab, Food Process Engineering, Swiss Federal Institute of Technology Zurich (ETH), Switzerland (Chair)

Organizing Committee (ISUD7):
Johan Wiklund
Emma Levenstam Bragd
Sébastien Manneville

Organizing Committee (AERC2010):
Mats Stading
Mikael Rigdahl
Susanna Edrud
Rodney Rychwalski
Henrik Persson
Marcus Schmidt
Alexandra Andrén

Proceedings of the 7th International Symposium on Ultrasonic Doppler Methods for Fluid Mechanics and Fluid Engineering

Editors:
Johan Wiklund
Emma Levenstam Bragd
Sébastien Manneville

ISBN: 978-91-7290-292-3

Published and distributed by:
SIK– The Swedish Institute for Food and Biotechnology
Box 5401
Frans Perssons Väg 6
SE-402 29 Gothenburg
Sweden

Official websites:
http://www.sik.se/isud7/
http://www.rheology-esr.org/AERC/2010/
http://www.isud.ethz.ch/

Agenda

Wednesday April 7

8:00--	Registration	Chalmers Conference Center
9:00-9:20	Welcome ceremony AERC 2010	Chalmers, Runan
9:20-10:00	Plenary lecture 1 AERC 2010	Chalmers, Runan
10:40-17:10	ISUD7	Chalmers, lecture hall VH
10:40-11:20	Keynote lecture 1 – Y. Takeda	Chalmers, lecture hall VH
15:10-16:10	Poster session 1	Chalmers Conference Center
18:00-19:00	AERC / ISUD7 Reception	City Hall (Börsen)
19:15-19:20	Trip with “Älvsnabben” harbour ferry	Departure from ”Lilla Bommen”
19:30--	ISUD7 Dinner	River Café

Thursday April 8

8:00--	Registration	Chalmers Conference Center
9:00-9:40	Plenary lecture 2 AERC 2010	Chalmers, Runan
10:00-16:00	ISUD7	Chalmers, lecture hall VH
10:00-10:40	Keynote lecture 2 – M. Fink	Chalmers, lecture hall VH
12:20-12:40	ISUD7 Board meeting	Chalmers
16:00-17:00	Poster session 2	Chalmers Conference Center
19:00--	AERC / ISUD7 Conference dinner	Park Avenue

Sponsors

The following sponsors are gratefully acknowledged for contributing to the conference:

MET-FLOW SA
CHALMERS
Sik
formas
Vetenskapsrådet
SCA
VOLVO
Volvo Car Corporation
Tetra Pak
Anton Paar
Lantmännen
LS instruments
TA Instruments
AkzoNobel
Tomorrow's Answers Today

Maps of the conference area

Chalmers Conference Center
(including ”Runan”)

Chalmers Conference Center
(including ”Runan”)

Entrance to lecture hall VH

Chalmers Conference Center

Entrance to lecture hall VH

Table of Contents

Author Index

Keynote Lectures

Paradigm shift in experimental fluid dynamics (EFD)

Yasushi Takeda[1, 2]
1. Hokkaido University, N13-W8, Kita-ku, Sapporo, 060-8628, Japan
2. Tokyo Institute of Technology, 2-12-1-N1-13 Ohokayama, Meguro-ku, Tokyo, 152-8550, Japan

As often mentioned, UVP has three main advantages over the conventional techniques of flow measurements; (1) space-time velocity field, (2) Applicable to opaque liquids and (3) Efficient flow mapping. Among these advantages, the information of space-time velocity filed is a sort of solution of the basic equations and it was the ultimate goal to invent novel flow measurement method. The development of the UVP was a pioneering work for this generation and it surely influenced on the development of PIV using laser. A successful development of such measurement techniques which enables us to obtain spatio-temporal velocity field compelled us change the methodology in physics. Hydrodynamic instability problem received its benefits. In the industrial applications too, two important branches in fluid engineering are currently faced to the paradigm shift in their application principles. One is a principle in flow metering and another is a flow behavior of viscoelastic materials. These current changes will be explained in detail with examples.

Multi-wave Imaging: A solution to image rheological properties of soft tissues

Mathias Fink
Institut Langevin, Ecole Supérieure de Physique et de Chimie Industrielles, 75005, Paris, France

We describe a new concept for imaging soft solids. The idea is that very different waves -- one to provide contrast, another to provide spatial resolution -- can be productively combined to generate something akin to near-field imaging. We will focus specifically on imaging rheological properties of soft biological tissues. Here, the multi-wave approach relies on the simultaneous use of both sonic shear waves and ultrasonic compressional waves. The sonic shear wave has typically centimetric wavelengths and propagates at low velocity in tissues (between 1 and 10 m/s). They are progressively distorted by the viscoelastic inhomogeneities of encountered tissues. When coupled to an ultrafast ultrasound scanner (10.000 images per second), it allows for the follow up of the propagation of these waves with a sub millimetric resolution over a large zone of interest. From the spatio-temporal evolution of the displacement fields, inversion algorithms are used to recover the rheological properties with sub-millimetric resolution. These techniques are no more diffraction limited because, the near field of the shear waves is directly observed. Here, the shear wave gives the contrast (viscoelasticity) while the ultrasonic wave gives the spatial resolution. Various examples of *in vivo* images will presented in breast, liver, eyes, muscles, cardiac applications that show the interest of this quantitative imaging technique in diagnostic and therapy monitoring.

Ultrasound rheometry

Ultrasound Doppler rheometry from spin response of viscoelastic and bubbly Liquids

Yuichi MURAI, Yuji TASAKA, Kosuke SAKURAI, Kazuya OYAMA, and Yasushi TAKEDA
Faculty of Engineering, Hokkaido University, N13-W8, Kita-ku, Sapporo, 060-8628, Japan
(e-mail: murai@ring-me.eng.hokudai.ac.jp)

Ultrasound Doppler technique for velocity profile measurement is applied for the estimation of rheological properties such as viscosity, elastic module, yield stress as well as effective and complex shear viscosities. Scanning of transient velocity profiles on a single ultrasound measurement line allows the measurement to complete the shear strain rate - shear stress characteristics only by a single run of spinning fluids inside a cylindrical container. The rheometrical performance is evaluated by several test cases for viscoelastic liquid (PAA), and applied for the measurement of those properties in bubbly liquid to seek the viscoelastic response in Newtonian-gas-liquid combination. The results for bubbly liquid in transient spinning response show that the effective shear viscosity increases high when bubbles are stretched with the shear stress. This trend is totally different from the effective viscosity of bubbly liquid in equilibrium deformation such in a steady Couette flow.

Keywords: Ultrasound rheometry, Spin response, Ultrasonic velocity profiling, Viscoelasticity

1 INTRODUCTION

Liquid foods have an extremely wide range in rheological properties. Food rheology is thus positioned in high priority field in a part of life science. One concern that tightly relates to accident is the behavior of visco-elastic liquid food. These liquids sometimes cause unexpected resistance in swallowing them, and also worsen the quality control of food manufacturing process. In order to estimate these visco-elastic properties in liquid foods, a high-accurate but convenient method is desired to build up. Conventional methods for estimating them utilize indirect information obtained from differential pressure in a tube (Poiseulle viscometry), torque caused by the wall shear stress (torsional Couette viscometry), or terminal velocity of sphere (Stokes viscometry). In these methods, the measurement of global properties needs time-consuming work for changing the shear rate repeatedly. Handling of thixotropic liquid becomes difficult when such a time-marching measurement is adopted. In addition, these indirect measurements cannot provide any information in terms of internal structure of the flow. This problem slows down the scientific understanding of the rheological behavior of liquid food.

Since ultrasonic velocity profiler (UVP)[1] can acquire the velocity profiles as a function of time, it has a potential to become a high-performance rheometry. Because of ultrasonic principle, most of liquid foods can be measured regardless of the opaqueness, such as milk, yogurt, chocolates, and foam-shaped food. In this study, our objective is set to develop such a UVP-base rheometry by choosing the best flow configuration. The best configuration is call so when the spatio-temporal two-dimensional velocity information is fully utilized to determine the liquid properties. We propose here a transient shear response of fluid driven by spinning in a container. This flow has rich velocity fluctuation both in space and in time, and hence the wide relationship between the shear stress and the shear rate is acquired.

In this paper, we describe about the method of UVP-based rheometry, and the verification using polyacrylamide (PAA) solution. The internal structure of fluid deformation is also visualized from the UVP data for PAA solution. The present method is applied for experimental detection of viscoelastic property in bubbly liquid.

2 FLOW CONFIGURATION

Figure 1 shows general description of the present flow configuration. Comparing with pipe flow[2-5] the spinning flow enables one to acquire the transient shear response from quiescent state. Therefore, wall-clinging effect for the elasticity, fluidized behavior departing from the yield point, and shear-thinning effect are all captured simultaneously with a single run of the measurement. Furthermore, any liquid reaches at the rigid rotation in steady state so that the transient region is easily judged from the radial velocity profiles. Furthermore, temperature and pressure conditions are controlled easily because of packed liquid in the container. Detailed dimensions are as follows. The UVP measurement line is set at the distance of e=7mm from the central axis of the container which is made of acrylic resin with D=150 mm and 2 mm in thickness. Temperature is controlled to be constant at 20 deg C at atmospheric pressure. An ultrasonic absorber is put on the backside of the transducer. The basic frequency is set at 2 MHz. High-porous polymer particles (HP20SS) are mixed to be ultrasonic reflector in target fluid. The speed of sound for PAA solution is 1485 m/s. Sampling period is 20 msec, and the number of profiles is 1024. Spatial resolution is 0.75 mm while the number of channels is 230. The flow velocity resolution is 1.5 mm/s. The rotational speed of the container can vary from 50 to 150 rpm.

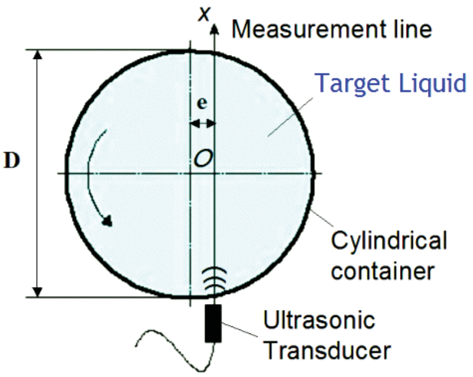

Figure 1: Measurement line of UVP for liquid filled in circular container. *x*: distance from ultrasonic transducer along the path of ultrasonic pulse. *e*: distance from the center axis of the container to the nearest point on the measurement line. *D*: internal diameter of the container.

3 SUDDEN SPINNING RESPONSES

Three types of spinning response are investigated for 1wt% PAA solution. Comparing these three flow structures, we deduce which response the best reflects to the flow for estimating the rheological properties.

Figures 2, 3, and 4 represent spatio-temporal velocity measured by UVP for three different spinning modes; spinning up, spinning down, and impulsive spinning, respectively. In all figures, the velocity shown there is the circumferential component that is decomposed from the on-beam velocity along the measurement line of UVP. The method of the decomposition is reported in our previous paper[6].

On the spinning up mode shown in Figure 2, the circumferential velocity takes the largest value at t=0.6s and it oscillates a few times before reaching the rigid rotation. This oscillation comes up due to elastic property of PAA solution and appears more obviously on the spinning down mode shown in Figure 3. On this mode, flow orientation changes repeatedly after the container is suddenly stopped. Calculating the damping ratio of velocity amplitudes during single cycle enables the average viscosity to be estimated while the oscillation frequency can be used for determining the system elasticity of liquid in this flow configuration.

These two responses are combined when impulsive spinning is given to the fluid as shown in Figure 4. The impulsive spinning is defined so when the quiescent fluid experiences instantaneous spinning within 0.5 second. On this mode, rigid rotation does not appear in the response.

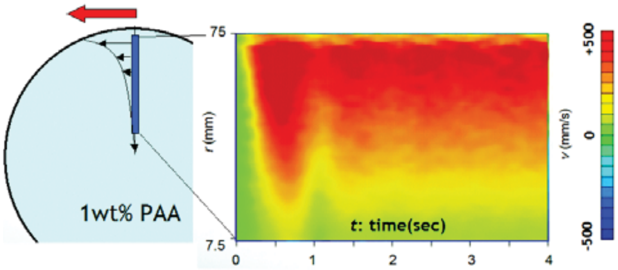

Figure 2: Circumferential velocity measured by UVP for spinning up flow in 1wt% PAA solution.

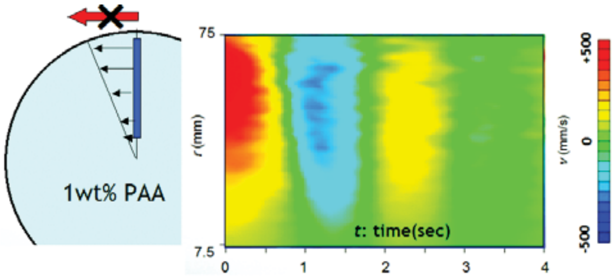

Figure 3: Circumferential velocity measured by UVP for spinning down flow in 1wt% PAA solution.

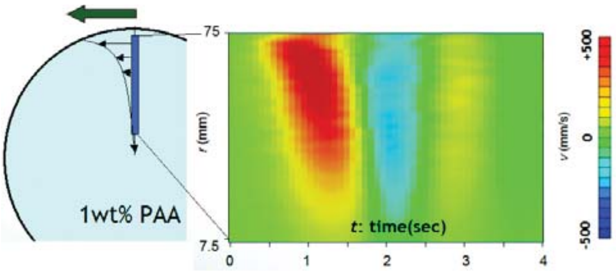

Figure 4: Circumferential velocity measured by UVP for impulsive spinning in 1wt% PAA solution.

By integrating the velocity profiles in time, the actual fluid deformation is visualized as shown in Figures 5 to 7. Among a number of representations, two cases are shown here: one is particle tracers being originally arranged in radial direction, and another is mesh tracers being square shape in the initial condition.

Figure 5 shows the fluid deformation on spinning up mode. The initial particle arrangement changes after the flow reaches the rigid rotation because of yielding of the fluid near the container wall. In contrast, the fluid in the core keeps the radial arrangements for pure elastic response there. Figure 6 shows the same visualization on spinning down mode. The particles are scattered inside the layer near the container wall while they keep the original arrangement in the core. As seen in mesh pattern, the core part is more rigidly kept its original square pattern. Thus, the spinning down mode provides radial stratified structure stronger than the spinning up mode. Figure 7 shows the deformation on impulsive spinning mode. Obviously the particle displacement is limited in a shallow layer near the wall, and the mesh structure is unmodified in comparison with the other two spinning modes.

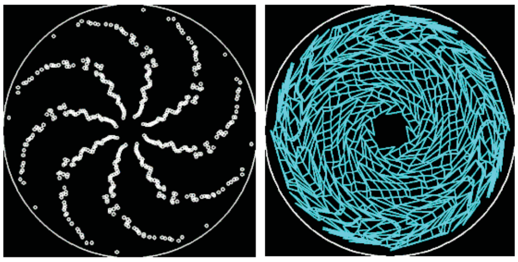

Figure 5: Distortion of fluid in PAA solution on spinning up mode. Left: particle tracers; right: mesh tracers.

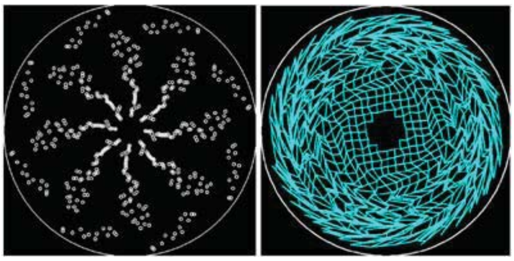

Figure 6: Distortion of fluid in PAA solution on spinning down mode. Left: particle tracers; right: mesh tracers.

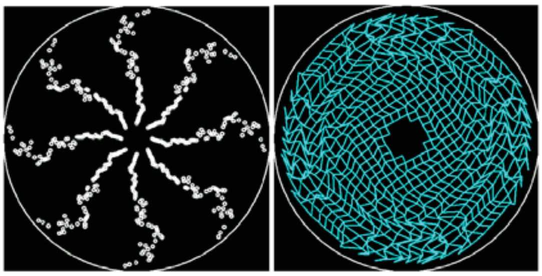

Figure 7: Distortion of fluid in PAA solution on impulsive spinning mode. Left: particle tracers; right: mesh tracers.

4 RHEOLOGICAL PROPERTIES

The following equation of circumferential momentum conservation is satisfied for any type of fluid when the internal shear stress is described as τ.

$$\rho\left(\frac{\partial v}{\partial t}+u\frac{\partial v}{\partial r}+\frac{uv}{r}+v\frac{\partial v}{r\partial\theta}\right)=\frac{1}{r^2}\frac{\partial}{\partial r}\left(r^2\tau\right) \quad (1)$$

Here ρ is density, t the time, v the circumferential velocity, u the radial velocity, r the radial coordinate, and θ the angle. The velocity v is obtained by UVP. When the radial velocity is negligible and the flow keeps axisymmetric structure, Eq.(1) is simplified to

$$\rho\frac{\partial v}{\partial t}-\frac{1}{r^2}\frac{\partial}{\partial r}(r^2\tau)=0 \quad (2)$$

For visco-elastic liquid, the following Herschel-Bulkley model suitably expresses the shear stress.

$$\tau=E\gamma=E\int\frac{\partial\gamma}{\partial t}dt=E\int\left(\frac{\partial v}{\partial r}-\frac{v}{r}\right)dt \quad (\tau<\tau_y) \quad (3)$$

$$\tau=K\left(\frac{\partial v}{\partial r}-\frac{v}{r}\right)^n+\tau_y \quad (\tau\geq\tau_y) \quad (4)$$

Four independent constants involved in the model are determined from velocity information based on least square approach. The cost function *g*, which should be zero when the model completely matches the properties of actual fluid, is defined as follows.

$$g(K,E,n,\tau_y)=\left\{\rho\frac{\partial v}{\partial t}-\frac{1}{r^2}\frac{\partial}{\partial r}(r^2\tau)\right\}^2 \quad (5)$$

We call *g* as cost function because dimension of the error assessment is arbitrary. In the case of Eq.(5), the dimension of *g* is squared force per unit volume, i.e. N/m^3 or Pa/m. Fully utilizing the spatio-temporal velocity information, the global cost function is defined as

$$G(K,E,n,\tau_y)=\iint g(K,E,n,\tau_y)drdt\rightarrow\min \quad (6)$$

Here the four constants are determined by random search algorithm to find out the condition that *G* gets minimum value. Using Eq.(6), the least value of *G* indicates the discrepancy of the employed rheological model from the actual property of the fluid. In this sense, the present method can assess the validity of the rheological model quantitatively.

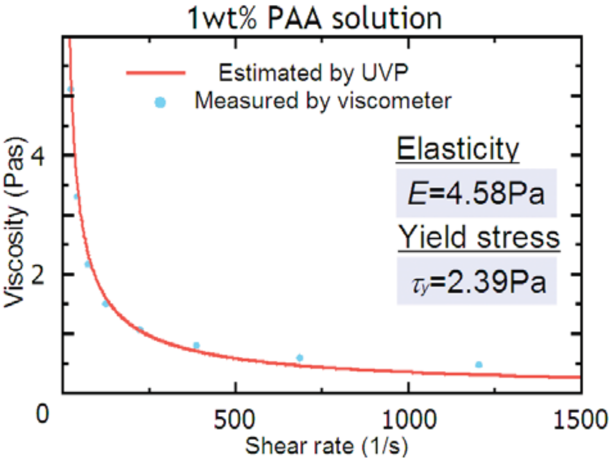

Figure 8: Viscosity estimated by the present UVP-base rheometry (red curve) and that measured by a torsional viscometer (blue plots) for 1wt% PAA solution from the data of impulsive spinning mode. Elasticity and yield stress are obtained by UVP simultaneously.

Figure 8 shows the results of rheological properties estimated by the present method. The shear-thinning characteristics of the viscosity in PAA solution are validly measured to have small error relative to the data measured by torsional viscometer. Simultaneously, the elasticity and the yield stress are obtained. These properties are determined only from the single-run measurement which takes only 5 seconds.

5 APPLICATION TO BUBBLY LIQUID

Rheology of bubbly liquid has already a long history beyond a century[5]. The recent topic relates to complex viscosity that provides interaction to turbulent eddies in high deformation rate with rich unsteadiness[6]. Now we are trying to detect viscoelastic property in bubbly liquid that consists of Newtonian gas-liquid combination.

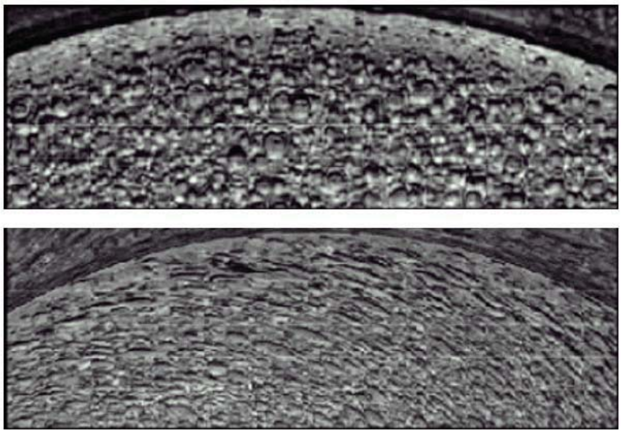

Figure 9: Shape of bubbles captured by high-speed video camera. Top picture in stagnant state (thus, capillary number is zero), bottom picture for during spin at maximum capillary number of 1.2

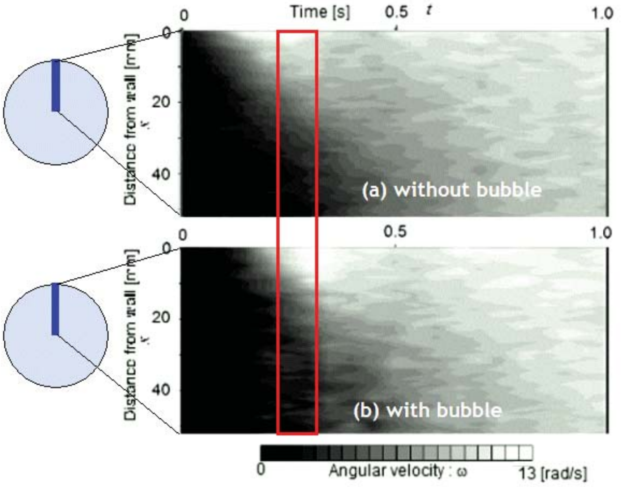

Figure 10: Spinning responses of bubbly liquid obtained by UVP shown by angular velocity. Mixing of bubbles delays the momentum transfer in the initial stage, and provides large acceleration later for surface tension.

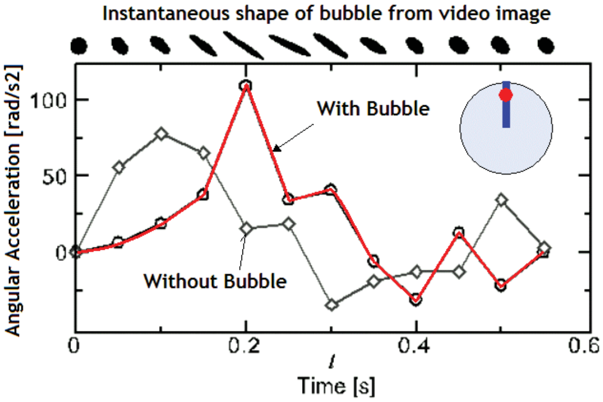

Figure 11 Spin responses of angular acceleration (time derivative of liquid angular velocity) for two cases with and without bubbles.

Figure 9 shows typical samples of interfacial distribution of bubbles in a part of cylindrical container. At capillary number of 1.2, many bubbles are stretched largely in circumferential direction. Figure 10 shows UVP data of single spin response to compare the effect of bubble mixing. As seen in Figure 11, which is a comparison of angular acceleration of liquid, mixing of bubbles delays the initial momentum transfer for interfacial yielding effect, and later provides large acceleration for recovery force of bubbles. This 0.2s-order time scale creates frequency characteristics of bubble rheology, which should impact the modulation of turbulence in bubbly liquid.

6 CONCLUDING REMARKS

UVP will be excellent rheometry since it obtains spatio-temporal velocity information with which closure problem in rheological models is completely solved. Spinning is one of the best configurations for capturing rheological properties because of well-posed informatics.

REFERENCES

[1] Y. Takeda, Velocity profile measurement by ultrasonic Doppler method, Exp. Fluid Sci. 10-4(1995), 444-453.

[2] B.H. Birkhofer, Ultrasonic in-line characterization of suspensions, Diss. ETH (No.17331), Zurich (2007).

[3] I. Fyrippi, I. Owen, M.P. Escudier, Flowmetering of non-Newtonian liquids, Flow Meas. Instr., 15 (2004), 131-138

[4] B.Ouriev, E.Windhab, Novel ultrasound based time averaged mapping method for die entry visualization in flow of highly concentrated shear-thinning and shear-thickening suspensions, Meas. Sci. Tech., 14 (2003), 140-147.

[5] A.C. Rust, M. Manga, J.Colloid & Interface Sci., 249 (2002), 476-480.

[6] Y. Murai, H. Oiwa, Fluid Dyn. Research., 40 (2008), 565-575.

Velocity profiling of viscoelastic fluids around a falling sphere

Takahisa SHIRATORI, Kazuya OYAMA, Yuji TASAKA, Yuichi MURAI, and Yasushi TAKEDA
Graduate School of Engineering, Hokkaido University, N13-W8, Kita-ku, Sapporo, 060-8628, Japan
(e-mail: t.shiratori@ring-me.eng.hokudai.ac.jp)

A method to measure two-dimensional velocity vector field around a falling sphere in viscoelastic fluids is developed by means of UVP (Ultrasonic Velocity Profiling). It bases on single-line measurement of fluid velocity component coupled with equation of continuity under the assumption of axisymmetric field. The aim of the study is to validate the UVP measurement performance for the application to opaque viscoelastic fluids. The validation is made with PIV (Particle Image Velocimetry) measurement under the same condition in order to compare the velocity vector field obtained. From the comparison, the flow structure such as toroidal circulation beside the sphere has been validly measured. Instead, negative wake phenomenon so-called has not been extracted by UVP for two reasons in the present technique. The handicap of UVP for viscoelastic fluid and the method of improvement are also discussed.

Keywords: Viscoelastic fluid, Falling sphere, Ultrasonic velocity profiling, Multi-dimensional flow

1 INTRODUCTION

For decades, several interesting flow behaviors have been reported in terms of falling sphere system with viscoelastic fluids. One of the most noticeable phenomena is reversing flow in a wake of the moving sphere, called “negative wake.” The negative wake is induced by combined stress [1], which is difficult to be characterized directly in most of commercial rheometers. Therefore falling sphere system should be handled by multi-dimensional velocimetry when its rheological response of fluid surrounding the sphere is investigated. However, most of non-Newtonian fluids in application are opaque, and hence optical method such as PIV or LDV measurements are unavailable as long as visible light is applied. X-ray and Neutron scanning are applicable for limited types of fluid while those are generally poor in spatial resolution.

Because of these backgrounds, a method to measure multi-dimensional fluid velocity vector distribution in falling sphere system in non-optical way is targeted in the present study. The method is established by means of ultrasonic velocity profiling (UVP[2]). There are two types of methodology in UVP measurement for acquiring two-dimensional velocity distribution. One is to simply employ two UVP-measurement lines with different angles in the target flow. This set-up enables us to conduct two-component velocity measurement. When flow field is completely steady state on Lagrangian frame that moves with the sphere, the two-dimensional two-component (2D-2C) velocity distribution can be reconstructed. Another technique is to couple the velocity profile along single UVP measurement line with equation of continuity. This combination allows space-time two-dimensional flow measurement for unsteady flows. When the sphere velocity and the flow around the sphere are steady, the space-time frame can be converted to space-space two-dimensional coordinate.

In this paper, we describe the method and the result of the latter case, i.e. single-UVP measurement coupled with equation of continuity, for detecting some key characteristics in viscoelastic fluids that take place around the falling sphere. The measurement performance is validated with the data obtained by particle image velocimetry (PIV) applied for the same experimental conditions. Since some technical problems come out in the result, we also discuss the reasons and the future improvements in the final part of the paper.

2 EXPERIMENTAL SET-UP

A schematic illustration of the experimental apparatus is shown in Figure 1. It mainly consists of a cylindrical container, a reservoir and a sphere. The inner diameter of the cylindrical container is 124 mm. It is filled with a test fluid, 1 wt% polyacrylamide (PAA, AP805C Dia-Nitrix) solution. As tracer particles, high-porous polymer particles (HP20SS, Mitsubishi Chemical) are mixed into the solution both for UVP and PIV measurements. The liquid top surface is set at 406 mm height from the bottom of the cylindrical container. The cylindrical container is settled in the reservoir that is filled with water in order to relax reflections of ultrasonic pulse on the container wall, and to prevent refractions of light in PIV measurement. A sphere is hung up with a thread just under the top free surface. The sphere falls along center axis of the cylinder straightly after the thread is cut. The mass of the sphere is 47.8 g, and diameter is 39.5 mm.

The rectangular area shown in Figure 1 indicates the measurement area of PIV. This area is illuminated vertically with a laser sheet. A high-speed video camera (FASTCAM-MAX Photron) is used to photograph the particle images. Frame rate and spatial resolution are 60 fps and 0.17 mm/pixel, respectively.

In UVP measurement, the ultrasonic transducer is located at 186 mm from the top surface of test liquid. The direction of the measurement line crosses perpendicularly with center axis of the cylinder. A UVP monitor (UVP-DUO, MET-FLOW) is used for Doppler velocity computation. Spatial resolution is 0.37 mm while the number of channels is 373. Velocity and time resolutions are 0.15 mm/s, and 0.084 sec, respectively.

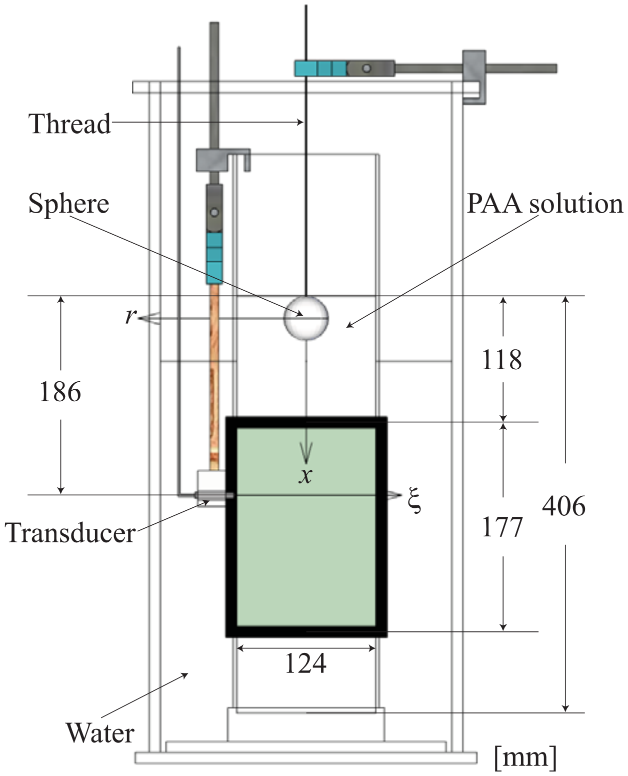

Figure 1: Schematic illustration of experimental apparatus

3 FRAME CONVERSION

UVP obtains radial velocity component u_r on the measurement line as a function of r and t. When translational velocity of the sphere is given as U, temporal information of the velocity can be converted into spatial distribution around the sphere using eq. (1).

$$dx = Udt \tag{1}$$

Here U can be treated as constant when the sphere reaches terminal falling velocity. Since the test liquid is incompressible, equation of continuity stands regardless to rheological properties as

$$\frac{\partial u_x}{\partial x} + \frac{\partial u_r}{\partial r} + \frac{u_r}{r} = 0 \tag{2}$$

where u_x is axial velocity component. From eqs. (1) and (2), axial-radial two-dimensional distribution of liquid velocity is estimated by

$$u_x(x,r) = \int \frac{\partial u_x}{\partial x} dx = -\int \left(\frac{\partial u_r}{\partial r} + \frac{u_r}{r} \right) Udt \tag{3}$$

where initial condition; $u_x = 0$ at $t = 0$, is applied for temporal integration of the kernel function.

It is noted that the spatial resolution of u_x in the axial direction varies with the sphere velocity U and temporal resolution of UVP. In order to keep the homogeneous resolution in 2-D space, a suitable averaging filter is introduced into preprocessing of UVP data. The present case employs median value filter that has 15 (r direction) times 3 (x direction) matrix.

4 RESULTS

4.1 PIV measurement

The instantaneous velocity vector field around the falling sphere is shown in Figure 2. Each vector field is obtained in different shot in the same movie. The distribution is shown on cylindrical coordinate system, x-r, whose origin corresponds to the center of the sphere. Both of axes are non-dimensionalized with the radius of the sphere, R = 19.8 mm. Velocities are non-dimensionalized with the terminal velocity of the sphere, U = 62.5 mm/s.

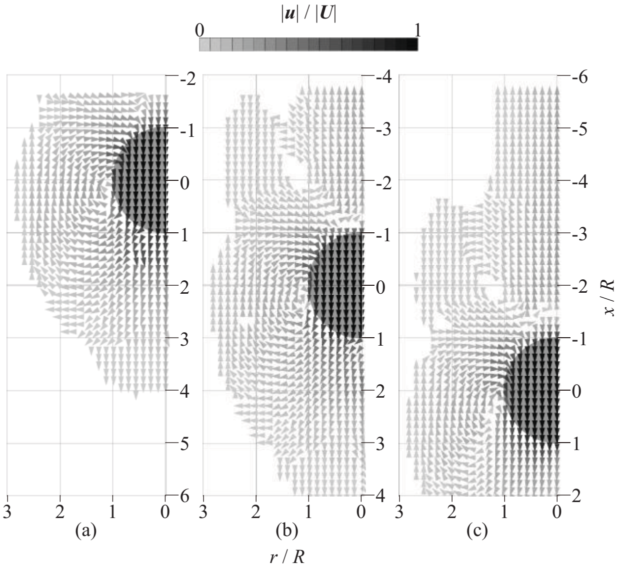

Figure 2: Velocity vector fields obtained with PIV at different shot of sphere

As seen in the results, the negative wake [1] is identified at x / R < -2, which has upward velocity for long distance in the downstream direction. The negative wake is considered as strong elastic recovery of the liquid behind the sphere after large strain is subject to the liquid beside the sphere. In addition, two circulation zones are observed in

Figure 2 (b) (c). One is at the side of the sphere (x / R = 0, r / R = 1), and another is at the side of negative wake (x / R = -2, r / R = 1.2). The former circulation is caused by an existence of the wall of the cylindrical container. The latter one is a specific phenomenon for viscoelastic flow, which is connected with the negative wake.

4.2 UVP measurement

The two-dimensional distribution of u_r obtained by UVP is shown in Figure 3 (a). The center of the sphere is estimated from the flow pattern which we have known from PIV measurement. The region around the point (x / R = 1, r / R = 1) indicates that fluid is pushed away by the sphere, i.e. potential displacement. The region around the point (x / R = -2, r / R = 1) has a flow direction approaching the sphere.

Figure 3 (b) shows the velocity vector field obtained by applying the equation of continuity to the data of Figure 3 (a). There is a circulation identifiable around x / R = 0, r / R = 1.5. However, compared to Figure 2 (c), the magnitude of velocity vector near the sphere is much smaller in Figure 3 (b), and a negative wake is not seen clearly. The reason of these differences is discussed below.

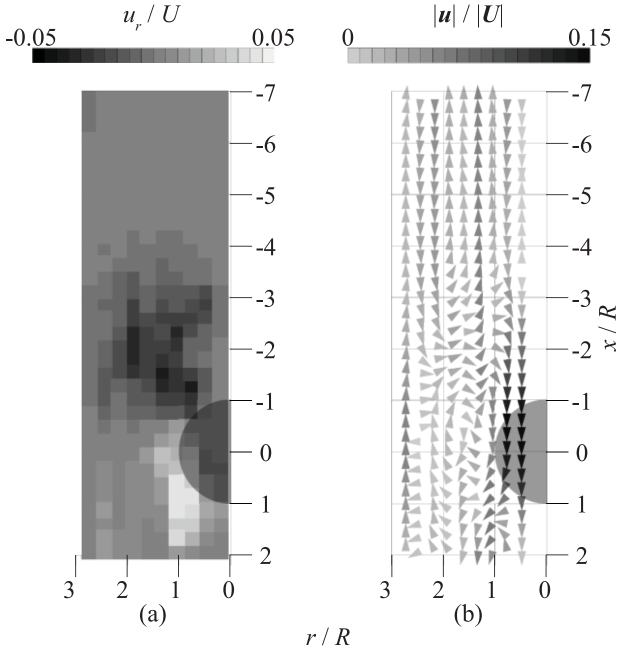

(a) (b)

Figure 3: (a) Distribution of u_r velocity component obtained with UVP (b) Velocity vector field obtained by applying the equation of continuity to Figure 3 (a)

5 DISCUSSIONS

5.1 On frozen hypothesis

Figure 3 (b) is obtained under the assumption that sphere reaches terminal velocity. There are reports about oscillatory falling of a sphere in non-Newtonian fluids, and this must be checked in the present case for judging the validity of the frozen assumption. Figure 5 shows the time change of the position of the sphere, which is obtained from PIV. The vertical axis indicates the position of the sphere, z at every time. The origin of z corresponds to the initial position of the sphere. The dotted line indicates the position of UVP measurement line. It is determined from Figure 4 that the sphere reaches the terminal velocity around the measurement line. And more, it seems the flow field is steady in Figure 2. Therefore frozen hypothesis is applicable to the flow field.

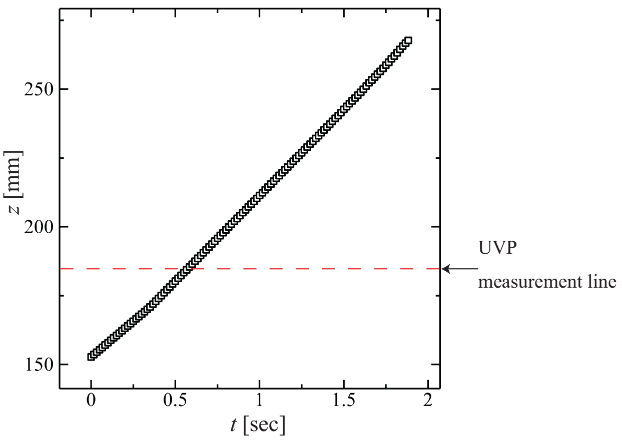

Figure 4: The position of the sphere in absolute coordinate

5.2 Equation of continuity

Relevancy of applying the equation of continuity is verified by calculating the experimental divergence ε defined as eq. (4).

$$\varepsilon = \frac{\partial u_x}{\partial x} + \frac{\partial u_r}{\partial r} + \frac{u_r}{r} \tag{4}$$

The equation of continuity is fulfilled when $\varepsilon = 0$. The spatial distributions of ε both for PIV and UVP measurements are shown in Figure 5. The data in (b) are lacked near the center axis because of differentiation disabled. The magnitudes of ε in Figure 5 (a) are much larger than those in Figure 5 (b). This fact indicates that the equation of continuity is unsuitable for the reconstruction of two-dimensional flow. One of the necessary conditions to regard the flow field axismmetry is that the sphere falls along the center axis of the cylinder precisely. A slight deviation of the sphere from the axis might lose the axial symmetry. This is the intrinsic problems when methodology of multi-dimensional velocimetry is built up at simplified equipment in falling sphere system.

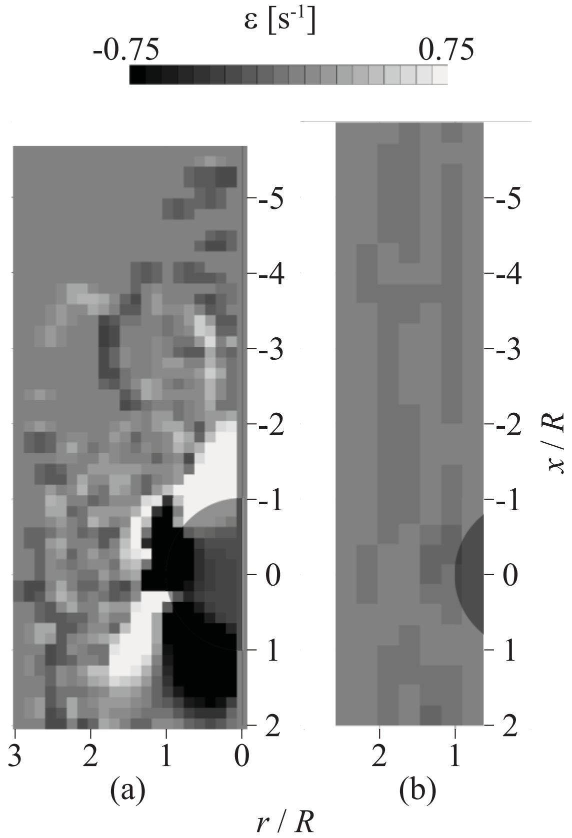

Figure 5: Distribution of ε obtained from (a) PIV measurement (b) UVP measurement

5.3 Comparison of u_r component

Comparison of the radial velocity distributions u_r obtained by PIV and UVP is shown in Figure 6. It is noted that the measurement is done for different shot of the sphere, and thus the two results need not to be completely the same for the reasons mentioned in the former subsection. Nevertheless, a common structure is recognized in the two results, which is the potential displacement of flow upstream the sphere (shown by white region). The remarkable difference is seen in the location of inward flow (shown by dark color) behind the sphere. The reason of the diffference between PIV and UVP may be explained by reflection of ultrasonic pulse on the surface of the sphere. At the time around the sphere passes the UVP measurement line, measurement errors appear prominently. Futhermore, near the negative wake (around x / R = -2.5, r / R = 1, shown by glay region in Figure 6 (a)), the magnitude of u_r is relatively small. Considering that the magnitude of velocity in Figure 6 (b) is smaller globaly than that in Figure 6 (b), it seems dificult to distinguish the negative wake from the errors shown above. This problem can be considered as a new fiding in UVP's application to viscoelastic flow.

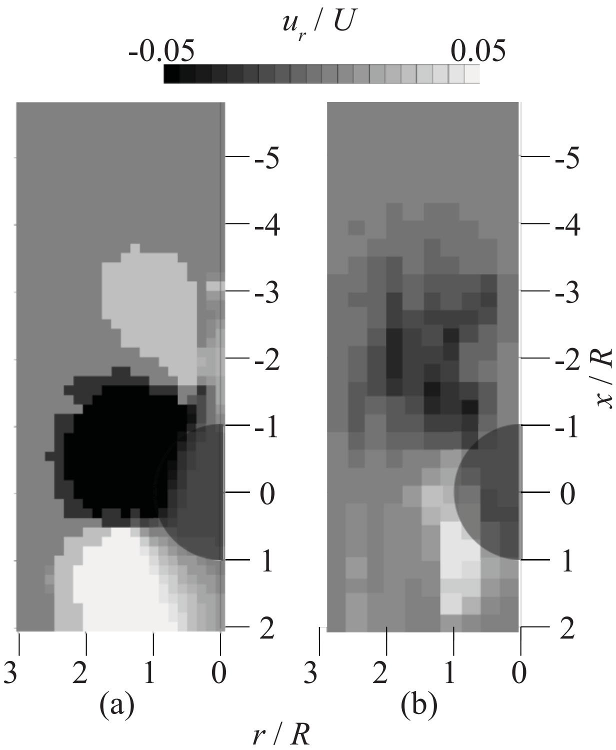

Figure 6: Distribution of radial velocity distribution u_r obtained by (a) PIV, and (b) UVP

6 SUMMARY

A method of two-dimensional viscoelastic flow field measurement by means of UVP has been proposed. Key flow structures futuring the viscoelastic responce in falling sphere system have been discussed as the measurement performance was assessed. With the results, we have picked up two technical problems; magnitude of velocity near the negative wake, and departure from axial symmetricity in coupling equation of continuity. At present, we are now thinking that these problem will be overcome when multiple transducers are utilized simultaneously [3]. We are to examine this strategy in the next step of the study.

REFERENCES

[1] O. Harlen, The negative wake behind a sphere sedimenting through a viscoelastic fluid, J. Non-Newtonian Fluid Mech. 108 (2002) 411–430
[2] Y. Takeda, Velocity profile measurement by ultrasonic Doppler method, Exp. Fluid Sci. 10-4(1995), 444-453.
[3] H. Obayashi, Y.Tasaka, S.Kon, Y.Takeda, Velocity vector profile measurement using multiple ultrasonic transducers, Flow Meas. Inst., 19 (2008), 189-195.

Wall shear measurement based on ultrasonic velocimetry for process in-line rheometry

Pauline Petit[1], Beat Birkhofer[2*] and Didier Lootens[1]
[1]Sika Technology AG, [2]Sika Services AG
Tüffenwies 16, CH-8048 Zürich, Switzerland (*Corresponding author: birkhofer.beat@ch.sika.com)

In this paper we demonstrate that the ultrasonic velocimetry in pipe flow is a tool which can be used to measure quantitatively in-line rheological properties of polyurethane based adhesives and sealants. In such concentrated suspension, the velocity profile is only measurable in the first few millimeters at the wall of the pipe due to the high acoustic attenuation. However, we show that the wall shear rate can be quantitatively measured by using a new velocity estimation method based on the analysis of the spectral data across different depths. The resulting profiles in the wall region were not visibly affected by changes of the ultrasonic sample volume (pulse length, frequency) and allow the determination of rheological parameters of the adhesive over a large range of volume flow rates.

Keywords: in-line rheometry, shear thinning suspensions, ultrasonic velocimetry, pipe flow

1 Introduction

In many industries such as chemical, food, pharmaceutical and cosmetics the rheology is an important part of the product quality. At the same time the rheological properties are often difficult and time consuming to measure, especially for complex fluids. For Sika, producing all kinds of construction chemicals, it is important to be able to characterize the rheological properties of the products [13]. The possibility to measure the shear thinning behavior of a product directly in-line in a continuous production process would have further advantages. Dealing with highly filled, opaque suspensions such as polyurethane based adhesives and sealants, the ultrasound velocimetry based rheometer concept [1–4, 11, 12, 14, 15, 19, 20, 22] is an interesting option. The method is based on the measurement of the velocity profile in steady and laminar pipe flow and often pressure drop. With this information it is possible to obtain the viscosity by either fitting to a fluid model (e.g. power law or Herschel Bulkley) or by using directly the velocity gradient as local shear rate combined with the local shear stress derived from the pressure drop (known as gradient or point wise method).

First measurements in different types of adhesives showed that velocity profile measurements are possible but the penetration depth is limited to at most a few millimeters due to the high attenuation. Therefore we tried to optimize ultrasound transducer and signal processing for the measurement of the velocity profile close to the wall, as this contains also important rheometric information. For industrial applications it is important to have a quantitative measurement of the rheology and therefore the influence of the ultrasonic pulse parameters, such as length and frequency, were varied to investigate their effect on the velocity profile and the derived rheological properties.

2 Material and methods

2.1 Suspension

The adhesive studied in this paper is a filled polyurethane with high adhesive strength. It belongs to a class of adhesives used for making permanent elastic seals of different types of substrate materials such as wood, metal, metal primer, ceramic material, plastic and can be used to assemble windows on their frames either for the construction or for the car industry. These products must have features to suit the customers' expectations: sealing properties, strength, color, curing kinetic but should also have special rheological properties (viscosity, yield stress) for their correct application. Consequently they are the result of a complex formulation work. High strength polyurethane sealing products are composed of: (i) polyurethane (20 – 30 w%) responsible for the adhesive and reactive properties of the paste, (ii) fillers (20 – 40 w%), that, depending on the system, consist in chalk, kaolin, titan dioxide, alumino-silicates or carbon black and are used to increase the viscosity of the paste and its final strength, (iii) other materials (10 – 30 w%) which can be plasticizers, stabilizers and catalysts [5].

2.2 Flow setup

The material was pumped by a dosing unit as it is used for the robotic application of the material e.g. to windscreens in the automotive industry. The dosing unit itself has a capacity of 614 ml and is supplied with another pump directly connected to a 200 L barrel. With the used adhesive the volume flow rate can be varied between 1 and 40 ml/s thus the phases of constant flow (corresponding to one filling of the dosing unit) are between 10 minutes and 15 seconds respectively.

The flow cell for the ultrasonic measurement was attached to the end of a temperature controlled tubing of a total length of 15 m. The pipe diameter in the flow cell was 25 mm. The cell was also equipped with two temperature and two pressure sensors.

2.3 Electronics and transducer

We used an ultrasound apparatus developed in the Microelectronics Systems Design Laboratory of the University of Florence [16] that allows the control of several transmission and reception parameters. The system was connected to a home-made 5.5 MHz pencil transducer featuring a 80 % -3 dB bandwidth and a 1.2 mm beam-width in the focus region. The transducer was excited with frequencies between 2 and 8 MHz and pulse width between 1 and 32 cycles. The data received from the transducer in each pulse repetition interval were sampled at 64 MS/s, demodulated, decimated to up to 16 MS/s (corresponding to a maximum gate resolution in water (c = 1480 m/s) of 46 µm), and finally saved in a file for post processing.

2.4 Signal processing

The convolution of sample volume and the actual flow profile [9, 10] results in a significant distortion of the measured velocity profile towards the wall. Literature describes mainly two different strategies to recover the actual profile: (i) deconvolution in the frequency domain [7–10] or (ii) use of the envelope profile [17, 18]. The first method requires knowledge of the sample volume which would be difficult to obtain in our highly attenuating suspension. While the envelope profile is

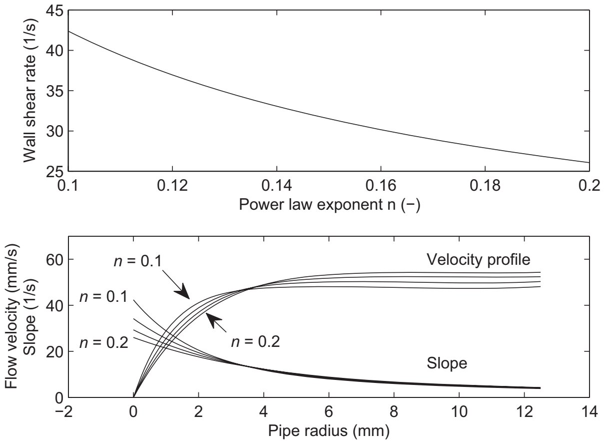

Figure 1: Theoretical calculations for power law fluids with *n* ranging from 0.1 to 0.2. Top: wall shear rate in function of *n*, bottom: velocity profiles and corresponding slopes.

easier to calculate as it only requires one correction factor describing the transducer characteristics, this method has a reduced accuracy due to the high attenuation. In this work we tested an alternative profile estimation method which was successfully used for the wall shear rate determination without requiring a sample volume dependent correction factor.

2.5 Rheometry

For most of the measured velocity profiles the available information covers only 5 to 10 % of the pipe radius. Altough the measured fluid is highly shear thinning, the onset of the velocity plateau in the central part of the pipe is not always visible.

Figure 1 shows some theoretical pipe flow calculations for a power law fluid for which viscosity η is a function of shear rate $\dot{\gamma}$, the coefficient K and the exponent n: $\eta = K\dot{\gamma}^{n-1}$. For the calculations the exponent n was varied from 0.1 to 0.2, the pipe radius $R = 12.5$ mm and the flow rate $Q = 20$ ml/s. Those parameters are typical for the presented measurements. For the power law fluid the wall shear rate $\dot{\gamma}_\mathrm{w}$ can be calculated using:

$$\dot{\gamma}_\mathrm{w} = \frac{3n+1}{4n}\,\frac{4Q}{\pi R^3} \qquad (1)$$

The resulting $\dot{\gamma}_\mathrm{w}$ varies from 42 to 26 s^{-1} for n equal 0.1 and 0.2 respectively. Thus $\dot{\gamma}_\mathrm{w}$ has the potential to be used for characterization of the shear thinning behavior of the fluid. The second plot of figure 1 shows the resulting velocity profiles and in addition the slope of the velocity profile calculated from the wall to the radial position. This indicates the shear rate can be determined from a linear interpolation in the corresponding region. It also shows that it would be ideal to be able to measure the shear rate in the first millimeter from the wall as this results in the most important differences.

3 Results and discussion

3.1 Off-line rheometry

Figure 2 shows the evolution of the viscosity as a function of the shear rate for different temperatures ranging from 25 to 50 ℃. The onset of the flattening of the infinite viscosity region is in the range of the expected wall shear rate which varies between 5 and 40 s^{-1}. Thus the power law model is only an approximation of the actual shear thinning characteristics of the fluid.

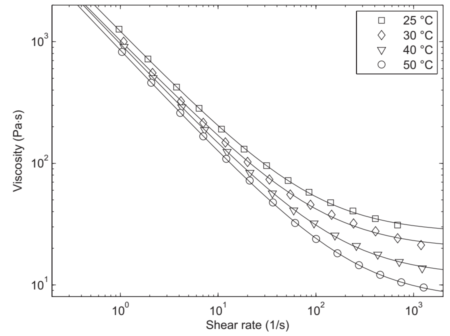

Figure 2: Viscosity curves of the adhesive used for the profile measurements obtained with a laboratory rheometer at different temperatures.

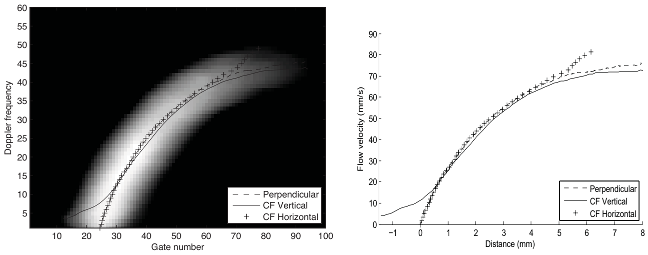

Figure 3: Example of a velocity profile measured for a flow rate of 30 ml/s with a pulse length of 4 cycles and a base frequency of 3.5 MHz. The left side shows the spectral intensities and the estimated profiles. The right side just the profiles estimated with three different methods.

3.2 Acoustic properties

The material has a relatively high attenuation coefficient of 0.4 Np/cm and a sound velocity of 1376 m/s at 20 ℃ with a temperature dependency of $-3.4\,\mathrm{m\,s^{-1}\,℃^{-1}}$.

3.3 In-line rheometry

Figure 3 shows a typical result for a profile measurement at a volume flow rate of 30 ml/s. The full line («CF Vertical») shows the conventional profile estimated from the channel-wise central frequency. It is obvious that this profile is not usable to extract the wall shear rate. The «+» symbols («CF Horizontal») indicate the central frequency determined across different depths. The resulting profile is realistic over the first 5 mm from the wall until the penetration limit of the measurement is reached. Finally a dashed line («Perpendicular» shows the result of an estimation of the central frequency analyzing the spectral information perpendicular to the velocity profile. This approach results in a profile overlapping with the horizontal central frequency over a wide radial range. Towards the end of the measured profile the result is better but not necessarily very reliable. Very close to the wall the method is not usable with the available spectral information.

3.4 Variation of physical measurement parameters

3.4.1 Pulse length

The pulse length was varied from 1 to 32 cycles for a base frequency of 3.5 MHz for a flow rate of 1 ml/s. The surface plots of the spectral intensity distribution (figure 4) show the expected broadening of the signal, the estimated velocity profile is shifted proportionally to the number of cycles away from the wall. The pulse length has no visible effect on the profile shape.

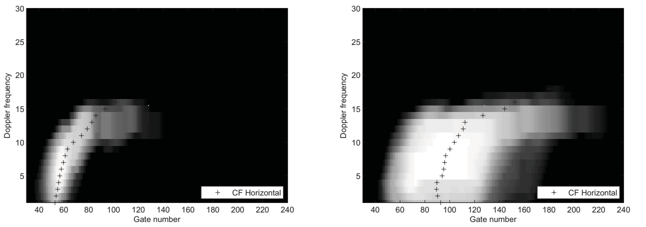

Figure 4: Spectral intensities for a pulse length of 1 (left) and 32 (right) cycles.

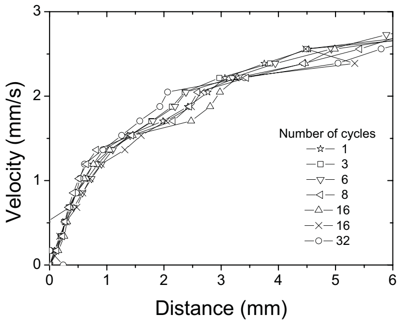

Figure 5: Profiles estimated for different pulse lengths. All curves were normed to distance zero.

3.4.2 Frequency variation

The result of a variation of base frequency from 2 to 6.5 MHz (figure 6) looks similar to the one for the pulse length variation. The profiles are just shifted in radial direction (not visible in the figure as the profile locations are normalized) while the estimated wall shear rate is not affected (within the limited available precision).

3.4.3 Gain variation

Also a variation of the analog gain (figure 7), the amplification of the received signal, does not influence the shape of the profile and the resulting wall shear rate significantly.

3.5 Variation of post processing parameters

3.5.1 Assumed Doppler angle

The transducer was not directly in contact with the fluid. Therefore the Doppler angle (angle between flow- and beam directions) in the fluid has to be calculated by Snells law ($c_2 \sin\theta_1 = c_1 \sin\theta_2$) which correlates incidence θ_1 and refraction θ_2 angles with the sound velocities (c_1 and c_2) in two different media [6]. The wall shear rate is sensitive to the Doppler angle (figure 8) but even an error of 50 m/s in the sound velocity of the fluid would only result in an error of the Doppler angle of less than 1 ° and accordingly 1.5 s^{-1} in the wall shear rate. Thus the relative errors in sound velocity and wall shear rate are approximately equal.

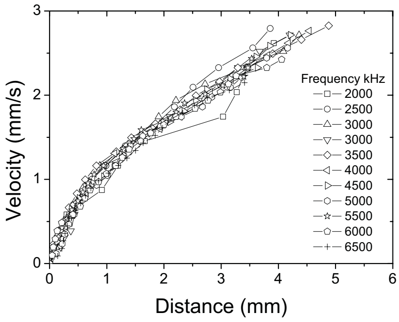

Figure 6: Profiles measured at different frequencies. All curves were normed to distance zero.

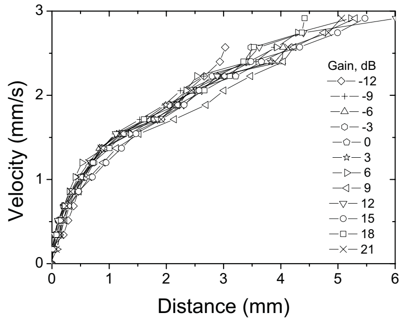

Figure 7: Profiles measured with different amplification settings.

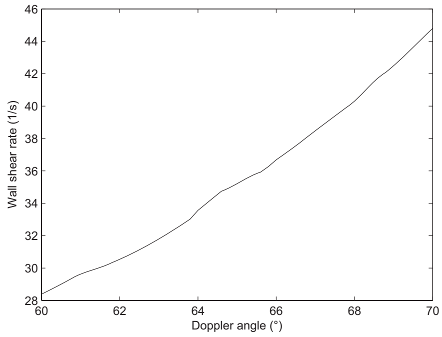

Figure 8: Influence of assumed Doppler angle on wall shear rate.

3.6 Flow rate variation

The flow rate was varied in steps of 5 ml/s from 5 ml/s to 30 ml/s and back to 5 ml/s. The wall shear rate was determined using the velocity data in the first 0.5 mm from the wall (corresponding to 4 % of the pipe radius). In a first step the velocity information was used to to fit the power law exponent n with following equation [21]:

$$v(r) = \bar{v}\frac{3n+1}{n+1}\left(1-\left(\frac{r}{R}\right)^{\frac{n+1}{n}}\right) \tag{2}$$

where $\bar{v}$ the average flow velocity ($\bar{v} = \frac{Q}{\pi R^2}$). Next the wall shear was calculated using equation 1. Fitting to the power law based velocity profile equation was chosen to obtain more realistic wall shear rates compared to a simple polynominal fit.

The resulting wall shear rates are shown as circles in figure 9. The shear rate predicted using a constant power law exponent n equal 0.2 and equation 1 is indicated with «×» symbols in the same figure. In this case the wall shear rate is simply direct proportional to the volume flow rate. But as shown in the laboratory rheometer measurements (section 3.1 and figure 2) the power law model is only an approximation, especially for the high shear rates. Therefore we used a second approach and calculated a «local» power law fit of the viscosity curves measured with the rheometer using one decade of shear rates around the approximate wall shear rate. Those calculations also consider the fluid temperature measured in the flow cell. The resulting n varies between 0.20 and 0.33 for flow rates of 5 and 30 ml/s respectively.

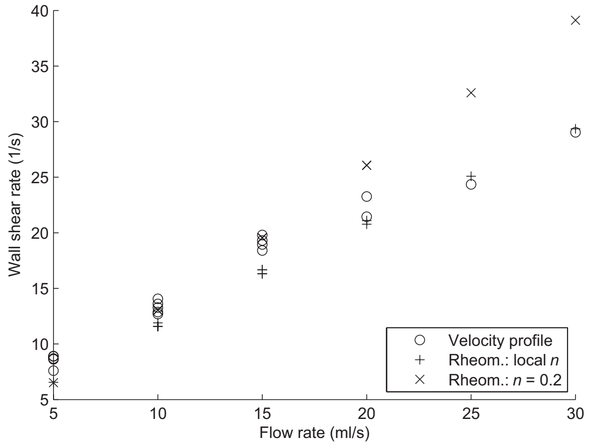

Figure 9: Wall shear rates in function of the flow rate extracted from the measured velocity profiles and predicted based on the rheometer measurements.

The resulting wall shear rates, again calculated using equation 1 are indicated with «+» symbols in figure 9. Especially for the higher flow rates those wall shear rates match the ones extracted from the velocity profiles quite well. For the lower flow rates the wall shear rate extracted from the flow profiles is slightly overestimated. This corresponds to an increase of the velocity slope very close to the wall also visible in figures 5 to 7. It is assumed that this artifact is due to the fact that in this region only a part of the sample volume is inside the fluid. More sophisticated spectral analysis methods should enable a compensation of this effect.

4 Conclusions

It was shown that an optimized measurement setup and profile estimation method allow to obtain the velocity profile in the wall region. The presented velocity estimation method has the additional advantage that the wall shear rate is insensitive to the sample volume, thus ultrasound parameters such as pulse length, base frequency and amplification. Further measurements, for example in fluids with different shear thinning characteristics at a constant flow rate, are necessary to test accuracy and precision the measurement system. Also a CFD calculation of the velocity profile based on the rheometer measurements will be of interest.

Acknowledgments

We would like to thank Dr. Stefano Ricci and Prof. Piero Tortoli from the Microelectronics Systems Design Laboratory of the University of Florence for their help optimizing the measurement setup. We are also thankful to Kurt Berli from Sika Services Widen for the help conducting the flow measurements and Patrik Kuhn from Sika Technology for the laboratory measurements.

References

[1] B. H. Birkhofer, S. A. K. Jeelani, E. J. Windhab, B. Ouriev, K.-J. Lisner, P. Braun, and Y. Zeng. Monitoring of fat crystallization process using UVP-PD technique. *Flow Measurement and Instrumentation*, 19(3-4):163–169, 2008.

[2] N. Dogan, M. J. McCarthy, and R. L. Powell. Comparison of in-line consistency measurement of tomato concentrates using ultrasonics and capillary methods. *Journal of Food Process Engineering*, 25:571–587, 2003.

[3] N. Dogan, M. J. McCarthy, and R. L. Powell. Measurement of polymer melt rheology using ultrasonics-based in-line rheometry. *Measurement Science and Technology*, 16:1684–1690, 2005.

[4] H. Fock, J. Wiklund, and A. Rasmuson. Ultrasound velocity profile (UVP) measurements of pulp suspension flow near the wall. *Journal of pulp and paper science*, 35:26–33, 2009.

[5] C. Hepburn. *Polyurethane Elastomers*. Elsevier, 2nd edition edition, 1992.

[6] C. R. Hill, J. C. Bamber, and G. R. ter Haar, editors. *Physical Principles of Medical Ultrasonics*. Wiley, 2nd edition, 2004.

[7] P. E. Hughes and T. V. How. Quantitative measurement of wall shear rate by pulsed Doppler ultrasound. *Journal of Medical Engineering & Technology*, 17(2):58–64, 1993.

[8] P. E. Hughes and T. V. How. Pulsatile velocity distribution and wall shear rate measurement using pulsed Doppler ultrasound. *Journal of Biomechanics*, 27(1):103–110, 1994.

[9] J. E. Jorgensen and J. L. Garbini. An analytical procedure of calibration for the pulsed ultrasonic Doppler flow meter. *Transactions of the ASME/Journal of Fluids Engineering*, 96:158–167, 1974.

[10] J. E. Jorgensen, D. N. Campau, and D. W. Baker. Physical characteristics and mathematical modeling of pulsed ultrasonic flowmeter. *Medical and Biological Engineering*, 11(4):404–421, 1973.

[11] R. Kotze, R. Haldenwang, and P. Slatter. Rheological characterisation of highly concentrated mineral suspensions using an ultrasonic velocity profiling with combined pressure difference method. *Applied Rheology*, 18(6):62114, 2008.

[12] T. A. Kowalewski. Velocity profiles of suspension flowing through a tube. *Archives of Mechanics*, 32(6):857–865, 1980.

[13] D. Lootens, P. Jousset, C. Dagallier, P. Hebraud, and R. Flatt. The "dog tail test": a quick and dirty measure of yield stress. application to polyurethane adhesives. *Applied Rheology*, 19(1): 13726, 2009.

[14] M. Müller, P. Brunn, and C. Harder. New rheometric technique: The gradient-ultrasound pulse Doppler method. *Applied Rheology*, 7(5):204–210, 1997.

[15] B. Ouriev and E. J. Windhab. Rheological study of concentrated suspensions in pressure-driven shear flow using a novel in-line ultrasound Doppler method. *Experiments in Fluids*, 32:204–211, 2002.

[16] S. Ricci, E. Boni, F. Guidi, T. Morganti, and P. Tortoli. A programmable real-time system for development and test of new ultrasound investigation methods. *IEEE Transactions on Ultrasonics, Ferroelectrics, and Frequency Control*, 53(10):1813–1819, 2006.

[17] P. Tortoli, F. Guidi, G. Guidi, and C. Atzeni. Spectral velocity profiles for detailed ultrasound flow analysis. *IEEE Transactions on Ultrasonics, Ferroelectrics, and Frequency Control*, 43(4):654–659, 1996.

[18] P. Tortoli, T. Morganti, G. Bambi, C. Palombo, and K. V. Ramnarine. Noninvasive simultaneous assessment of wall shear rate and wall distension in carotid arteries. *Ultrasound in Medicine & Biology*, 32(11):1661–1670, 2006.

[19] J. Wiklund and M. Stading. Application of in-line ultrasound Doppler-based UVP-PD rheometry method to concentrated model and industrial suspensions. *Flow Measurement and Instrumentation*, 19(3-4):171–179, 2008.

[20] J. Wiklund, I. Shahram, and M. Stading. Methodology for in-line rheology by ultrasound Doppler velocity profiling and pressure difference techniques. *Chemical Engineering Science*, 62:4277–4293, 2007.

[21] W. L. Wilkinson. *Non-Newtonian fluids: fluid mechanics, mixing and heat transfer*, volume 1. Pergamon Press, 1960.

[22] T. Wunderlich and P. O. Brunn. Ultrasound pulse Doppler method as a viscometer for process monitoring. *Flow Measurement and Instrumentation*, 10(4):201–205, 1999.

Ultrasonic velocimetry in carbon black suspensions

Thomas Gibaud, Damien Frelat and Sébastien Manneville
Laboratoire de Physique, Université de Lyon - Ecole Normale Supérieure de Lyon, CNRS UMR 5672,
46 allée d'Italie, 69364 Lyon cedex 07, FRANCE (e-mail: sebastien.manneville@ens-lyon.fr)

Attractive colloidal gels display a solid-to-fluid transition as shear stresses above the yield stress are applied. This shear-induced transition is involved in virtually any application of colloidal gels. It is also crucial for controlling material properties. Still, in spite of its ubiquity, the yielding transition is far from understood, mainly because rheological measurements are spatially averaged over the whole sample. Here, the instrumentation of creep and oscillatory shear experiments with high-frequency ultrasound opens new routes to observing the local dynamics of opaque attractive colloidal gels. We show that the transition proceeds from the cell walls and heterogeneously fluidizes the whole sample with a characteristic time whose variations with applied stress suggest the existence of an energy barrier linked to the gelation process.

Keywords: colloidal gels, ultrasonic velocimetry, velocity profile, yielding.

1 INTRODUCTION

Colloidal particles with strong enough short range attraction are known to aggregate into fractal clusters that may form a space-spanning network leading to solid-like properties even at very low volume fractions [1]. In such a gel state, the system is kinetically arrested and displays non-ergodic features such as ultraslow relaxations, aging, and dynamical heterogeneities [2]. These glassy features have raised the issue of unifying the behaviour of colloidal gels and that of more concentrated amorphous jammed systems, e.g. colloidal glasses or concentrated emulsions [3].

Here, we focus on the stress-induced solid-to-fluid transition in carbon black suspensions, a totally opaque colloidal gel made of weakly attractive soot particles. We use high frequency ultrasound as a new tool to follow the local deformation and flow of the sample under an external stress. Both creep tests and oscillatory shear experiments show that, above a critical yield stress σ_y, (i) yielding proceeds from the cell walls in a spatially and temporally heterogeneous way and (ii) the time needed for total fluidization of the sample decreases exponentially with the applied shear stress.

2 MATERIALS AND METHODS

2.1 Carbon black gel preparation

Carbon black is widely used in industry, e.g. for coatings, printing, rubbers, tires, paints, or batteries [4]. These colloidal carbon particles result from partial combustion of fuel and are made of unbreakable aggregates of permanently fused nanometric primary particles. These aggregates have a typical diameter of 500 nm. When dispersed in a light mineral oil (from Sigma, density 0.838, viscosity 20 mPa.s) at a weight concentration of a few percents, carbon black particles (Cabot Vulcan XC72R of density 1.8) form a space-spanning network due to weakly attractive interactions of typical strength 30 k_BT [3].

Our samples are prepared by vigorous mixing of 6% w/w carbon black particles into the mineral oil. Since the resulting gel is transparent to ultrasound, 1% w/w hollow glass microspheres of mean diameter 6 µm (Sphericel, Potters) are added in order to provide enough acoustic contrast (see below). The sample is further sonicated for 1 hour.

2.2 Ultrasonic echography under shear

In our experiments, classical rheology in Couette geometry is combined to ultrasonic echography in order to access local properties of the gel such as its velocity or deformation fields. Rheological measurements are performed in a smooth Plexiglas Couette cell (rotating inner cylinder radius 24 mm, gap width 1 mm, and height 30 mm) by a stress-imposed rheometer (Bohlin C-VOR 150, Malvern Instruments).

In creep experiments, we use ultrasonic speckle velocimetry (USV) as described in Ref. [5] to record temporally-resolved velocity profiles across the gap at about 15 mm from the cell bottom (Fig. 1a,b). USV is based on the interaction between ultrasound and micronsized scatterers embedded in the gel (here, the glass microspheres that act as contrast agents). It gives access to the local velocity of the gel with a spatial resolution of about 40 µm.

For oscillation experiments, we take advantage of ultrasonic echography in a new way by focusing on the spatiotemporal diagrams of the successive speckle signals (Fig. 1c-f). Indeed, the spatial variation of the speckle intensity provides crucial information on the local deformation of the sample. When pulses are sent with a sufficiently high repetition frequency f_{prf} compared to the oscillation frequency f, tracking the local oscillatory motion of the gel becomes possible (Fig. 1c and e). Here, we rather set $f_{\mathrm{prf}} = f$ so that the material is probed by ultrasound only once per oscillation period. Data analysis is then straightforward: if two successive speckle signals are fully correlated, then the gel is solid-like since it comes back exactly to the same position every period (Fig. 1d). On the other hand, we interpret any significant degree of decorrelation in the speckle signal from one period to the other as the signatureof fluid-like behaviour due to motions of the scatterers induced by local rearrangements inside the gel (Fig. 1f).

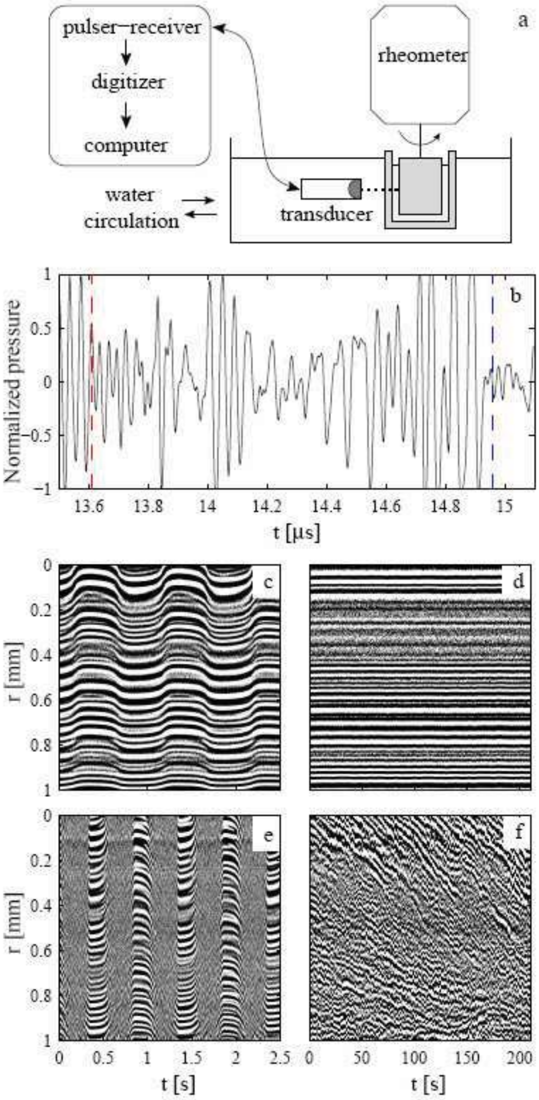

Figure 1: Ultrasonic echography under shear. (a) Schematic of the rheology experiment combined with USV. (b) Typical normalized pressure signal backscattered by glass microspheres embedded in a carbon black gel as a function of time after the incident pulse is emitted at *t*=0 s. The times-of-flight corresponding to the positions of the stator and the rotor are indicated by a red and blue dashed line respectively. The corresponding gap is 1 mm. (c and d) Spatiotemporal diagrams of the normalized pressure signal during an oscillation experiment at f=1 Hz and σ=15 Pa. The pressure is coded in linear grey levels and plotted against the time at which the incident pulse is sent (*x*-axis) and the radial distance *r* to the rotor (*y*-axis). In (c), the pulse repetition frequency f_{prf} is 400 Hz, which is large enough to resolve the deformation due to the oscillations of the rotor, while in (d), $f_{\mathrm{prf}}=f$=1 Hz. (e and f). Same as in (c and d) but for a higher shear stress σ =30 Pa.

The spatiotemporal tracking of the transition from correlated speckle signals (i.e. solid-like state) to decorrelated speckle signals (i.e. fluidized state) is made quantitative by using a threshold for the correlation coefficient of successive signals over small time windows, thus identifying the boundary between solid and fluid regions as a function of time up to a spatial resolution of 40 μm (see Fig. 3d).

3 RESULTS

3.1 Creep experiments

Figure 2a gathers the results of creep experiments for a wide range of imposed shear stresses. The critical shear stress σ_y = 8.5±0.5 Pa clearly separates two regimes. For $\sigma<\sigma_y$, the gel remains solid-like and does not flow, whereas for $\sigma>\sigma_y$, the sample eventually flows with a measurable shear rate, a transition known as the “viscosity bifurcation" in the soft glassy literature [6].

In order to get better insight into the fluidization process, we correlate the rheological measurements to the local velocity field *v*(*r*) measured with USV for the typical creep experiment at σ=10 Pa shown in Fig. 2b. In the early stage where the shear rate slowly increases (t<1500 s), solid-body rotation is observed, i.e. the sample is in an unsheared solid-like state except for thin lubrification layers along the cell walls that allow the gel to slide as a solid block (Fig. 2c). The average velocity in the solid-like material slowly increases following the trend in the shear rate. At the beginning of the sharp upward bend in the shear rate, for 1500 s < t < 1800 s, the bulk sample starts to experience a non-zero shear rate. Fluidization then proceeds in a spatially heterogeneous way. Indeed, in this regime, velocity profiles present a highly sheared region close to the rotor that coexists with a low-shear band next to the stator and whose size increases in time (Fig. 2d). Such a shear localization suggests that the gel progressively sticks to the cell walls and gets dragged along the rotor. The fluidized zone expands from the rotor until, for t≈1800 s, the gel flows homogeneously without any apparent wall slip, as seen from the linear velocity profiles of Fig. 2e.

Our local measurements refute the simple scenario in which yielding occurs abruptly and homogeneously at σ_y and rather support a yielding mechanism that is heterogeneous in both space and time, where fluidization starts at the walls and propagates through the whole sample. Such front dynamics is reminiscent of heterogeneous nucleation as predicted by a phenomenological “fluidity" model [7]. The present experiment also allows us to define unambiguously a characteristic time τ for fluidization as the time when homogeneous shear is first observed, e.g. τ = 1850±100 s for σ=10 Pa. The fluidization time roughly corresponds to the inflection point in the shear rate curve.

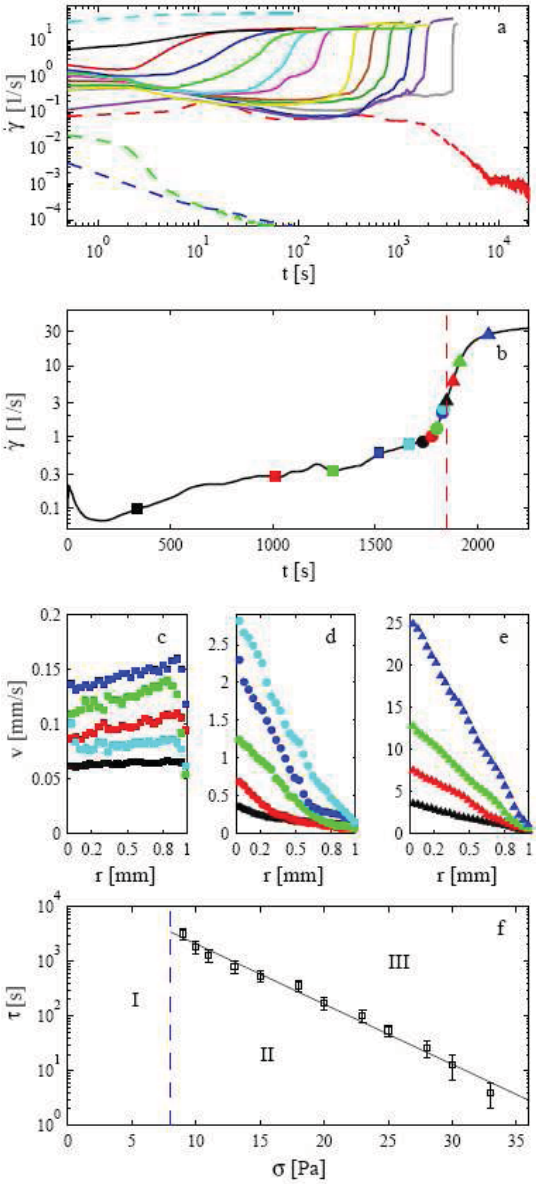

Figure 2: Creep experiments in a 6% w/w carbon black gel. (a) Temporal evolution of the shear rate for (from bottom to top) σ =5, 7, 8, 9, 10, 11, 13, 15, 18, 20, 23, 25, 28, 30, 33 and 40 Pa. (b-e) Combined rheological and USV measurements for σ =10 Pa. (b) Shear rate as a function of time. The red dashed line indicates the fluidization time τ discussed in the text. (c, d, e) Instantaneous velocity profiles *v*(*r*) recorded with USV at the times shown in (b) using the same symbols. (f) The fluidization time τ as a function of the applied shear stress σ. The black line is an exponential fit to the experimental data.

Fig. 2f sums up the behavior of our colloidal gel in creep experiments. Below σ_y (region I), the gel remains solid for all times, while above σ_y, the gel first undergoes solid-body rotation or shear localization for $t<\tau$ (region II) and eventually flows homogeneously for $t>\tau$ (region III). Remarkably, over the whole range σ=8-33 Pa, the fluidization time follows an exponential law: $\tau \propto \exp(-\sigma/\sigma_0)$ where $\sigma_0=4.0\pm0.2$ Pa. In other words, with $\sigma_0=k_BT/v$, where *v* is some characteristic volume, this behaviour is equivalent to an Arrhenius law $\tau \propto \exp(E(\sigma)/(k_BT))$, where the energy barrier $E(\sigma)=-\sigma v$ decreases linearly with the applied stress.

3.3 Oscillatory shear experiments

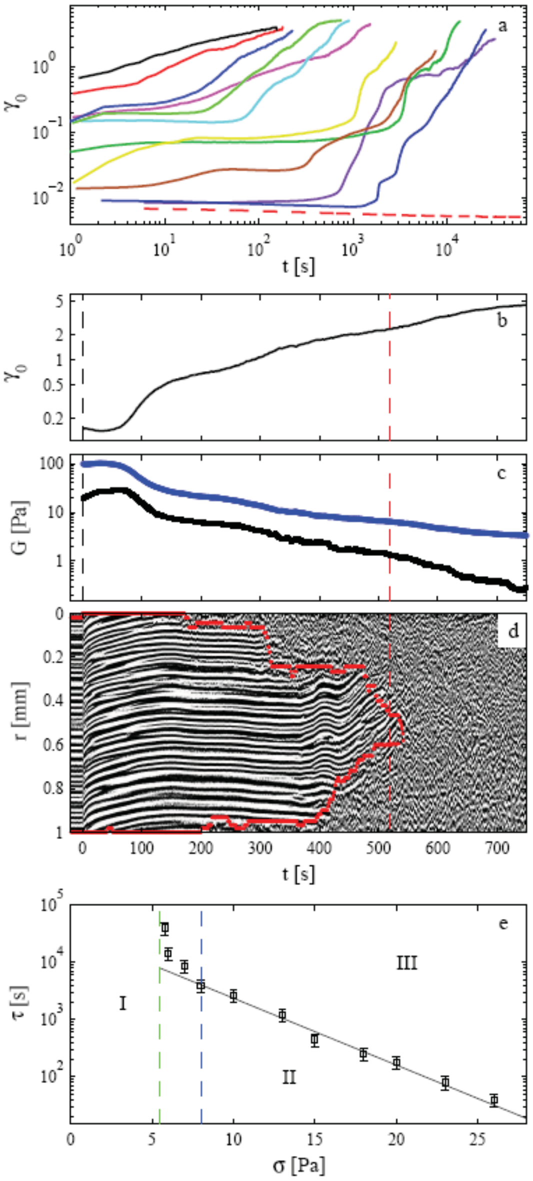

Figure 3: Large amplitude oscillatory shear experiments at *f*=1 Hz in a 6% w/w carbon black gel. (a) Temporal evolution of the deformation amplitude γ_0 for (from bottom to top) σ =5, 5.8, 6, 7, 8, 10, 13, 15, 18, 20, 23, 26 Pa. (b-d) Combined rheological and USV measurements for σ=15 Pa. (b) σ_0 and (c) *G*' (black) and *G*'' (blue) as a function of time. (d) Spatiotemporal diagram of the ultrasonic speckle signal coded in linear grey levels. The USV sampling frequency is equal to the oscillation frequency *f*=1 Hz. Red dots indicate the boundary between solid-like and fluid-like regions. The red dashed line shows the time τ at which 90% of the gel across the gap is fluidized. (e) The fluidization time τ as a function of the stress amplitude σ. The black line is an exponential fit to the experimental data (only data above 8 Pa are considered in the fit).

In a second series of experiments, the gel is submitted to oscillatory shear stress of given amplitude σ and frequency f=1 Hz. The strain amplitude γ_0 is monitored and again, we observe that when σ is large enough γ_0 eventually increases with time, suggesting that the sample becomes fluid over time (Fig. 3a,b). To confirm this scenario, we track the local deformation of the gel with USV (see Section 2.2). For $\sigma<5$ Pa, the gel indeed remains solid: no decorrelation of the ultrasonic speckle signals, i.e. no rearrangement within the gel, was observed during waiting times as long as 10^5 s. However, for stress amplitudes above 5 Pa, rearrangements and fluid-like behaviour are detected first close to the cell walls (see $t\approx100$-300 s in Fig. 3d). The fluidized zone then progressively expands through the bulk material ($t\approx300$-550 s) until the whole sample gets fluid ($t>550$ s).

It is important to note that fluidization does not have such a dramatic signature on γ_0 under oscillatory stress as on the shear rate during creep tests. Moreover, as shown in Fig. 3c, the loss modulus is larger than the elastic modulus throughout the whole experiment. In view of the USV results, this can only be explained by the presence of lubrication layers at the walls. A naive interpretation of standard viscoelastic data would thus wrongly conclude that the sample is fluid as soon as stress is applied. Here simultaneous spatially-resolved measurements show that solid-fluid coexistence comes into play and reveal a highly heterogeneous fluidization pattern. In oscillation experiments, the fluidization time, defined as the time τ for which 90% of the gel is in the fluid-like state, follows an exponential law $\tau \propto \exp(-\sigma/\sigma_0)$ with $\sigma_0=3.9\pm0.3$ Pa for $\sigma>8$ Pa (Fig. 3e). This is strikingly similar to the behaviour obtained in creep experiments (Fig. 2f). However, under an oscillatory stress of amplitude 5 Pa$<\sigma<$8 Pa, a strong departure from exponential behaviour is observed, pointing to a divergence at $\sigma\approx5.5$ Pa. In this stress range, no fluidization was observed during creep tests.

4 DISCUSSION AND CONCLUSIONS

The creep tests and the oscillation experiments above have shown the benefit of local measurements in establishing a spatiotemporal scenario for yielding: fluidization is initiated at the walls and propagates into the entire sample within a characteristic time τ that follows an Arrhenius law. Such a scaling provides evidence for the relevance of activated processes and barrier hopping in the context of yielding in colloidal gels. Although such ingredients have recently been incorporated into theoretical approaches based on mode-coupling theory [8] or on the shear-transformation zone (STZ) theory [9], local dynamical descriptions are still missing from microscopic models of the stress-induced solid-to-fluid transition.

To conclude, ultrasonic echography constitutes a versatile tool to follow yielding and fluidization in both space and time even in optically opaque materials. Its mesoscopic resolution of a few 10 µm bridges the gap between microscopic imaging techniques and global rheological measurements. Indeed, coarse-grained models for soft glassy materials use local strains and stresses averaged over intermediate sizes [10,11], so that gathering information at a mesoscopic scale is a key issue for comparing experiments to such models. From the fundamental point of view, our observations not only emphasize the importance of activated processes in yielding but also reveal a complex interplay between boundaries and bulk dynamics.

REFERENCES

[1] W. B. Russel, D. A. Saville, and W. R. Schowalter, Colloidal Dispersions, Cambridge University Press (New York), 1989.

[2] L. Cipelletti et al., Phys. Rev. Lett. 84 (2000) 2275-2278.

[3] V. Trappe et al., Nature 411 (2001) 772-775.

[4] J.-B. Donnet, R. C. Bansal, and M.-J. Wang, Carbon black: Science and technol ogy, Marcel Dekker Inc. (New York), 1993.

[5] S. Manneville, L. Bécu, and A. Colin, Eur. Phys. J. AP 28 (2004) 361-373.

[6] P. Coussot et al., J. Rheol. 46 (2002) 573-589.

[7] G. Picard et al., Phys. Rev. E 66 (2002) 051501.

[8] V. Kobelev and K. S. Schweizer, Phys. Rev. E 71 (2005) 021401.

[9] M. L. Falk, J. S. Langer, and L. Pechenik, Phys. Rev. E 70 (2004) 011507.

[10] L. Bocquet, A. Colin, and A. Ajdari, Phys. Rev. Lett. 103 (2009) 036001.

[11] S. M. Fielding, M. E. Cates, and P. Sollich, Soft Matter 5 (2009) 2378-2382.

Ultrasound based methods for acoustic characterization, in-line viscosity and solid fat content (SFC) measurements of fat blends

Emma Levenstam Bragd[1], Johan Wiklund[1], Paul Wassell[2, 3] and Niall W.G. Young[2, 3]
1. SIK – The Swedish Institute of Food and Biotechnology, P.O. Box 5401, SE-402 29, Gothenburg, Sweden

2. Danisco A/S, Multiple Food Applications, Edwin Rahrs Vej 38, 8220 Braband, Denmark

3. University of Chester, Environmental Quality and Food Safety, Research Unit, Department orf Biological Scence, Parkgate Road, Chester, CH1 4BJ, U.K.

Fat and fat crystallization are today studied by methods that are time consuming, expensive and not optimized for in-line measurements. Therefore, new methods are being developed at SIK (Gothenburg, Sweden). Previously, a method for in-line rheometry combining the Doppler-based Ultrasound Velocity Profiling (UVP) technique with Pressure Difference (PD) measurements, commonly known as UVP-PD, has been developed. In this work, the in-line UVP-PD method was successfully applied to highly concentrated and opaque fat blends. The UVP-PD method could rheologically characterize and differentiate between different fat blends. In addition, new ultrasound based methods have been developed for acoustic characterization, for monitoring crystallization kinetics under dynamic conditions and for determination of the solid fat content (SFC). Experimental results showed, for example, that the SFC can be determined in-line using ultrasonics with good agreement with pNMR. Ultrasound based methods can thus be regarded as rapid and powerful research tools as well as a feasible in-line tool for process monitoring and quality control.

Keywords: Ultrasound, in-line, rheometry, viscosity, SFC

1 INTRODUCTION

Removal and reduction of trans fatty acids (TFA) and saturated fats from foods is becoming increasingly prevalent within the food industry because of the potential dangers these fats can cause in the diet. The problem is to maintain the fat blends' functionality since the TFA and the saturated fats give structure to the fat blends. Successful alternative structurants which have found commercial relevance are based on crystalliser technology, which involves adding small quantities of a long chain hydrophobic moiety that positively affect the fat-crystallization kinetics [1] [2]. Methods available today to monitor crystallisation processes include rheological and microscopic methods, pNMR, DSC and X-ray diffraction. These methods are time consuming, expensive and they are not optimized for in-line measurements. New methods to analyse the crystallisation processes under dynamic conditions are therefore required and are being developed at SIK - The Swedish Institute for Food and Biotechnology (Gothenburg, Sweden). The aim of this work was to evaluate ultrasound based in-line methods for determination of rheological parameters and solid fat content (SFC) in an industrial pilot plant under true dynamic processing conditions, thoroughly described in [1] and [2]. In addition, a light microscopy based method for determining the particle size and particle size distribution of the crystals in different fat blends has been improved and tested. The aim is to replace this method with new ultrasound based methods.

2 MATERIALS AND METHODS

2.1 Materials

The fat blends used for rheology measurements consisted of 25 % Chocofill BR 60, a non-*trans*, vegetable fat filling from Aarhus Karlshamn (Karlshamn, Sweden), in rapeseed oil. To one of the systems 1 % of GRINDSTED® CRYSTALLIZER 110 from Danisco A/S (Copenhagen, Denmark) was added. The fat blends used for SFC measurements consisted of 30% palm stearin (Danisco A/S) dispersed in 70% rapeseed oil. The fat and fat blends used for microscopy studies were Chocofill NH 50, 6 % oil absorber in liquid oil and different concentrations of palm stearin dispersed in rapeseed oil, all from Danisco A/S. The cocoa butter came from Cloetta Sverige AB (Ljungsbro, Sweden).

2.2 UVP technique and the UVP-PD method for in-line rheometry

Ultrasound velocity profiling (UVP) is a technique for measuring an instantaneous velocity profile in liquid flow along the pulsed ultrasonic beam axis. The instantaneous velocity profile is obtained by detecting the Doppler shift frequency of backscattered ultrasound as a function of time. The velocity profiles can then be used for determination of the volumetric flow rate (by integration) and for determination of the shear rate distribution (the velocity gradient). If the UVP technique is combined with pressure difference (PD) measurements, the resulting UVP-PD method can be used for in-line rheometry. The UVP-PD method is well described in literature and allows e.g. real-time measurements of radial velocity profiles and rheological properties, such as yield stress, directly in-line. If a flow in a tube can be approximated by a power-law model according to Eq. 1, then, the radial velocity profile is given by Eq 2 [3].

$$\tau = K\dot{\gamma}^{n} \qquad (1)$$

$$v(r) = \left(\frac{R\Delta P}{2LK}\right)^{1/n} \cdot \frac{R}{(1+1/n)} \cdot \left[1 - \left(\frac{r}{R}\right)^{(1+1/n)}\right] \qquad (2)$$

τ is the shear stress, $\dot{\gamma}$ is the shear velocity, K is the consistency index and n is the power law index. R is the pipe radius, ΔP is the pressure drop and L is the distance over which the pressure drop is measured. The viscosity and the rheological model parameters can be determined by making a non-linear fit of Eq. 2 to the measured velocity profile and pressure drop data.

2.3 UVP-PD System

A custom made UVP-PD testing section comprising a flow adapter cell with ultrasound transducers and a by-pass loop with a differential pressure sensor was developed and is thoroughly described in [2]. The UVP-PD system further comprised a custom pulser/receiver, UVP-DUO-MX with integrated multiplexer (Met-Flow SA, Lausanne, Switzerland). The instrument firmware and driver software were modified to give access to the complex demodulated baseband signal (I/Q). The modified firmware combined with the RheoFlow™ software enabled velocity profile estimation from the UVP-Duo instrument with two options; time-domain algorithmn or fast Fourier transform (FFT). In this work, 4 MHz, 150 V, 2-4 cycles per pulse and 512 repetitions were used and 25-40 profiles were processed and averaged in real-time thus giving a total measurement time of 450 ms per reading. The use of a high-speed digitizer card (Agilent Acquiris, Agilent Technologies Sweden AB) as a part of the data acquisition scheme enabled not only measurements of the velocity profiles, but also the simultaneous determination of the acoustic properties. A high-speed DAQ card from National Instruments Sweden AB (Kista, Sweden) was used for acquisition of data from the differential pressure sensor. The pulser/receiver and the differential pressure sensor were connected to a master PC. UVP data was implemented with an ActiveX library (Met-Flow SA). The novel software RheoFlow™, developed at SIK for in-line UVP-PD based rheological measurements, was used for all data acquisition, processing and analysis.

2.4 Solid fat content (SFC)

The ultrasound based in-line method for determination of the SFC is based on the technique described by McClements and Povey [4-5]. If the sound velocity in a suspension or emulsion is approximately the same as in an ideal solution of the substances, and, if the size of the particles or droplets is much smaller than the wavelength of the sound, then the velocity of sound in the suspension or emulsion is given by Eq. (3) [6].

$$c = \frac{1}{\sqrt{\kappa\rho}} \qquad (3)$$

ρ and κ is given by Eqs. (4) and (5) respectively.

$$\rho = (1-\phi)\rho_1 + \phi\rho_2 \qquad (4)$$

$$\kappa = (1-\phi)\kappa_1 + \phi\kappa_2 \qquad (5)$$

c refers to the velocity of sound, κ to the adiabatic compressibility, ρ to the density and ϕ to the volume percentage of the dispersed phase. The subscripts 1 and 2 refer to the continuous and the dispersed phase respectively. Eq. (3) can be rewritten as a quadratic equation in terms of ϕ that for oils and fats has one solution given by Eq (6) [5]

$$\phi = \left(-B - \left(B^2 - 4AC\right)^{1/2}\right)/2A \qquad (6)$$

where A, B, and C are given by Eqs. (7), (8) and (9) respectively.

$$A = c_1^2(1-\rho_1/\rho_2) + c_2^2(1-\rho_2/\rho_1) \qquad (7)$$

$$B = c_2^2(\rho_2/\rho_1 - 2) + c_2^2\rho_1/\rho_2 \qquad (8)$$

$$C = c_2^2\left(1 - c_1^2/c_{total}^2\right) \qquad (9)$$

By converting the volume percentage into a mass percentage, the SFC can be calculated according to Eq. (10).

$$SFC = 100\phi\rho_2/\rho \qquad (10)$$

Thus, if both the speed of sound in and the density of both the continuous and dispersed phases are known, the SFC can be calculated by measuring the speed of sound in the dispersion. For validation, the SFC, determined with in-line ultrasonic measurements, was compared to the SFC determined off-line with the established IUPAC pulsed nuclear magnetic resonance (p-NMR) technique [7] and calculation principle by van Putte & van den Enden [8]. The densities were determined using a Densito-30PX from Mettler-Toledo (Stockholm, Sweden).

2.5 Microscopy

A light microscopy method, developed and improved at SIK, was used to study fat crystals with polarized light. The method was used for determination of the particle size distribution of the fat crystals. A Nikon Microphot FXA microscope (Japan) was used with a 20x objective. The images were taken with an Altra 20 camera from Olympus. The fat that was to be studied was melted and allowed to solidify in a schukoff flask. A small sample was taken and placed on a pre-cooled objective glass. Light microscopy images were taken and the diameter of the particles was determined using image analysis.

3 RESULTS AND DISCUSSION

3.1 Velocity profiles and rheology

Figure 1 shows the arithmetic average velocity profile and corresponding power-law fit of the control system (25% Chocofill BR 60 and 75% rapeseed oil) measured in the direction of the flow (flow rate 70 kg/h). The consistency index was calculated to be 6.7 Pas^n and the power-law index was 0.20 (R^2 = 0.998).

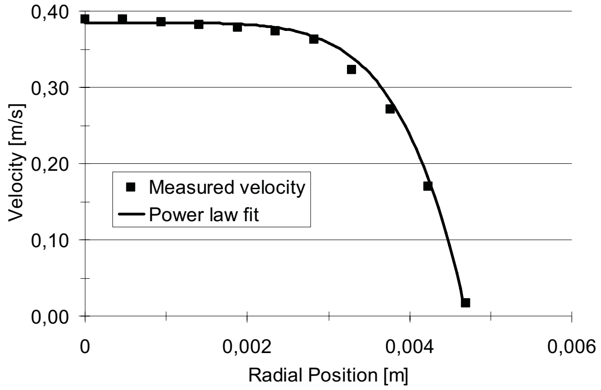

Figure 1. Rheological data and resulting power-law fit for the control system with 25% Chocofill BR 60 and 75% rapeseed oil.

Figure 2 shows the arithmetic average velocity profile and corresponding power-law fit of the blend with 25% Chocofill BR 60, 74% rapeseed oil and 1% GRINDSTED™ CRYSTALLIZER 110, measured in the direction of the flow (flow rate 70 kg/h). The consistency index was calculated to be 14.3 Pas^n and the power-law index was 0.09 (R^2 = 0.983).

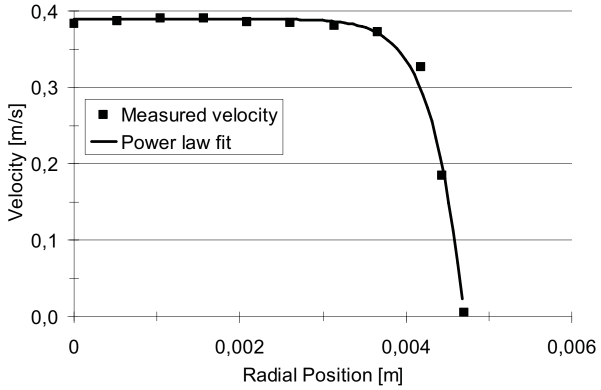

Figure 2. Rheological data and resulting power law fit for the system with 25% Chocofill BR 60, 74% rapeseed oil and 1% GRINDSTED® CRYSTALLIZER.

The low power-law indices indicate that both blends are shear-thinning which is in accordance with the shape of the velocity profiles, showing close to plug-flow. The consistency index for the fat blend with added crystallizer is higher than the consistency index for the control system, even though the composition essentially is the same. The viscosity of the sample with added crystallizer at a shear rate of 1 s^{-1} is about double the viscosity of the sample without added crystallizer. Hence, the viscosity of a fat blend can be significantly increased by addition of a small amount of crystallizer.

3.2 Solid fat content (SFC)

Following results comes from in-line SFC measurements during true dynamic processing conditions without the need of a calibration curve. The density of palm stearin was 899 ± 1 kg/m³ and the sound velocity at 10°C was determined to be 1548 ± 5 m/s. The density of rapeseed oil was 916 ± 1 kg/m³ and the sound velocity was determined to vary with temperature according to the equation $c=1536.4–3.487\times T$ (R^2 = 0.997). Figure 3 shows how the SFC in a blend consisting of 30% palm stearin and 70% rapeseed oil varies with temperature. The SFC is measured both with the standard p-NMR method and with the ultrasonic method.

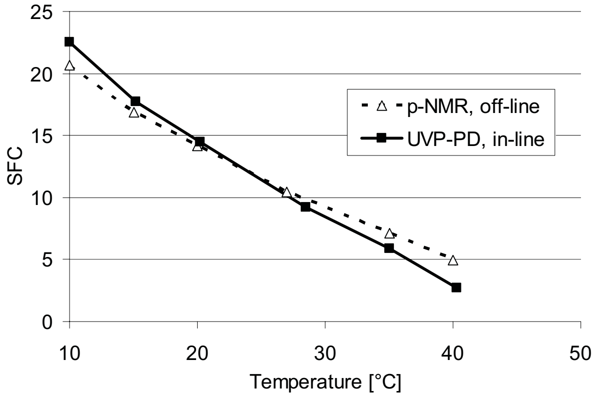

Figure 3. Solid fat content measured with ultrasonic's and p-NMR.

Figure 3 shows that there is a good correlation between the measurements made with the ultrasonic method and the measurements made with the standard IUPAC p-NMR method. The ultrasound based method can thus be used as a non-invasive in-line method for measuring SFC.

3.3 Microscopy

Light microscopy images were taken of the different fat or fat blends (not shown) and the images could be used to determine the size distribution of the fat crystals. Figure 4 shows an example of how the PSD was determined from light microscopy images. The microscopy based method works well but it is time consuming. A new method for determining the PSD using ultrasound is under development at SIK.

The method is based on measurements of the ultrasound velocity and attenuation over a wide frequency range, typically 0.5-100 MHz and the PSD can be calculated using multiple scattering theory [9]. The method is rapid and has good chances of in the future replacing the more time consuming microscopy method.

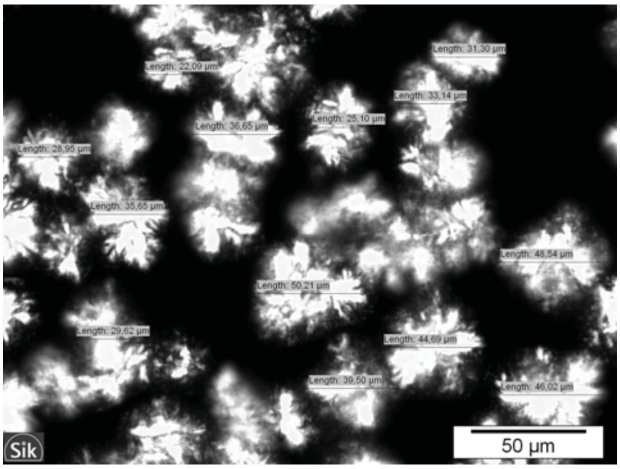

Figure 4. Fat crystals in Chocofill NH 50. The particles sizes are determined with the light micrscopy based method.

Nevertheless, the microscopy images give us insights of the structure of the fat crystals in a way not possible with ultrasonic techniques. Figure 3 shows a microscopy image showing crystals of palm stearin in rapeseed oil.

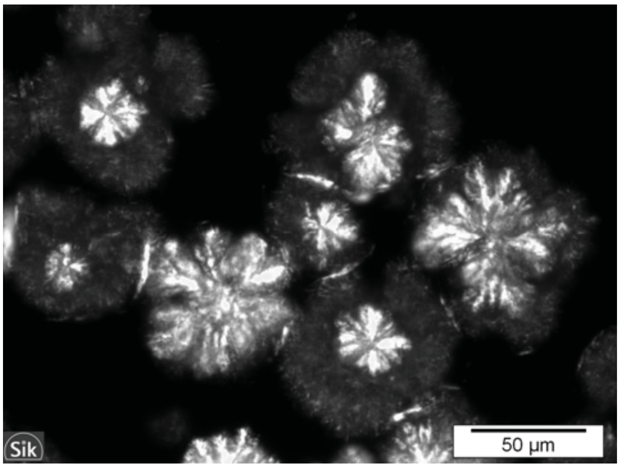

Figure 5. Growing fat crystals in a blend with 30% palm stearin and 70% rapeseed oil.

The light microscopy image in Figure 5 is taken soon after the sample preparation. Some crystals are assembled into diffuse clusters while others can be found in more compact, ordered structures. Light microscopy images of the palm stearin/rapeseed oil samples taken a longer time after sample preparation show that the palm stearin with time becomes arranged into smaller and more ordered structures.

4 CONCLUSIONS

The results show that the developed UVP-PD system and ultrasound based methods can be used to study both the rheology and SFC of opaque fat blends in-line and under true dynamic processing conditions. The SFC measured with the ultrasonic technique showed a strong correlation with the SFC measured with standard p-NMR. The UVP-PD method is an attractive tool for monitoring and characterization of fat blends in-line. The next step is to be able to measure the size and size distribution of the fat crystals with ultrasound in order to replace the time consuming microscopy techniques.

ACKNOWLEDGEMENTS

Graham Bonwick, Christopher Smith and Eva Almiron-Roig, University of Chester, U.K. are acknowledged for scientific collaboration. Lisbeth Dahl Pedersen, Danisco A/S, Braband, Denmark is acknowledged for experimental assistance. Met-Flow SA, Lausanne, Switzerland is acknowledged for technical support.

REFERENCES

[1] Young N et al.: Monitoring struturants of fat blends with ultrasound based in-line rheometry (ultrasonic velocity profiling with pressure difference), International Journal of Food Science and Technology 43 (2008) 2083-2089.
[2] Wassell P et al.: In-line viscosity and solid fat content (SFC) measurement of fat blends with ultrasound based in-line rheometry. International Journal of Food Science and Technology 45 (2010) 7 pages (doi: 10.1111/j.1365-2621.2010.02204.x).
[3] Wiklund J & Stading M: Application of in-line ultrasound Doppler-based UVP–PD rheometry method to concentrated model and industrial suspensions, Flow Measurement and Instrumentation 19 (2008) 171–179.
[4] McClements & Povey: Solid fat content determination using ultrasonic velocity measurements, International Journal of Food Science and Technology 22 (1987) 491-499.
[5] McClements & Povey: Comparison of pulsed NMR and ultrasonic velocity techniques for determining solid fat contents, International Journal of Food Science and Technology 23 (1988) 159-170.
[6] Urick RJ: A sound velocity method for determining the compressibility of finely divided substances, Journal of Applied Physics 18 (1947) 983-987.
[7] IUPAC: 2.150 - Solid content determination in fats by NMR (low resolution nuclear magnetic resonance) (ex 2.323). In: Standard Methods for the Analysis of Oils, Fats and Derivatives, 7th Edition, Blackwell Scientific Publishing, Oxford (1987).
[8] Van Putte K & van den Enden J: Fully automated determination of solid fat content by pulsed NMR, Journal of the American Oil Chemists’ Society 51 (1974) 316-320.
[9] McClements DJ & Coupland JN: Theory of droplet size distribution measurements in emulsions using ultrasonic spectroscopy, Colloids and Surfaces A. Physicochemical and Engineering Aspects 117 (1996) 161-170.

Suspensions and sediments

USV procedure for flowing fluids and suspensions

Maxime Chinaud[1], Thomas Delaunay[1] and Philippe Tordjeman[2]
[1]Institut d'Electronique du Sud, Groupe Micro Rhéo Acoustique, UMR CNRS 5214, Université Montpelier 2, France
[2]Institut de Mécanique des Fluides, CNRS, Université de Toulouse, INPT, France

[1]CC82, Place Eugène Bataillon, 34095, Montpellier
[2]1 Allée du Professeur Camille Soula, 31400, Toulouse

To measure fluid velocity in flow and also powders under sedimentation a non-invasive method is developed in this paper: the Ultrasonic Speckle Velocimetry (USV). Sedimentation of polymethyl metacrylate and silica particles in water, with known diameter distribution, is carried out to improve the method where the USV procedure, the signal processing and data analysis is particularly described. The optimization conditions are linked to space resolution, temporal resolution, dynamic and results show that USV is a useful technique to measure velocities between 10^{-5} and 1 m/s, using appropriate ultrasonic transducers. The choice of speckle window allows a 0.1ns temporal resolution obtained after signal processing. In the context of our sedimentation experiments, we showed that velocities measured by USV are in close agreement with those predicted by theory.

Keywords: Ultrasonic Speckle Velocimetry, Sedimentation flow, Signal processing, Data analysis

1 INTRODUCTION

Fluids research need more and more data about velocity fields for many applications. Ultrasonic techniques are well known to characterize opaque fluids compared to optical techniques such as Particle Image Velocimetry (PIV) [1, 2] and make this method a non-invasive quantitative techniques highly suited to study complex fluids. There are two main ultrasonic methods: Doppler echo ultrasound techniques - widely used in hydrodynamics, in particular, in clinical applications [3, 4], but hindered by complex electronic systems - and ultrasonic speckle techniques. The latter method is based on the ultrasonic speckle scattered by ultrasound contrast agents dispersed in flowing fluids. Ultrasonic Speckle Velocimetry (USV) is a recently developed technique [5] and does not require new transducer development. Moreover, USV has been recently successfully applied [6, 7] to measure the complex fluid velocity in all direction and to characterize flowing instabilities such as shear banding of opaque fluids. In spite of its interesting applications, USV is not widely used for flow velocities measurement due difficulties related to the signal processing description needed to improve the poor signal-to-noise ratio of the ultrasonic backscattered response [8]. However, recent recording system with efficient signal processing allows considering USV as a high-performance method compared to Doppler methods. Through the study of particle sedimentation in Newtonian fluid, this paper reports experimental procedures to optimize USV measurements. Signal processing conditions and data analysis are carried out and discussed in terms of accuracy, dynamics and resolution.

2 METHODS

2.1 USV Principles

An ultrasonic pulse backscattered by seeded particles in flowing fluids create a speckle signal [5, 7]. Its intensity results from the coherence of the all acoustic waves backscattered by the seeded particles - with a volume fraction of contrast agents comprised between 10^{-11} and $10^{-12}m^{-3}$ [5] - with a very high frame rate. Hence, the fluid vector velocity v can be determined by the cross-correlation (Eq. 1) of two successive speckles separated by a pulse repetition time t_{PRF} (Fig. 1 a).

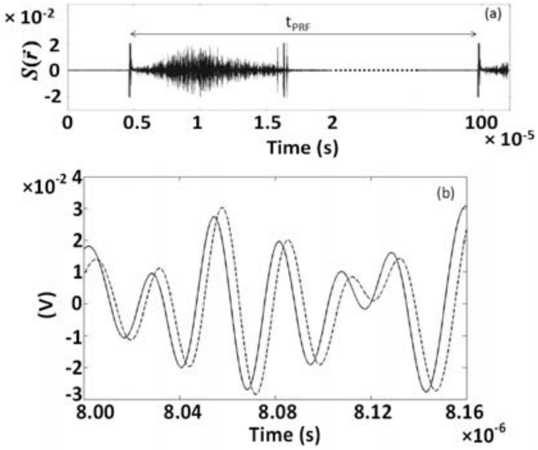

Figure 1: a) Speckle signal recorded between two successive acoustical pulses. t_{PRF} is the time between the two pulses; b) Zoom of two speckle signals at t (solid line) and $t + t_{PRF}$ (dashed line).

$$C(\vec{r}) = \sum_{r-\Delta r}^{r+\Delta r} S(\vec{r},0)S(\vec{r},t_{PRF}) \qquad (1)$$

t_{PRF} is a tunable parameter controlled by the pulser-receiver unit. Fig. 1.a presents the backscattered signal *S* between two successive pulse echoes while Fig. 1.b shows the coherence between two successive speckle signals. *C* is calculated for a speckle window $\Delta r=n\lambda$, where λ the acoustic wavelength and *n* is a whole number typically comprised between 2 and 20. The displacement of the scatterers at *r* is given by the time value δt that maximizes *C*. Finally, by assuming that the seeded particles behave as Lagrangian tracers, Eq. 2 give the fluid velocity along the ultrasonic beam axis.

$$v(\vec{r}) = \frac{1}{2} c \frac{\delta t}{t_{PRF}} \tag{2}$$

2.2 Particle Velocimetry Sedimentation

A sedimentation of particles in a Newtonian fluid is developed and built in a rectangular Plexiglas cell (2.4×3.6×5cm). The USV is then operated by placed the acoustic transducer in the base and the acoustic axis characteristic of the wave vector direction coincides with the sedimentation axis (Fig. 2).

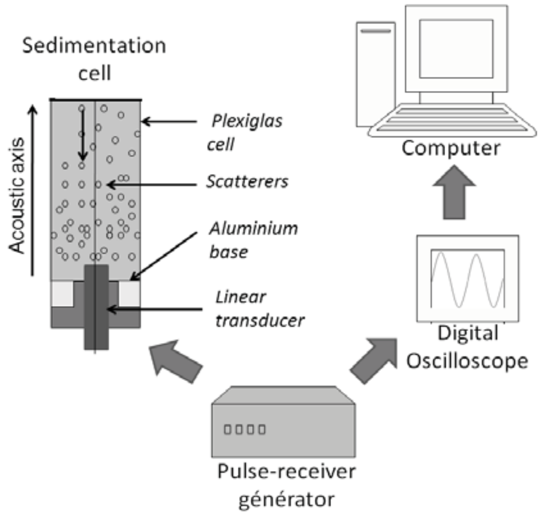

Figure 2: Schema of the sedimentation device.

Two commercial ultrasonic linear transducers (Olympus V312-SM), with 2.25MHz and 25MHz frequencies are controlled by a pulser-receiver generator Olympus Panametrics connecting to a digital oscilloscope Lecroy, Wave Runner MXi6400. Different speckle signals are recorded with the oscilloscope and triggered at a pulse repetition frequency, $PRF = (t_{PRF})^{-1}$, tunable from 0 to 20kHz.

Here, we studied the sedimentation of three different particle populations:

- Polymethyl méthacrylate (PMMA) particles (Dantec Dynamics). These particles contain rhodamine and are used for PIV experiment. Their mean diameter is around 10 µm and the impedance ratio between water and PMMA is about 0.5.
- Polydisperse silica particles (Arena) with a wide diameter distribution centred on 67.5 µm. The impedance ratio is about 0.1.
- Monodisperse silica particles with a narrow diameter distribution centred on 56.5 µm obtained by sifting of the polydisperse silica particles.

3 EXPERIMENTAL PROCEDURE

3.1 The device

The diameter distribution of the ultrasound scatterers allows choosing the ultrasonic transducer frequency [9]. 2.25MHz and 25MHz transducers are thus used to study the sedimentation of the silica and PMMA particles where the wavelengths are 670µm and 60µm, respectively.

The main parameters of the pulse generator are the bandwidth *BW* with the attenuation *A* and the gain *G* which limit the transducer frequency range, the damping current *C* controlling the shape of the ultrasonic pulse, and finally, the transducer energy *E*. For the following results, the setting is: *A*=-1dB, *G*= 54dB, *C*=50Ω and *E*=32µJ for both transducers. The bandwidths were comprised between 1 and 10MHz and comprised between 10 and 50MHz for the 2.25MHz and 25MHz transducers. Previous experiments or theory are necessary to evaluate the velocity particles in order to adjust the *PRF*. In our case, the particles velocity is estimated considering Stockian flows described by Eq. 3.

$$v(d) = \frac{\rho g d^2}{18\eta}\left(1 - \frac{\rho_w}{\rho}\right) \tag{3}$$

ρ and ρ_w are the volume weight of the particles and water and η is the water viscosity. Consequently, the *PRF* was fixed at 200Hz for the PMMA particles and 1kHz for the silica particles.

The signal recording is carried out with the oscilloscope using sampling frequencies of 500MHz and 50MHz for the PMMA and silica particles.

3.2 Signal Processing

In order to measure with high accuracy the velocity toward the sedimentation time, 10 successively *S* are recorded 200 times for each experimental condition. Between two acoustical pulses, the whole *S* is divided into *N* windows (Eq. 4) where each one has a 50% of overlapping with the previous windows, which allow measuring the velocity at *N* positions in the sedimentation cell.

$$N = \sum_i N_i \approx \frac{2L}{n\lambda} - 1 \tag{4}$$

Here *L* is the cell height. Typically, *N*=190 for PMMA with *n*=4. The cross-correlation function is then computed automatically for each speckle window couples $\{N_i(kt_{PRF}), N_i((k+1)t_{PRF})\}$, where *k* comprised between 1 and 9.

Fig. 3 present two 3D-representations of *S* in function of t_{PRF} and of the flowing time. Fig. 3.a shows a high level of coherence where *C* gives a well-defined maximum while Fig. 3b presents a low level of coherence and here the C are characterized by secondary maxima with amplitude close to the main peak.

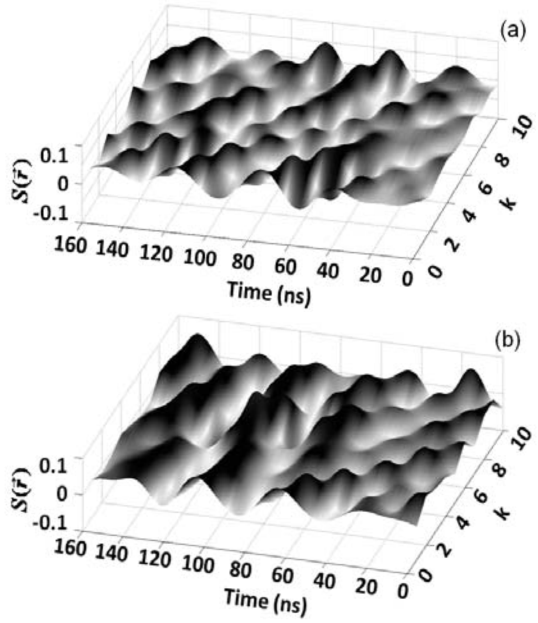

Figure 3: 3D-representations of speckle signal *S* vs time and the number of acoustic pulses. a) Example of a coherent speckle; b) Example of a noisy speckle.

This latter case is predominant and requires specific procedures to be analyzed: for each *i* speckle windows, we calculated the averaged cross-correlation functions C_i, determined the maximum C_{imax} and plotted the maxima in according to *i*.

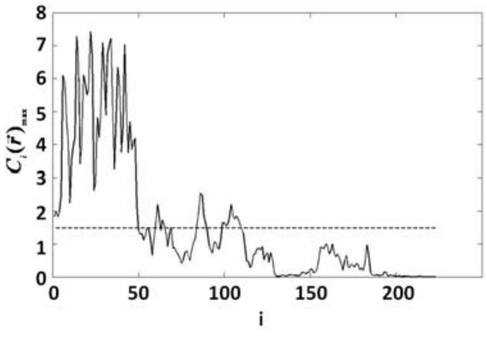

Figure 3: Maximum of the mean cross-correlation C_{imax} function vs the number of speckle windows *i*. Dashed line represents the criteria of 20 % of the maximum of C_{imax}

A criteria was defined to leave out all the cross-correlations given a C_{imax} value lower than 20% of the curve of the maxima and with all the cross-correlations having a secondary-primary peak amplitude ratio higher than 50%. From all C_i verifying the criteria, the velocities were finally calculated.

Space resolution is governed the speckle windows $\Delta r = n\lambda$. For PMMA, *n*=[4; 16] yield to [240; 960] µm and for silica particles *n*=[4; 8] yield to [2.6; 5.2] mm.

The measured minimum velocity is obtained from the minimum of δt while the maximum measured is given by Eq. 5 from the width of the speckle traces.

$$v_{\max} = \frac{n\lambda}{2t_{PRF}} \qquad (5)$$

Then, USV technique presents a very important dynamics, authorizing velocity measurements along the acoustic axis between [1.5 10^{-5}; 4.8] m/s for PMMA and [1.5 10^{-5}; 5.3] m/s for silica particles.

Three steps of procedure for signal processing are established. Firstly, the offset signal has to be removed. Secondly, numerical filter is applied between 10 and 50 MHz with -60 dB of attenuation to suppress the non-speckle signal. Subsequently, to obtain a temporal resolution of 0.1 ns with the 50 and 500 MHz sampling frequencies, the speckle data is re-sampled with a zero filling signal processing [10].

4 RESULT AND DISCUSS

Experimental velocities distributions of the three particle families are compared with those calculated from theory in Fig. 4, where mean velocities and standard deviations are assembled in Tab. 1.

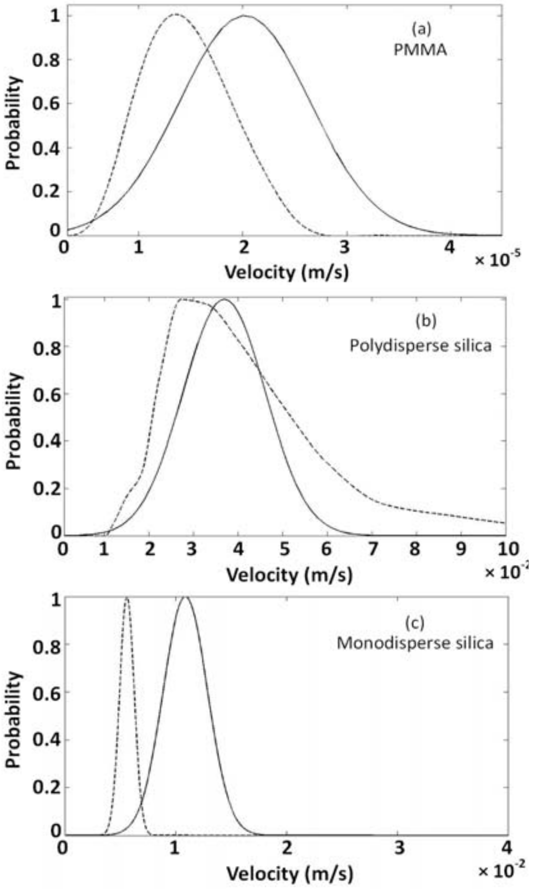

Figure 4: Velocities distribution of PMMA , polydisperse silica and monodisperse silica particles for a length of speckle window corresponding to n=4. Dashed lines represent the theoretical Stockian velocities and the solid lines represent the experimental values.

Table 1: Values of mean velocities and of standard deviations for PMMA, polydisperse silica and monodisperse silica particles for different length of speckle windows.

Particles	Mean velocity (m/s)		Standard deviation (m/s)	
n	4	8	4	8
Polydisperse silica (x10^{-2})	3.69	3.50	0.92	1.08
Monodisperse silica (x10^{-2})	1.12	1.21	0.29	0.40
PMMA (x10^{-5})	2.0	1.8	0.6	0.9

These results allow checking that USV has a significant dynamics and is able to measure the velocity over 6 decades. From the size distributions, it is possible to plot the theoretical velocity distribution in the Stockian regime (Fig. 4). Comparing both theoretical and experimental distributions, USV experiments clearly give mean velocities shifted towards the higher values. This shift is emphasized for the polydisperse silica particles and can be explained by considering that the multiple ultrasound scattering efficiency is obtained for the larger diameter particles when the theoretical velocity calculus gives the same weight for all the particles. The USV results in Fig. 4 also show the effect of the size distribution of silica particles. The mean velocity (1.12 and 3.69cm/s for monodisperse and polydisperse silica particles) depends on the mean particle diameter (56.5 and 67.5µm, respectively) while the velocity standard deviation increases with the particle size distribution.

The USV space resolution is studied by changing the speckle window length Δr (for n= 4, 8 and 16) for the three particle families and authors have show that the mean velocity is less affected by a change of Δr. On the other hand, the velocity distribution width changes with the speckle window length and the standard deviation seems to increase with *n*. This effect is due to a widening of the characterized area in the sedimentation cell.

Finally, Fig. 5 shows the variation of the velocity along the sedimentation axis for the polydisperse silica particles.

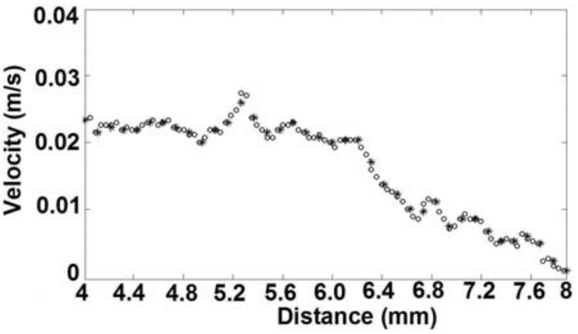

Figure 5: Velocity profile along the acoustical axis for polydisperse silica particles.

One can observe that the velocity decreases with the distance, which can be explained by the particle diameter effects on the sedimentation velocity.

5 CONCLUSION

USV is shown as a useful method to study the velocity profile in full flow on the basis of particle sedimentation experiments. Here three numerical stages have been developed before data processing. Moreover, a cross correlation criteria was defined to optimize data processing. We studied the effects of speckle window length on the measured velocities and found that the results are more accurate with the smallest window length.

The sedimentation velocities are measured for three different particle families - PMMA, monodisperse and polydisperse silicate particles, which are characterized by different density, acoustical impedance and size distribution - using 2.25 and 25MHz transducers were used. In our signal processing conditions, the temporal resolution could reach 0.1 ns for both the transducers. We measured velocities comprised between 20µm/s and 3cm/s, showing the wide dynamic potentiality of USV and the coherence with theoretical velocities.

ACKNOWLEGMENTS

The authors would like to thank V Roig, F Risso and M Roudet for numerous fruitful discussions. Our sincere thanks are also extended to C André for the characterization of monodisperse silica particles.

REFERENCES

[1] Cummins HZ, Pike ER: Photon Correlation Spectroscopy and velocimetry, Plenum, New York (1977)

[2] Berne BJ, Pecora R: Dynamic Light Scattering General Publishing Company ed., Toronto, Ontario, Canada (2000)

[3] Gens F, Remenieras JP, Patat F, Diridollou S, Berson M: Potential of a high-frequency correlation method to study skin blood flow, Skin research and technology (2000) 6 21-6

[4] Atkinson P, Woodcock JP: Doppler ultrasound and its use in clinical measurement, Academic Press, London (1982)

[5] Nakajima M, Itoh T, Shingyouuchi M, Akiyama I, Yuta S: Ultrasonic Speckle Velocimetry Ultrasonic Symposium IEEE (1988) 2 1007-12

[6] Gharib M, Beizaie M: Correlation between negative near-wall shear stress in human aorta and various stages of congestive heart failure, Annals of Biomedical Engineering (2003) 31 678-85

[7] Manneville S, Bécu L, Colin A: High-frequency ultrasonic speckle velocimetry in sheared complex fluids, Eur. Phys. J. A.P (2004) 28 361-73

[8] Cowan ML, Jones IP, Page JH, Weitz A: Diffusing acoustic wave spectroscopy, Phys. Rev.E (2002) 65 066605-1-11

[9] Born M, Wolf E: Principles of optics, University Press, Cambridge (1964)

[10] Carlson AB: Communication systems, Macmillan publishing company, New York (1986)

A new high resolution velocity and acoustic turbidity profiler for open-channels

Stéphane Fischer
UBERTONE, 1, rue de Molsheim, 67000 Strasbourg, France
(email : stephane . fischer @ ubertone . fr)

Hydraulic studies in rivers and sewers need a detailed metrology of flow and sediment transport at all spatial and time scales. We have developed an ultrasonic profiler for open-channel flows that allow high resolution measurements of velocity and acoustic turbidity in environmental and industrial applications. The system is fully integrated in a hydrodynamic box connected by an Ethernet cable. It is equipped with two transducers placed in the front for the measurement over two axes at different angles and frequencies. The electronic board is composed by a low noise analog stage for adaptive amplification and demodulation of the acoustic signal, a digital part dedicated to real time sequencing and signal processing and a low power processor that manage the data storage and the embedded web interface. This new profiler allow high speed sampling of velocity and backscattered acoustic energy profile with a high spatial resolution in sever conditions. Typical applications for this profiler are velocity measurement on river or channels, flowmetering in partially filled pipes, sediment transport studies, velocity field around submerged structures, concentration measurements.

Keywords: velocity profiler, acoustic turbidity, field instrument

1 INTRODUCTION

The Ultrasonic Velocity Profiler is one of the more efficient tools in hydraulic research and studies [1]. It is useful in accessing the main velocity field in open channel flows, and the interpretation of backscattered signal amplitude at different frequencies can lead to the concentration of suspended particles [2]. This amplitude profile can also be used to detect interfaces [3]. The good spatial and time resolution of Doppler coherent systems allows the study of turbulence [4]. Ultrasonic techniques are widely used in environmental and industrial flows due to their non-intrusive nature and their ability to work with opaque fluids.

A better knowledge of hydrodynamic processes and sediment transport in sewer systems may improve their efficiency and reduce the pollution of natural flows.

We have developed an ultrasonic profiler for open-channel flows that allow high resolution measurements of velocity and acoustic turbidity in environmental and industrial applications.

2 INSTRUMENT DESCRIPTION

The UB-Flow F156 (figure 1) has been designed for studies in the field of hydrodynamic and sediment transport as well as sewer diagnoses.

2.1 Device

The instrument is integrated into one single immersed hydrodynamic box. It is placed along the flow, and can be oriented in order to get either a horizontal or a vertical velocity profile. It is powered and communicates through the same cable. The device is handy and compact.

Figure 1: The UB-Flow F156 profiler is equipped with 2 transducers and integrates the whole electronic and software

2.2 Transducers

The device is equipped with two transducers placed at the front of the instrument.

The large band transducers are centered on two different frequencies (1.5 and 6.0 MHz) in order to match a wide range of particle sizes, beginning at 30 µm.

Frequency	Diameter	Angle
1.0 to 2.1 MHz	*20 mm*	*75°*
4.0 to 8.3 MHz	*5 mm*	*55°*

2.3 Electronic

The hardware is composed of three main parts : analog, digital and computing. All electronics are integrated in an immersed box and weighs less than 150 g.

The analog part is equipped with a low noise 82 dB amplification/demodulation channel. The ultrasonic emission bloc allows instantaneous power of 25 W (RMS) at frequencies going from 800 kHz to 9.25 MHz, selected by the user.

The digital part manages the ultrasonic sequencing, the data sampling and the first stage of real-time signal processing.

The computing part lies on an operating system embedded in a low power processor associated with 4 GB on board storage. This part communicates by Ethernet with any computer or smartphone accessing to the network.

The system is powered by the same Ethernet cable using the IEEE 802.3af norm (*PoE*).

2.4 Software

The software for data management and user interfaces is fully embedded in the device.

The web interface allow the user to configure the instrument, to visualize the velocity and acoustic turbidity profiles in real time and to download the data files.

The software allows to store instantaneous velocity and acoustic turbidity profiles at the selected sampling rate. As the software of the device is autonomous, it can collect data during a few weeks without being connected to a PC.

2.5 Configuration

Many parameters are modifiable to finely tune the instrument to fit the application :

- transducer selection
- emission frequency (1.0 to 2.1MHz and 4.0 to 8.3MHz)
- phase coding
- pulse duration (0.5 to 1000µs)
- number of cells (2 to 100)
- distance between cells (from 2.5 mm)
- pulse repetition frequency (up to 5kHz)
- automatic or manual amplification gain

3 MEASUREMENT

3.1 Profiling method

One of the main advantages of the pulsed ultrasonic techniques is the ability to measure from a distance without perturbation of the flow. The emission of an ultrasonic pulse in a narrow beam allows you to observe a profile which is composed of many measurement cells (or volumes) distributed along the beam axis. Thereby, the pulse is transmitted along the beam in the medium and is backscattered by the particles suspended in the flow. The echoes of the particles are received by the same transducer, the signal is conditioned, amplified, demodulated and sampled. This signal contains informations on velocity and concentration, the travel time of the ultrasound is relative to the position of the concerned particles. Thus, the windowing of the backscattered signal in several blocs leads to the profile.

3.2 Velocity estimation

The UB-Flow F156 uses the coherent pulse Doppler method in order to estimate the velocity. This method uses the observed phase shift of the acoustic signal in a same volume during consecutive emission-reception cycles. Each cycle generates one data sample per volume. The set of data samples coming from the same volume is called “Doppler signal” and has a frequency f_D which is related to the flow velocity v in the corresponding volume according to:

$$v = \frac{c \cdot f_D}{2 f_0 \cdot \cos\beta} \tag{1}$$

where c is the speed of sound in the medium, f_0 the carrier frequency and β the angle between flow and ultrasonic beam.

The Doppler frequency in one volume is given by the calculation of the first order moment of the signal (samples of the complex envelope with in-phase and quadrature components). Several methods may be used for Doppler frequency estimation. The UB-Flow uses the Pulse-Pair method [5]; another approach may be spectral analysis of the signal [6]. With the Pulse-Pair method, the estimated value of Doppler frequency is given by:

$$f_D = \frac{1}{2\pi T_{PRF}} \arctan \frac{\mathrm{Im}\left(R_{xx}\left(T_{PRF}\right)\right)}{\mathrm{Re}\left(R_{xx}\left(T_{PRF}\right)\right)} \tag{2}$$

where $R_{xx}(\tau)$ is the autocorrelation function of the Doppler signal and T_{PRF} the sampling repetition period.

The coherent pulse Doppler method has been largely studied [7,8]. This method ensures good temporal and spatial resolution and low variance on velocity estimation.

3.3 Acoustic turbidity estimation

The turbidity of fluid is generally measured by optical techniques. This parameter is used more and more in sediment transport studies in sewers and rivers because it can be linked to the suspended sediment concentration (SSC).

The acoustic turbidity is defined as the ability of the suspended particles to diffuse an acoustic wave. It relates, in each volume, for a given emission frequency, to the turbidity ratio :

$$T_r = \frac{v_r^2}{v_e^2 \cdot \Delta t_p \cdot G_t(z)} \left(\frac{z}{R_t} \right)^2$$

where :

v_r is the reception voltage,

v_e the emission voltage,

Δt_p the pulse emission duration,

$G_t(z)$ the electro-mechanical gain of the transducer in emission/reception at the working frequency, including the near field correction (modelled from the data given by [9]),

z the distance to the transducer,

R_t the transducer's radius.

This parameter T_r is proportional to the backscattered acoustic intensity and compensate all the transducer and instrument effects. Thereby, T_r only depends on the characteristics of the liquid (attenuation) and of the suspended particles (concentration, size, nature, form). This parameter can be used to evaluate the SSC with granulometric (*i.e.* particle size) estimation [2].

4 EXPERIMENTAL SETUP

Figure 2: UB-Flow F156 installed on the river Aar.

The instrument has been configured according to table 1.

It was installed on the Aar (figure 2), an arm of the river Ill in Alsace. The river is 12 meters large. The Reynolds number of the flow is approximatively $3 \cdot 10^5$. The beam is horizontal, placed 10 cm under the free surface.

Table 1: Parameters of the instrument

Variable	Symbol	Value
Carrier frequency	f_0 (MHz)	1.5
Pulse duration	Δt_p (µs)	20
Pulse repetition frequency	PRF (Hz)	700
Number of volumes	N_{vol}	54
Time between volumes	Δt_v (µs)	25
Samples per estimation	N_s	300

5 RESULTS

The mean velocity profile measured from the border of the river is in agreement with the observed flow.

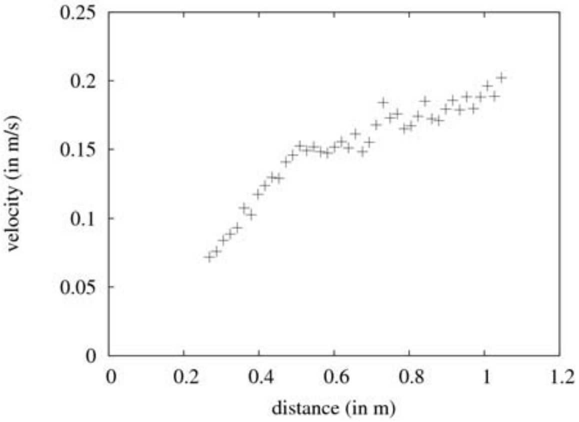

Figure 3: Mean velocity profile averaged over 133 successive instantaneous profiles

The standard deviation of the mean estimation is mainly due to the velocity dispersion in the flow.

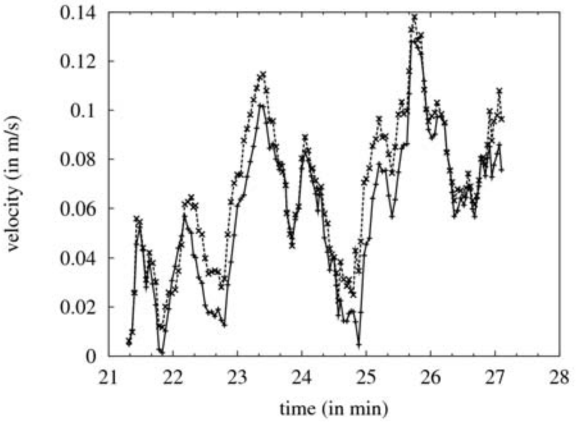

Figure 4: Evolution of the velocity in two measurement cells distant from 7.5 cm at 36 cm from the transducer.

The evolution of the velocity through the time is observed at a distance of 36 cm from the transducer and presented in figure 4.

This time series shows the large effect of the turbulence on the velocity fluctuation. The slowest velocity variation (approx. 0.01 Hz) corresponds to the energy injection frequency which is approximatively equal to the mean velocity divided by the hydraulic diameter.

The high correlation between the evolution of the velocity in the two cells distant from 7.5 cm is due to the coherence in the turbulent vortex.

The figure 5 compares the turbidity ratio T_r in the same measurement cell in two different flow conditions. The first measurements have been done in low water conditions during July 2009, the second have been done during rainy conditions in December 2009.

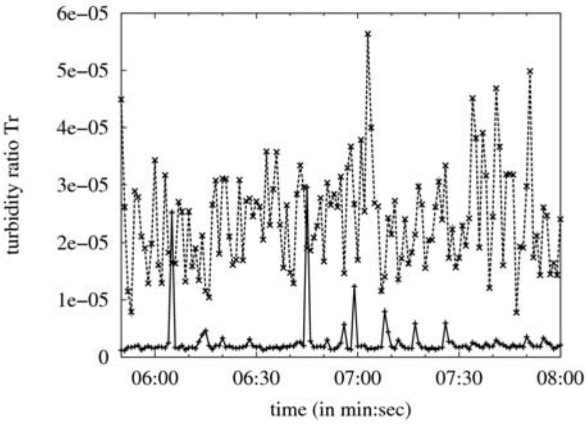

Figure 5: Evolution of the turbidity ratio T_r during time in two different concentration conditions (continuous line : July 2009, dash line : December 2009)

In low water conditions the turbidity is lower and presents some random peaks. This may correspond to a low homogeneous concentration of small particles associated with the random transit of isolated particles.

In rainy conditions, the turbidity ratio is greater and presents an important variation around the mean value. This may be due to local variation of the concentration of the particles.

6 CONCLUSION

We have developped an ultrasonic velocity and turbidity profiler, integrated in a compact immersed device equipped with two transducers. The instrument is designed for outdoor conditions.

This new instrument offers the possibility to measure velocity and turbidity profiles in industrial or natural flows with high spatial and temporal resolutions.

7 ACKNOWLEDGEMENT

This work has been done with the support of the ”concours national d'aide à la création d'entreprises de technologies innovantes” from the French Ministry of Research.

8 REFERENCES

[1] G. De Cesare and J.-L. Boillat, Flow velocity measurements using ultrasound Doppler method - 10 years experience in hydraulic modeling, Proceedings of the Fifth International Symposium on Ultrasonic Doppler Methods for Fluid Mechanics and Fluid Engineering, (2006) 113-116.

[2] Abda F., Azbaid A., Ensminger D., Fischer S., François P., Schmitt P., Pallarès A. : Ultrasonic device for real-time sewage velocity and suspended particles concentration measurements, Water Science & Technology, 60.1(2009) 117-125.

[3] S. Kojima, Y. Tasaka, Y. Murai and Y. Takeda, UVP Measurement for Flows Accompanying Free Surface, Fifth International Symposium on Ultrasonic Doppler Methods for Fluid Mechanics and Fluid Engineering, (2006) 117-120.

[4] D. Hurther, 3-D acoustic Doppler velocimetry and turbulence in open-channel flow. PHD Thesis EPFL, (2001).

[5] Miller, K.S., Rochwarger, M.M.: A covariance approach to spectral moment estimation, IEEE Transactions on Information Theory, 18(1972) 588-596.

[6] Fischer, S. et al.: A New Velocity Estimation Method using Spectral Identification of Noise, Flow Measurement and Instrumentation. 19 (2008) 197-203.

[7] Lhermitte, R., Serafin, R.: Pulse-to-Pulse coherent Doppler sonar signal processing techniques, Journal of Atmospheric and Oceanic Technology, Vol.1(1984),NO. 4.

[8] Abeysekera S., Performance of pulse-pair method of Doppler estimation. Aerospace and Electronic Systems, IEEE Transactions, vol.34 (1998) 520-531.

[9] Pallarès A., François P., Azbaid H., Schmitt P., Fischer S., Abda F.: Acoustic characterization of sewage effluents, CFA (2006).

Experiments on water jet induced cyclonic circulation - measurement of flow pattern and sediment concentration at reservoir outlet works

Jenzer Althaus, J. M. I.; De Cesare, G.; Schleiss, A.J.
Laboratoire de Constructions Hydrauliques (LCH), Ecole Polytechnique Fédérale de Lausanne (EPFL), Station 18, CH-1015 Lausanne, Switzerland, e-mail: jolanda.jenzer@epfl.ch

In the framework of the reservoir sedimentation problematic, a new innovation employing water jets in order to maintain the fine sediments in suspension and to release them through the water intake is studied. Laboratory experiments as well as numerical simulations are performed. The experimental facility consists of a prismatic basin, in which four equal water jets are placed in a circle on a horizontal plane near the bottom where each jet directs in a right angle to the end of the potential core of its neighbouring jet. This jet arrangement creates a cyclonic circulation. Light weight crushed walnut shells with an mean diameter of 60 microns are used as sediments. Turbidity measurements give information about the time evolution of the sediment concentration at strategically interesting locations. Flow velocities and patterns are measured by UVP technique. It could be observed by the laboratory experiments and from the numerical simulations that the flow velocities induced by this jet configuration are strong enough to keep fine sediments in suspension. A sensitivity analysis regarding the momentum flux and the position of the jets has been performed in order to evaluate which configuration gives the optimal combination regarding the suspended sediment release.

Keywords: Reservoir sedimentation, water jet, experiment, flow field, suspended sediment, sediment concentration

1 INTRODUCTION

The process of sedimentation is a severe threat to the man-made lakes serving as reservoirs for hydro power production, drinking water supply or flood protection. It is a long term problem with economical consequences calling therefore for a sustainable solution [1]. The simplest concept is to release continuously the sediments out of the reservoir in order to achieve almost the natural conditions before the dam construction. The method may apply for fine sediments only. This can be done even without loosing precious water volume by releasing them through the turbines.

The present study focuses on the fine sediments right in front of the power intake. Evacuating the sediments in this area avoids clogging of the outlet works and guarantees its functionality. Most of the fine sediments reach this area when they are transported by turbidity currents.

A well arranged set of four water jets creates an artificial turbulence, means a rotational and upward flow, lifting the fine sediments to the height of the water intake from where they are evacuated during operating hours. In alpine reservoirs, these jets are fed by water derived from neighboring water catchments. In this way a minimum of external energy is used when evacuating the fine sediments.

2 MODEL SETUP AND INSTRUMENTATION

2.1 Main parameters

In the physical experiments, a jet layout consisting of four equal water jets placed in a circle on a horizontal plane where each jet points in a right angle to the end of the potential core of its neighbouring jet is tested (Figure 2). Since it is assumed that the influence on the flow of such an arrangement is locally limited, the physical model is reduced to the reservoir section in front of the dam. The experimental model is an elongated basin in a prismatic shape, with a total inner basin length of 4 m and an inner width of 1.97 m. The total basin height is 1.50 m. The front wall of the basin is considered to represent the dam, and the two lateral vertical walls confine the reservoir volume (Figure 1). In case of a locally limited circulation in front of the dam, the elongated basin form guarantees with its water body in the upper part a boundary condition as it exists in nature.

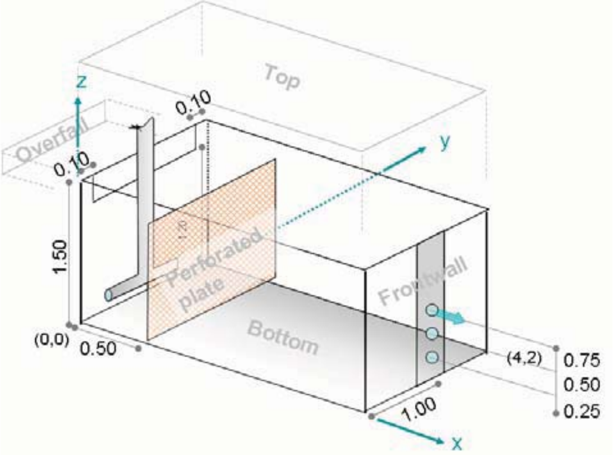

Figure 1: Schematic view of the physical model

The jet nozzle velocities in the experiments are between U_0 = 2.8, 5.6 and 7.5 m/s, while the nozzle diameters d_j are 3, 6 and 8 mm. According to [2], the jet centerline velocity $u_{CL}(s)$ at distance s from nozzle of a turbulent axisymmetric round jet, assuming discharge in s-direction is indirectly proportional to s as follows in Eq. 1:

$$u_{CL}(s) = 6.43 \frac{U_0 d_j}{s} \tag{1}$$

This means that the jet velocity decreases quite rapidly and the range of velocities to be measured in the jet area is rather big.

Figure 2: Picture from the interior of the physical model showing the jets fed from above in the foreground and the front wall with the water intake in the back.

2.2 Sediments

Walnut shell powder has been chosen for the physical experiments as seeding material. This material has been tested in former studies in the research field of sedimentation in shallow reservoirs [3] and has been proofed to be very well adapted to this kind of tests. It suits well for sediment concentration measures as well as tracer for UVP measurements. It is almost cohesionless, light weight (specific density is $\rho_s = 1500$ kg/m^3) and homogeneous. The particle size distribution is relatively narrow and the settling velocity is small (according to Stokes' theory: $w_s \approx 0.8$ mm/s in water at 15°C). The particles have a median diameter of $d_m = d_{60} = 0.06$ mm. Normal initial concentration was 0.3125 kg/m^3.

2.3 Experimental procedure

First, a water-sediment mixture is spread out on the bottom of the basin. Thereafter, the basin is slowly filled (Q_{in} = 1.7 l/s) with water from the back wall, while pressurized air (approx. $6 \cdot 10^5$ Pa) is blown out of the three irrigation pipes lying on the basin bottom thus creating a strong whirling pool. The bubbles have the effect of putting and maintaining the sediments in suspension. Once the basin is filled up to the selected water level (e.g. 1.20 m) the pressurized air is stopped and the experiment starts: The jets get started and the water intake is opened. Turbined water is replaced by clear water entered by the jets, thus maintaining the water depth constant. A normal experiment lasts for four hours, within this period the evacuated sediment amount decreases significantly from a maximum value reached in the first minutes to a small one. After four hours the value remains small and its decrease is insignificant during a long time.

2.4 Measurement technique

The following measurements are taken: suspended sediment concentration (SSC) with SOLITAX sc sensors, and flow velocity measurements by means of ultrasonic velocity profilers (UVP, [4-5]).

The outflowing suspended sediment concentration is measured continuously (one record every 5 seconds), SSC on the horizontal axis of the water intake (at a distance of 0.25, 0.45, 0.65, 0.75, 0.85, 0.95 and 1.00 m from the front wall) and on the rotational (vertical) axis of the jet configuration (on levels 0.10, 0.20, 0.30, 0.40, 0.50, 0.75 and 1.00 m over bottom) are measured sporadically.

Flow velocity measurements are performed in the area of the jet's arrangement and close to the water intake. Therefore, a rack of 5 x 5 2-MHZ-UVP-transducers is fixed at the lower end of a vertical stem (Figure 3). The lateral distance from one sensor to another is 200 mm; the distance between the sensors and the wall is 200 mm. This rack is moved within the front cube from one quadrant to another such that 4 displacements have to be done to get all records on one level, providing a horizontal 2D flow pattern on a plane of 2 x 2 m^2, consisting of a map with totally 100 points each with velocity information in both horizontal directions.

Figure 3: The 5 x 5 UVP-transducers rack fixed on the vertical stem with its remote computer installed on the bridge.

Such horizontal measurements are taken at four different levels: 0.10, 0.30, 0.50 and 0.70 m from the bottom. Vertical measurements are taken on two axes: the longitudinal middle axis corresponding to the water intake axis, and the transversal axis, crossing the rotational axis.

The number of channels was 557, the number of repetitions was 128, the number of cycles was 4 and the number of multiplexer cycles was 8 with 6 profiles per burst.

3 FLOW PATTERN

From the measured flow pattern, it can be observed that water is sucked vertically from the reservoir bottom up and from above down to the level of the jet's plane, from where the water is spread horizontally again. Because of its high 3-dimensionality, the flow pattern is very complex (Figures 4 and 5).

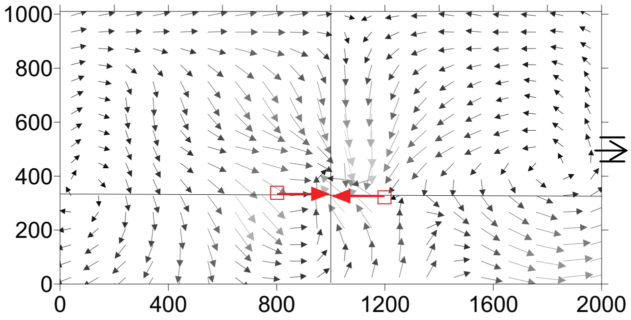

Figure 4: Measured flow pattern in the longitudinal axis, with the water intake at the right edge at the level of h_i = 500 mm. Units in mm. Dark colored arrows: low flow velocities, bright colored arrows: high flow velocities. Total jet discharge equals water intake discharge: 1.125 l/s, constant water depth h = 1.2 m, nozzle diameter d_j = 8 mm, distance between rotational axis and front wall d_{axis} = 1.05 m, jet plane height h_j = 0.35 m, distance between jets l_j = 0.3 m.

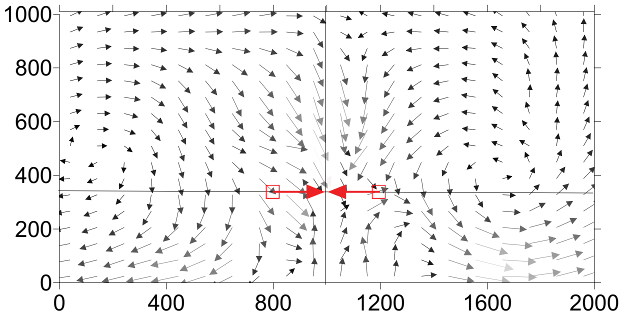

Figure 5: Measured flow pattern in the transversal axis, right through the rotational axis. Units in mm. Dark colored arrows: low flow velocities, bright colored arrows: high flow velocities. The same parameters as in Figure 4 have been adopted.

Numerical steady state simulations performed with the Navier-Stokes-equation based solver ANSYS-CFX confirm these observations (Figures 6 and 7).

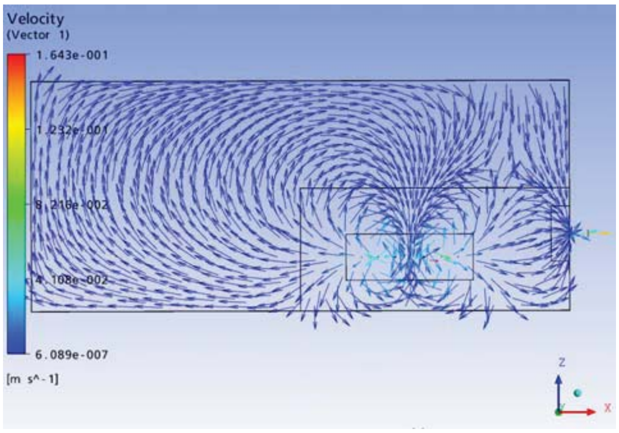

Figure 6: Calculated flow pattern in the longitudinal axis, with the water intake at the right edge (see arrows). Red: high velocities, blue: low velocities.

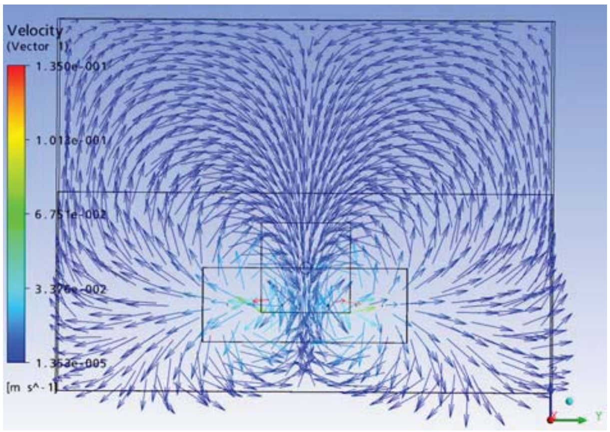

Figure 7: Calculated flow pattern in the transversal axis, right through the rotational axis. Red: high velocities, blue: low velocities.

4 EVACUATED SEDIMENTS

Raw SSC data of six geometrically identical experiments recorded outside of the power intake are displayed in Figure 8. Each experiment was performed with a different jet discharge. They are compared with the SSC measured during the first 4 hours of the experiment where no inflow and no outflow of the basin took place. The latter measurements were recorded on the level z = 0.5 m over the basin bottom.

In case the jets were used, it could be observed that the evacuated sediment ratio ESR, defined in Eq. 2 as the evacuated sediment volume V_{out} compared to the sediment volume initially added to the basin V_{in}, is almost proportional to the sum of the jet nozzle discharges Q times the square root of the current time t in seconds (Eq. 3):

$$ESR = V_{out} / V_{in} \tag{2}$$

$$ESR = 1.0465 \cdot \left(\frac{Q}{h} \cdot \sqrt{\frac{t}{\Pi \cdot V_{\tan k} \cdot v_{ss}}} \right)^{1.04} \tag{3}$$

where h is the water depth, V_{tank} is the basin volume, v_{ss} is the estimated settling velocity of an average walnut shell powder grain (see paragraph 2.2). This equation is valid for h/d_j higher than 400, for t less than four hours and for test conditions. Its validity hasn't been tested yet for prototype scale.

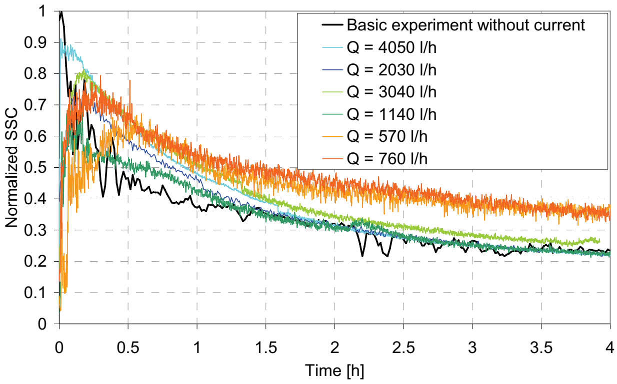

Figure 8. Raw data of outflowing suspended sediment concentration (SSC) measurements and of SSC measured in the basic experiment. Each experiment is done with 4 equivalent jets. Two of the experiments were performed with a jet diameter d_j = 8 mm, two with d_j = 6 mm, and another two with d_j = 3 mm. The jet diameters were combined with three different jet velocities, v_j, leading to 6 different total jet nozzle discharges Q.

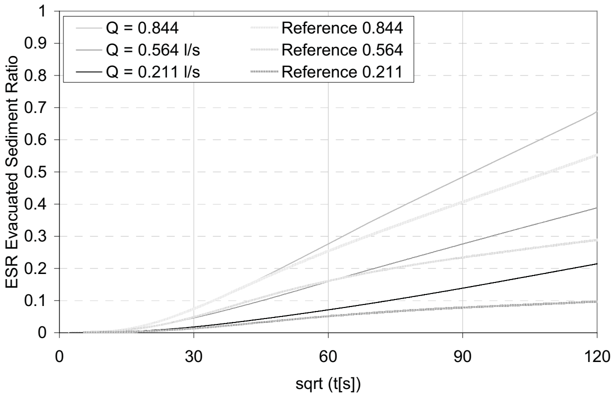

Figure 9: After around 15 minutes (sqrt (t [s]) = 30) the evacuated sediment ratio is proportional to the square root of time in seconds. Higher jet discharges are more effective, the evacuated sediment ratio is higher. The evacuated sediment ratio achieved using jets is after 2 hours approximately as high as after 4 hours without jets.

The experiments varying other parameters like the jet position relative to each other, relative to the basin bottom and relative to the front wall let arise, that the influence of these geometrical parameters is in the range of the error, thus negligible.

In Figure 9 it can be observed that in case no jet is used ESR is smaller than in case jets are employed.

SUMMARY AND CONCLUSION

With an experimental set-up systematic experiments have been performed concerning the continuous evacuation of suspended sediment in reservoirs. In an elongated cuboidal basin, four equivalent jets are arranged in a circular configuration. The described installation is used to investigate the most efficient jet configuration regarding the evacuated sediments quantity. The sediments are simulated with ground walnut shells.

Several combinations of jet diameters and jet velocities are tested, as well as their position relative to each other, relative to the basin bottom and water intake elevation as well as relative to the front wall.

In case jets are used, the experiments show that after two hours the evacuated sediment ratio is approximately as high as after four hours in case no jets are used when releasing the same water discharge through the water intake. In other words, after four hours without jets approximately 80 % of the sediment quantity released with jets is achieved. Thus it seems that this method could be very promising bearing in mind that no extra energy consumption is needed apart from the head and discharge provided by water tunnels. Moreover, the analysis of the experiments conducted with water jets and sediments put in evidence that the evacuated sediment ratio is proportional to the sum of the jet discharges and to the square root of time.

Further studies will compare the results of numerical simulations performed with ANSYS-CFX. The measures obtained with the experiments will be analyzed in detail.

ACKNOWLEDGMENTS

The research project is supported by "swiss*electric research*".

REFERENCES

[1] Jenzer Althaus, J., and De Cesare, G. 2006. Reservoir Sedimentation, Interreg III Alpreserv Project "Sustainable Sediment Management in Alpine Reservoirs considering ecological and economical aspects", Volume 3 / 2006, Publisher Institut für Wasserwesen, Universität der Bundeswehr München, Germany, ISSN 1862-9636

[2] Jirka, G.H. (2004). "Integral model for turbulent buoyant jets in unbounded stratified flows. Part I: single round jet". Environmental Fluid Mechanics, 4: 1-56.

[3] Kantoush, S.A. (2008) Experimental study on the influence of the geometry of shallow reservoirs on flow patterns and sedimentation by suspended sediments. Communication No. 37 of Laboratory of Hydraulic Constructions (LCH), ed. Prof. Dr. A. Schleiss, Lausanne, EPFL, ISBN: 1661-1179

[4] Takeda, Y. (1995) Instantaneous velocity profile measurement by ultrasonic Doppler method. Int. J. Japan. Soc. Mech. Eng., Series B, 35, 8-16.

[5] Met-Flow SA (2002) UVP Monitor – User Guide, Lausanne, Switzerland.

Suspended particles in wastewater : acoustical characterization and modeling

Philippe SCHMITT[1], Anne PALLARES[1], Pierre FRANCOIS[1], Marie-Noëlle PONS[2]

[1]Institut de Mécanique des Fluides et des Solides, Université de Strasbourg,
2, rue Boussingault, 67000 Strasbourg, France

[2]Laboratoire des Sciences du Génie Chimique -CNRS, Nancy Université (ENSIC –INPL)
1, rue Grandville, BP 451, F-54001 Nancy cedex, France

Wastewater regulation and treatment is still a major concern in planetary pollution management. Some pollutants, referred to as particulate matter, consist of very small particles just suspended in the water. Various techniques are used for the suspended particles survey. Few of them are able to provide real-time data. The development of new, real time instruments needs the confrontation with real wastewater. Due to the instability of wastewater, its modeling in terms of suspended solids was performed. Hence, its sedimentation and acoustical behaviour was studied and modelled on an artificial matrix.
Knowing the description of real wastewater, we tried to produce an artificial mixture made of basic ingredients. A good agreement in terms of turbidity and settling velocity was observed between the artificial wastewater matrix and the real one. After a brief outline of the self-developed multi-frequency fluxmeter, this paper will investigate the individual contribution of the different compounds to the acoustical signal. A good comparison of acoustical and turbidity behaviour of wastewater will thus be obtained.

Keywords: acoustic, suspended solids, settling velocity

1 INTRODUCTION

Environmental protection became a major concern in many countries. One of its aspects is wastewater management. As for regulation of industrial processes, sewage supervision needs real time flow control.

Urban wastewaters are a complex medium with variable characteristics. Currently, the suspended particles concentration in wastewater is either measured through sampling either through turbidity. The major drawback of the first method is the time delay between the sampling and the measurement which forbids any real time retroaction on the water regulation. On the other side, turbidity measurements might be biased by a punctual modification of the granulometric repartition of total suspended solids (TSS), by a variation of the particle type or by the presence of a dye, factors which all lead to a change of the turbidity/concentration relationship. The major hindrance for the use of ultrasound concentration measurements in wastewater is the huge variety of encountered materials in various proportions. Within the common particles found in wastewater, only sands have been exhaustively studied by acoustics. Preliminary work on various materials like paper pulp, loess, garden earth, soups and excrements was carried out. It showed that none of these materials has an identical behavior to sand. Anyhow, the analysis of the ultrasonic spectrum in terms of size distribution, based on the known behavior of sand, reflects at least qualitatively the real evolution of particle size. For example, by sifting garden earth (which is a mixture of organic and mineral particles) through larger sieves, the ultrasonic spectrum analysis shows a growth of the mean diameter of particles.

Note that the aim of our work is not the exact decryption of the acoustical behavior of wastewater particles. This would need the production of calibrated particles of natural materials for which even the size notion is often problematic (like for example for fibers at different flocculation levels). On a semi-empirical basis, our aim is to build reliable indicators of the TSS evolution relying on the acoustical spectrum without or as less as possible calibration steps.

2 SUSPENDED SOLIDS CONCENTRATION MEASUREMENTS

2.1 Standard methods

Different techniques were used to measure the suspended solids concentration.

A first technique is the time dependant collection of wastewater samples. After sampling, the water is filtered on a 1 µm filter and the TSS concentration is calculated from the solid depot on the filter after evaporation.

An estimate of total suspended solids can also be obtained by an optical measurement known as turbidity. The correlation between the turbidity and the TSS concentration will hold only for the particular wastewater from which it was derived. A

HACH turbidimeter was used for the nephelometric turbidity measurements of wastewater and artificial matrix.

2.2 Acoustic investigation

The acoustic characterization was done with a self-developed multi-frequency fluxmeter [1]. This instrument allows the measurement of the concentration of several size classes of suspended particles (see figure 1).

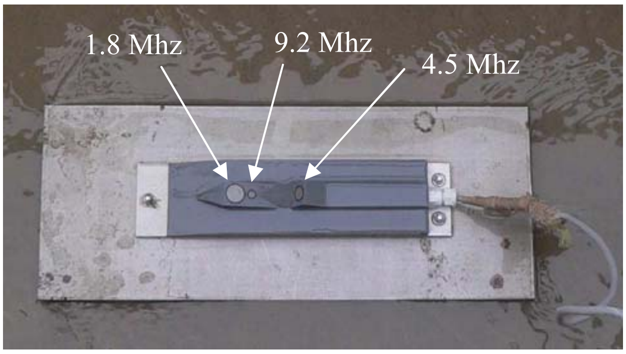

Figure 1: Our multi-frequency fluxmeter.

The acoustic signal can be expressed in terms of :

$$T_j(r) = \beta_{p,j}(r)\exp\left[-4\int_0^r \alpha_{p,j}(r)dr\right] \quad (1)$$

T_j stands for the acoustic backscattered signal at frequency j. The acoustic backscattering and attenuation coefficients for each particle type p are respectively $\beta_{p,j}$ and $\alpha_{p,i}$ both depending on frequency. We assume that the particle distribution, independently of their size, is uniform along the beam. Thus, there's no distance dependency of the backscattering and attenuation coefficients. However, the attenuation coefficient is usually a small value. Hence, its estimation error might be huge in regard to its mean value. Thus, only the acoustic spectra obtained for frequencies above 6 MHz give significant attenuation information. In its current configuration, our instrument gives only a single exploitable profile for attenuation at 11.7 MHz.

Another assumption is an identical size distribution of all particles whatever the value of their density is. On the basis of the semi-empirical formulae describing the behaviour of sand, the backscattering coefficient becomes :

$$\beta_{p,j} = \frac{C_m}{\rho_{mean}}\sum_{i=1}^{n} F_{j,i}\gamma_i \quad (2)$$

where C_m stands for the total massic concentration in kg/m^3. The mean density of all particles is ρ_{mean} and γ_i stands for the fraction of the ith size class. The mean value $F_{j,i,}$ of the ratio of the form function by the particle radius over 5 diameter classes (12, 30, 70, 170 et 400 µm) is given by the following expression where a_s is the particle radius :

$$F_{j,i} = \left\langle \frac{f_{j,\infty}^2}{a_s} \right\rangle_i \quad (3)$$

The form function itself is calculated from [2,3,4] :

$$f_{\infty,j} = C_0\left(\frac{1.1x^2}{1+1.1x^2}\right) \text{ with } x = k_j a_s = \frac{2\pi}{\lambda_j}a_s$$

$$C_0 = 1.1\left[1-0.25e^{\left(-((x-1.4)/0.5)^2\right)}\right]\left[1+0.37e^{\left(-((x-2.8)/2.2)^2\right)}\right] \quad (4)$$

From there, the granulometric distributions and the massic concentrations of suspended particles are estimated. A second step in the data analysis is the use of the attenuation data. The attenuation coefficient can be written :

$$\alpha_{p,j} = \frac{C_m}{\rho_{mean}}\sum_{i=1}^{n} A_{j,i}\gamma_i \quad (5)$$

The mean massic attenuation factor can be expressed in a similar way as previously:

$$A_{j,i} = \left\langle \frac{3\chi_j}{4a_s} \right\rangle_i \quad (6)$$

As for backscattering, a common model exists for the normalized total scattering section χ_j. Under the same assumption as previously that wastewater suspended solids behave as sand, its value might be obtained through the modified high-pass model [2,3,5] for attenuation under its usual form :

$$\chi_j = \frac{1.1(4/3)0.18x^4}{1+1.3x^2+(4/3)0.18x^4} \quad (7)$$

On this basis, the attenuation is recalculated and compared to the one obtained by analysis of experimental data through the T_j equation (1).

3 WASTEWATER CHARACTERISTICS

Wastewaters are usually the combination of industrial and urban effluents. Their composition is variable, function of the time of the day (reflects human habits and weather conditions), of their localisation (urbanised, commercial or industrial zone). Wasterwaters were studied on two sites : the wastewater treatment plant of Greater Nancy (1) and in the sewer of the city of Nantes (2).

For the site (1), the average turbidity value is 150 NTU and the usual acoustic coefficients are 0.08 for backscattering and 0.8 for attenuation. These values are comparable to the one observed on site (2).

3.1 Sampling study

It is well known that the amount of suspended solids varies with time and localisation. However, as shown by figure 2, the mean suspended solids concentration value is 150 mg/l. The associated granulometry is known to be mostly > 150 µm.

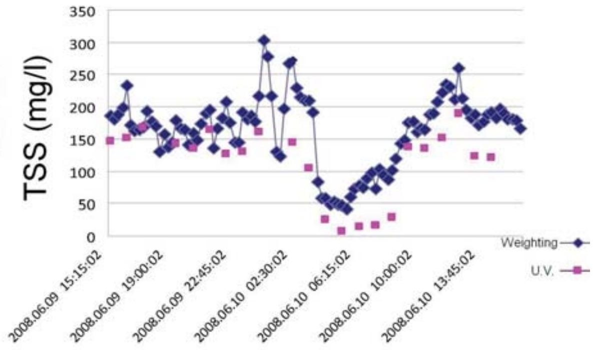

Figure 2: Total suspended solids concentration evolution as a function of time on site (1).

We tried to build our artificial wastewater matrix according to these mean concentration and size distribution.

3.2 Turbidity and acoustical behaviour study

As above for sampling, as can be seen on figure 3, the turbidity and the acoustical behaviour of wastewater are a function of time, reflecting human activities and weather conditions. On this other measurement site (2), turbidity and acoustic measurements were compared to the TSS concentration measured by sampling and show that there is a direct link between the measured data and the total suspended solids concentration. The mean value of TSS is 220 mg/l on this second site.

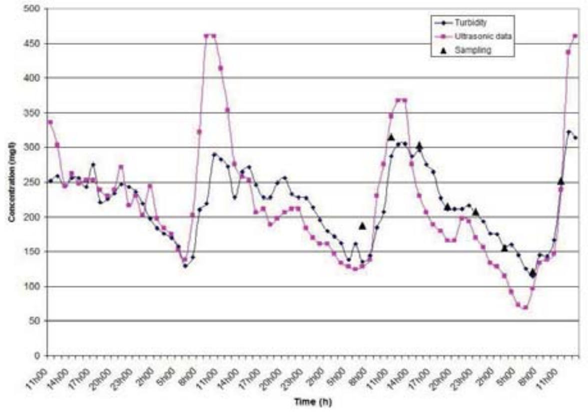

Figure 3: Total suspended solids concentration as a function of time and of measurement technique on site (2).

4 ARTIFICIAL WASTEWATER MIXTURE

Knowing the description of real wastewater, we tried to produce an artificial mixture made of simple ingredients like various kind of starches (corn, wheat, rice, potatoe) and toilet paper. To reflect the trouble aspect of wastewater due to the organic matter, an alcohol-free pastis was also added to the mixture. The granulometry of the various compounds was measured by microscope and is mentioned in table 2.

4.1 Turbidity

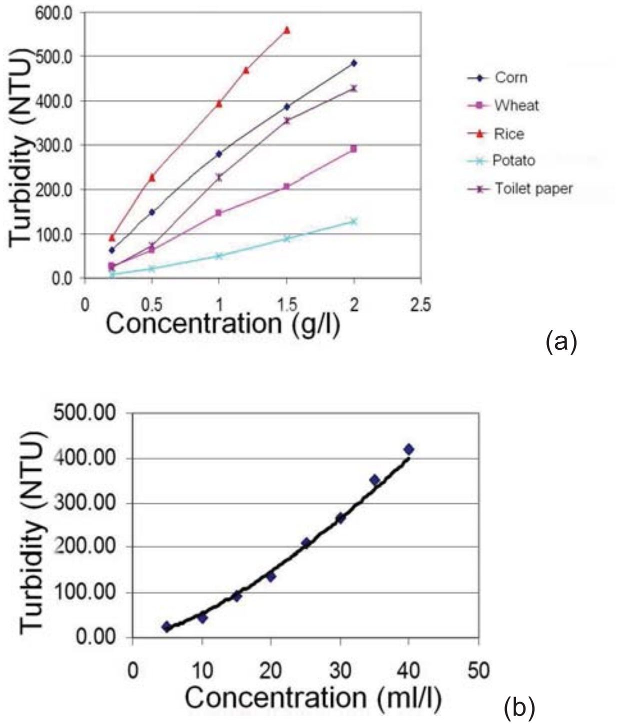

(a)

(b)

Figure 4: Turbidity evolution as a function of concentration and compound, (a) Various starches, (b) Pastis.

As can be seen on figure 4, turbidity is a roughly linear function of the ingredient concentration for all the starches and the toilet paper and is a power function of the pastis concentration.

Table 1 summarizes the turbidity behavior of the various ingredients :

Compounds	Turbidity (NTU)
Potato starch	60 * concentration (g/l)
Wheat starch	140 * concentration (g/l)
Toilet paper	220 * concentration (g/l)
Corn starch	250 * concentration (g/l)
Rice starch	340 * concentration (g/l)
Pastis	1.90 * concentration (g/l)
Wastewater	50 to 300 NTU

4.2 Settling velocity

The knowledge of the wastewater settling velocity is of major concern for the clarifiers in wastewater treatment plants [6]. The settling velocity is an indirect reflection of the TSS composition and concentration. The standardized VICAS protocol [7] was used on our samples.

Keeping in mind the mean turbidity value, several mixtures were created in order to reproduce the sedimentation velocity of real wastewater. Figure 5 shows the individual sedimentation velocities and the sedimentation velocity of two mixtures compared to the one of natural wastewater.

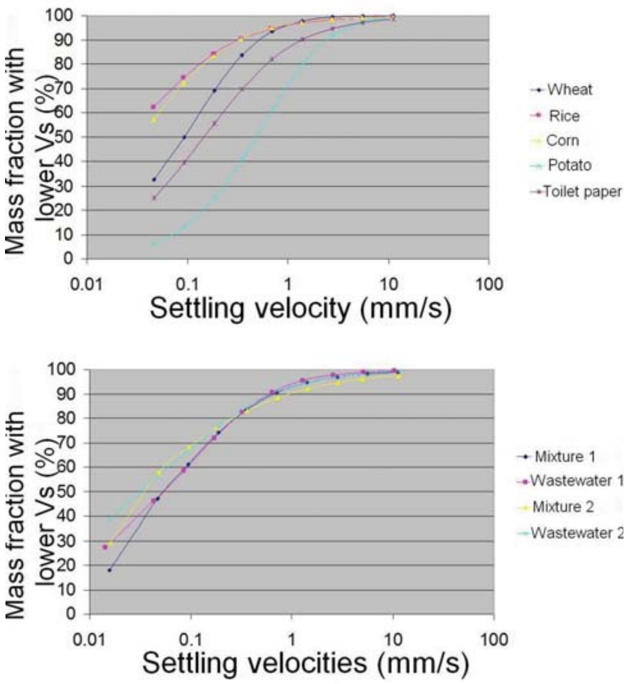

Figure 5: Settling velocities distributions, (a) Individual starches, (b) Natural and artificial wastewater.

A good agreement in terms of turbidity and settling velocity can be seen between the artificial wastewater matrix and the natural one.

4.3 Acoustical behavior

The acoustical behavior as yet only been evaluated on natural wastewater and the individual mixture components. Table 2 summarizes the results on granulometry and acoustic coefficients.

Data was obtained by multi-frequency measurements on various concentrations of each compound.

Table 2: Summary of optical and acoustical measurements

	Diameter by microscope (μm)	Diameter by US (μm)	Supposed density	β_p	α_p
Wastewaters	20 – 500	90	1.03	0.08	0.80
Potato starch	36 – 126	37	1.20	0.27	0.95
Wheat starch	18 – 72	22	1.20	0.12	0.81
Corn starch	14 – 36	16	1.20	0.11	1.14
Rice starch	6 – 18	16	1.20	0.08	1.08
Sand		145	2.60	0.28	0.32
Toilet paper		39	1.03	0.08	1.90
Alumina		19	2.4	3.38	6.26

The acoustic coefficients are expressed as mass response rate which allows the comparison of the different compounds. The mass response rate is the ratio of the diffused or attenuated intensity for a given particle type by the diffused or attenuated intensity for spherical particles of same size, of density 1 and having a form function identical to the one of sand. The corn, wheat and rice starch have acoustic coefficients close to the one of real wastewater. However, only a small fraction of wastewater suspended solids are as small. As already determined by other measurements, they might remain quite unseen by ultrasound. The toilet paper has an acoustic backscattering coefficient close to the one of wastewater but a much larger attenuation coefficient.

The coefficient of the sand are expected however the backscattering value is smaller as announced by theory. Alumina is quite “exotic” on the ultrasonic point of view, with huge backscattering and attenuation coefficients.

5 CONCLUSIONS

The size estimation given by the fluxmeter is comparable to the size distributions measured by microscope for each mixture. Thus, the average diameter extrapolating method from acoustic data gives encouraging results. However, the basic compounds with a combination of ultrasonic "reflection coefficient / attenuation coefficient" close to that of wastewater have an average diameter much smaller than the one of wastewater : a simple mixture of those compounds won’t describe the behavior of the wastewater.

Future work will be to analyze the acoustic response of mixtures mainly made of toilet paper (fibrous form) and potato starch (interesting diameter). These solutions should give an acoustic response close to wastewater and thus provide a stable and reproducible wastewater model for various laboratory experiments.

REFERENCES

[1] Abda et al.: (2009) Ultrasonic device for real time sewage velocity and suspended particles concentration measurements, Water Science and Technology 60-1 p117.

[2] Sheng J., Hay A.E., (1988) An examination of the spherical scatterer approximation in aqueous suspension of sand, J. Acoust. Soc. Am., 83, 598.

[3] Crawford A.M., Hay A. E., (1993) Determining suspended sand size and concentration from multifrequency acoustic backscatter, J. Acoust. Soc. Am., 94, 3312.

[4] Thorne P.D., et al.(1993) Measurements of the form function and total scattering cross section for a suspension of spheres, J. Acoust. Soc. Am.,93, 243.

[5] Richards S.D. et al., (1996) The effect of suspended particulate matter on sound attenuation in seawater, J. Acoust. Soc. Am., 100, 1447.

[6] De Clercq B. et al.(2002) On-line dynamic fluid velocity profiling in secondary clarifiers. Proceedings of AutMoNet2002, 281-288.

[7] Chebbo G. et al.(2003) Protocole Vicas : mesure de la vitesse de chute des MES dans les effluents urbains, 12, 39-49.

River intake and desander efficiency testing on a physical model using UVP and LSPIV

Giovanni De Cesare, Juliano M. Ribeiro[1], Sameh A. Kantoush[2], Matteo P.E.A. Federspiel
Laboratoire de Constructions Hydrauliques (LCH), Ecole Polytechnique Fédérale de Lausanne (EPFL), Station 18, CH-1015 Lausanne, Switzerland, e-mail: giovanni.decesare@epfl.ch
[1]formerly at the EPFL-LCH, now at STUCKY Ltd, P.O. Box, CH-1020 Renens, Switzerland
[2]Water Resources Research Center, Disaster Prevention Research Institute, Kyoto University, Gokasho, Uji, Kyoto 611-0011, Japan

Hydraulic model tests were carried out in order to establish the feasibility of the Teesta VI hydropower plant in Sikkim State, Northern India. An initial arrangement of barrage and river intake with four desander basins on the right bank of the Teesta River, tributary to the Brahmaputra, has been proposed. During high Monsoon floods, river bed load and suspended sediments shall be diverted through the spillway openings. During normal operation, the four desander basins of 250 m lenght with free flow conditions must be able to evacuate suspended sediments avoiding their entrainment into the power intakes. In order to study flow conditions and evaluate the river intake and desander design, LSPIV and UVP measurements were performed at several locations within the basins and the intake zone. The measurements were conducted for two different river intake designs. UVP allowed to measure mean flow velocity and evaluate the retention efficiency of the basins. Overall flow field comparisons for different scenarios over the entire model surface are reported by LSPIV technique.. The mean flow velocity is the main parameter to design a desander and it is directly related to the sediment grain size diameter to be removed. To improve the desander efficiency, flow disturbances as reverse flows, circulation cells and eddies must be avoided. Therefore the flow velocity must be well distributed all over the cross section and the flow velocity standard deviation must be minimized.

Keywords: Hydraulic model tests, run-of-river power plant, river intake, desander, UVP, LSPIV

1 INTRODUCTION

The 500 MW Teesta VI hydropower project, located on the Teesta River in southern Sikkim, India, is a run-of-river scheme. It is the last stage of the Teesta Cascade development within the state of Sikkim. Hydraulic model test have been carried out at the Laboratory of Hydraulic Constructions (LCH) of the Ecole Polytechnique Fédérale de Lausanne (EPFL). The model includes a part of the upstream river section, the barrage with the four spillway passages, the river intakes and the four desander basins, two power intakes, and a part of the downstream river (Figure 1).

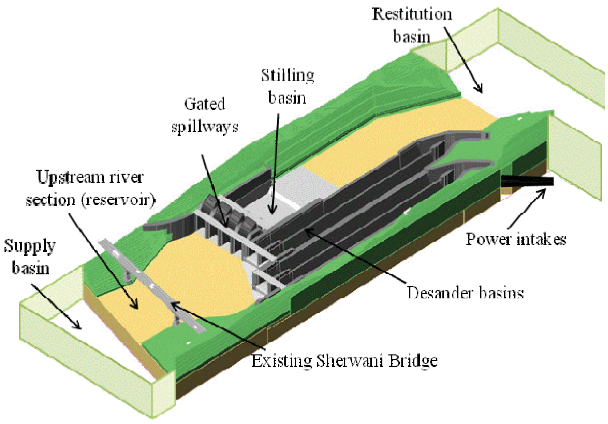

Figure 1: Boundaries and components of the physical model in its original river intake configuration.

The main purpose of the hydraulic model tests was to assess the viability of the arrangement of barrage, desanders and power intake. During high Monsoon floods, river bed-load and suspended sediment shall be diverted through the spillway openings placed at riverbed level. The mentioned head works consist of the following structures:

- dam with gated spillway (concrete structures);
- upstream river intakes on the right bank with four subsequent sediment settling basins (desanders)
- and power intake arrangement after the desanders with 2 head race tunnels.

In order to reduce the erosion wear at the guide vanes and runners of the turbines, desanding basins have to be provided. They were designed and dimensioned on the principal of a reduction of the water velocity that helps sediment particles to settle down. In this paper, special attention is given on the river intake design (orientation, form, etc.) and the desander basin size. The flow conditions have been assessed using Large-Scale Particle Image Velocimetry (LSPIV) and Ultrasonic Doppler Velocity Profiler (UVP) measurements. These techniques have been successfully applied in previous research studies by Kantoush et al. (2007) [1], Kantoush and Schleiss (2009) [2] and in general hydraulic modeling by De Cesare and Boillat (2008) [3] and Bieri et al. (2009) [4].

2 MODEL SETUP AND INSTRUMENTATION

2.1 Scale and main parameters

With respect to the objectives of the study, the size of the model and considering the similarity rules and possible scale effects, the comprehensive model has been constructed with a scale factor 1:75. It was operated with respect to Froude similarity, i.e. conserving the inertial and gravity forces ratio. The overall model covered a surface of 2.80 x 10.30 m^2. The maximum discharge for the Standard Project Flood (SPF) is 11’600 m^3/s at prototype scale. The design discharge for the hydropowerplant (HPP) is 531 m^3/s separated into four desander basins, two power intakes and headrace tunnels.

2.2 Instrumentation

Several parameters were measured during experimental tests, namely: 2D surface velocities, velocity profile in water column, water levels and discharge. The physical characteristics which were measured on the model and the corresponding instrumentation are summarised in Table 1.

Table 1: Main measuring devices and accuracy

Parameter	Instrumentation	Accuracy
Water level	Manual limnimeter	0.5 mm
Velocity profile	Ultrasound Velocity Profiler (UVP)	1 mm/s
Surface velocity field	Large Scale Particle Image Velocimetry (LSPIV)	1 mm/s
Pressure	Dynamic pressure transducers/piezometers	0.1 mm, 128 Hz sampling freq.
Discharge	Electromagnetic flowmeter	1% of max. capacity

The surface velocity field of the approach flow to the gated spillways and to the desanding basins were assessed using LSPIV technique. A Met-Flow SA UVP with a single 2 MHZ transducer has been used for the measurement of vertical velocity profiles at the intake axis as well as inside the desander basins at an angle of 30°. The number of channels was 220 inside the desander, 1024 profiles were taken to get average velocity and standard deviation per channel, the sampling time per profile was 64 ms.

3 RIVER INTAKE AND DESANDER DESIGN

The river intake is the most upstream element for run-of-river hydropower production. Its objective is for the powerhouse design discharge, regardless of river discharge, to ensure uniform water derivation over the width and water depth, to keep the entrance free from bed load and floating debris, and to present a homogeneous flow velocity at the trash rack section. Large eddies in the river approach zone should be prevented from entering the desanders, swirling flow at piers and upstream dead zone should not occur during normal flow conditions. The flow inside the desander should be as homogeneous as possible to allow an efficient sediment settling process. For general design criteria and example details for desilting chambers see Ortmanns and Minor 2007 [5].

The following tests have been performed on the physical model:

- Verification of approach flow conditions, occurrence of flow separation and vortex formation inside and upstream of the river intake;
- Study of the approach flow in front of the desander basins, considering the possibility of reverse currents and eddy formation;
- Investigation of the velocity distribution and approach flow conditions at each water intake opening and discharge distribution between the four openings;
- Verification of the flow and eddy formation inside the desanders.

The discharge has been fixed at half the powerhouse design discharge (531 m^3/s) per power intake and pair of desanders.

The overall flow behavior can be determined using LSPIV. The CMOS camera has been fixed some 3 m vertically above the model. Seeding was obtained by means of white plastic particles, with an average diameter of 3.4 mm and specific weight of 960 kg/m^3.

Figure 2 shows the surface velocity field for the upstream river section, water intake and desander basins for regular operation (design discharge and normal water level).

The angle between main approach flow and intake axis is at the origin of a non uniform discharge distribution. Desander 1 and 2 take more discharge, desander 3 functions below its design discharge. Any non uniform velocity, respectively discharge distribution lowers the efficiency of the entire desanding system.

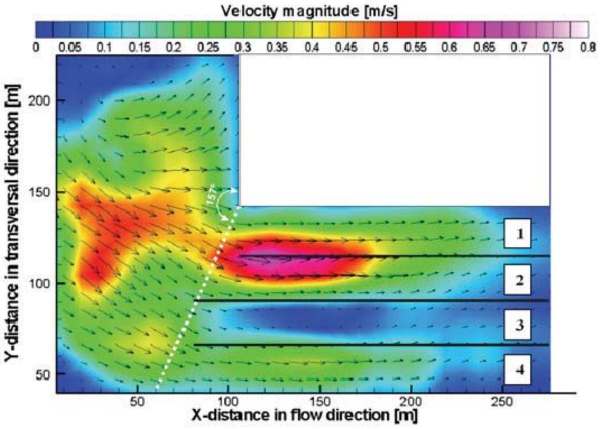

Figure 2: Average flow pattern with surface velocity vectors by LSPIV for the initial intake design ($Q = 531\ m^3/s$, water level 360 m a.s.l.). Note that desander 3 has very low velocities inside.

Vertical velocity profiles were taken at the intake axis and inside the desander chambers (Figure 6). Hydrogen bubble seeding was used to obtain good US echo. This technique has been proven to be very efficient in physical scale modeling by Meile et al. 2007 [6]. The seeding installation can be seen in Figure 4 placed at the intake to desander 3.

Three profiles were measured at the intake section in order to determine by surface integration the discharge passing through. Table 2 summarizes the discharge distribution. One can clearly see that especially desander 3 has a very low discharge compared to desander 4, which has therefore a reduced sediment settling efficiency. The discharge distribution is 43/57%, ideally it should be 50/50%.

The velocity profiles taken inside the 26 m deep desanding chambers show not only a non uniform distribution over the water column (and basin width), but also a rather high turbulence (see Figure 6, left below), which again leads to inefficient particle settling.

The main reasons for the malfunctioning are the orientation of the intake axis, creating a local detachment of the water flow and the four large entry sections. The original design with its large entry sections allowed eddies of the size of the intake width and smaller turbulent structure entering easily the desander basins thus reducing considerably their sediment trap efficiency.

4 MODIFIED RIVER INTAKE

The presence of a vortex at the entrance of the desanders, the disparity in discharge distribution between desanders, the turbulent flow inside the desander basins and the need of a larger width to install a trash rack led to a modification in the design of the water intake.

Based on the results of the previous chapter, the design engineers together with the research engineers of the EPFL-LCH proposed a modified river intake design.

The entrance section was oriented towards the main flow direction, it was enlarged and divided into three passages and then narrowed into the entrance of the desanders as shown in Figure 3 and 4.

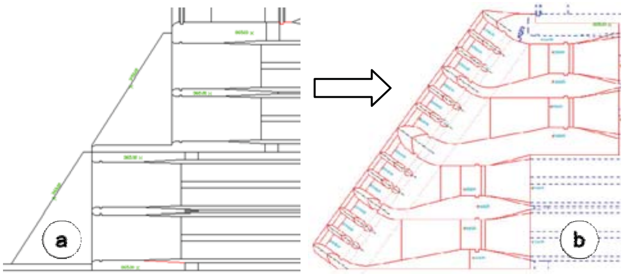

Figure 3: From initial (a) to the optimized (b) river intake design and transition to the desander basins.

The narrow passage prevents large eddies to enter the desander. The local contraction in width and depth (there is a small sill) between intake and desander with its streamline convergence prevents even small transversal flow turbulences from entering the desander.

Figure 4: New intake set-up for desanders with UVP and hydrogen bubble seeding installation for velocity measurements.

Figure 5 shows the surface velocity field for the upstream river section, new water intake and desander basins for regular operation obtained by LSPIV. The approach flow is well oriented and the velocity distribution at the entrance section of the desander chambers is improved compared to the previous design.

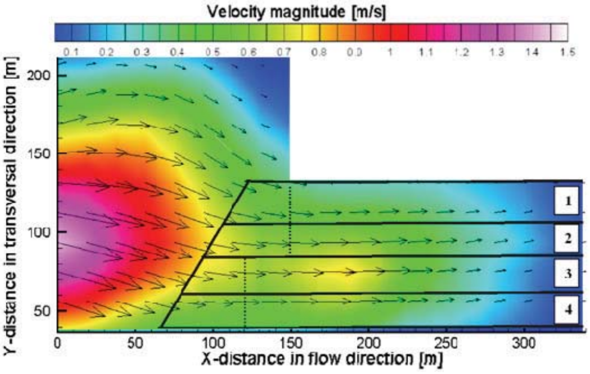

Figure 5: Average flow pattern with surface velocity vectors by LSPIV for the modified intake design (Q = 531 m^3/s, water level 360 m a.s.l.).

Figure 6b) and d) show a uniform velocity distribution both at the intake section and inside the desander chamber. Due to the reduced width of the intake section because of the two intermediate piers, the average velocity is higher, but a very homogeneous velocity distribution over the width and depth of the intake section results.

The velocity fluctuations inside the desander chamber are significantly reduced; see Figure 6c) and d) while the average velocity is increased due to the higher discharge.

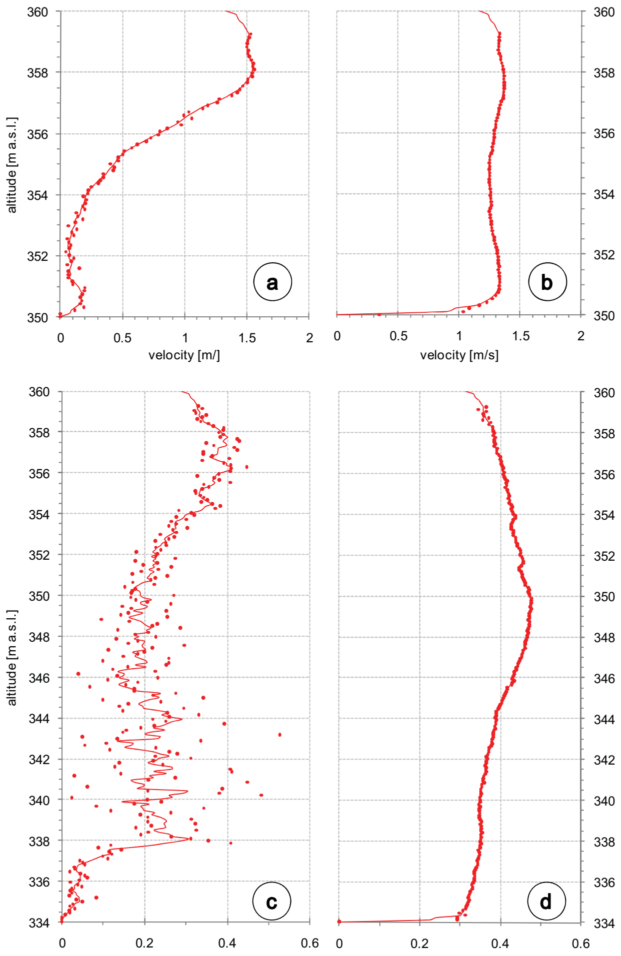

Figure 6: Velocity profiles at the rive intake N° 3 axis (a and b) and in the middle of the corresponding desander basin (c and d) for the original (a and c) and optimized (b and d) intake design (Q = 531 m^3/s, water level 360 m a.s.l.).

Again three profiles were measured at the intake section in order to determine the discharge by integration. Table 2 summarizes the discharge distribution for both old and new design.

Table 2: Discharge distribution between the 4 intake bays to the desander basins for the initial and optimized intake design. The discharge has been fixed per power intake, desander pair 1 and 2, resp. 3 and 4 together to half of the powerhouse design discharge of 531 m^3/s.

Basins	Initial intake design		Optimized design	
	m^3/s	%	m^3/s	%
1	121.8	45.9	129.8	49
2	143.7	54.1	135.7	51
1+2	265.5		265.5	
3	114.5	43.1	132.0	50
4	151.0	56.9	133.5	50
3+4	265.5		265.5	
Total	531.0		531.0	

Compared to the initial geometry, the discharge distribution with some 49/51% is nearly perfect for the desander pair 1 and 2 and 50/50% for 3 and 4. This is a remarkable result for an uncontrolled intake structure.

6 SUMMARY AND CONLCUSIONS

The headworks are a crucial component of any run-of-river hydropower project. These structures have to allow extracting the powerhouse design discharge properly minimizing problems cause by sediments in intake, settling basin and the flushing structures. Therefore special attention is required on layout and design of headworks.

Thanks to LSPIV and UVP measurements, the physical tests allowed putting in evidence the limits of the initial design and proposing a new river intake design which avoids uneven discharge distribution among desander chambers. Furthermore, this new design improves the flow conditions inside the chambers permitting a better functioning of the entire system.

In conclusion, the limitations of the initial design were identified during the physical model tests. Modifications were duly addressed which resulted in an improvement of the final design of the Teesta VI headworks.

REFERENCES

[1] Kantoush, S.A., De Cesare, G., Boillat, J.L., Schleiss, A.J.: Flow field investigation in a rectangular shallow reservoir using UVP, LSPIV and numerical modeling, Flow Meas. Instrum., 19/3-4 (2008), 139-144

[2] Kantoush, S.A., Schleiss, A.J.: Large-Scale PIV surface flow measurements in shallow basins with different geometries, Journal of Visualisation, 12/4 (2009), 361-373

[3] De Cesare G, Boillat J.-L: Flow velocity measurements using ultrasound Doppler method – 10 years experience in hydraulic modeling, Proc. of 5th ISUD international symposium on ultrasonic Doppler methods for fluid mechanics and fluid engineering, Zurich, Switzerland (2006), 113-116

[4] Bieri, M., Jenzer Althaus, J, Kantoush, S. A., Boillat, J.-L.: Large scale particle image velocimetry applications for complex free surface flows in river and dam engineering, Proc. of 33rd IAHR Congress, Vancouver, Canada (2009), 604-611

[5] Ortmanns C., Minor H.-E.: Flow and turbulence conditions on the design of desilting chambers, Dam Engineering 17/4 (2007), 257-269

[6] Meile, T., De Cesare, G., Blanckaert, K., Schleiss, A.: Improvement of Acoustic Doppler Velocimetry in steady and unsteady turbulent open-channel flows by means of seeding with hydrogen bubbles, Flow Meas. Instrum., 19/3-4(2008), 215-221

Flow in complex geometries

Flow field and sediment deposition in a rectangular shallow reservoir with non symmetric inlet and outlet configuration

Erica Camnasio*, Giovanni De Cesare and Sameh Kantoush**
Laboratory of Hydraulic Constructions, Ecole Polytechnique Fédérale de Lausanne, EPFL/ENAC/LCH, Station 18, 1015 Lausanne, Switzerland

* D.I.I.A.R. Department of Hydraulic, Environmental, Infrastructures and Surveying Engineering, Politecnico di Milano, Piazza Leonardo da Vinci 32, 20133 Milano, Italy
** Water Resources Research Center, Disaster Prevention Research Institute, Kyoto University, Gokasho, Uji, Kyoto 611-0011, Japan

UVP measurements were performed at the Laboratory of Hydraulic Constructions at EPFL in order to study the velocity flow fields developing in a rectangular shallow reservoir of adjustable length L and width B (B_{max} = 4 m, L_{max} = 6 m, inlet and outlet channel width b = 0.25 m). In fact, reservoir geometry influences the large turbulent flow structures developing in it. In particular, the results of UVP measurements in reservoirs having different locations of the inlet and outlet channel are presented. Because of the small water depth, compared to the horizontal dimensions of the reservoir, the velocity flow field can be considered in a first approximation two-dimensional; so, velocity measurements were carried out by a 2D horizontal movable square grid formed by 8 ultrasound transducers, which allowed measuring the two components of the horizontal velocity in 16 points simultaneously.

Keywords: UVP measurements, shallow reservoirs, velocity flow field, suspended sediments.

1 INTRODUCTION

The process of reservoir filling up with sediments is a serious problem questioning the sustainable use of reservoirs and which has to be considered in the optimization of sediments management. It is essential to understand which kind of flow fields can develop in a reservoir depending on its geometry that is to say on its dimensions, shape, and also on the inlet and outlet locations. In fact, flow patterns and water velocity strongly influence the sediments transport, deposition and erosion processes.

The laboratory experiments carried out focused on the schematic reference case of a rectangular shallow reservoir, endowed with free-surface rectangular inlet and outlet channels.

The present work is an extension of the experiments carried out by Kantoush [4], who started to analyze the influence of reservoir geometry on flow patterns and sediments deposition. A recently carried out study of the influence of inlet and outlet channel position on hydraulic and sedimentation is presented in this paper.

The flow field developing in the reservoir is mainly 2D, so the two components of the horizontal velocity were measured by UVP transducers (Metflow, [2]) forming a movable square grid, giving a good representation of the main large-scale eddies existing in the reservoir.

Since suspended sediments may represent for some reservoirs a big amount of the total solid load in certain flood conditions, leading to considerable deposits, tests with a constant concentration of sediments supplying were performed. Afterwards, the thickness of the resulting deposits on reservoir bottom was measured.

2 LABORATORY SET- UP

The experimental facility of the Laboratory of Hydraulic Constructions at EPFL is a rectangular shallow reservoir with a smooth horizontal bottom (Kantoush, [1]). The maximum depth is 30 cm and maximum horizontal dimensions are 6 m x 4 m. Movable PVC walls allow changing the length L and the width B of the reservoir, in the way to test different L/B ratios.

A free-surface inlet channel of fixed width b = 0.25 m and an equal outlet channel can be moved along the B side of the reservoir, giving raise to 4 configurations having different locations of the inlet and outlet channel. For the performed experiments, reservoir dimensions were fixed at L = 4.5 m and B = 4 m.

The hydraulic conditions of the tests were a discharge Q = 7 l/s and a reservoir water depth h = 0.2 m. This means that the Froude and Reynolds numbers at the inlet channel were Fr_{in}= 0.1 and Re_{in} = 28'000. The circulating discharge was monitored by an electromagnetic flow meter, and the water level was regulated by a flap gate placed at the end of the outlet channel.

3 UVP MEASUREMENTS

A horizontal movable square grid (overall dimensions: 1 m x 1 m) formed by 8 UVP transducers (2 MHz) allows to measure the two horizontal velocity components in 16 points, placed at the intersections between the velocity profiles recorded by each transducer (Figure 2). The distance between each point of measurement is about 24 cm.

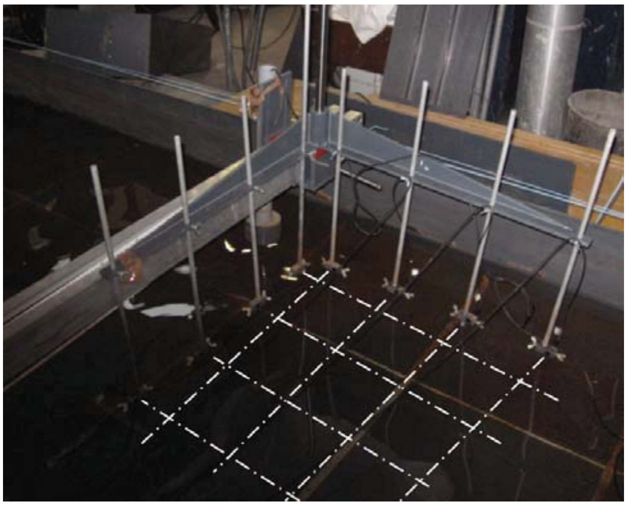

Figure 2: Photos of the movable square grid formed by the 8 UVP transducers. The directions of the measured horizontal velocity profiles are represented by dashed lines.

Since the water depth is much smaller than reservoir horizontal dimensions, the vertical velocity component can be neglected, as typical for shallow free surface flows. UVP measurements of the vertical velocity component were carried out as well, to confirm the assumption of a negligible vertical velocity with respect to the horizontal components.

The transducers were placed at a distance of 8 cm from the bottom that is at 40% of the water depth. In fact, velocities at different height from the bottom were measured in different reservoir positions. It was found that placing the transducer at about one half of the water depth lead to a good approximation of the average horizontal velocity components. The grid was moved by steps, in order to cover the whole reservoir surface. Sixteen positions of the grid were necessary to cover the whole reservoir surface. Therefore, the resulting flow field was not instantaneous. Nevertheless, the flow steady state guarantees steadiness of velocity acquisitions. Acquisition time and the number of recorded profiles were optimised to depict the average flow field developing in the reservoir.

Every transducer can measure velocities up to a distance of 723 mm in the way that maximum recordable velocities are up to 0.189 m/s, which is more than the maximum expected velocity. The relationship linking the maximum distance of measurement $P_{\max}$ to the recordable velocity range V_{range} is:

$$V_{range} = \frac{c^2}{4 \cdot f_0 \cdot P_{\max}} \quad (1)$$

where f_o = ultrasound basic frequency (2 MHz for the adopted transducers) and c = sound velocity (1480 m/s in water).

Equation (1) calculates the amplitude of the velocity measurement window that is 0.3787 m/s. In the present case, since velocities can be both negative and positive, the velocity recordable range is -0.18 ÷ +0.18 m/s.

The measurement window is formed by 232 channels; it means that every profile recorded by the transducer is formed by 232 points of measurement.

The minimum sampling time of 39 msec is assumed for the measurement of every profile. Ten profiles are taken for each transducer, then a pause of 100 msec occours, and the registration of the other 10 profiles of the successive transducer starts.

Table 1: Characteristic parameters used for UVP acquisition.

Maximum measurable depth	723 mm
Velocity range of measurement	-0.189 m/s ÷ + 0.187 m/s
Number of samples: profiles acquired for every transducer during one cycle	10
Number of transducers	8
Number of cycles	20
Minimum sampling time	39 ms
Delay between transducers	100 ms
Delay between cycles	100 ms
SIGNAL	
Transmitting frequency	2 MHz
Number of cycles per pulse	4
Number of repetitions	32
Channel width (spatial resolution)	1.48
MEASUREMENT WINDOW	
Start - End	33 - 721 mm
Number of channels forming every profile	232
Channel distance	2.96

So, every cycle is formed by 10 profiles times 8 transducers resulting in 80 velocity profiles. After the first cycle, a 100 msec delay occours, and another cycle of all the transducer starts: on the whole, 20 cycles are taken.

An average map for every cycle is produced, showing the velocity vectors in the 16 points of intersection of the profiles recorded by the transducers. Then, a final average map is obtained, averaging the 20 maps produced for every cycle. The whole measure lasts about 2 min. Afterwards the grid can be moved to the following position. In the end, placing the vector maps in the reference coordinate system of the reservoir, it is possible to compose all the registered average maps, in the way to depict the whole reservoir flow field.

4 TESTS WITH SEDIMENTS

After carrying out measurements of the velocity flow field developing in clear water conditions (during which only a small amount of suspended particles was added to water, in the way to provide a sufficient echo for UVP measurement) for the different reservoir configurations, a sediment supply was added to the inflowing discharge by a mixing tank. Sediments were fed from a sediment tank into the mixing tank, where they were mixed uniformly with water by a rotating propeller. The resulting mean inflowing concentration was about 2 g/l that corresponds to a solid discharge of 50 kg/h. The sediment supply lasted for 4 hours, for a total sediment inflow of 200 kg. The experiment was stopped after the first 2 hours, to measure the intermediate thickness of sediments deposited on reservoir bottom by a laser (Baumer, OADM13). Then, other 2 hours of sediment supplying were performed, and the final thickness of sediments deposits was measured. The concentration was monitored at the inlet and at the outlet channels by two turbidimeters (Solitax SC, [6]). The values of turbidity measured at the outlet were about 50% of the Inlet concentration, with some differences on reservoir trapping efficiency depending on the geometrical configuration.

The sediments used for the experiments were crashed walnut shells of mean diameter d_{50} = 89 μm, with bulk density of the dry sediments ρ_{dry} = 550 kg/mc and a grain density ρ_s = 1500 kg/mc. Their mean settling velocity is v_{sed} = 1.9 mm/s, according to the Stokes' law applied on d_{50}.

5 RESULTS

The first tested configuration was the symmetric one, having the inlet and outlet channel placed both on the longitudinal axis of the reservoir. This configuration leads to a stable symmetric flow pattern formed by 2 main symmetrical gyres on both sides of the main water jet that links directly the inlet to the outlet channel. It was chosen to start from this initial configuration to analyze the influence of asymmetrical positions of inlet and outlet channels on flow field and sediments deposits.

Two extremes configurations were tested: one (Figure 3 b) has the inlet and the outlet channels placed both near the corners adjacent to the right side of the reservoir; the other one (Figure 3 c) has the two channels placed at opposite reservoir corners. In the end, an intermediate configuration (Figure 3 d) was investigated: the inlet channel was in the middle of the upstream side, while the outflow was placed on one corner of the downstream side.

The main water jet presents, near the entrance of the reservoir, the highest velocity values, about 140 mm/s, as the average velocity expected for the 0.25 m x 0.2 m inlet channel subjected to a discharge of 7 l/s. Downstream, the water jet begins its spreading and mixing process with the water of the reservoir. Velocity begins to decay, the jet width increases, and vortexes develop, originating recirculation zones. The maximum thickness of sediments deposits is placed along the main jet pattern, showing bed forms and reaching a maximum height of about 40 mm. On the contrary, in correspondence of the recirculation zones which are characterized by low velocities, sediments deposits have a smaller thickness (about 10-20 mm) and a more uniform distribution.

A remarkable phenomenon happens for configuration (c): the flow pattern developing during tests with sediments (c2) is different from the one that develops during clear water tests (c1). For clear water tests, the main jet is deflected towards the side of the reservoir nearer to the inlet channel, then the jet follows the right reservoir wall and downstream wall, and it reaches in the end the outlet channel. A big recirculation clockwise zone develops in the centre of the reservoir. On the contrary, during tests with sediments, after 30 minutes of sediment supply the deposits on the bottom create a roughness sufficient to deflect the main jet towards the centre of the reservoir. The main jet follows a direction oriented towards the outlet channel, even if the inlet and the outlet are not directly linked by the main jet. It flows against the downstream wall then it divides itself in two parts, giving raise to 2 big recirculation zones. This flow structure remains then stable for the remaining part of the experiment.

The last configuration (d) is the intermediate one: the main jet reaches directly the exit of the basin and two eddies of different size and shape develop on each side of the main jet.

6 CONCLUSIONS

By the help of UVP measurements it could be observed that in some cases a different flow field can develop in the same reservoir configuration during clear water tests or during tests with sediment supply. This fact shows that not only the velocity flow field influence sediments deposition, but also that the deposits themselves have a strong feedback on the flow field. In fact, they can completely modify the flow patterns, and in particular the direction of the main jet from the inlet to the outlet.

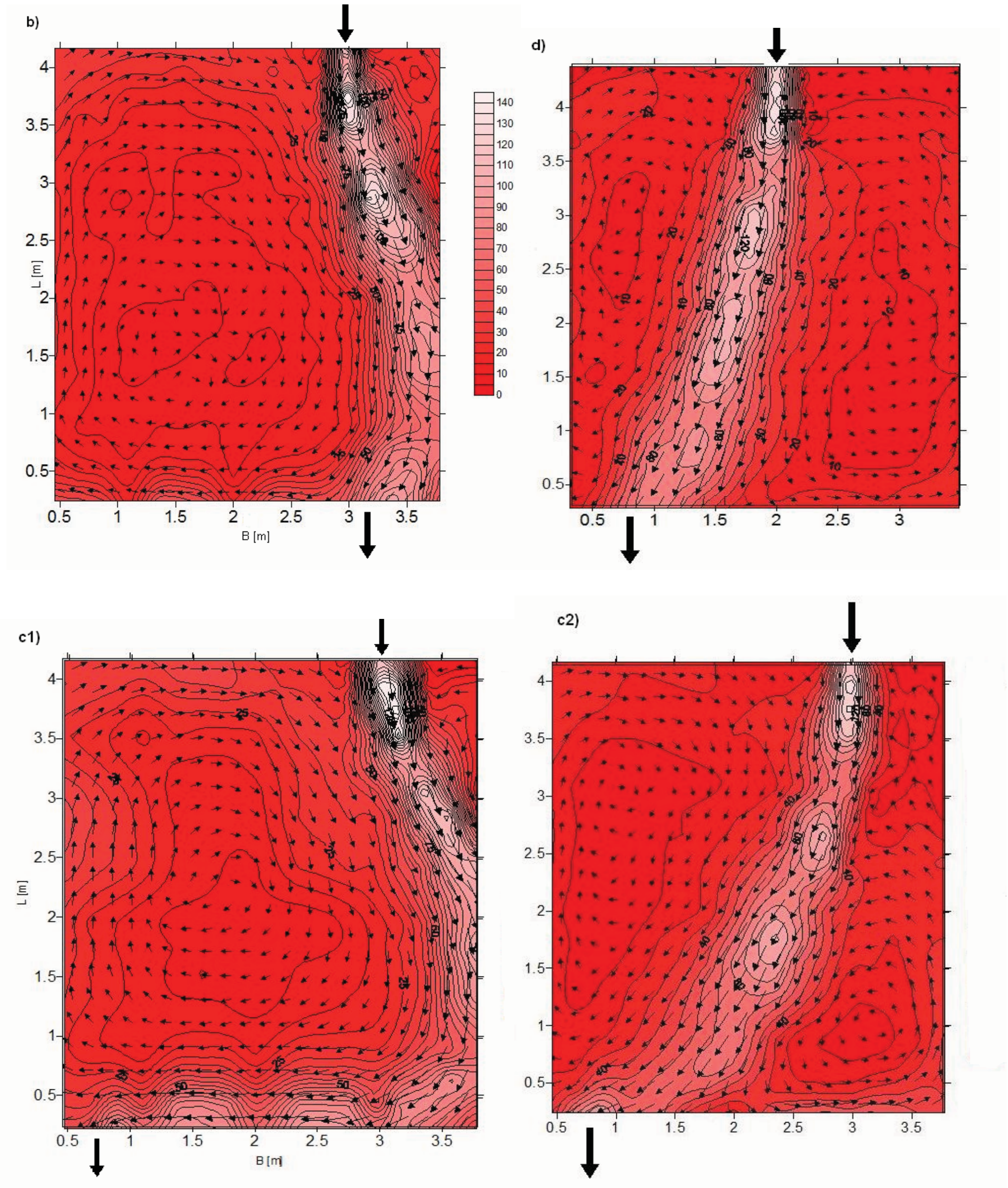

Figure 3: Examples of velocity maps [mm/s] for some of the tested reservoir configurations. b) inlet and outlet channel on the right side – c1) inlet on the right and outlet on the left, test without sediments supplying – c2) inlet on the right and outlet on the left, test with sediments supplying – d) inlet in the centre and outlet on the left. (Q = 7 l/s – h = 0.2 m).

AKNOWLEDGEMENT

Experiments were carried out at the Laboratory of Hydraulic Constructions of EPFL, within the framework of collaboration between Ecole Polytechnique Fédérale de Lausanne and Politecnico di Milano for a Ph.D. research financed by a scholarship of the Italian Ministry of Education, University and Research.

REFERENCES

[1] S. Kantoush et al.: Flow field investigation in a rectangular shallow reservoir using UVP, LSPIV and numerical model, 5th International Symposium on Ultrasonic Doppler Methods for Fluid Mechanics and Fluid Engineering, Zurich, Switzerland (2006) 129-133.

[2] Metflow. UVP Monitor – Model UVP-DUO with Sofware version 3. User's guide, Metflow SA, Lausanne, Switzerland, (2002).

[3] S.A. Kantoush et al.: Suspended load transport in shallow reservoirs, XXXI IAHR Congress, Seoul, South Korea (2005) 1787-1799.

[4] S.A. Kantoush: Experimental study on the influence of the geometry of shallow reservoirs on flow patterns and sedimentation by suspended sediments, Ph.D. Thesis, Ecole Polytechnique Fédérale de Lausanne, (2008).

[5] Fan, J., and Morris, G. L.: Reservoir sedimentation Handbook. Design and management of dams, reservoirs, and watersheds for sustainable use. McGrow Hill, New York (1997).

[6] Hach. Solitax SC User Manual, (2005).

Application of the Ultrasound Doppler Velocimetry in a Czochralski crystal growth model experiment

Andreas Cramer, Josef Pal and Gunter Gerbeth
Institute of Safety Research, Magneto-Hydrodynamics Division
Forschungszentrum Dresden-Rossendorf, P.O. Box 51 01 19, 01314 Dresden, Germany

The present work is concerned with ultrasound and temperature measurements in a Czochralski crystal growth model experiment. In the Czochralski growth, primary strong horizontal temperature gradients are present at the solidification front, which should lead to an axisymmetric flow pattern in the melt volume. To study the flow structure a modified Rayleigh-Bénard configuration was built up in which the upper thermal boundary condition in a Czochralski system is accounted for by a partially cooled surface. The measurements show, that rather a large scale flow pattern develops known as wind in real Rayleigh–Bénard configurations. The wind was always found as the only stable flow pattern for all performed Grashof numbers. Applying a rotating magnetic field (RMF) to the melt volume, the wind starts to co-rotate with the RMF. By analogue with the superposition of the primary and the secondary flow in an RMF, the swirl evoked by the RMF is also superimposed to the wind without any remarkable interaction. Not until the weaker secondary flow produced by the RMF becomes similar in vigour to the buoyant wind does the flow structure in the modified Rayleigh-Bénard system change basically. The results show the applicability of the Ultrasound Doppler Velocimetry (UDV) in the detection and identification of complex flow patterns.

Keywords: Ultrasound Doppler Velocimetry, Temperature gradients, Czochralski crystal growth, Fluid flow,

1 INTRODUCTION

Electromagnetic processing of materials provides the means to gain control of the flow in metallurgical and crystal growth tasks. Still to date, the strategy in quite a lot of work done on the field is to apply magnetic fields, observe their influence on the flow field, and to analyse the modification of the final product. A more promising approach goes the opposite direction: as flow control is merely a tool, the goal is to be expressed with objective functions. These targets are most reasonably formulated in terms of the relevant quantities, which are often distribution and transport of the scalars temperature and concentration. One example in Czochralski crystal growth is the ratio $r^* = \Delta T_\mathrm{h} \,/\, \Delta T_\mathrm{v}$ of the horizontal and the vertical temperature gradient within the silicon melt at the perimeter of the growing crystal.

Once an objective function is defined, the task formulation is to solve a multi-step inverse problem: a flow field that fulfils the target function is to be sought. Given this flow field, it has to be realised by means of applying magnetic fields, or, as is the case in crystal growth, the buoyant convection intrinsic to the process is to be accordingly controlled electromagnetically. Finally, a coil system producing the fields determined in the previous step has to be designed. As the problem is extraordinarily difficult if ever solvable, known results from the corresponding forward strategies are to be adopted for each step.

Prior describing the apparatus employed to study the effect of the RMF used hitherto on the ratio r^* and the flow field, the action of this field type on a cylindrical liquid metal volume is briefly recalled. An AC magnetic field of strength $\boldsymbol{B}_0$ applied to an electrical conductor induces an eddy current $\boldsymbol{j}$ within that medium. The interaction of $\boldsymbol{j}$ with the field that produced it results in a Lorentz force $\boldsymbol{F}_\mathrm{L} = \boldsymbol{j} \times \boldsymbol{B}_0$, which may drive a flow in the case that the electrical conductor is liquid. In [1], $\boldsymbol{F}_\mathrm{L}$ is expressed as

$$\boldsymbol{F}_\mathrm{L} = \mathrm{Ta}\, r\, f(r,z)\, \boldsymbol{e}_\varphi, \mathrm{Ta} = \frac{\sigma\,\omega\, B_0^2\, \mathrm{R}^4}{2\rho\nu^2}, \qquad (1)$$

where the Taylor number Ta is a measure for the relative strength of the driving force, σ, ρ, and ν are electrical conductivity, density and kinematical viscosity of the melt, R is the radius of the liquid metal column, and ω is the frequency of the RMF. The shape function f vanishes at the top and the bottom walls. Eq. 1 is valid for the low-frequency and low-induction approximation. Low frequency means $\mu\sigma\omega\mathrm{R}^2 < 1$ with μ being the magnetic permeability, whereas low-induction stands for the case that the characteristic angular velocity of the resulting flow is much smaller than the field frequency ω. The flow developing under the influence of an RMF is a primary swirl following the mere azimuthal direction of $\boldsymbol{F}_\mathrm{L}$ in Eq. 1. Initiated by an imbalance between pressure and centrifugal force at non-vertical rigid walls, a meridional motion is superimposed. This secondary flow exhibits a toroidal structure with two vortices lying on top of each other, leading to a jet moving radially outward at mid-height of the liquid column [2].

2 EXPERIMENTAL SETUP

The apparatus, shown in Fig. 1, is a modified Rayleigh-Bénard configuration, in which the upper thermal boundary condition in a Czochralski system is accounted for by a partially cooled surface. This partial cooling covering approximately the same area as the growing crystal in an industrial facility is realised with a circular heat exchanger mounted concentrically within the upper lid. Some compromise had to be made with respect to the entity of all boundary conditions. The surface between the crystal and the crucible is free, whereas it is covered by a PTFE lid in the model. This construction was motivated by the thermal boundary condition. Both the heat exchanger at the top and the bottom heating plate are made from copper to approximate isothermal boundary conditions. This approach is further supported by a branched structure of flow channels machined into the copper parts. A precise control of temperatures is realised by supplying the heat exchanger and the bottom heater with coolant/heating fluid at high flow rate from thermostats having a large reservoir, the latter being regulated by a PID circuit. Differences to the set-point and inhomogeneity were monitored by platinum resistance wires mounted within the heat exchanger and the bottom heater at various positions and found to be less than 0.05 K. Water may be used as a coolant, whereas the aim to reach high temperature gradients necessitates a heating fluid with a high boiling point. The experiments were thus performed with silicone oil. It is noted that all copper parts in contact with the fluid are covered by a thin electrically insulating layer of aluminium oxide. Otherwise electric current may circulate between the fluid under investigation and those parts, which is likely to modify the distribution of the Lorentz force and in turn the flow structure.

A borosilicate glass pipe 90 mm in inner diameter and also in height was chosen for the reasons of being electrically insulating, relatively poor heat conducting so as to approach what is commonly referred to as adiabatic boundary condition, allowing transmission of ultrasound for flow measurements, and standing relatively high temperatures. Sealing of the cell is realised by clamping the glass cylinder between the bottom heater and the PTFE top cover by means of thread rods screwed into the bottom plate. Different thermal expansion coefficients of the constructional materials are accounted for with springs inserted between the PTFE disc and the upper fastening nuts. The upper limit on temperature is imposed by the o-rings, which are located in the annular grooves machined into the PTFE disc (c.f. Fig. 1) and the bottom heater. These sealings are made from highly fluorinated synthetic elastomer and may be used at permanent load up to 280 °C. During the measurements, the whole apparatus was embedded in mineral wool serving the minimisation of the lateral heat loss.

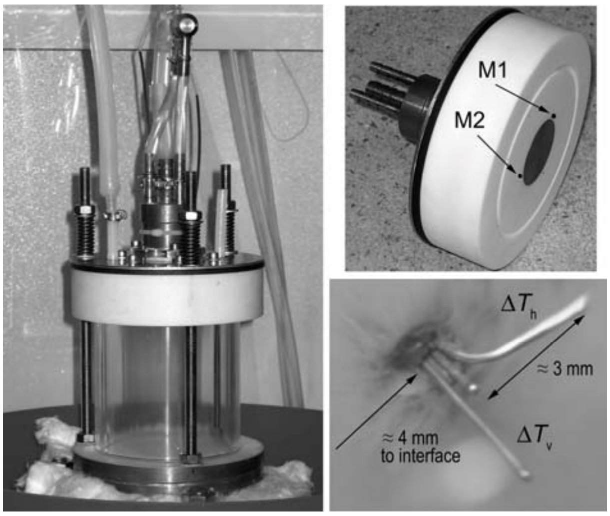

Figure 1: On the left a photo of the whole experimental setup, the right upper picture an oblique view from below of the PTFE top cover. M1 and M2 are the locations of the thermocouple-tripods close to the circumference of the heat exchanger. The right lower figure shows the equilateral-triangular arrangement of the three thermocouples comprising a measuring point.

Temperatures in the melt are measured with mineral insulated type K thermocouples with protective tubes of 250 μm in total diameter. Three thermocouples in a triangular arrangement as shown in Fig. 1 allow determination of both horizontal and vertical temperature gradients. It can be seen, that two such tripods are mounted at the perimeter of the top heat exchanger. As we shall see immediately below, the advantage thereof is not restricted to having solely a second measuring station. Because of the relatively small size of the thermocouples, transients of temperature may be recorded together with the mean values. Ultrasound Doppler Velocimetry in conjunction with the presence of two metering points for the temperature gradients proves a valuable tool in the detection and the characterisation of non-axisymmtric convective patterns. Acoustic properties of the borosilicate glass and the smooth surface of the pipe permit attaching a transducer to the outside of that wall to measure the radial velocity component along the entire ultrasonic beam. UDV has matured during the past years and is commercially available from a variety of manufacturers to date. Here, a DOP2000 (Model 2032, Signal-Processing, Lausanne, Switzerland) was used. The principle of operation of UDV is described in the pioneering work of Takeda [3], and a demonstration of the ability to work for liquid metals may be found in [4].

The RMF was generated by the home-made MULTIpurpose MAGnetic field system, which is described in detail in [5]. Besides an RMF, MULTIMAG offers also other magnetic field types, even linear superpositions thereof. Such flexibility will certainly be the experimental basis for future work on the present topic of tailored flow control.

3 RESULTS

Naturally, the first measurement series has to cover the flow without control. The only parameter subject to variation is the total temperature drop ΔT between the bottom heater and the top heat exchanger. Even though the surface is cooled only partially, the system may be described by the Grashof number

$$\mathrm{Gr} = \frac{\beta\, \mathrm{g}\, \Delta T\, \mathrm{H}^3}{\nu^2} \qquad (2)$$

where β, g, and H are volumetric expansion coefficient, acceleration of the free fall, and height. For Rayleigh-Bénard systems with homogeneous upper and lower temperature boundary conditions, a flow phenomenon often termed wind is known. Instead of an axi-symmetric convective pattern, fluid rising in a more or less kidney-shaped region at one side, moving along the surface to the opposing side, descending there, and closing the loop along the bottom is frequently observed. It was not expected to find any wind in the system with partially cooled surface because of the primary strong horizontal temperature gradient at the perimeter of the heat exchanger directed radially everywhere, which gradient should lead to kind of a forced symmetrisation. Quite the contrary, the wind always showed up as the sole and stable flow pattern for all Gr - albeit in statistical orientation.

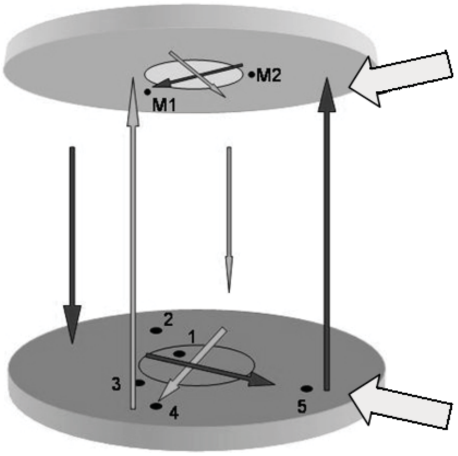

Figure 2: Statistically oriented flow directions. The big grey arrows indicate the UDV sensor positions.

This mono-cellular pattern was detected as an asymmetry in the temperature data recorded with both tripods, and confirmed by UDV measurements. Fig. 2 shows schematically both such statistically oriented flow directions and the position of the ultrasonic sensors, whereas Fig. 3 illustrates the measured ultrasonic velocity profiles for several temperature gradients and gives evidence to the previously described wind.

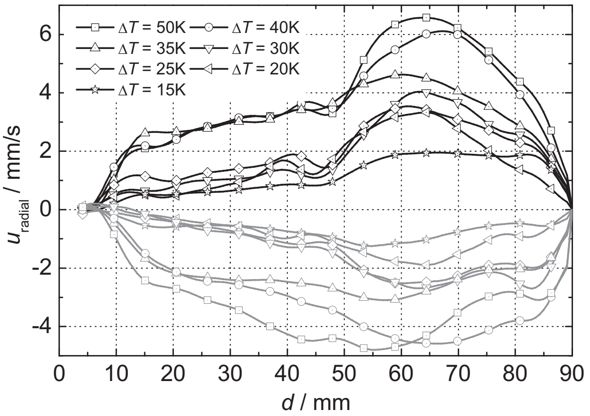

Figure 3: UDV profiles of the wind for several temperature gradients between heater and cooler. Positive values (upper sensor) indicate a flow away from the sensor, negative values (lower sensor) a flow toward the sensor.

When the RMF is switched on the wind starts to rotate as indicated schematically in Fig. 4. By analogue with the superposition of the primary and the secondary flow in an RMF, the swirl evoked by the RMF is also superimposed to the wind without any remarkable interaction. Not until the weaker secondary flow produced by the RMF becomes similar in vigour to the buoyant wind does the flow structure in the modified Rayleigh-Bénard system change basically. The scenario for strengths of the RMF below this threshold is shown in Fig. 5 in the form of a spatio-temporal representation of velocity.

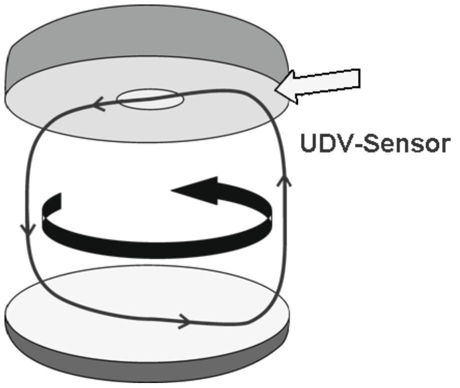

Figure 4: Schema of the buoyant wind co-rotating with the applied RMF.

Concerning the objective function without applying the RMF it arises $r^* \approx 3$. It is reminded that it should not be expected to observe highly precise and reproducible values for that magnitude. r^* is calculated from two differences out of three absolute measurements of temperature, each of the differences being quite small because of the short distance between the thermocouples. However, Fig. 6 evinces that r^* deteriorates for weak magnetic fields up to the threshold described above in the previous paragraph.

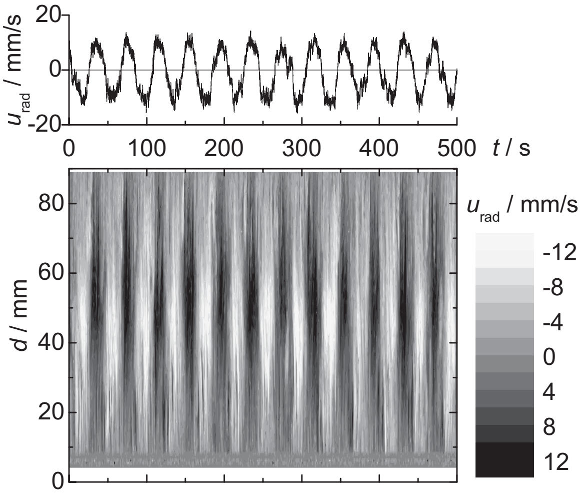

Figure 5: Dependence of the radial velocity component on time at Ta = 5•10^5 in a contour plot along the ultrasound beam (lower panel) and for a selected location (upper panel). While the RMF is weak the buoyant wind co-rotates with the magnetic field.

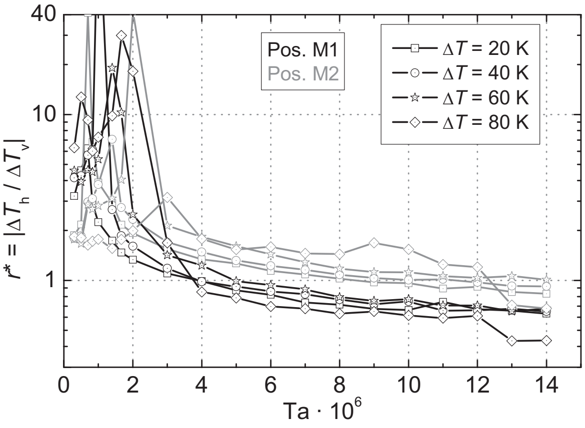

Figure 6: Dependence of the objective function r^* on the strength of the RMF.

Although the representation of the ordinate is logarithmic, the plot is cropped at the upper end – r^* reached values exceeding 100. Increasing the field strength leads to the secondary flow produced by the RMF forcing dominating the wind; r^* starts to decrease. As the mono-cellular buoyant flow structure vanishes completely above a certain value of Ta, Fig. 6 clearly shows that $r^* \approx 1$ is accomplishable whatever the vertically applied temperature difference. MULTIMAG would allow raising Ta for more than two orders of magnitude while the four ΔT contained in Fig. 6 are yet in the range of industrial interest ($Gr_{\Delta T=20K} = 1.7 \cdot 10^8$ … $Gr_{\Delta T=80K} = 1.1 \cdot 10^9$).

It is well known that an RMF may reduce the temperature fluctuations, which are inherent to turbulent natural convection. Hence, it was worth while to study also the transients of temperature. Fig. 7 shows the temperature signals recorded with one of the six thermocouples comprising the two tripods. The amplitude of the fluctuations decreases to 7% when Ta is increased about 50 times.

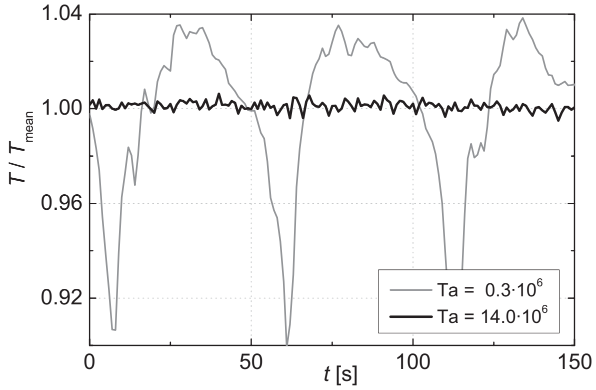

Figure 7: Temperature signals recorded at two different strengths of the magnetic field.

4 SUMMARY

Firstly, local gradients and fluctuations of the temperature field in the vicinity of the solid-liquid interface in a physical model of the Czochralski crystal growth process were studied experimentally. A comparable magnitude of the horizontal ΔT_h and the vertical temperature gradient ΔT_v at the triple point melt-crystal-atmosphere was chosen as a target function for an optimisation via electromagnetic flow control. It is shown that this task may be accomplished yet with an RMF alone: for any vigour of the buoyant convection investigated in the experiments. The application of RMF also reduced the temperature fluctuations.

Secondly, for flow measurements, the UDV technique was proved as a valuable tool in the detection and the characterisation of non-axisymmetric convective patterns.

5 ACKNOWLEDGEMENTS

This work was financially supported by “Deutsche Forschungsgemeinschaft” in the framework of the Collaborative Research Centre SFB 609.

REFERENCES

[1] Gorbatchev L P et al: Magnetohydrodynamic rotation of an electrically conductive liquid in a cylindrical vessel of finite dimensions, Magnetohydrodynamics 10 (1974) 406-414.

[2] Davidson P A, Hunt J C R: Swirling recirculating flow an a liquid-metal column generated by a rotating magnetic field, J. Fluid Mech. 185 (1987) 67-106

[3] Takeda Y: Development of an ultrasound velocity profile monitor, Nucl. Eng. Design 126 (1991) 277-284.

[4] Cramer A et al.: Local flow structures in liquid metals measured by ultrasonic Doppler velocimetry, Flow Meas. and Instrum. 15 (2004) 145-153.

[5] Pal J et al.: MULTIMAG – A MULTIpurpose MAGnetic system for physical modelling in magnetohydrodynamics, Flow Meas. Instr. 20 (2009) 241-251.

Steady and unsteady flow characteristics of a shear thinning fluid through a collapsed elastic tube

S. Nahar, S. A. K. Jeelani and E. J. Windhab
Laboratory of Food Process Engineering, Institute of Food, Nutrition and Health
ETH Zurich, Schmelzbergstrasse 7, 8092 Zurich, Switzerland.

It was observed that for a given steady volume flow rate Q of a shear thinning (1.5 wt.% carboxymethyl-cellulose, CMC) aqueous solution, the tube was buckled from an elliptical shape to a line or area contacted two lobes as the critical external pressure P_e increased. The downstream transmural pressure P_{tm} was found to be more negative than that at the upstream as the outlet pressure decreased due to stronger tube collapse resulting in reduced cross sectional area. The tube cross sectional area decreased about an order of magnitude from the undeformed one when the compressive P_{tm} was about 30 mbar at downstream, which was investigated using image analysis near the tube outlet at different P_e. The corresponding maximum flow velocity at the tube center increased about a factor of two as monitored using pulsed Ultrasound Doppler Velocimetry (UVP). A bi-modal velocity profile was observed in the two lobed tube shape from the plane above the horizontal axis of tube center by UVP. The periodic flow characteristics of CMC solution during ramp up and down were found to be different for the same range of Q, due to instantaneous inlet pressure response than that at outlet. The evolution of flow velocity profiles during the periodic ramp flow was measured and the velocity at the tube center increased by an order of magnitude as the time elapsed from 18s to 188s.

Keywords: bio-medical application, deformed elastic tube, intestinal flow, non-Newtonian fluid, steady and unsteady flow, transmural pressure, ultrasound Doppler velocity profile.

1 INTRODUCTION

The knowledge on the flow characteristics of non-Newtonian fluids in elastic inflatable and collapsible tubes is important to the biological applications especially for the understanding of the mixing and propulsion mechanism of food in small intestine during digestion. The mechanisms of pharyngeal, esophageal and intestinal transport of food and liquids are useful for the treatment of patients with malfunctioning of these transport processes [1]. Moreover, the flow behavior of non-Newtonian fluids in elastic tubes depends on the micro-structural properties of the fluids, solid mechanics of the elastic tube, the interaction between the deformation of the tube and fluids, and the applied stresses to induce flow [2]. The extensive experimental and theoretical contributions made by several authors [3,4,5] are mostly for the understanding of the complexity of the laminar and turbulent flows of Newtonian fluids through collapsible tubes together with the solid mechanics of the tube. However, there is little literature on the experimental flow characteristics of non-Newtonian fluids through elastic tubes under the influence of different transmural pressures and the corresponding velocity distribution in the collapsed tube. There are several publications on the velocity profiles measured using the ultrasound Doppler velocimetry (UVP) technique during steady and unsteady laminar flow of non-Newtonian fluids and particulate suspensions [6] in non-collapsible pipes. We have used [7] this technique to study the flow profiles of a non-Newtonian shear thinning solution during steady laminar flow through a partially collapsed elastic tube using Starling Resistor set up. In this paper, we investigate both the steady and unsteady laminar flow characteristics of shear thinning carboxymethyl-cellulose (CMC) aqueous solution (inelastic up to 2%) through a collapsible elastic tube under compressive transmural (internal minus external) pressures P_{tm}. As the external chamber pressure increased, the width at the tube center and cross sectional area of the deformed tube decreased; consequently the maximum flow velocity increased as measured by UVP. This technique was also used to study the temporal evolution of instantaneous flow velocity profiles during the periodic ramp flow in a collapsible elastic tube.

2 EXPERIMENTAL

2.1 Starling Resistor setup

The Starling Resistor is widely used [e.g. 5] to investigate flow through elastic tubes relevant to many applications. The experimental setup (Figure 1) in the present study consists of a cylindrical Plexiglass (PG) pressure chamber (300 mm inner diameter, 5.66 mm thick and 620 mm long) with two side metal flanges through each of which an aluminum pipe is fixed. A 20 mm inner diameter, 1 mm thick and 320 mm long silicone elastic tube (Lindemann GmbH, Germany) is mounted between the two aluminum pipes. The right pipe is connected to a rotor pump and a PVC tank containing the non-Newtonian liquid. Two pressure sensors (Sensor-Technics, Type: CTEM9350GY7) are installed on two PVC connectors for both the inlet and outlet aluminum pipes to measure the pressures of liquid.

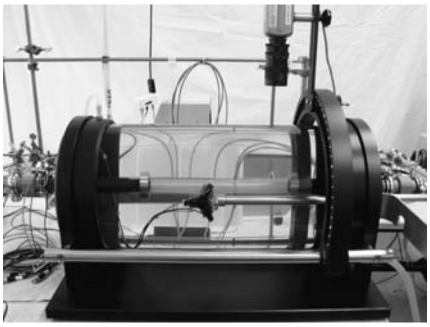

Figure 1: Photograph of the experimental setup for flow structure measurement of non-Newtonian fluids in elastic tubes using Starling Resistor.

One additional pressure sensor is connected to the pressure chamber to measure the externally applied pressure to deform the elastic tube. The three pressure transducers are connected to a data acquisition board (type USB-6221, National Instruments) with a resolution of 16 bits. A Canon PowerShot G2 camera with the resolution of 2272X1704 is used to obtain images of deformed elastic tube. The camera is mounted on an aluminum arm, which can be rotated to obtain images of the deformed tube at different angles. The steady and unsteady flows of a shear thinning non-Newtonian aqueous solution of 1.5 % carboxymethyl-celullose (Blanose CMC 7MF, IMCD Switzerland AG) at a range of volume flow rates and different values of the external chamber pressure, were carried out at 22°C.

2.2 Shear thinning solution

In the present work, a shear thinning solution was used to investigate the flow structure of non-Newtonian fluids in elastic tubes. A carboxymethyl-cellulose (CMC) aqueous solution (1.5 % wt/wt with 0.1 M NaCl; M_W = 2.5 $\times 10^5$ g/mol) was used based on literature [8], which showed inelastic behaviour for concentrations up to 2%. Hence the rheological measurements of this solution at different concentrations were carried out using Physica (MCR 300, CC27) rheometer with concentric cylinder geometry (gap width = 1.13 mm).

2.3 UVP measurement in elastic tube

A UVP-Duo (Met-Flow SA, Lausanne, Switzerland) instrument was used to measure the velocity profiles of CMC solution flowing through the elastic tube in the Starling Resistor setup.An ultrasound transducer with 4 MHz emission frequency and 5 mm active and 8 mm housing diameters (Met-Flow SA, Lausanne, Switzerland) was used as transmitter and receiver. One transducer arm together with holder to house the ultrasound transducer (for single or multiple transducer measurements) was immersed in the Perspex cylindrical pressure chamber filled with water. By adjusting the Doppler angle (20° with respect to the normal to the horizontal axis), the velocity profile during flow through the elastic tube can be measured using single transducer at different radial and axial locations of the (undeformed and deformed) elastic tube. The transducer submerged in water in the pressure chamber was in direct contact with the elastic tube without causing tube deformation. The communication with the UVP-Duo was made with an active X Library from Met-Flow SA. The number of cycles per pulse was 2 and the channel width was 0.38 mm. The measured velocity of sound in the CMC solution at 22°C was 1516 m/s.

2.4 Deformation measurement of elastic tube

In order to determine the parameters during a steady flow of non-Newtonian fluid through the elastic tube, the shape and cross sectional area along the length of both the undeformed and deformed sections of tube were measured optically using images taken from different angles over the circumference.

A MATLAB based software was used to implement the computer tomography (CT) method for the 2D reconstruction of the elastic tube. The CT method was based on the backward projection of several images, which were obtained in different angles. The grid pattern was painted on the tube and pictures were taken by rotating the radially oriented camera around the tube shown in Figure 1. The angle between the pictures taken was known. Image processing (contrast maximization etc.) was applied to identify the grid lines drawn on the tube surface (left and center part of Figure 2). Then a rotation matrix (according the angle of the camera position) was applied to the images, which were combined (using addition or multiplication of the grayscale values). The projection beam lines for the lines on the tube cross in one point, which resulted in the position in 2D (right part of Figure 2). In addition to the CT-method, cell tracker software (also written in MATLAB) was used for the 3D reconstruction of the elastic tube. In this step, iteration was done over the tube length with a certain step change and several positions in 2D are constructed. Then, by using the cell tracker all the crossing points obtained at several positions in 2D were detected and 3D reconstruction was done.

3 RESULTS AND DISCUSSION

3.1 Rheology of CMC solution

The measured shear rate $\dot{\gamma}$ dependent viscosities η of different concentration CMC aqueous solutions were found to be shear thinning. 1.5 % CMC solution was further investigated, the measured (Figure 2a) viscosity of which was well represented by the Carreau model (Eq.1) with the fitted constants: $\eta_0 = 0.1452$Pa.s, $\lambda = 0.02673$ and $m = 0.7588$. The dynamic moduli measured under linear viscoelastic conditions by the oscillatory shear for 1.5 % CMC solution are shown in Figure 2b. The viscous (loss) modulus *G``* can be seen to be at least an order of magnitude higher than the elastic (storage) modulus *G`* indicating that the fluid is almost inelastic.

$$\eta = \eta_0 \left[1 + (\lambda\dot{\gamma})^2\right]^{(m-1)/2} \tag{1}$$

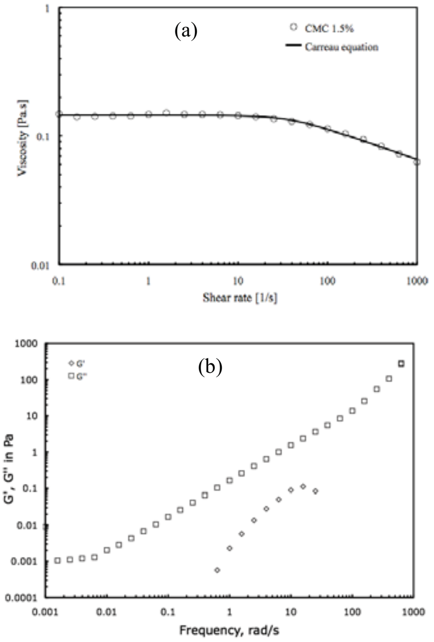

Figure 2: (a) Shear rate dependent viscosity (symbols: experimental; line: Carreau model) and (b) Dynamic moduli under oscillatory shear with a constant deformation of 5% at 22 °C for 1.5% (w/w) CMC solution.

3.2 Steady Flow of CMC solution in Collapsible tubes

The flow behavior of non-Newtonian fluids in elastic tubes depends on the microstructural properties of the fluids, solid mechanics of the elastic tube, the interaction between the deformation of the tube and fluids [3], which includes the nonlinear pressure drop/flow rate relation [2]. Figure 3 shows that the pressure drop in the tube ($dP = P_i - P_o$) increases with increase in flow rate Q (17 ml/s) during steady flow of 1.5 % CMC solution up to a critical external pressure (about 95 mbar) due to increase of friction in uncollapsed tube. In contrast, above the critical external pressure the collapsed tube walls come closer and the pressure drop at a given Q increased as P_e increased. On the other hand, when Q is further increased, internal pressure slowly increased and the tube recovered its original shape at higher flow rates decreasing the pressure drop. Moreover, the downstream transmural pressure was found to be more negative than the upstream one as the outlet pressure decreases when the tube collapses more strongly (Figure 4).

In addition, when the transmural pressure P_{tm} is negative, the mechanics of the flow is closely coupled to the structural mechanics of the tube and is characterized by the 'tube law': the relationship between cross-sectional area and transmural pressure [9] as shown in Figure 4. The tube cross sectional area decreased about an order of magnitude from the undeformed one when the compressive P_{tm} was about 30 mbar at downstream and the corresponding maximum flow velocity at the tube center increased about a factor of two.

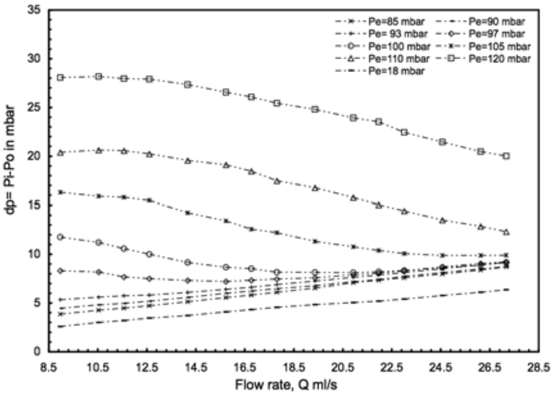

Figure 3: Influence of P_e on the variation in pressure drop with flow rate .

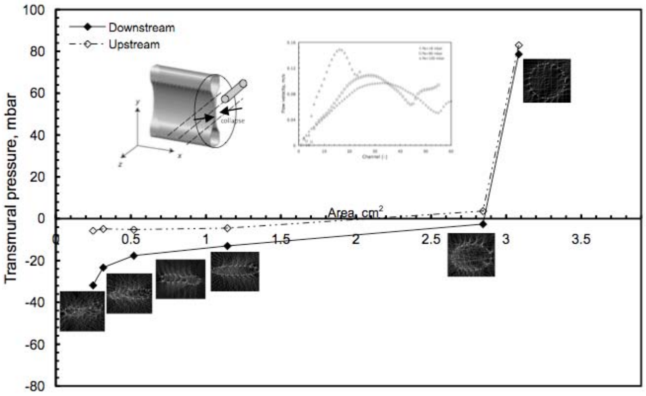

Figure 4: Transmural pressure versus tube cross sectional area during CMC solution steady flow in the elastic tube. The average maximum velocity versus area and schematic collapsed tube view is also inserted.

For a given flow rate (Q=17 ml/s) and an applied external chamber pressure of about 105 mbar lead to a change in the tube shape along the length. There was a section along the tube length where a two lobed shape was observed having a bi-modal velocity profiles for the corresponding tube shape as shown in Figure 5.

3.3 Unsteady Flow of CMC solution in Collapsible tubes

The experimental flow characteristics of CMC solution under a periodic ramp flow (4.7×10^{-3} cycle/s and a flow rate amplitude of 13 ml/s) through elastic tube in the Starling resistor setup are shown in Figure 6.

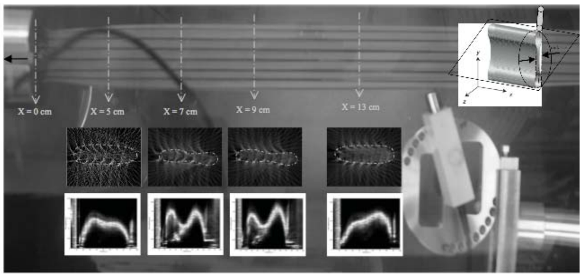

Figure 5: Variation in velocity profile,tube shape and cross sectional area along the tube length during steady flow of 1.5%CMC at 18 mbar downstream transmural pressure.

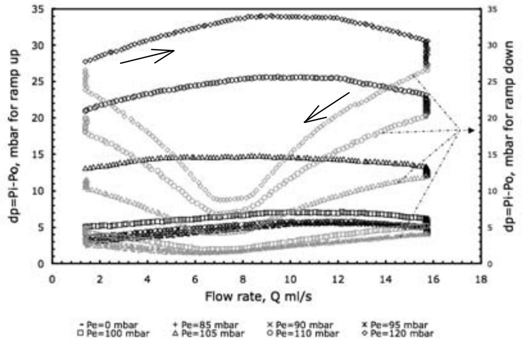

Figure 6: Variation in pressure drop with flow rate during periodic ramp flow of 1.5 % CMC solution through silicone elastic tube at different chamber pressures.

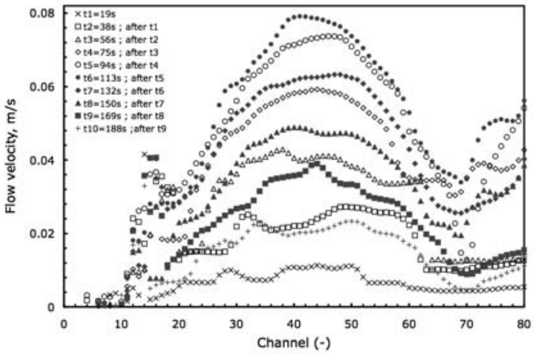

Figure 7: Temporal evolution of average flow velocity of 1.5 % CMC solution during a periodic ramp flow through elastic tube (open symbols: 10 s^{-1} ramp up; closed symbols: 10 s^{-1} ramp down).

In an unsteady flow (Figure 6) during the ramp up (10 s^{-1}), the flow characteristics of CMC solution can be seen to be similar to those of steady laminar flow for the same range of Q in section 3.2. In contrast, during the ramp down (10 s^{-1}) at higher applied external pressure (90 to 120 mbar), the pressure drop in the tube sharply decreases as Q decreases due to the instantaneous change of pressure response at the inlet than that at the outlet. Moreover, as Q reduces significantly, the tube walls come closer with a line/area contact of tube shape where the tube frictional force become dominant thereby increasing the pressure drop. Even for undeformed elastic tube, a higher average maximum velocity for the ramp down than that for the ramp up flow was observed. Figure 7 shows the temporal evolution of the average flow velocity at the tube center, which increased by about an order of magnitude during 1 cycle of the periodic ramp flow as time elapsed from 18s to 188s.

4 CONCLUSIONS

The steady and unsteady laminar flow characteristics of non-Newtonian shear thinning CMC aqueous solution through an elastic tube were investigated at different compressive transmural pressures in a Starling Resistor setup. The tube cross sectional area decreased by an order of magnitude from the undeformed one when the compressive P_{tm} was 30 mbar at downstream and the corresponding maximum flow velocity at the tube center increased about a factor of two. A critical external chamber pressure caused collapse of elastic tube to form a two lobe-shaped cross-section, where measured UVP based velocity profiles are bi-model. The velocity profiles evolution during periodic ramp flow was measured and the velocity at the tube center increased by an order of magnitude as the time elapsed from 18s to 188s.

5 ACKNOWLEDGEMENTS

Swiss National Science Foundation (SNF) for funding this project; B. Birkhofer and P. Horvath for the software development; D. Kiechl, J. Corsano, B. Pfister and P. Bigler for construction of the experimental setup; Y. Takeda and Y. Murai for collaboration.

REFERENCES

[1] Meng et al.: Computer simulation of the pharyngeal bolus transport of Newtonian and non-Newtonian fluids, Trans IChemE, Part C, *Food and Bioproduct Processing*, 83 (2005) 297-305.

[2] Grotberg JB, Jensen OE: Biofluid Mechanics in Flexible Tubes, Annu. Rev. Fluid Mech.36 (2004)121-147.

[3] Heil M: Stokes flow in collapsible tubes – computation and experiment, J. Fluid Mech. 353 (1997) 285-312.

[4] Hazel AL, Heil M: Steady finite-Reynolds-number flows in three-dimensional collapsible tubes, J. Fluid Mech. 486 (2003) 79-103.

[5] Lyon et al. : Flow through collapsible tubes at low Reynolds numbers – Applicability of the Waterfall model, Circulation Res. 47 (1980) 68-73.

[6] Birkhofer et al. : Monitoring of fat crystallization process using UVP-PD technique, Flow Meas. Instrumen. 19 (2008) 163-169.

[7] Nahar et al. : Non-Newtonian fluid flow in elastic tubes, 6th International Symposium on Ultrasonic Doppler Method for Fluid Mechanics and Fluid Engineering (ISUD6), Prague, Czech Republic, September 9-11, (2008) 131-134.

[8] Stranzinger M: Numerical and Experimental Investigations of Newtonian and Non-Newtonian Flow in Annular Gaps with Scraper Blades, PhD thesis (Diss. ETH No. 13369), ETH Zürich (1999).

[9] Shapiro AH: Steady Flow in Collapsible Tubes, ASME J. Biomech. Engg. 99 (1977) 126-147.

Measurement and Analysis of Flow Behaviour in Complex Geometries using Ultrasonic Velocity Profiling (UVP) Technique

Reinhardt Kotzé[a], Johan Wiklund[b], Rainer Haldenwang[a] and Veruscha Fester[a]
[a]*FPRC - Flow Process Research Centre, CPUT - Cape Peninsula University of Technology, PO Box 652, Cape Town, 8000, South Africa.*
[b]*SIK - The Swedish Institute for Food and Biotechnology, PO Box 5401, Göteborg, Sweden.*

In order to derive models for estimating fluid momentum and kinetic energy in complex geometries, the shape of the velocity profile is critical in determining accurate quantities. In some applications, such as flow through pipe fittings and flow through abrupt contractions and enlargements, theoretical velocity profiles in combination with mathematical models have thus far been used to determine fluid momentum, kinetic energy and loss coefficients. In this project a non-Newtonian CMC model fluid was tested in two different complex geometries using the Ultrasonic Velocity Profiling (UVP) technique. Velocity profiles were measured at three different positions at the center (contraction) of a specially manufactured 50% open diaphragm valve. A range of velocity profiles from developed to contracting flow were also measured by scanning the transducer along a hyperbolic contraction using a high precision robotic arm set-up. Experimental results obtained using UVP showed good agreement with theoretical predictions. Results showed that the most important problem is that it is not possible to accurately measure from the transducer front, which is due to the ultrasonic transducer's near-field. Wall interfaces could be calculated to a certain degree of accuracy, but information of the high velocity gradient close to the wall region is still inaccurate, which could influence results significantly. This problem can be eliminated by the introduction of a next generation transducer, which is currently under development.

Keywords: Velocity profiles, Complex geometries, Diaphragm valve, contraction-expansion, non-Newtonian

1 INTRODUCTION

Flow through complex geometries such as abrupt contractions and enlargements, as well as valves are important problems in fluid dynamics, because they are integral components and frequently occur in pipeline systems. In order to design pipeline systems efficiently, understanding the energy loss mechanisms in complex geometries is a prerequisite [1]. According to literature, there are many different techniques for studying flows of multiphase and complex fluids. However, experimental and cost limitations forces one to consider an alternative approach [2]. UVP is both a method and a device to measure an instantaneous unidimensional (1D) velocity profile along a measurement axis [3-5] and is accepted as an important tool for measuring flow profiles in opaque liquids used in research and engineering. This method has been used for flow mapping in complex geometries such as stirred tanks [6], open channel [7], contractions [8-9], liquid metal target of neutron spallation source configuration [10] and cylindrical hydrocyclone [11].

In this work velocity profiles were measured using UVP at the center (contraction) of a specially manufactured diaphragm valve and at multiple positions along a hyperbolic contraction. The industrial applicability of the UVP technique for measurement of non-Newtonian flow behaviour in two complex geometries was evaluated in this work.

2 THEORY

2.1 Pipe flow

The radial velocity profile for non-Newtonian shear-thinning pipe flow can be described by the integrated form of the power-law model:

$$v = \left(\frac{nR}{(1+n)}\right)\left(\frac{R\Delta P}{2LK}\right)^{\frac{1}{n}}\left(1-\left(\frac{r}{R}\right)^{1+\frac{1}{n}}\right). \qquad (1)$$

In pipe flow integration of the velocity profile yields the volumetric rate of fluid flow and is given by:

$$Q = 2\pi\int_{0}^{R} vr dr, \qquad (2)$$

where v is the velocity at a radial point, r, along the pipe radius. The volumetric flow rate, Q, in a steady state process is given by:

$$Q = VA, \qquad (3)$$

where V is the bulk velocity and A the total area of a particular geometry [12]. In order to calculate a flow rate from measured velocity profiles inside the valve center geometry, separate flow rates were calculated for manually drawn area/flow segments (see Fig. 2) and added together to yield a total volume flow rate:

$$Q_T = \sum_{n=1}^{N}\left(V_n \cdot A_n\right), \qquad (4)$$

where V_n is the measured velocity across a particular flow/area segment, A_n, which is calculated by Solidworks 2009 and N is the total number of segments.

3 MATERIAL AND METHODS

3.1 Material

The Carboxymethylcellulose (CMC) (Protea Chemicals, Bryanston, South Africa, http://www.proteachemicals.co.za) solution used was 6.15% w/w for the valve tests at FPRC. CMC sodium salt (Alfa Aesar GmbH & Co KG, Karlsruhe, Germany, www.alfa.com) 2.63% w/w was used for the hyperbolic contraction tests at SIK. Controlled stress rheometers (Paar Physica MCR300, Anton Paar, Randburg, South Africa, www.advancedlab.co.za and Rheologica StressTech, Rheologica Instruments, Lund, Sweden) were used to obtain flow curves for the CMC 6.15% w/w (K = 0.07, n = 0.85) and 2.63% w/w (K = 0.68, n = 0.82) solutions (cup and roughened bob geometry, measuring gap = 1.13 mm). The rheological parameters were used to calculate Reynolds numbers [13] for non-Newtonian pipe flow. In this research all measurements were conducted in laminar flow.

3.2 Experimental flow loops and UVP setup

In this work the latest UVP instrument (UVP-DUO-MX, Met-Flow SA, Lausanne, Switzerland) was used for velocity profile measurements. Ultrasonic Doppler, Immersion type transducers (TN and TX-line, Imasonic, Bensancon, France) with a base frequency of 4 MHz, 5 mm active element were used [14]. A special flow adapter cell made from stainless steel was designed at SIK for simultaneous in-line measurements of velocity profiles and acoustic properties for straight pipe flow. This transducer installation has previously been described [4, 15] and the same setup was used for the valve tests in this work. Two experimental flow loops were used in this work, one for the valve and one for the contraction flow measurements. Both flow loops share similar methodology of equipment setup and transducer installation. The first flow loop (valve) consisted of a 52.8 mm PVC pipe and is fully described elsewhere [16]. The second flow loop (contraction) consisted of stainless steel pipes of internal diameters 48.5 and 22.5 mm and is described in Zatti *et al*. [9]. Fig. 1 shows a schematic diagram of the valve flow loop at the FPRC.

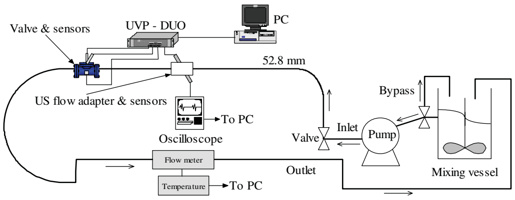

Fig. 1. Schematic illustration of the valve flow loop.

3.3 Diaphragm valve

A commercial diaphragm valve (Dynamic Fluid Control Pty Ltd, Johannesburg, South Africa, www.dfc.co.za) was reverse engineered and re-manufactured using a rapid prototyping (3DP^{TM}) technique of multilayer printing [17]. The spatial co-ordinates of the valve were obtained from 3D imaging using a special camera and were relayed to a CAD drawing package, Solidworks 2009 (Dassault Systèmes SolidWorks Corp., Concord, MA, USA, www.solidworks.com). With the valve geometry known, it was then possible to design and create ports in which to install ultrasonic transducers in the valve, especially with regard to, and as close as possible to the valve center. Information from the CAD drawing was relayed to a 3D printer (Z-Corp., Burlington, MA, USA, www.zcorp.com), which was used to grow the 3-dimensional object. Fig. 2 shows both the design and the positions (TDX Lines 1-3) of the ultrasonic transducers at the center valve geometry.

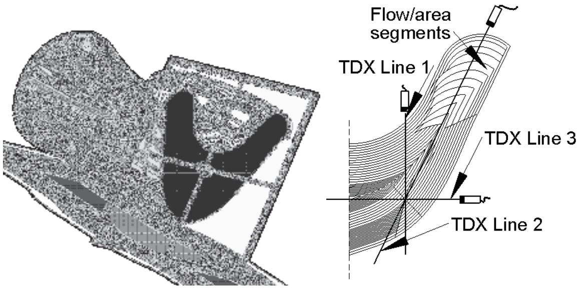

Fig. 2. Isometric view of diaphragm valve design and transducer positions.

3.4 Hyperbolic contraction

Fig. 3 shows the experimental setup for the contraction tests. The hyperbolic contraction used in this work was made of Polymethylmethacrylate (PMMA). The contraction was installed in a 20 l tank and was filled with CMC, thus using it as a coupling fluid. The contraction wall thickness was also optimised to integers of half wavelengths for maximum ultrasonic energy transfer. In this case velocity profiles were measured through the contraction wall interface and not by installing transducers in direct contact with the test fluid, as described for the valve tests.

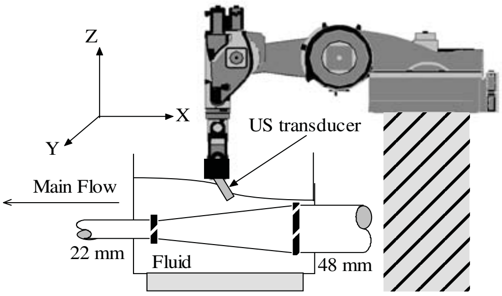

Fig. 3. Contraction setup with robotic arm.

The ultrasonic transducer was moved along the contraction (X-direction) using a high precision (+/-0.03mm) robotic arm (KUKA Roboter GmbH, http://www.kuka-robotics.com). This enabled measurement of a range of velocity profiles from developed to contracting flow and from the results a complete flow map of the velocity field inside the hyperbolic contraction was determined. More details are presented elsewhere [9].

4 RESULTS AND DISCUSSION

4.1 Valve geometry

Velocity profiles measured at three different flow rates (0.5 l/s, 0.99 l/s, 1.7 l/s) inside the valve across TDX Lines 1-3 (see Fig. 2) is shown in Figs. 4-6. Results obtained from measurements across TDX Line 3 are symmetrical around the center position (dotted lines) and was expected due to measuring across a symmetrical axis in the valve. Fig. 5 shows a sharp increase in velocity close to the near wall for all of the lateral measurements.

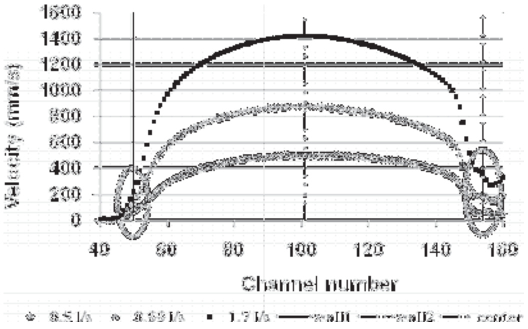

Fig. 4. Radial profiles measured in valve across TDX Line 3 for CMC 6.15% w/w.

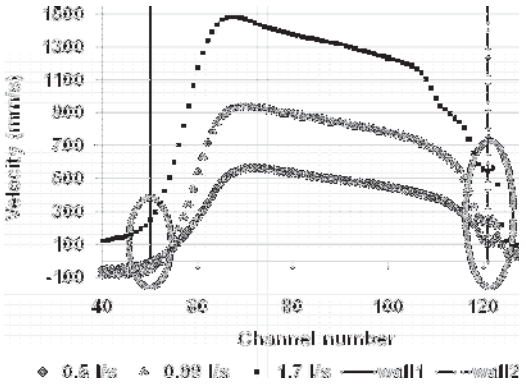

Fig. 5. Lateral profiles measured in valve across TDX Line 1 for CMC 6.15% w/w.

This could be due to the fluid pushing against and under the diaphragm creating higher velocities than compared with velocities measured at a different position in the valve. Velocity profiles measured across the diagonal position (TDX Line 2) shows an increase of velocity from the near wall and steady decrease from the center area of the valve. What is interesting is that at higher flow rates the linear increase of velocity from the near wall to the maximum velocity (as in the 0.5 l/s case) seems to stay constant for some distance, which suggest that most of the fluid flow occurs beyond the valve's upper regions or 'ears'.

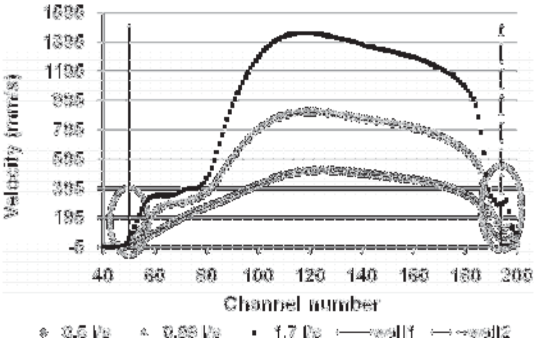

Fig. 6. Diagonal profiles measured in valve across TDX Line 2 for CMC 6.15% w/w.

It can be observed that every experimental velocity profile has non-zero velocities (marked with circles) at the wall interfaces (marked with solid and broken lines, wall1-wall2). Firstly, the increase in velocity at the first wall interface (wall1) is due to the cavities situated in front of the transducer surfaces, where flow occurs before the actual wall position. The increase in velocity at the opposite wall interface (wall2), is due to multiple ultrasonic reflections from the wall, which is inherent in UVP [4]. A velocity distribution colourmap, constructed using Solidworks and Matlab, is presented in Fig. 7.

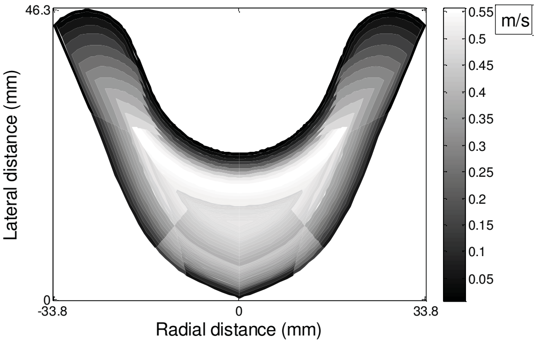

Fig. 7. Velocity distribution 3 colourmap.

The measured volume flow rate was 0.5 l/s and the error difference percentage between the calculated flow rate (0.43 l/s) was 14.86%. Some important observations can be made from the colourmap in Fig. 7. The majority of the flow seems to be at the center area of the valve and not at the upper regions (see Fig. 6). Also, the highest measured magnitudes of velocity appear to be just below the valve diaphragm (see Fig. 5).

4.2 Hyperbolic contraction

Fig. 8 shows the theoretical and experimental velocity distribution inside the hyperbolic contraction using Eq. 1 and UVP. The average error difference percentage between the theoretical and experimental results was 10.37%.

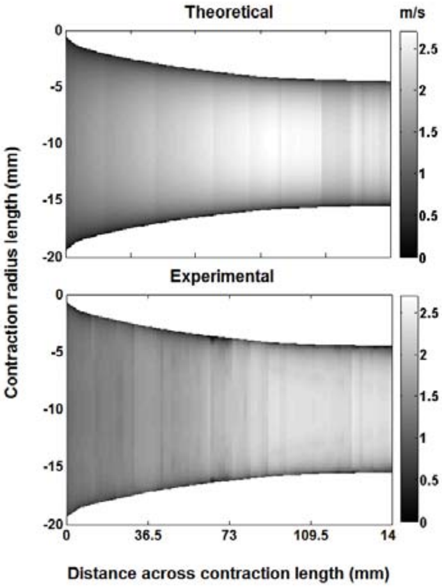

Fig. 8. Experimental and theoretical velocity distribution across contraction length for CMC 2.63% w/w.

This error was mainly due to the temperature dependant properties of the CMC sodium salt, which showed a decrease in viscosity with increasing temperature from fluid pumping effects. A significant amount of energy is required to overcome ultrasonic absorption and penetration depths when measuring through material layers. This loss of energy can also cause problems when measurements inside attenuating fluids are of interest, which is the case with most industrial suspensions.

5 SUMMARY

From our results we conclude that UVP is a suitable method for measuring velocity distributions inside complex geometries. The most important remaining problem in order to increase overall measurement accuracy is velocity measurements from the transducer front at the wall region, where velocity gradients are high. This problem could be reduced by the introduction of new ultrasonic transducers that allows measurements directly at the transducer front. A transducer of this kind where the focal point of the ultrasonic beam is located at the transducer front/wall, is currently under development [4].

ACKNOWLEDGEMENTS

The National Research Foundation of South Africa (NRF), the CPUT and Vetenskapsrådet – The Swedish Research Council, Research Links, for funding. The Adaptronics Advanced Manufacturing Technology Laboratory (AMTL) at CPUT is acknowledged for manufacturing and installation of the diaphragm valve. SIK is gratefully acknowledged for scientific collaboration. Wi-Ka mekaniska are acknowledged for assistance with design and manufacturing of the flow cells. Anders Petterson is acknowledged for assistance with the robotic set-up at SIK.

REFERENCES

[1] McNeil DA, Morris SD: A Mechanistic Investigation of Laminar Flow Through an Abrupt Enlargement and a Nozzle and its Application to Other Pipe Fittings, Technical Report No. Report EUR 16348 EN (2005), European commission, Institute for Safety Technology, Ispra.

[2] Powell RL: Experimental techniques for multiphase flows, Physics of Fluids 20 (2008) 1-22.

[3] Takeda Y: Velocity Profile Measurement by Ultrasound Doppler Shift Method, Int. J. Heat. Fluid. Fl. 7 (1986) 313-318.

[4] Wiklund J, Shahram I, Stading M: Methodology for in-line rheology by ultrasound Doppler velocity profiling and pressure difference techniques, Chem. Eng. Sci. 62 (2007) 4277-4293.

[5] Jensen JA: Estimation of Blood Velocities Using Ultrasound: A Signal Processing Approach, Great Britain, Cambridge University Press (1996).

[6] Bouillard J, Alban B, Jacques P, Xuereb C : Liquid flow velocity measurements in stirred tanks by ultra-sound Doppler velocimetry, Chem. Eng. Sci. 56 (2001) 747-754.

[7] Meile T, De Cesare G, Blanckaert K, Schleiss AJ: Improvement of Acoustic Doppler Velocimetry in steady and unsteady turbulent open-channel flows by means of seeding with hydrogen bubbles, Flow. Meas. Instrum. 19 (2008) 215–221.

[8] Ouriev B, Windhab E: Novel ultrasound based time averaged flow mapping method for die entry visualization in flow of highly concentrated shear-thinning and shear-thickening suspensions, Meas. Sci. Technol. 14 (2003) 140-147.

[9] Zatti D, Wiklund J, Vignali G, Stading M: Determination of Velocities Profiles in Hyperbolic Contraction using Ultrasound Velocity Profiling, Annual Transactions of the Nordic Rheology Society (2009) Vol. 17.

[10] Takeda Y, Kikura H: Flow mapping of the mercury flow, Exp. Fluids. 32 (2002) 161-169.

[11] Bergström J, Vomhoff H: Velocity measurements in a cylindrical hydrocyclone operated with an opaque fiber suspension, Miner. Eng. 17 (2004) 599-604.

[12] Chhabra RP, Richardson JF: Non-Newtonian Flow in the Process Industries. Oxford, Great Britain, Butterworth-Heinemann (1999).

[13] Slatter PT: The role of rheology in the pipelining of mineral slurries, Min. Pro. Ext. Met. Rev. 20 (1999) 281-300.

[14] Met-Flow SA: UVP Monitor Model UVP-DUO User's Guide, Software version 3. Met-Flow SA, Lausanne, Switzerland (2002).

[15] Kotzé R, Haldenwang R, Slatter P: Rheological characterisation of highly concentrated mineral suspensions using an Ultrasonic Velocity Profiling with combined Pressure Difference method, Appl. Rheol. 18 (2008) 62114-1-10.

[16] Fester VG, Kazadi DM, Mbiya BM, Slatter PT: Loss Coefficients for Flow of Newtonian and Non-Newtonian Fluids Through Diaphragm Valves, Chem. Eng. Res. Des. 85 (2007) 1314-1324.

[17] Jacobs P: Stereolithography and Other RP&M Technologies. ASME Press, New York, NY (1996).

Two phase flow

Identification of liquid-gas interface based on ultrasonic reflected signal for two-phase flow velocity measurement

Hideki Murakawa, Ryosuke Sakagami, Katsumi Sugimoto and Nobuyuki Takenaka
Department of Mechanical Engineering, Kobe University
1-1 Rokkodai, Nada, Kobe, 657-8501 Japan

When an ultrasonic velocity profile (UVP) method is applied to two-phase flow measurements, ultrasonic pulses are reflected on both the seeded micro-particles in liquid phase and the gas-liquid interfaces. Hence, the velocity data measured by the UVP method includes velocity information of both phases. Therefore, the phase separation has been a long out standing problem. In order to analyze the reflected signal, UVP system was developed by using a pulser/receiver and a digitizer. The method can select two velocity calculation algorithms that are the Ultrasonic Doppler Method (UDM) and the Ultrasonic Time-domain Cross-correlation method (UTDC). Synchronizing measurement with a high-speed camera and the UDM was established, and measured two-phase flow in a horizontal duct at 2 ms interval. Furthermore, signal analysis of the reflected on liquid-gas and liquid-particles interfaces were conducted. The phase change based on the acoustic impedance. Based on the property, it was found that it was possibly to distinguish between liquid-gas interfaces and micro-particles in liquid phase.

Keywords: UVP, UDM, UTDC, two-phase flow, gas-liquid interface, identification method

1 INTRODUCTION

Two-phase flow has been investigated over the past several decades. However, due to its complexity, some characteristics of the phenomena have not yet been thoroughly understood such as turbulent phenomena, bubbles' motion, and so on. The velocity of rising bubbles is an important parameter to obtain both void fraction and drift velocity in two-phase flow. For understanding the two-phase flow, ultrasonic measurement technique is a powerful tool to obtain the flow parameters. The technique has several desirable characteristics; it is non-intrusive and is applicable to existing pipes. When the ultrasonic velocity profile (UVP) method is applied to the two-phase flow measurements, ultrasonic pulses are reflected on both the seeded micro-particles in liquid phase and the gas-liquid interfaces. Hence, the velocity data measured by the UVP method includes velocity information of both phases. Therefore, the phase separation has been a long out standing problem. Suzuki et al. [1] applied a statistical method based on the velocity different between liquid and bubbles in a vertical duct for measuring the liquid velocity distributions around a bubble. For the other approach, signal intensity method using two ultrasonic frequencies was developed for measuring liquid and bubble velocity distributions individually [2,3]. Velocity analysis is applied for detecting liquid-gas interface measured by a commercial system of UVP [4]. These methods mainly calculated from the obtained velocity profiles.

In order to analyze the reflected signal, ultrasonic velocity profile system was developed. The method can select two velocity calculation algorithms that are the ultrasonic Doppler method (UDM) and the ultrasonic time-domain cross-correlation method (UTDC) [5]. At first, the system was evaluated by measuring single-phase flow. Furthermore, a synchronizing measurement with a high-speed camera and the UDM was established, and measured two-phase flow in a horizontal duct at 2 ms interval. Furthermore, signal analysis of reflected on liquid-gas and liquid-particles interfaces were conducted.

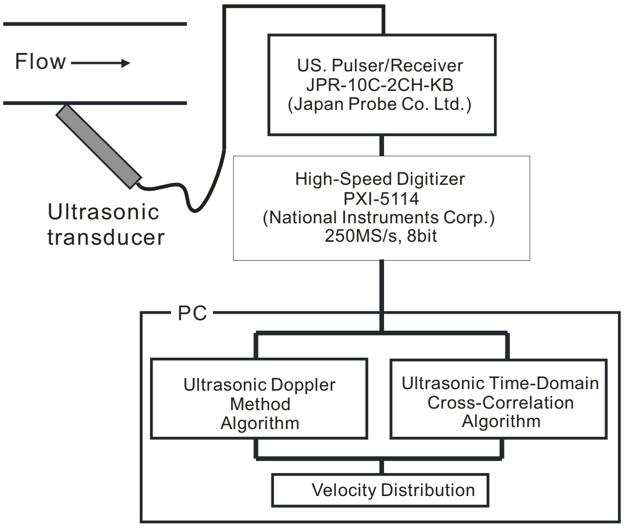

Figure 1: Block diagram of ultrasonic measurement system.

2 ULTRASONIC MEASUREMENT SYSTEM

2.1 Algorithm of velocity measurement

UVP method can be divided into two methods. The one is UDM and the other is the UTDC. The UDM requires multiple ultrasonic emissions for obtaining the Doppler shift frequency [6]. The number of pulse (N_{pulse}) for the velocity calculation and the ultrasonic repetition frequency (f_{prf}) are usually set at 32-128 and 1-8 kHz. Hence, the time resolution is over 4 ms. On the other hand, the UTDC requires only two ultrasonic pulses for obtaining an instantaneous velocity distribution. If the f_{prf} is set at 1 kHz, the time resolution is 1 ms. Therefore, the UTDC is good for measuring the turbulent phenomena in a flow. However, the UTDC is easily affected by noises compared with the UDM. Hence, the UDM is suitable to make understanding or monitoring flow fields.

2.2 Measurement system of UDM and UTDC

In order to select the UVP algorithm, the system was developed as shown in Figure 1. The system composes of an ultrasonic pulser/receiver (JPR-2CH-KB, Japan Probe, Co., Ltd.), a high-speed digitizer (PXI-5114, National Instruments Corp.) and a PC. The measurement software was developed by using C++ and LabView. Ultrasonic is emitted by ultrasonic transducer (TDX) and the pulser/receiver. The reflected signals from seeded particles in water are digitized by the high-speed digitizer, and the signals are computed by the PC. The measurement software was made by the LabView, and instantaneous velocity distributions are confirmed at the software on time. The velocity algorithm of the UDM and the UTDC can be selected.

2.3 Experimental facilities

Experimental facility is shown in Figure 2. Experiments were conducted at a horizontal duct made of acrylic with 50mm –width and 25 mm –height. The working fluids were water and air (for two-phase flow), and the water temperature was kept at 20 – 25 °C. The water was seeded with nylon micro tracer particles at a ratio of 0.1 g/l. The specific density of these particles was 1.02 and the average diameter was 80 µm. The TDX was set at outside of the bottom of the test section. The TDX was submerged in the water in order to adjust the acoustic impedance. The basic frequency of the TDX is 8 MHz with sensor diameter of 3 mm.

3 VELOCITY MEASUREMENTS

3.1 Single-phase flow

In order to confirm accuracy of the developed system, velocity measurements in single-phase flow were conducted by using the UDM and the UTDC algorithm. Flow condition was Reynolds number (*Re*) of 8,000.

The results in the UDM are shown in Figure 3 and 4.

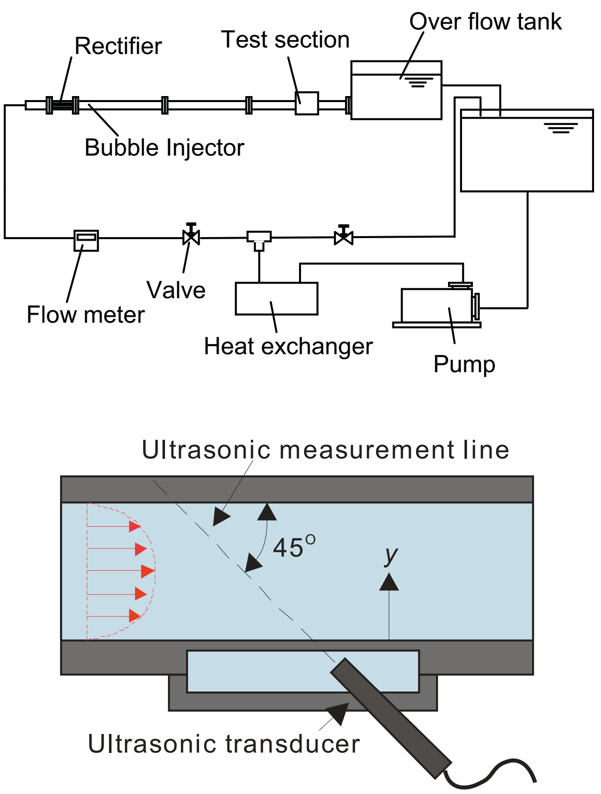

Figure 2: Test loop and the test section. The test loop is a horizontal duct with 50 mm –width and 25 mm –height. TDX was set at outside of the bottom with contact angle of 45°.

Number of instantaneous velocity profile was 10,000. The UDM parameters were N_{pulse} = 128 and f_{prf} = 8 kHz. Hence, 16 ms was required for obtaining the 128 reflected pulses. In the measurement, about 40 ms was taken for an instantaneous velocity profile including the calculation and the data storing time. Figure 3 shows the velocity histogram at center of the channel measured by the UDM. Total number of instantaneous velocity profile is 10,000. It can be confirmed that data of 0 m/s are counted. This means there were some data that could not measure the velocity at the position. In theoretically, the UDM algorithm cannot distinguish if there is not reflected signal or the velocity is 0 m/s at a position. For calculating the average velocity distribution, 0-data was eliminated from the all over the measured data as shown in Figure 4. For easy understanding, the horizontal axis indicates the average velocity, and the vertical axis indicates the distance from the bottom surface of the channel. It can be confirmed that the average velocity distribution could be obtained. However, it is difficult to distinguish between 0 m/s and no-data from the velocity histogram at lower velocity such as around near wall region. Therefore, the distinction method whether there is a particle or not is required for more accurate measurement.

A result measured by the UTDC is shown in Figure 5. In the experiment, f_{prf} was set at 1 kHz, and the time resolution was 1 ms. The black bar represents effective data number at the position. Although the total number of measurement is set at 20,000, obtained data changes with the position. If the reflected signal didn't obtained, or the calculated cross-correlation function is less than the setting values at a position, the velocity is recorded as no-velocity data. Therefore, the number of calculated velocity normally decreases with the distance from the TDX because the ultrasonic signal weakens. The method is difficult to obtain an instantaneous velocity distribution at all the measurement positions in the flow. In order to understand the flow field, ensemble average might be required. However, it can distinguish the data of 0 m/s and no-data. If the number of reflector particles is low, the average velocity distribution can be obtained. Therefore, the method is useful for measuring turbulent flow.

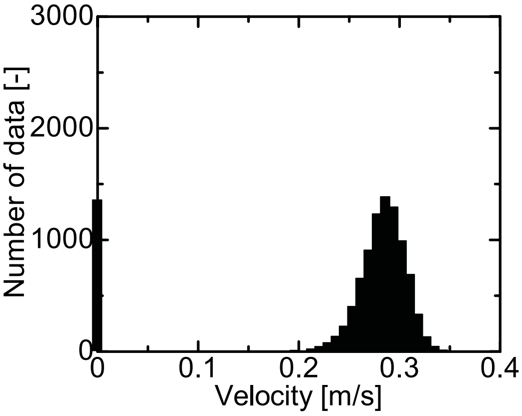

Figure 3: Velocity histogram at center of the channel. The data include 0 m/s which is no-data.

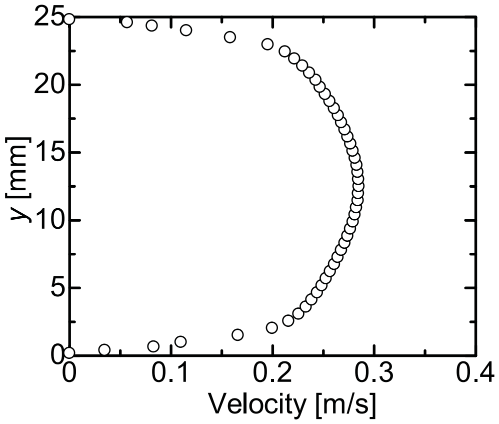

Figure 4: Average velocity distribution measured by using the UDM. 0-data was eliminated for averaging the velocity.

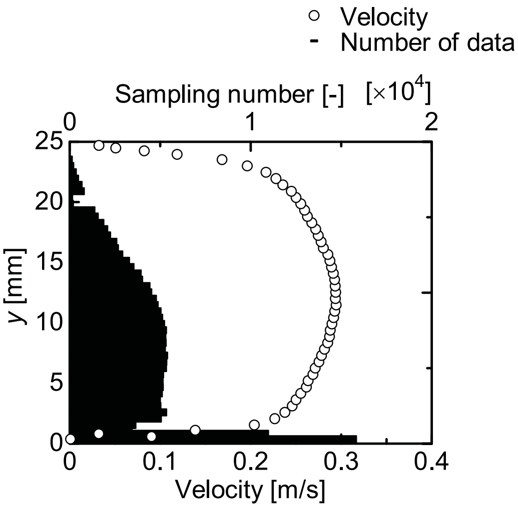

Figure 5: Average velocity distribution measured by using the UTDC. Number of data changes with measuring position.

3.2 Two-phase flow

In order to determine the liquid-gas interface, synchronized measurement of high-speed camera and the UDM was conducted. Frame rate of the high-speed camera was set at 500 fps, and the N_{pulse} and f_{prf} of the UDM were 128 and 8 kHz. For the UDM measurement, reflected signal was recorded continuously up to maximum onboard memory in the digitizer. After all the wave signals

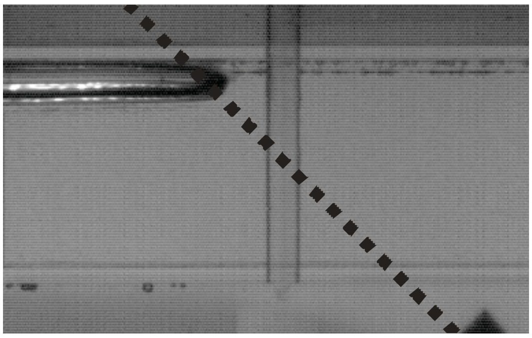

(a) A picture of two-phase flow taken by the high-speed camera.

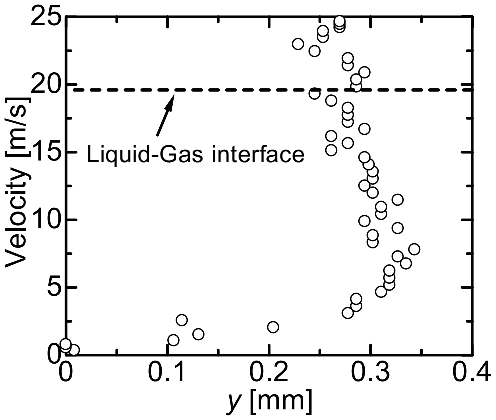

(b) Instantaneous velocity distribution around the bubble nose.

Figure 6: Synchronized measurement of high-speed camera and the UDM in two-phase flow. The liquid-gas interface was determined by the picture.

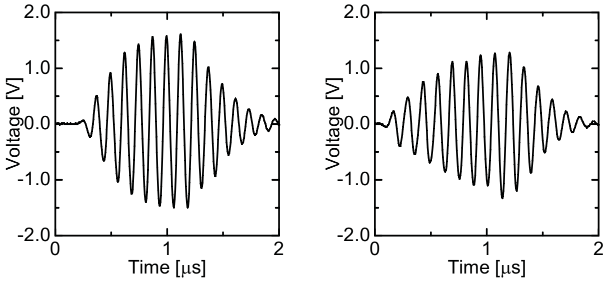

(a) Water-Air interface (b) Water-Acrylic interface

Figure 7: Reflected signal from the interfaces

Table 1 Acoustic impedance of materials

	Acoustic impedance [kg/(m^2·s)]
Water	1.5×10^6
Air	4.3×10^2
Nylon-6,6	2.9×10^6
Acrylic	3.2×10^6

were recorded, instantaneous velocity distributions were calculated. As 32 waves were shifted from the previous calculation waves, velocity distributions were obtained every 2 ms.

A result of the measurement is shown in Figure 6. The superficial liquid velocity (J_L) was 0.24 m/s, and the superficial gas velocity (J_G) was 0.024 m/s. The flow regime was plug flow as shown in the picture. The bubble velocity obtained from the pictures was about 0.25 m/s. Synchronizing with the system, the liquid velocity distributions around a bubble could be obtained. It was observed that the bubble affects the liquid velocity, and the bubble induced the liquid turbulence. However, it is difficult to determine the liquid-gas interface from the instantaneous velocity distribution.

4 ANALYSIS OF ULTRASONIC REFLECTED WAVE

For applying the method for measuring two-phase flow in an opaque pipe, the synchronization with the high-speed camera cannot be applied. Therefore, identification method of liquid-gas interface by using the reflected signal was studied.

Figure 7 shows comparison of ultrasonic reflected signal from water-air and water-acrylic. It is confirmed that the phase of the wave changed in 180° depending on the interface. Because phase of the wave changes when the wave reflects on an interface from higher to lower acoustic impedance. Table 1 shows acoustic impedance of several materials. From the table, it is also confirmed that the reflected signal from nylon particles doesn’t change the phase. If the phase detection technique is applied for the UTDC under low particle concentration, the reflection signal can be distinguished between liquid-particle and liquid-gas interfaces.

5 SUMMARY

In order to apply the UVP method for measuring two-phase flow, a system was developed. It can select velocity algorithms of the UDM and the UTDC. It was confirmed that the system can be used for measuring single-phase flow. In order to measure two-phase flow in a horizontal duct, the system was synchronized with a high-speed camera. The liquid velocity aroud bubbles were obtained by detecting the interface. In order to apply the technique for measuring two-phase flow in an opaque pipe, wave analysis of the reflected signals was studied. It was confirmed that the difference of the phase shift depending on the accousitc impedance might be used for identification of the interfaces.

ACKNOWLEDGEMENTS

The authors acknowledge Kansai Research Foundation for technology promotion (KRF) for their financial support. Part of this work was also supported by KAKENHI (Grant-in-Aid for Young Scientists (B), 21760132)

REFERENCES

[1] Y. Suzuki, M. Nakagawa, M. Aritomi, H. Murakawa, H. Kikura, M. Mori: Microstructure of the flow field around a bubble in counter-current bubbly flow, Exp. Thermal and Fluid Sci., 26 (2002) 221-227

[2] H. Murakawa, H. Kikura, M. Aritomi: Application of ultrasonic doppler method for bubbly flow measurement using two ultrasonic frequencies, Exp. Thermal and Fluid Sci., 29 (2005) 843-850

[3] H. Murakawa, H. Kikura, M. Aritomi: Application of ultrasonic multi-wave method for two-phase bubbly and slug flows, Flow Measurement and Instrumentation, 19 (2008) 205-213

[4] Y. Murai, H. Fujii, Y. Tasaka, Y. Takeda: Turbulent bubbly channel flow investigated by ultrasound velocity profiler, J. Fluid Sci. and Tech., 1 (2006) 12-23

[5] G. Yamanaka, H. Kikura, M. Aritomi: Study on the development of novel velocity profiles measurement method using ultrasonic time-domain cross-correlation. Proc.3rd Symp. Ultrasonic Doppler Methods for Fluid Mech. and Fluid Eng., Lausanne, Switzerland, (2002) 109-114

[6] Y. Takeda: Velocity profile measurement by ultrasound Doppler shift method, Int. J. Heat & Fluid Flow, 7 (1986) 313-318.

Two-phase flow monitoring using ultrasonic multi-wave technique

Daisuke Ito, Hiroshige Kikura and Masanori Aritomi
Research Laboratory for Nuclear Reactors, Tokyo Institute of Technology, Japan
2-12-1-N1-13 Ohokayama, Meguro-ku, Tokyo 152-8550

Two-phase flow has been recognized as one of the most important phenomena in fluid dynamics. In order to clarify the flow structure, two-phase flow parameters have been measured by using many effective measurement techniques. The velocity profile as one of the important flow parameter has been measured by using ultrasonic velocity profiling technique. This technique can measure velocity distributions along a measuring line, which is a beam formed by pulse ultrasounds. Furthermore, a multi-wave sensor with more than two oscillators can measure the velocity profiles of both gas and liquid phase by separating the reflected echo signals. In this study, multi-wave sensors are applied to air-water bubbly flow monitoring. At first, the transmitted sound pressure fields were investigated to apply these sensors to flow measurement by experimental and numerical approaches, and the beam formation was estimated. Then, the echo signals reflected from air-water bubbly flow in a vertical rectangular channel were measured by using the sensors, and the flow structures were estimated from statistical analysis and velocity profiling process of echo signals.

Keywords: Two-phase flow, ultrasonic velocity profile measurement, multi-wave sensor

1 INTRODUCTION

Gas-liquid two-phase flow is a flow phenomenon which usually appears in the nuclear and thermal power plants, and it is one of the keys to the proper operation of many instruments in the plants. For the clarification of gas-liquid two-phase flow, the experimental studies have been performed. In conventional studies, a number of measuring techniques have been developed and investigated in order to clarify the flow structure. As one of the most effective two-phase flow monitoring method, wire-mesh tomography (WMT) has been developed [1] and applied to many two-phase flow measurements. In WMT, two-phase flow parameters (instantaneous void fraction distribution, bubble size and bubble velocity etc.) can be estimated by measured electrical conductivity between crossing wires. However, the intrusive effect to the bubble velocity cannot be ignored [2]. Therefore, the authors focused on ultrasonic velocity profiling (UVP) technique not only for the bubble velocity measurement but also for the liquid measurement. As the previous studies, UVP method has been successfully applied to air-water bubbly flow measurement with multi-wave sensor which has more than two oscillators [3]. In addition, as a high time-resolution UVP technique, ultrasonic time-domain cross-correlation (UTDC) method has been developed and applied to flow measurement [4].

In this study, multi-wave sensors are used for multi-wave ultrasonic velocity monitoring in two-phase bubbly flow. The ultrasonic sound field transmitted into water is important to improve the UVP measurement accuracy, because the measuring volume is defined by the beam diameter and channel distance. As the previous study, sound pressure distributions have been investigated by experimental method. So the ultrasonic transmission characteristics of multi-wave sensors are investigated by experimental and numerical analysis, and the effect on the measurement volume or ultrasonic beam formation is evaluated. In air-water bubbly flow in a vertical rectangular channel, the echo signals are measured and the bubble velocity profiles are estimated by using UTDC algorithm.

2 CHARACTERISTICS OF ULTRASONIC TRANSMISSION

2.1 Sound field measurement

The sound pressure distributions transmitted into water were measured by the hydrophone technique. This system consists of a pulser devise, a receiver device, an automatic 3D stage and a thermostatic water bath, as shown in Fig.1. The pulse signal sent from pulser is transmitted into water by the sensor. The water temperature is maintained at 30 degrees Celsius by the thermostatic water bath. At this temperature, the sound speed in water is 1510 m/s.

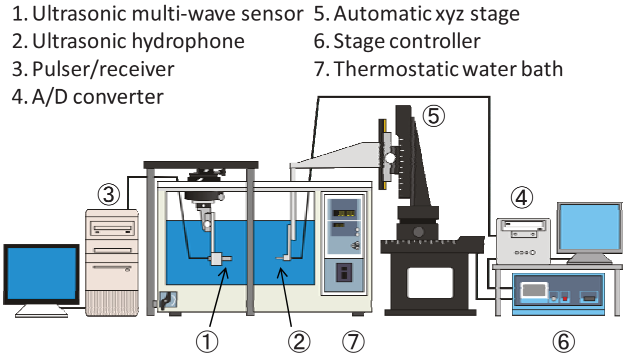

Figure 1: Schematic diagram of sound field measurement system.

The ultrasonic hydrophone fixed on the 3D stage was traversed in the test region and it receives the electrical signals with the piezoelectric element of the hydrophone. This element has a detecting area of 1×1mm^2. This technique can measure the time series data of received signals and it is applicable to the transmitting path analysis of ultrasonic pulse in three-dimensional space.

2.2 Sound field calculation

The numerical analysis of the sound field was carried out to compare with the measurement and to obtain smaller spatial resolution. The sound pressure *p* is given by Rayleigh equation, as shown in the following equation.

$$P = \rho \int_{S_T} v'_T \left(t - \frac{r}{C} \right) \frac{dS}{2\pi r} \tag{1}$$

The Rayleigh equation with ring function [5] was applied to simplify the calculation and to reduce the time in sound field calculation. From this numerical analysis, the spatial sound pressure distribution and the temporal change of ultrasonic pulse can be estimated.

2.3 Sound pressure distributions

The measured and calculated sound pressure distributions with 2MHz multi-wave sensor are shown in Fig.2. The color map represents the intensity normalized by the maximum value of detected voltage in the test area. There are only a few differences between experiment and simulation. It may result in the hydrophone size. This means that the size of 1mm^2 is little bit small in the experiment. From this sound field estimation, it shows that there is a weak area of ultrasonic intensity in the near region. This sound pressure attenuation attributed to the doughnut-shaped element of the 2MHz multi-wave sensor.

The 3D distributions of ultrasonic beam with iso-surface of -3dB of maximum pulse intensity are shown in Fig.3. Although the beam of the normal sensor has good shape, the beam near the sensor (x=0~20mm) becomes bicylindrical shape in multi-wave sensor. It is called “hollow effect”. In these regions, it is difficult to define the measurement volume. However the beam after x=20mm has single cylindrical shape and a nearly-constant diameter. Therefore, the ultrasonic beam without hollow effect should be used for the flow measurement.

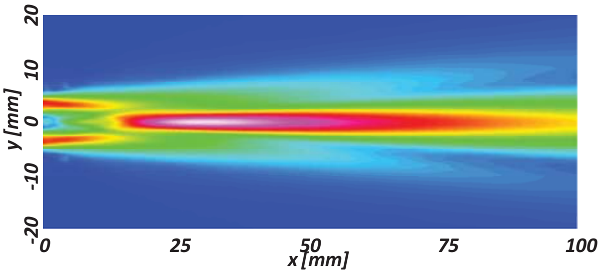

(a) Experimental result

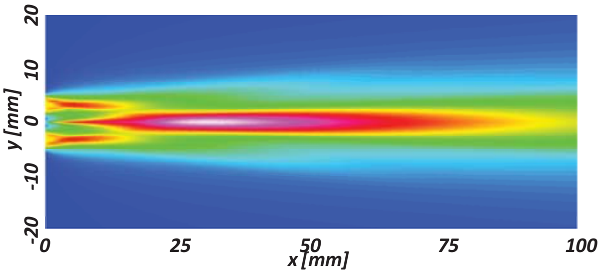

(b) Calculation result

Figure 2: Comparison of sound pressure distributions measured and calculated in *f*=2MHz, 2cycle/pulse, D_{out}=1mm and D_{in}=3mm.

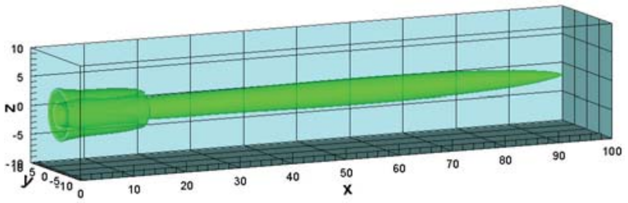

(a) 2MHz multi-wave sensor

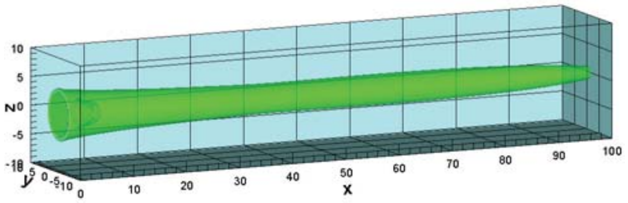

(b) 2MHz normal sensor

Figure 3: 3D sound field calculating results in *f*=2MHz, 2cycle/pulse, D_{out}=1mm and D_{in}=3mm.

3 EXPERIMENTAL SET-UP

The experimental set-up consists of an air-water circulation system, a test channel section and a measurement system, as shown in Fig. 4. Working fluids are air and water. Water temperature is kept around 20 degrees Celsius by the cooling water. Air flow quantity is measured by a laminar flow flowmeter. Air inlet is made of 5 metal needles set at 100mm downstream from the flow straightener. The outer diameter of each needle is 2 mm and the diameter of holes drilled in each needle is 1 mm. The tip of the needle is round in order to reduce influence on the flow. All the needles are set in parallel to give the same performances. In this study, gas flow rates from 5 nozzles were controlled individually and non-uniform distribution was formed in the test section with G1~G5, as shown in Fig.5.

The total length of the test channel is 1,800 mm and the length between gas injection and test section is about 1,200 mm. The channel cross section is rectangular, 20×100 mm^2, so the hydraulic equivalent diameter is about 33 mm.

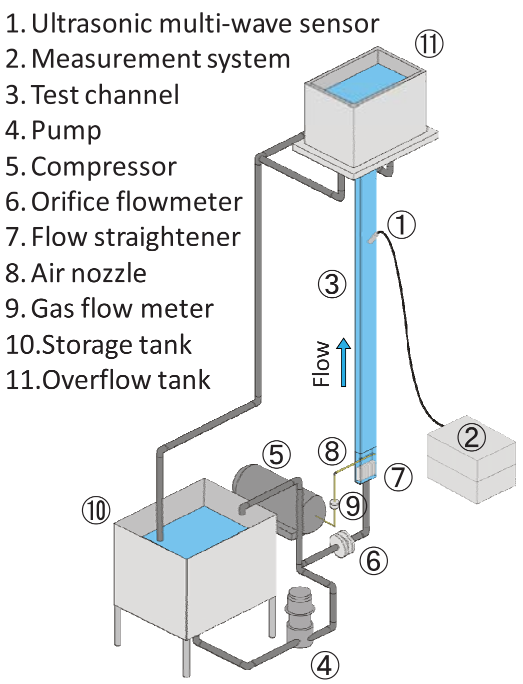

Figure 4: Schematic diagram of experimental set-up.

Table 1: Flow condition

Working fluid	Air, water
System pressure	Atmosphere
Superficial liquid velocity	0.1 m/s (constant)
Superficial gas velocity	1 ~ 5 mm/s (varied)
Temperature of water	20 °C

The measuring section with the ultrasonic multi-wave sensor is made of acrylic glass because it has almost the same acoustic impedance as water. In consequence, it is also useful for image or optical measurement. An ultrasonic multi-wave sensor was set up at 45 degrees in the outside of the channel and the wall thickness of test section was 1mm due to increase the transmission intensity of ultrasound and to decrease the influence of the reflected echo from the wall. Furthermore, as the results of ultrasonic sound field analysis, the ultrasonic beam without the hollow effect was applied to the measurement using 2MHz multi-wave sensor. The multi-wave measurement system is illustrated in Fig.6. A pulse ultrasound is transmitted from the sensor connected to an ultrasonic pulser/receiver (TIT-10B-USB; Japan Probe) controlled by PC. After the ultrasonic pulse was transmitted, the same element detects a reflected echo from an interface of water and bubbles, and then the signal amplified by the receiver was recorded using a digital oscilloscope (WaveRunner 44Xi; LeCroy). The measured signals were analyzed by statistical work and UTDC method.

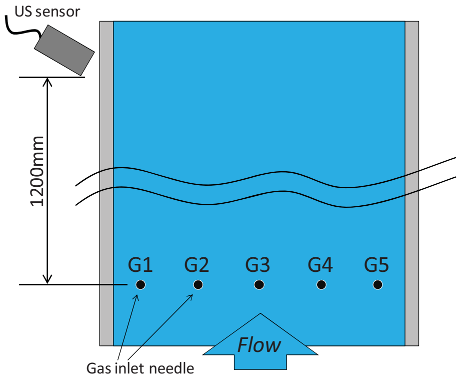

Figure 5: Air nozzle and gas inlet condition.

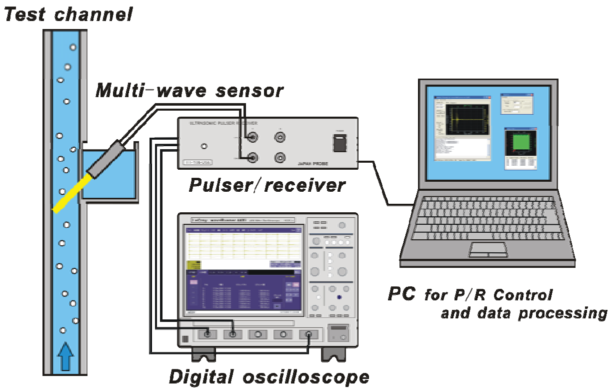

Figure 6: Ultrasonic multi-wave measurement system.

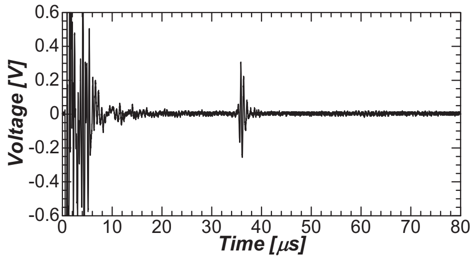

(a) t=0ms

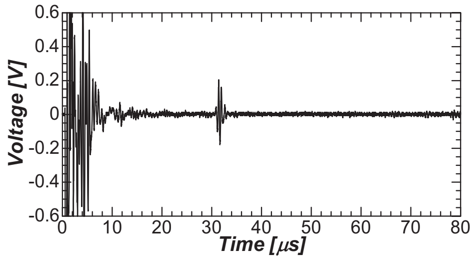

(b) t=10ms

Figure 7: Typical instantaneous echo signals reflected from bubbles (J_G=5mm/s).

4 RESULTS AND DISCUSSION

The typical echo signals reflected from bubbly flows are shown in Fig.7. The horizontal axis is time and the vertical axis is the detected voltage. The signal reflected from bubble appears and the echo moves toward the sensor surface as the bubble goes up.

Then, UTDC velocity estimation was applied to the

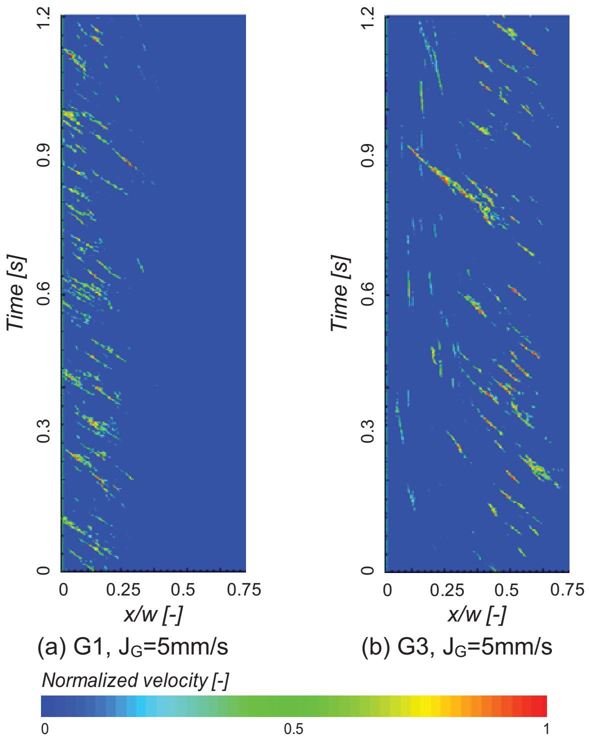

(a) G1, J_G=5mm/s (b) G3, J_G=5mm/s

Figure8: Spatio-temporal bubble velocity distributions estimated by UTDC method from measured echo signals.

measured echo profiles, and the instantaneous bubble velocity profiles were obtained. The spatio-temporal distributions of estimated bubble velocity with 2MHz sensor are shown in Fig.8. The velocity normalized by the maximum velocity was represented by the color plot. Bubble velocities were measured when bubbles pass through the ultrasonic beam. The presence of bubble and passing frequency were found from these figures. The approximate size of bubbles may be estimated by the length of bubble trajectory. Comparing the gas inlet condition, bubbles flow near the wall in Fig.8 (a). On the other hand, there are many bubbles in the center of channel, as shown in Fig.8 (b). In addition, the dispersion of the bubbles is larger than gas inlet from G1.

The measured velocity profiles were averaged and illustrated in Fig.9. In the horizontal axis of this figure, 0mm means the wall of the flow channel and 50mm means the channel center. The profile shapes were changed by depending on the gas inlet condition with the same superficial velocity. However the relation between measured profiles, void distribution and ultrasonic transmission characteristics should be evaluated for high accurate measurement.

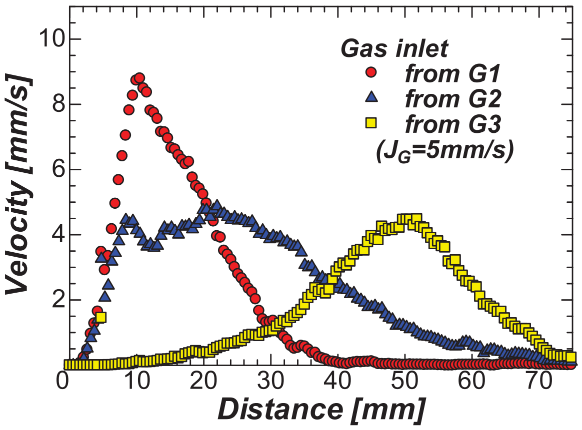

Figure 9: Averaged velocity profiles (averaging whole instantaneous velocity profiles).

5 SUMMARY

The applicability of the ultrasonic multi-wave sensors to air-water bubbly flow in the rectangular channel were investigated. The ultrasonic transmission characteristics of the sensor were investigated by experimental and numerical analysis and the effect on the measurement volume and ultrasonic beam formation, especially hollow effect, were evaluated. In air-water bubbly flow in a vertical rectangular channel, the reflected echo signals were measured using multi-wave sensor and the bubble velocity profiles are estimated by UTDC method. The effect of the ultrasonic beam characteristics should be clarified for the accurate ultrasonic velocity measurement.

REFERENCES

[1] Prasser H-M: A new electrode-mesh tomograph for gas-liquid flows, Flow Meas. Instrum. 9 (1998) 111-119.

[2] Ito D, Kikura H, Aritomi M, Prasser H-M: Bubble velocity estimation with three-layer wire-mesh sensor, ISFV13 (2008).

[3] Murakawa H, Kikura H, Aritomi M: Application of an ultrasonic array sensor to air-water bubby flow measurement, Flow Meas. Instrum. 19 (2008) 205-213.

[4] Yamanaka G, Kikura H, Aritomi M: Study on the development of novel velocity profiles measurement method using ultrasonic time-domain cross-correlation, Proc. ISUD3 (2002) 109-114.

[5] Ohtsuki S: Calculation method for the nearfield of a sound source with ring function, J. Acous. Soc. Japan, 30-2 (1974) 76-81.

Liquid metals

Investigations of the bulk flow inside a cylindrical liquid metal column generated by diverse AC magnetic fields

Dirk Räbiger[1], Chaojie Zhang[1], Ilmars Grants[2], Sven Eckert[1] and Gunter Gerbeth[1]

[1] MHD Department, Forschungszentrum Dresden-Rossendorf, P.O. Box 5101119, 01314-Dresden, Germany

[2] Institute of Physics, University of Latvia, Miera iela 32, LV-2169 Salaspils, Latvia

This presentation considers various situations where the flow inside a liquid metal column is driven by different configurations of AC magnetic fields. The Ultrasound Doppler Method has been used to determine profiles of the fluid velocity in the ternary alloy GaInSn. The azimuthal and vertical velocity components have been measured allowing for an analysis of both the swirling flow in the horizontal planes and the flow pattern in the radial-meridional plane. In the first part we study the combination of a traveling and a rotating magnetic field which may generate a specific flow phenomenon in form of a concentrated vortex with properties similar to a tornado. The second part is concerned with the transient liquid metal flow which is generated by the discontinuous application of a rotating magnetic field (RMF). Such new approaches have been recently suggested for melt stirring during solidification of metal alloys. Finally, we consider an RMF-driven flow which is influenced by an oxide layer at the free surface of the metallic melt. Our measurements demonstrate that the occurrence of the oxide layer may lead to an unexpected oscillating behaviour of the bulk flow.

Keywords: Ultrasound Doppler Method, liquid metal, electromagnetic stirring, mixing

1 INTRODUCTION

Alternating (AC) magnetic fields are widely used in casting, metallurgy and crystal growth for melt stirring. For instance, the electromagnetic stirring is applied to provide an efficient mixing of metallic melts, to control the flow at the mold region in the continuous casting process or to achieve a purposeful alteration of the microstructure of casting ingots. In general, the principle of electromagnetic melt stirring can provide a diversity of flow pattern according to the requirements of the application under consideration. Besides simple variations of magnetic field strength and frequency, combinations of various kinds of magnetic fields and/or temporal modulations of the magnet field parameters are possible to produce different structures of the flow-driving Lorentz force. A detailed knowledge about the transient flow structures arising from the field modifications is necessary for a well-defined flow control. A mismatch of the relevant modulation parameters may lead to worse results.

2 EXPERIMENTAL SETUP

We consider an axisymmetric configuration of a finite, closed cylinder filled with liquid metal which is affected by diverse AC magnetic fields. The flow measurements have been carried out using the ternary eutectic alloy Ga68In20Sn12, which has a melting point of about 10°C and shows the following properties at room temperature: electrical conductivity $\sigma = 3.2\times10^{6}$ Sm^{-1}, density $\rho = 6.36\times10^{3}$ kgm^{-3} and viscosity $\nu = 3.4\times10^{-7}$ m^{2}s^{-1}. A schematic view of the experimental setup is depicted in Fig. 1. Fluid vessels were made from Perspex with a radius *R* of 30 mm and 45 mm, respectively. The height of the liquid metal column *H* was chosen to be 60 mm or 90 mm ensuring an aspect ratio *2R/H* of unity. The experiments were performed in the magnetic induction system COMMA at FZD. Six coils are arranged in a pole-pair connection to create the rotating magnetic field with an effective magnetic induction up to a maximum value of 25 mT. The fluid vessel was placed concentrically in the bore diameter of the magnetic system. In order to preclude flow artifacts arising from symmetry deviations of the experimental set-up (vertical alignment, conformity of both the cylinder and the magnetic field axis), special care was necessary to ensure a precise positioning of the cylinder inside the magnetic system. The homogeneity of the magnetic field was checked using a 3-axis Gauss meter (Lakeshore model 560, sensor type MMZ2560-UH). Within the radial dimension of the fluid container, the variance of the magnetic field strength was found to be smaller than 3%.

The flow velocities were measured by a DOP2000 velocimeter (model 2125, Signal Processing SA) equipped with 8 MHz (TR0805LS) transducers. Two pairs of ultrasound transducers were arranged horizontally at the cylinder side wall to measure the azimuthal velocities. Sensor 1 and 2 were positioned 15mm above the cylinder bottom, while sensor 3 and 4 were situated 15mm below the free surface. The radial distance between the two pairing sensors is 2*d* = 16 mm. Each transducer acquired directly the velocity component projected on the ultrasound beam line. The distribution of the fluid azimuthal velocity along the cylinder radius can be reconstructed based on the method described in [1]. In the experiment, we also measured the vertical velocity profiles by arranging an array of transducers vertically along the diameter at the cylinder bottom. Fig. 1 shows an example with a single transducer at the center of the cylinder bottom. Because of the divergence of the ultrasonic beam the lateral size of the measuring volume increases with the distance from the transducer. Hence, the spatial resolution in lateral direction varies from 5 mm at the sensor to approximately 7.5 mm at the opposite wall of the fluid vessel. In axial direction a spatial resolution of about 1.4 mm was achieved. The velocity data were acquired with sampling frequencies between 3.5 and 25 Hz. The accuracy of the velocity data can be assessed to be better than 0.15 mm/s.

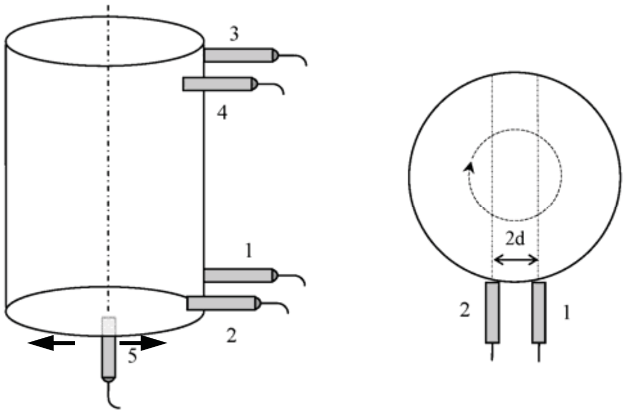

Figure 1: Sketch of the experimental setup showing the arrangement of the ultrasonic transducers to measure the swirling flow (sensors 1-4) and the vertical velocity (sensor 5).

3 RESULTS

3.1 Superposition of different AC magnetic fields

When rotation is added to a converging flow, an intense vortex appears which may become manifest in many spectacular flows ranging from bathtub vortex tropical cyclones. Both, the converging flow and the rotation can be induced by magnetic forces in a volume of liquid metal. We consider here a GaInSn melt in a cylindrical container. The poloidal flow is driven by an axial upwards traveling magnetic field, and the azimuthal flow is produced by a rotating magnetic field. Both resulting forces are schematically drawn in Fig. 2(a). A separate application of a TMF causes a converging flow at the top of the cylinder as shown in Fig. 2(b).

Acting alone the TMF drives a downward mean flow in the central portion of the cylinder (Fig. 3(a)). The negative velocities correspond to a descending flow. The superposition of an additional RMF suppresses the downward motion along the axis until a reversal of the flow direction can be observed. The condition of this flow reversal was found to occur at a constant ratio of axial and azimuthal forces [1]. This axial velocity reversal is associated with the formation of a two-cell structure as shown in Fig. 3(b). Similar flow patterns have been observed in tropical cyclones and tornados as well as in respective laboratory models [2, 3] or numerical simulations [4]. Such structures are generated when the radial inflow is stopped and turned back at some equilibrium radius by inward increasing centrifugal forces.

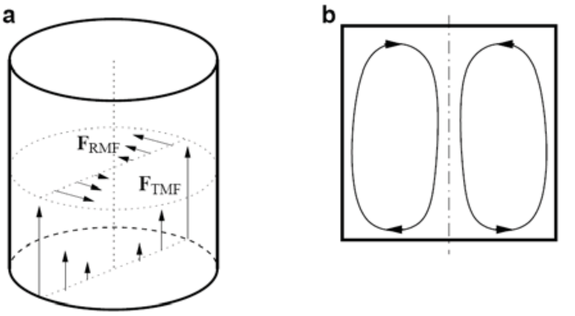

Figure 2: (a) Schematic representation of the body forces induced by TMF and RMF, respectively; (b) the meridional flow pattern in an upwards TMF-driven flow.

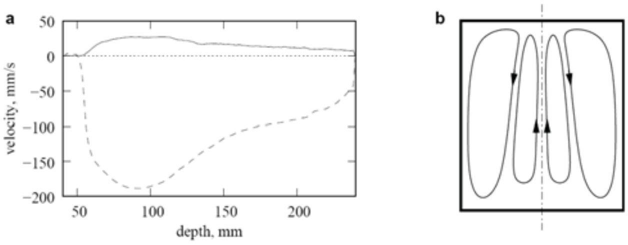

Figure 3: (a) Axial velocity along the cylinder axis for the application of a TMF (dashed line) and combined TMF and RMF (solid line); (b) schematic representation of the two-cell regime.

3.2 Electromagnetic stirring using a time-modulated RMF

Recently, it has been demonstrated that a melt stirring using a modulated RMF can enforce higher mixing rates, but at lower energy consumption as compared with a continuously applied RMF [5]. We investigated the case if an RMF acts upon a cylindrical column of liquid metal, while the field strength is modulated in two different ways. First, we used a succession of RMF pulses that always have the same rotational direction. Second, we applied an RMF pulse sequence of alternating direction.

The problem of macrosegregation has to be considered as a key problem concerning magnetic field application for melt stirring during the solidification of metal alloys [6]. This phenomenon is attributed to the secondary flow driven by the Ekman-pumping specifically arising in a rotating fluid in form of a double vortex. The radial component of the secondary flow, which passes along the solidification front, conveys solute-rich melt towards the axis of rotation. Consequently, the radial convection along the solid-liquid interface causes an accumulation of solute in the central region of the sample, whereas a corresponding depletion of solute has to be registered in regions near the lateral walls. Thus, the segregation problem could likely be avoided by melt stirring with a permanent change of flow direction at the solidification front.

A pronounced double vortex structure with a periodic inversion of the sign of vorticity can be obtained by melt stirring using a pulsed RMF [5]. However, such a flow pattern can only be obtained for a very narrow range of pulse frequencies. This is illustrated by the time series of the local velocity presented in Fig. 4. A frequency of 0.475 Hz provides regular oscillations of the vertical velocity. The realization of lower or higher frequencies implies a weakening of the secondary flow and a loss of the periodicity of the flow.

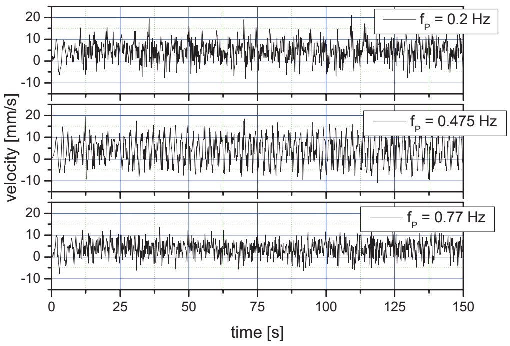

Figure 4: Time series of the vertical velocity in case of RMF pulses with unidirectional sense of rotation showing the effect of variations of the pulse frequency f_p.

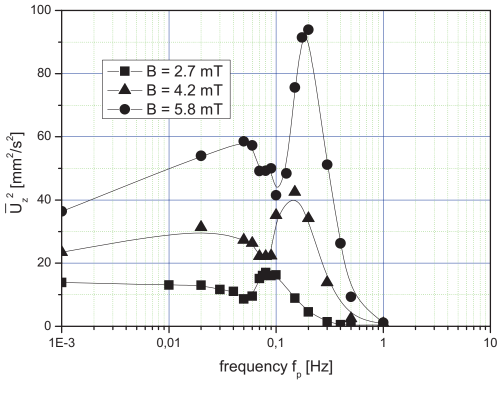

Figure 5: Dependence of the intensity of the secondary flow on the frequency of reversals of rotational direction f_p.

The parameter f_p plays an important role also in the case of an RMF pulse sequence of alternating direction. The square value of the vertical velocity U_z represents an indication with respect to the intensity of the secondary meridional flow. Fig. 5 displays this quantity as function of the frequency f_p. It becomes obvious that pronounced maxima of the energy of the secondary flow occur at selective frequencies, varying for different values of the magnetic field strength. Recent investigations have demonstrated that the optimal values of these modulation frequencies correspond to characteristic time scales of the RMF spin-up process [5, 7].

3.3 Influence of oxide layers on an RMF-driven flow

Liquid metal flows driven by an RMF inside a cylindrical container have been frequently investigated by numerical simulations for both situations of a free surface of the melt or a solid boundary at the top of the fluid vessel. The solid end walls are responsible for the existence of an axial gradient of the angular velocity which drives the secondary motion in the radial-meridional plane in form of a double vortex structure. Albeit the ideal assumptions taken as boundary conditions for the numerical calculations almost all technical applications of melt stirring occur with a free surface of the melt which is covered by an oxide layer.

We conducted measurements of the bulk flow inside a liquid metal column at which the fluid surface was covered by a layer of oxides. Figure 6 reveals a peculiar phenomenon which was observed within a particular parameter range. In case of a complete coverage of the free surface with oxide particles the secondary flow may become unstable and exhibits distinct periodic oscillations.

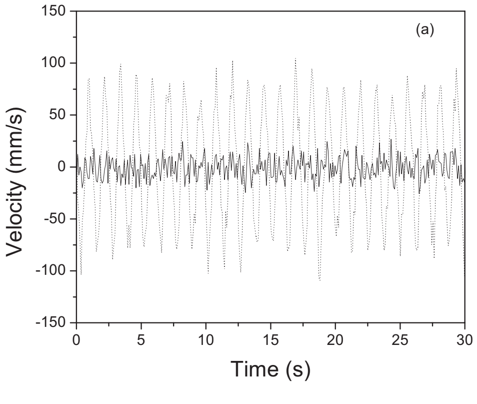

Figure 6: Time series of the vertical velocity on the cylinder centerline in the case of a regular RMF-driven flow (solid line) and in case of appearing flow oscillations (dotted line)

This effect can be explained by the nonlinear interaction between the primary swirling flow and the secondary flow [8]. This interaction manifests itself in a variation of the poloidal vortex lines, the best known example of which is the inertial wave in case of an RMF spin-up [9]. The secondary flow, which is induced by an axial gradient in the swirl, tends to eliminate the non-uniformity in the angular velocity by a redistribution of angular momentum. The inertial oscillations during the RMF-driven spin-up are forced by the rapid increase in the rotation rate. Because of viscous damping, these oscillations decay and can be observed therefore only over a finite period of time. The permanently occurring oscillations in the present case are triggered by the oxide layer at the surface. This covering layer is affected by a torque induced due to the swirling fluid below and a friction force from the side walls. At the beginning of the process, if the rotation rate is low, the layer is coupled with the wall and not moving therefore. This situation is similar to the case of an enclosed cylinder.

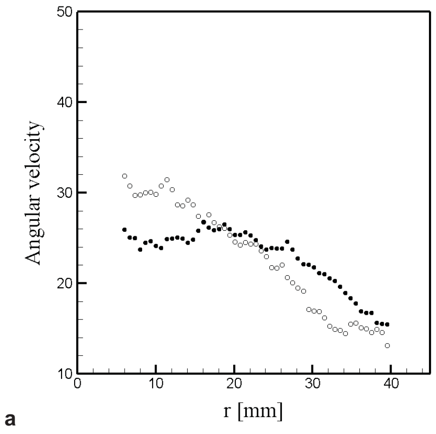

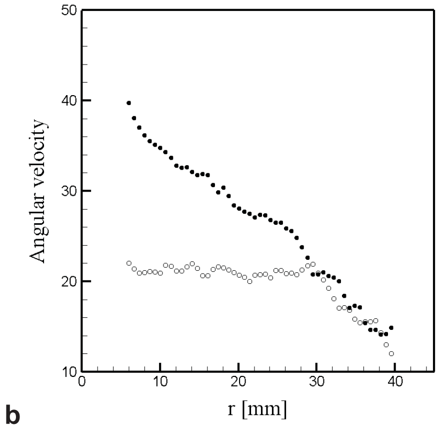

Figure 7: Two snapshots showing the differential rotation in the cylinder. Solid dots represent the angular velocity profile 15 mm above cylinder bottom (transducer 1); open circles represent the angular velocity profile 15 mm below the free surface (transducer 3). (a) the core of the fluid column rotates faster at the surface; (b) the core rotates faster at the bottom of the cylinder.

An acceleration of the liquid provokes a separation of the oxide layer from the side walls. Owing to the uneven boundary conditions the fluid rotates faster now at the surface. A poloidal flow comes up which redistributes the angular momentum leading to an acceleration of the liquid above the bottom of the vessel accompanied by a deceleration of the swirl near the surface. The oxide layers may reattach to the side wall and finally an inversion of the swirl distribution occurs. As a result, the azimuthal velocities in the upper and the lower part of the cylinder are always in anti-phase, i.e. the rotation beneath the surface reaches a maximum if the rotation rate is lowest near the bottom. The existence of the differential rotation is demonstrated in Fig. 7, which contains two typical snapshots from our measurements of the azimuthal flow showing the different angular velocities below the surface and above the bottom of the fluid vessel at two selected moments.

4 SUMMARY

Miscellaneous examples have been presented within this paper illustrating the variety of flow phenomena arising from the application of different kinds of magnetic fields on a liquid metal column. The Ultrasound Doppler Method appears as an effective tool for exploring the diverse structures of the bulk flow. Especially, this technique provides a valuable insight into the vortex dynamics of such non-transparent, unsteady flows.

Acknowledgement

The research is supported by the Deutsche Forschungsgemeinschaft (DFG) in form of the SFB 609 “Electromagnetic Flow Control in Metallurgy, Crystal Growth and Electrochemistry”.

REFERENCES

[1] Grants I, Zhang C, Eckert S, Gerbeth G: Experimental observation of swirl accumulation in a magnetically driven flow, J. Fluid Mech. 616 (2008) 135-152.

[2] Church CR, Snow JT, Baker GL, Agee EM: Characteristics of tornado-like vortices as a function of swirl ratio: a laboratory investigation, J. Atmos. Sci. 36 (1979), 1755-1776..

[3] Montgomery MT, Vladimirov VA, Denisenko PV: An experimental study on hurricane mesovortices, J. Fluid Mech. 471 (2002), 1-32.

[4] Nolan DS, Farrell BF: The structure and dynamics of tornado-like vortices, J. Atmos. Sci. 56 (1999), 2908-2936.

[5] Eckert S, Nikrityuk PA, Räbiger D, Eckert K, Gerbeth G: Efficient melt stirring using pulse sequences of a rotating magnetic field: Part I – Flow field in a liquid metal column, Metall. Mater. Trans. 38B (2007), 977-988.

[6] Nikrityuk PA, Eckert K, Grundmann R: A numerical study of unidirectional solidification of a binary alloy under the influence of a rotating magnetic field, Int. J. Heat Mass Transfer 49 (2006), 1501-1515.

[7] Nikrityuk PA, Ungarish M, Eckert K, Grundmann R: Spin-up of a liquid metal flow driven by a rotating magnetic field in a finite cylinder: A numerical and an analytical study, Phys. Fluids 17 (2005), 067101.

[8] Davidson PA: The interaction between swirling and recirculating velocity components in unsteady, inviscid flow, J. Fluid Mech. 209 (1989), 35-55.

[9] Räbiger D, Eckert, S, Gerbeth, G: Measurements of an unsteady liquid metal flow during spin-up driven by a rotating magnetic field, Exp. Fluids. 48 (2010), 233-244.

The sensitivity of the flow driven by a travelling magnetic field to axial alignment

Josef Pal, Andreas Cramer and Gunter Gerbeth
Institute of Safety Research, Magneto-Hydrodynamics Division
Forschungszentrum Dresden-Rossendorf, P.O. Box 51 01 19, 01314 Dresden, Germany

The present experimental study is concerned with the sensitivity of the flow driven by a travelling magnetic field (TMF) to axial alignment. Referring to the center axis of the TMF generating coil system the fluid volume was stepwise dealigned. Because the flow induced in a TMF is, basically, of a torus type, vertical velocity components are representative for the motion in the meridional plane. To acquire velocity profiles the Ultrasound Doppler velocimetry (UDV) was used which allows gathering the whole profile along the ultrasonic beam. Several transducers were mounted at the bottom of the fluid covering vessel and connected to the multiplexer channels of the UDV device. Eutectic GaInSn was used as working fluid. Analysing mean velocity profiles and the spatiotemporal properties of the flow, the study shows, that already for small deviations from coaxial conditions the flow topology changes.

Keywords: Ultrasound Doppler Velocimetry, Fluid flow, Travelling magnetic field, Stirring

1 INTRODUCTION

In crystal growth, the transport and distribution of the melt components, such as oxygen, as well as particles emitted from the covering crucible is influenced by the flow. In its native form, without any external influence, the flow is a buoyant convection intrinsic to the specific crystal growth method. Externally applied magnetic fields provide a useful contactless method to influence the flow in particular when material transport inside the melt in a definite way is required.

Studies on travelling magnetic fields in crystal growth started first at the mid/end of the 1990s [1-2] and still are matter of investigation [3-7]. Usually, and to our best knowledge common to scientific investigations hitherto, numerical flow simulations are based on coaxial conditions between the axis of the coil system and that of the fluid containing vessel. Such ideal assumptions are in experimental setups and in particular on industrial scale hardly accomplishable, if ever feasible. Comparisons between theory and experiment have, therefore, to be done in a careful and critical manner.

The aim of the present work is to study experimentally the sensitivity of the fluid flow driven by a TMF displacing the covering vessel stepwise away from the coaxial position. Prior to the experimental setup, measuring technique and results the principle of the action of a TMF on electrically conducting melts will be briefly recalled.

2 THE MAGNETICALLY DRIVEN FLOW

Applying any AC magnetic field with strength ***B*** to a volume of liquid metal induces an eddy current ***j*** within the fluid and the interaction of the current with the magnetic field that produced it leads to an electromagnetic Lorentz force $\boldsymbol{f}_L = \boldsymbol{j} \times \boldsymbol{B}$. Consequently, the fluid will be set in movement towards the direction of the acting force. Under axisymmetric conditions, Grants and Gerbeth [5] derived a simple analytical expression for $\boldsymbol{f}_L$ acting by a TMF on a melt with height H and radius R as

$$\boldsymbol{f}_L = \tfrac{1}{2} F r^2 \boldsymbol{e}_z \, , F = \frac{\sigma \omega B^2 k R^5}{4 \rho \nu^2}, \tag{1}$$

with the forcing parameter F and *k* the wave number being a measure for the axial extension of the coil system. σ, ρ and ν are the electrical conductivity, density and kinematical viscosity of the melt, and ω is the frequency of the TMF. Besides low-frequency and low-induction approximations a long wavelength TMF with $2\pi/k \gg R$ was assumed in Eq. (1).

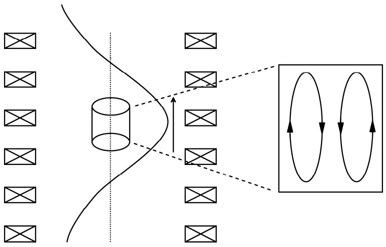

Figure 1: Sketch of the flow in an upward travelling magnetic field. The fluid follows the travelling direction at the perimeter of the container and closes in the centre opposing the Lorentz force, which is weaker there.

The force is of pure axial character and increases radially from the centre of the melt toward the surrounding coils. Thus, it drives a flow in the meridional plane, which is sketched in Figure 1 for an upward travelling magnetic field. Detailed information on the fluid flow may be found in [6-8].

3 SETUP AND MEASUREMENT TECHNIQUE

For the present study eutectic GaInSn was chosen which is liquid at room temperature and has the properties ρ = 6361 kg/m^3, ν = 3.4·10^{-7} m^2/s, and σ = 3.3·10^6 S/m. In order to investigate the driving action of the applied TMF on the fluid, the covering container was positioned inside the home-made MULTIMAG (MULTIpurpose MAGnetic field) facility in which the TMF is generated by six circular solenoids in an axial linear arrangement. Supplying the coils with a 60°-phase-shifted current results, depending on the phase sequence, in a downward or upward travelling field. For further technical details on MULTIMAG [9] is referred to.

The Ultrasound Doppler Velocimetry technique was applied to acquire velocity profiles u_z in the vertical direction at several radial positions. The measuring principle is well known and described in the literature [10]; merely a short description will be recalled here. An ultrasonic transducer acting as emitter sends short ultrasonic pulses with a certain repetition frequency into the fluid. After a pulse sequence, the transducer switches into the receiver mode and collects the scattered echoes, which come back from small tracer particles inside the fluid. The measured time of flight of the ultrasonic pulse relates to the position of the tracers whereas small differences in the time of flight between consecutive pulses are determined by a correlation technique. This phase shift is a measure for the velocity of the particles in the particular measuring volume. Two main features make this technique attractive for our purposes. Firstly, in contrast to optical measurement methods, such as PIV, the applicability in opaque fluids and secondly the possibility to acquire a whole velocity profile along the ultrasonic beam line. To acquire the velocity profiles the commercial DOP2000 velocimeter (Model 2032, Signal-Processing, Lausanne, Switzerland) with an integrated multiplexer module was equipped with seven 8 MHz transducers. All sensors were mounted at the bottom of the fluid covering vessel with the inner dimension of 60 mm in diameter and height. Six of them were azimuthally allocated every 60° near to the vessel rim at the radial position 24 mm, the seventh in the centre. The mean time between consecutive sensors or multiplexer channels was about 150 ms, to acquire one complete set of profiles the time amounts to slightly over 1 second. 6000 profiles per channel were acquired for each measurement, which results in a total recording time of almost two hours.

For an accurate and well-defined displacement between the vessel and the TMF axis, the vessel was mounted on a non-magnetic XY-stage with a positioning sensitivity of 0.01 mm.

4 MEASUREMENTS AND RESULTS

Naturally, the first measurement has to cover the axisymmetric case. Thus, the aligned "zero"-position was deduced in a multistep procedure by recording the ultrasonic profiles and repositioning the vessel. Figure 2 shows the recorded velocity profiles in this case.

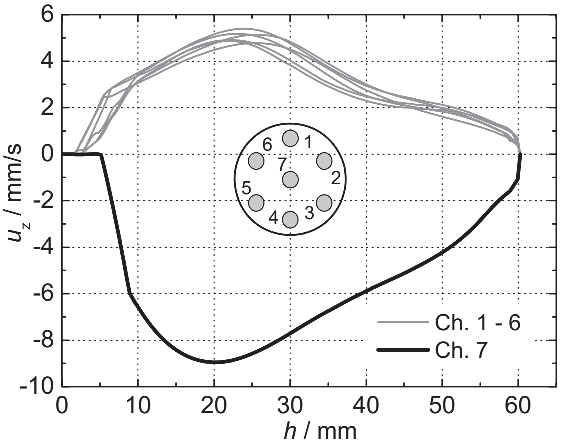

Figure 2: Mean velocity profiles recorded for F=1.0·10^6 under axisymmetric conditions. Positive values indicate a flow away from the sensor, which means here an upward oriented flow. Negative values mean a flow towards the sensor, here downward oriented. The inset shows the allocation of the sensors.

Displacement steps, afterwards, each 0.125 mm were applied between the centered zero-position and 1 mm. The displacement was always along one of the axis of the XY-stage, which accords with the diameter between the sensors no. 2 and 5. Displacing the filled vessel in this manner the fluid volume gathered by sensor no. 2, called outer sensor henceforth, gets closer to the surrounding coils. By contrast, the region gathered by sensor no. 5 (called inner sensor) will get closer to the center axis of the TMF.

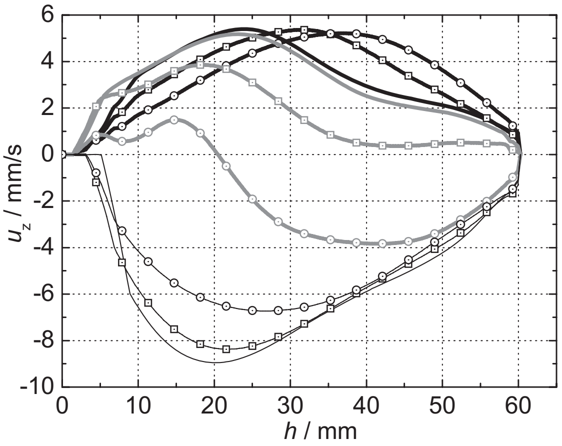

Figure 3: Mean velocity profiles at selected positions along the shifting diameter. Thick black lines indicate the outer, thick grey lines the inner and the thin black lines the centre sensor. Lines without symbol refer to the axisymmetric case, squares and circles to the shifted steps of 0.5 and 1.0 mm, respectively.

As can be seen in the figure, a displacement of up to 1 mm shows no qualitative influence on the flow in the volume part gathered by the outer and centre sensors. This becomes also obvious from the spatiotemporal structure shown in Figure 4 and extracted time series in Figure 5. A dealignment of up to 1.0 mm, cf. Figure 5, causes rather a certain stabilizing effect on the flow regarding the amplitude of velocity fluctuations.

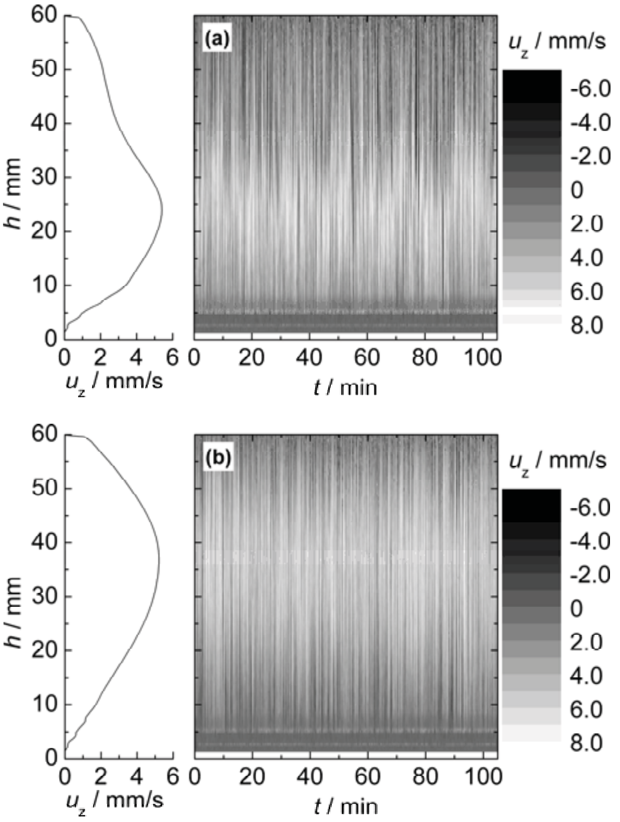

Figure 4: Spatiotemporal flow structure recorded with the outer sensor; (a) illustrates the coaxial zero position and (b) the 1.0 mm dealigned case. The calculated mean velocity profiles are shown on the left side.

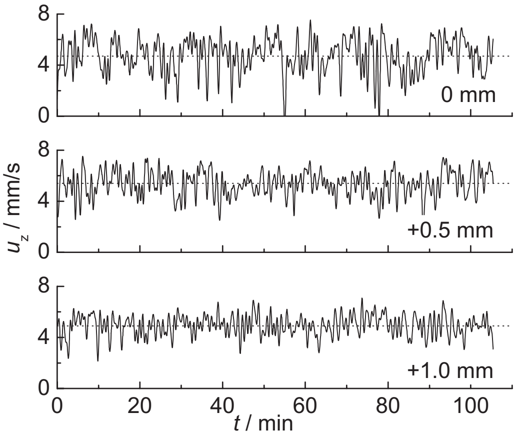

Figure 5: Extracted time series at the half height of the fluid volume from data recorded with the outer sensor. The dealignment steps are indicated in the figures just as with dotted lines the calculated mean velocities.

On the other hand, through dealignment of the vessel, the part of the fluid measured by the inner sensor gets more and more toward the axis of the TMF where the driving action of the Lorentz force is weaker. Depending from the dealignment distance, the Lorentz force cannot balance the recirculating flow coming from the outer side and the flow at the inner side becomes therefore less stable and even reverses its flow direction. Figure 6 illustrates this behaviour by means of time series extracted from the ultrasonic data stemming from the inner sensor.

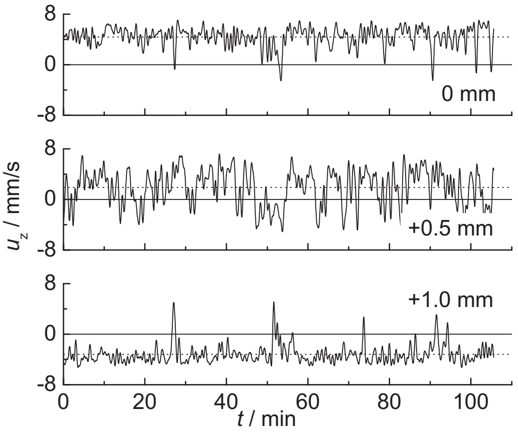

Figure 6: Extracted time series at the half height of the fluid volume from data recorded with the inner sensor. The dealignment steps are indicated in the respective figure, dotted lines are calculated mean velocities.

Regarding the calculated mean profiles, Figure 7 illustrates in detail the sensitivity of the flow to the dealignment of the vessel by steps of 0.125 mm. Starting from the aligned position, for a displacement of about 0.5 mm the vertical flow velocity decrements to almost zero in the upper half of the container. With further displacement the flow changes its structure from a single vortex to rather a double vortex in which the upper vortex becomes more and more distinct.

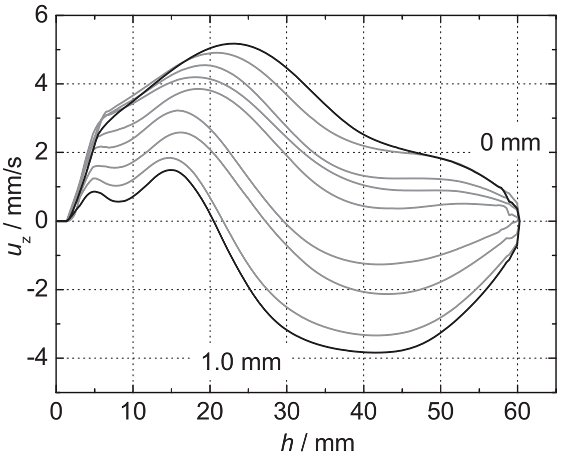

Figure 7: Mean vertical velocity profiles recorded with the inner sensor for displacement steps of 0.125 mm between the coaxial zero-position and the 1.0 mm shifted one.

In comparison to Figure 4, Figure 8 shows the spatiotemporal structure for the inner sensor.

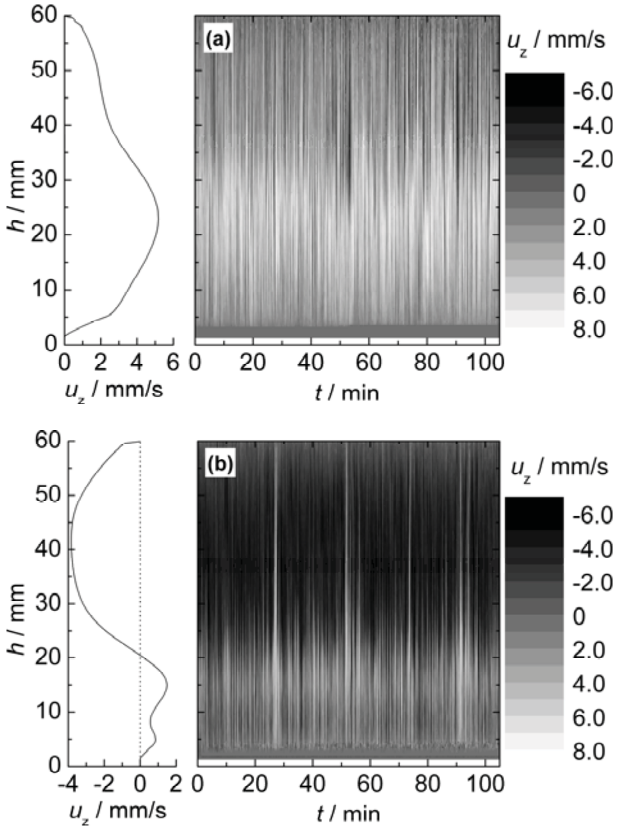

Figure 8: Spatiotemporal flow structure recorded with the inner sensor. Legends for (a) and (b) are the same as in Figure 4.

5 SUMMARY

The present study gives insight into the flow driven by a TMF. In contrast to the usual coaxial arrangement between the fluid and the axis of the magnetic field, in the present work the corresponding axis were stepwise displaced. Performed ultrasonic measurements evince clearly the sensitive behaviour of the TMF driven flow to the axial alignment with the coil system producing the TMF.

6 ACKNOWLEDGEMENTS

This work was financially supported by “Deutsche Forschungsgemeinschaft” in the framework of the Collaborative Research Centre SFB 609.

REFERENCES

[1] Ono N, Trapaga G: A Numerical Study of the Effects of Electromagnetic Stirring on the Distributions of Temperature and Oxygen Concentration in Silicon Double-Crucible Czochralski Processing, J. Electrochem. Soc. 144 (1997) 764-772.

[2] Ramachandran N: Use of Travelling Magnetic Fields to Control Melt Convection, J. Jpn. Soc. Microgravity Appl. 17 (2000) 98-103.

[3] Rudolph P: Travelling magnetic fields applied to bulk crystal growth from the melt: The step from basic research to industrial scale, J. Crystal Growth 310 (2008) 1298-1306.

[4] Klein O et al.: Numerical simulation of Czochralski crystal growth under the influence of a traveling magnetic field generated by an internal heater-magnet module (HMM), J. Crystal Growth 310 (2008) 1523-1532.

[5] Grants I, Gerbeth G: Stability of melt flow due to a travelling magnetic field in a closed ampoule, J. Crystal Growth 269 (2004) 630-638.

[6] Lantzsch R et al.: Experimental and numerical results on the fluid flow driven by a traveling magnetic field, J. Crystal Growth 305 (2007) 249-256.

[7] Mazuruk K: Control of melt convection using traveling magnetic fields, Adv. Space Res. 29 (2002) 541-.548

[8] Cramer A et al.: Local flow structures in liquid metals measured by ultrasonic Doppler velocimetry, Flow Meas. and Instrum. 15 (2004) 145-153.

[9] Pal J et al.: MULTIMAG – A MULTIpurpose MAGnetic system for physical modelling in magnetohydrodynamics, Flow Meas. Instr. 20 (2009) 241-251.

[10] Takeda Y: Development of an ultrasound velocity profile monitor, Nucl. Eng. Design 126 (1991) 277-284.

2d-2c Ultrasound Doppler Array Velocimeter for Flow Investigations in Liquid Metals

Sven Franke[1], Hendrik Lieske[1], Andreas Fischer[1], Lars Büttner[1], Jürgen Czarske[1],
Dirk Räbiger[2], Sven Eckert[2]
[1] Laboratory of Measurement and Testing Techniques, Faculty of Electrical Engineering and Information Technology, Technische Universität Dresden, 01062 Dresden, Germany
[2] Department Magnetohydrodynamics, Institute of Safety Research, Forschungszentrum Dresden-Rossendorf, P.O. Box 510119, 01314 Dresden, Germany

A novel ultrasound Doppler measurement system for investigating the velocity field in electromagnetically driven liquid metal flows is presented. Two orthogonally arranged ultrasound sensor line arrays facilitate a two-dimensional measurement of two velocity components (2d-2c) within a square area of 70 x 70 mm². The array elements are controlled by a specific time multiplex technique in order to achieve both a high spatial and a high temporal resolution. The design of the sensor, the multiplex electronics and the operation mode of the measurement system are described. First velocity field measurements of liquid metal flows in a cubic vessel driven by a rotating magnetic field were performed and will be presented.

Keywords: Ultrasound Doppler Velocimetry, Flow Field Measurements, Ultrasound Sensor Array, Liquid Metals, Magnetohydrodynamics, Rotating Magnetic Field

1 INTRODUCTION

Magnetohydrodynamics (MHD) provides manifold possibilities of electromagnetic flow control in industrial processes (e.g. continuous casting). Beside ongoing numerical simulations a comprehensive understanding of the interactions between liquid metal flows and different kinds of applied magnetic fields requires also detailed experimental investigations. Reliable and precise data about the velocity structure are necessary for the validation of the theoretical computer models. Model experiments using low melting point liquid metals (e.g. GaInSn) are considered as an important tool to investigate the flow structure and related transport processes in liquid metal flows [1]. Because of the opaqueness of the fluid the instrumentation of respective experiments is challenging. Powerful optical methods like Particle Image Velocimetry (PIV) and Laser Doppler Anemometry (LDA) as used for measurements in transparent liquids can obviously not applied in opaque melts.

The pulsed wave ultrasound Doppler velocimetry (UDV) offers an attractive possibility to measure flow velocities in opaque fluids [2, 3]. Also two-dimensional flow mapping of stationary flows were performed with UDV using multiple transducers [4]. However, measurements with a high number of scanning lines as well as a high temporal resolution are desired for investigations of highly turbulent, three-dimensional flows occurring, for example, during the electromagnetic stirring of metal melts.

Few commercial UDV instruments are available on the market, however, merely providing measurements of one velocity component along one line. An upper limit of ultrasound transducers which can be controlled simultaneously by these instruments and an inadequate arrangement of the transducers restrict an efficient flow mapping.

For this reason, a novel pulsed wave UDV measurement system currently in development is presented, which provides 2d-2c flow field measurements with high temporal and spatial resolution using two linear sensor arrays.

2 MEASUREMENT SYSTEM

The UDV system deploys two linear ultrasound transducer arrays each equipped with 25 transducer elements [5]. Figure 1 shows an orthogonal arrangement of these arrays allowing a 2d-2c measurement of the flow pattern in a square plane of 70 x 70 mm². Thereby, each array facilitates the measuring of one of the two velocity components (2d-1c). The design of the linear arrays is determined by several requirements which are described next.

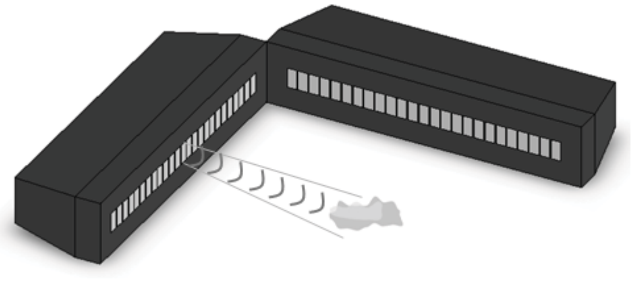

Figure 1: Two linear ultrasound transducer arrays arranged orthogonally for 2d-2c flow field measurements

The detection of small flow structures requires a high spatial resolution of the measurements. A high axial resolution necessitates a high ultrasound transmission frequency as well as a large transducer bandwidth. The lateral resolution also increases with higher transmission frequencies, since the angle of ultrasonic beam divergence in the far field becomes smaller with higher frequencies. However, the transmission frequency can not be chosen arbitrarily high as a result of acoustic attenuation inside the liquid metal which increases with rising frequency. For the present design the compromise of these considerations is found in an ultrasound transmission frequency of 8 MHz for the piezo elements with a -3dB-bandwidth of 2.5 MHz.

Regarding the size of the piezo elements opposite demands have to be considered. On the one hand, a small size of these elements is preferable to scan the flow field with a small lateral spacing. On the other hand, a low divergence of the ultrasound beam requires dimensions of the piezo elements being much larger than the ultrasound wavelength [6]. Hence, a specific sensor structure for the linear arrays was designed to meet both requirements. The sensor arrays consist of rectangular transducer elements with a cross section of 2.5 x 5 mm² (fig. 2). The elements are separated by a gap of circa 0.3 mm caused by the production process. Thus, the entire sensitive array length is about 70 mm. In operation adjacent rectangular piezo elements are driven in pairs acting as single piezo element with an effective square area of 5 x 5 mm² which can be shifted by 2.8 mm. This results in 24 controllable transducer pairs.

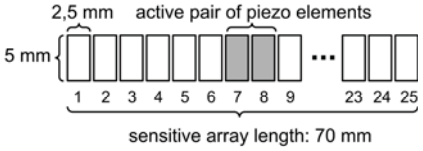

Figure 2: Design of a linear ultrasound array with 25 transducer elements

The requirement of a high temporal resolution is contrary to the demand of a high spatial resolution since the duration for sequentially scanning the entire flow field increases directly with a growing number of array elements. The idea for achieving a high temporal resolution despite the high number of array elements is to parallelize the measurement as much as possible. Thereby, the spacing between the active piezo pairs is chosen in such an extent that crosstalk can be neglected. The optimum spacing for the present measurement system was determined by sound field simulations and crosstalk investigations. Their results allow driving four piezo pairs in parallel reducing the scanning time by a factor of 4. This is implemented in the multiplex control scheme in figure 3. It features to scan the entire flow field in n = 6 switching steps. In order to minimize artefacts in the velocity profiles by multiple backplane echoes the control scheme ensures that no piezo element operates at two consecutive switching steps.

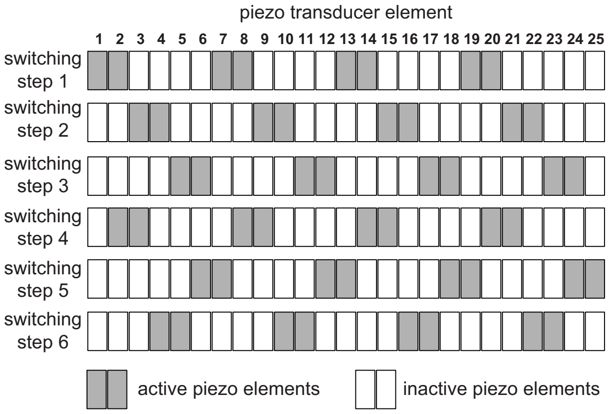

Figure 3: Transducer control scheme of 4-channel parallel operation mode

The measurement setup for one linear ultrasound array is shown in figure 4. The main component is a self-developed high speed, high voltage capable multiplexing electronics implementing the entire control scheme. The burst signal generated by an arbitrary function generator is amplified by a high voltage RF amplifier. Afterwards the high voltage burst is distributed by the transmitting multiplexer among the transducers being active in the respective switching step. The transmitting/receiving (T/R) switch separates the burst signal from the echo signal received by the particular transducer. The receiving multiplexer of the switching electronics transfers the amplified echo signals of the active transducers to four summing amplifiers. They sum the echo signals of the elements of each active transducer pair as well as filter and amplify the signals. A personal computer (PC) equipped with a four-channel data acquisition (DAQ) card acquires the echo signals with a sampling rate of 25 MS/s. A microcontroller controls the transmitting and receiving multiplexer as well as generates the trigger for the burst signal and the DAQ card.

For 2d-2c operation two measurement setups (compare figure 4) are required. Thereby, the linear arrays have to be driven alternating to prevent crosstalk due to diffuse scattering. For this reason, the multiplexing circuits of both linear arrays are synchronized.

The echo signals are processed offline in MATLAB after acquiring the data. A software-based digital quadrature demodulation provides the “I” and “Q” signal of each channel which are filtered afterwards [2, 7]. The flow velocity is estimated with the frequency-domain autocorrelator, see [8]. However, the acquisition of the full bandwidth signal also allows applying the time-domain cross-correlation technique to achieve higher temporal resolution for flow mapping [9].

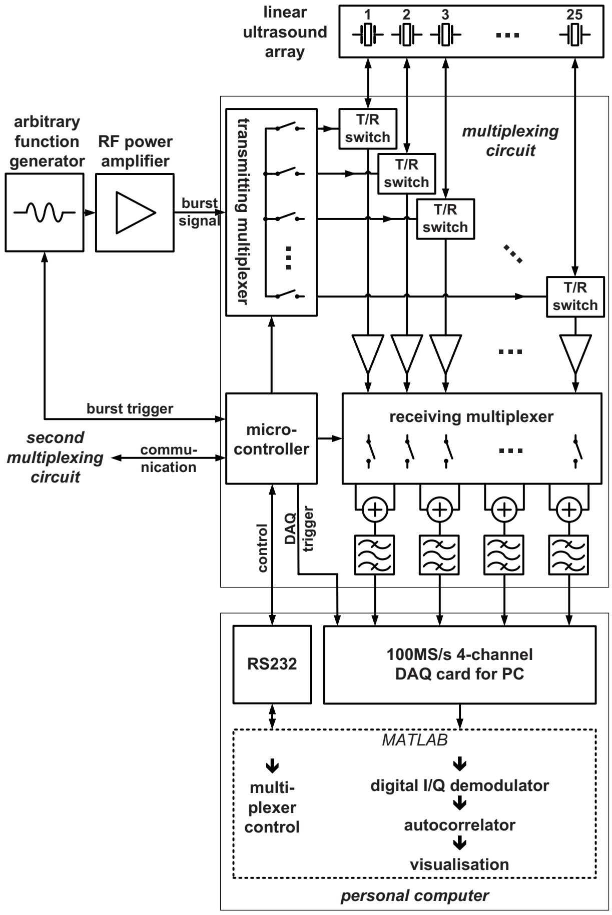

Figure 4: Measurement setup with multiplexing circuit to implement the control scheme

3. MEASUREMENTS

Up to now the measurement system features two-dimensional measurements of at first one velocity component (2d-1c). The second component is currently implemented.

First measurements were performed to validate the parallel operation mode and characterize the measurement system.

3.1 Measurement Setup

The experimental setup shown in figure 5 applies a magnetic field stirrer to drive a liquid metal flow inside a cubic vessel. The stirrer consists of a system of induction coils generating a rotating magnetic field (RMF). The cubic vessel with an inner edge length of 70 mm is made of acrylic glass and filled with the metal alloy GaInSn (c = 2740 m/s) which is liquid at room temperature. It is placed centrically in the magnetic stirrer.

The flow is generated as follows: The RMF rotates around the vertical vessel axis and induces electric currents inside the liquid metal. These currents interact with the imposed magnetic field and generate a dominating angular component of the magnetic field which drives a swirling flow of the melt [10].

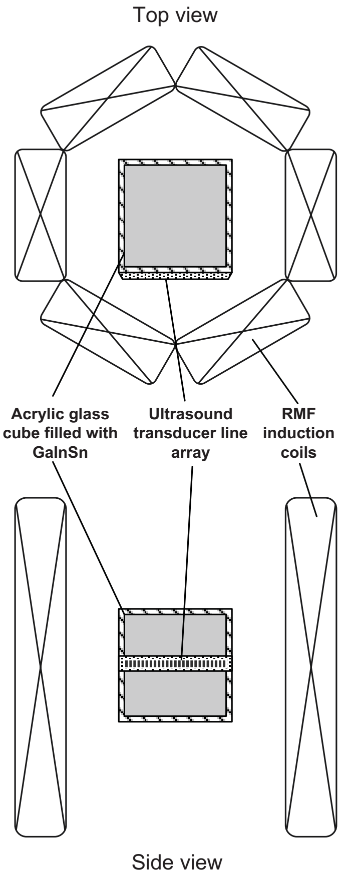

Figure 5: Experimental setup: Acrylic glass cube filled with GaInSn in a RMF stirrer

3.2 Spatial and temporal resolution

The number of wave cycles is a trade-off between a high axial resolution (i.e. a low number of cycles), transducer bandwidth and high acoustic energy or rather a high signal-to-noise-ratio (i.e. a large number of cycles). For the present investigations ultrasound bursts of 8 sinusoidal wave cycles at a frequency of 8 MHz are deployed. From this follows an axial resolution of $\Delta z \approx 1.4$ mm in GaInSn.

The lateral resolution of ultrasound transducers is defined as the -6 dB intensity width in the focal point (or rather the near field depth) of the sound beam. The sound field simulation of a square transducer of 5 x 5 mm² yields a lateral resolution of $\Delta x \approx 3$ mm in GaInSn for the applied measurement system. Hence, the lateral resolution is approximately equal to the traversing step width of 2.8 mm.

The temporal resolution of the flow mapping is determined by the burst repetition frequency which depends on the measurement depth. A depth of the cube of 70 mm results in a calculative repetition frequency of maximum 3.2 kHz related to the control scheme shown in figure 3. Due to technical reasons (i.e. switching time and programming time of the transmitting and receiving multiplexer; see figure 4) the maximum burst repetition frequency is set to 1.6 kHz. In the prospective 2d-2c operation the linear arrays will be driven alternately which leads to half of burst repetition frequency above.

3.3 Measurement results and discussions

For mapping the swirling flow in the cube the linear array is mounted in the vessel wall as depicted in figure 6. There, the measurement plane coincides with the x-y-plane of the cubic vessel at z = 35 mm.

Figure 7 shows one single frame of a 2d-1c flow mapping. There, the y-axis equals the alignment of the array and the velocity component according to the x-axis is measured. A flow toward the transducers is depicted as negative velocity and a flow away from the transducers as positive velocity. As a conclusion figure 7 presents a clockwise rotating vortex flow (compare with figure 6).

For this full frame 50 emissions per profile with a burst repetition frequency of 830 Hz were used which results in a duration of merely 63 ms for capturing the entire flow structure. This corresponds with a frame rate of 16.6 fps.

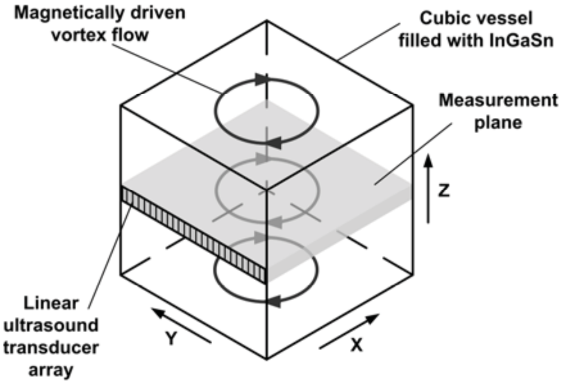

Figure 6: Measurement configuration for visualization of flow field (2d-1c) in the plotted measurement plane

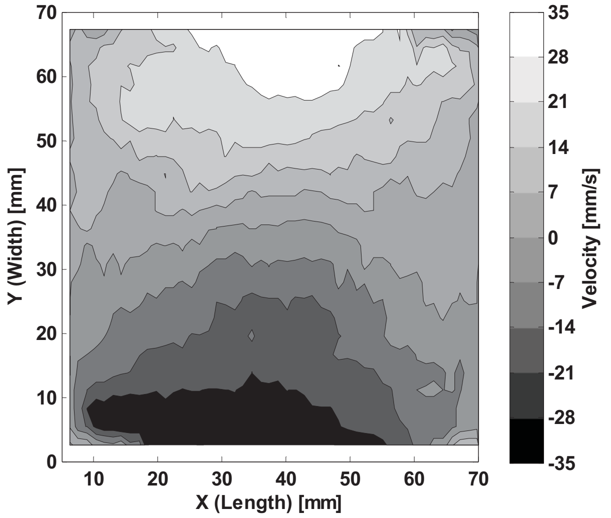

Figure 7: Single frame (Δt = 60 ms) of RMF-driven clockwise vortex (f = 50 Hz; B = 1.4 mT); the velocity component in x-direction is measured

By applying the maximum burst repetition frequency of 1.6 kHz (50 emissions per profile) frame rates up to 33 fps were achieved. Reducing the number of emissions the frame rate may be increased further.

4 SUMMARY

A 2d-2c ultrasound Doppler velocimeter for measuring flow fields in liquid metals is developed. There, two linear ultrasound transducer arrays each with 25 elements are arranged orthogonally to each other to cover a measurement plane of 70 x 70 mm². A specific array design and a parallelized operation mode facilitate a high temporal resolution contemporary with a high number of transducer elements.

Preliminary 2d-1c flow mappings of a RMF-driven liquid metal alloy were successfully performed achieving a full frame rate of up to 33 fps. Prospectively the second velocity component will be implemented and the frame rate will be increased further by faster signal processing methods.

ACKNOWLEDGEMENT

The research is supported by the Deutsche Forschungsgemeinschaft (DFG) in form of the SFB 609 “Electromagnetic Flow Control in Metallurgy, Crystal Growth and Electrochemistry”. This financial support is gratefully acknowledged by the authors.

REFERENCES

[1] Eckert S, Gerbeth G, Räbiger D, Willers B, Zhang C: Experimental modeling using low melting point metallic melts: Relevance for metallurgical engineering, Steel Res. Int. 78 (2007), 419-425.

[2] Takeda Y: Development of an ultrasound velocity Profile monitor, Nucl. Eng. Design 126 (1991), 277-284.

[3] Eckert S, Cramer A, Gerbeth G: Velocity measurement techniques for liquid metal flows, in “Magnetohydrodynamics - Historical Evolution and Trends”, Molokov S, Moreau R, Moffatt HK (Eds.), Springer-Verlag, Dordrecht (2007), 275-294.

[4] Takeda Y, Kikura H: Flow mapping of mercury flow, Exp. Fluids 32 (2002), 161-169.

[5] Franke S, Büttner L, Czarske J, Eckert S: Ultrasound Doppler Array Velocimeter Used for Vortex Investigations of Liquid Metals, 14th Int. Conference on Sensors, Technologies, Electronics and Applications 2009, Nuremberg (2009), vol. 1, 59-64.

[6] Hedrick WR, Hykes DL, Starchman DE: Ultrasound Physics and Instrumentation, Elsevier Mosby, St. Louis (2005), 4 ed.

[7] Jensen JA: Estimation of blood velocities using ultrasound, Cambridge University Press, Cambridge (1996).

[8] Kasai C, Namekawa K, Koyano A, Omoto R: Real-time two-dimensional blood flow imaging using an autocorrelation technique, IEEE Trans. Sonics. Ultrason. 32 (1985), 458-464.

[9] Ozaki Y, Kawaguchi T, Takeda Y, Hishida K, Maeda M: High time resolution ultrasonic velocity profiler, Exp. Therm. Fluid Sci. 26 (2002), 253-258.

[10] Davidson PA, Hunt JCR: Swirling recirculating flow in a liquid metal column generated by a rotating magnetic field, J. Fluid Mech. 185 (1987), 67-106.

Ultrasonic flow measurements in a low temperature liquid metal model of the continuous steel casting process

Klaus Timmel, V. Galindo, X. Miao, Sven Eckert and Gunter Gerbeth

MHD Department, Forschungszentrum Dresden-Rossendorf, P.O. Box 5101119, 01314-Dresden, Germany

Experiments have been performed at room temperature using a small-scale experimental set-up with the eutectic alloy GaInSn. The ultrasound Doppler method was applied for measuring the fluid velocity in the mould. An arrangement of 10 transducers was used to determine a two-dimensional distribution of the horizontal velocity component. According to the concept of the electromagnetic brake the impact of a DC magnetic field on the outlet flow from the submerged entry nozzle (SEN) has been studied. Our measurements deliver an authentic reproduction of the location and extension of the emergent jet and disclose the temporal behaviour of the flow inside the jet as well as in the recirculating zones. An important result of our study was the feature that a static magnetic field may give rise to non-steady, non-isotropic large-scale flow perturbations. The combination of cold liquid metal models and the ultrasound Doppler method as a powerful flow measuring technique in liquid metals appears as an important tool for an experimental investigation of the mould flow and provides valuable experimental data for the validation of numerical flow simulations.

Keywords: Ultrasound Doppler Method, liquid metal, continuous casting, mould flow, magnetic field

1 INTRODUCTION

Fluid flow in the mould cavity of the continuous casting process can be controlled by the application of magnetic fields. For instance, AC magnetic fields are employed as electromagnetic stirrers (EMS) for a homogenization of the melt and a promotion of the double-roll flow pattern in the mould, which is supposed to diminish many slab defects such as the entrapment of bubbles and non-metallic inclusions and to improve therefore the quality of the solidified steel strand [1, 2]. Another approach to ensure high quality slabs under high casting speeds is the utilisation of DC magnetic fields as electromagnetic brake (EMBR) [2, 3]. The DC field should directly reduce the velocity in the mould region and suppress recirculating flows which arise from the high intensity jet flow poured into the mould from the submerged entry nozzle (SEN). The EMBR technology had already been invented in the 1980’s and firstly applied to continuous casting plants in Japan and Sweden [4]. On one hand, second and third generation of EMBR’s are brought into industrial use meanwhile (see for instance [5]). On the other hand, the electromagnetic braking effect in highly turbulent, complex flow configurations is not fully understood until now. For instance, an experimental study has been published recently, which was concerned with the influence of a DC magnetic field on the liquid metal flow driven by rising gas bubbles inside a cylindrical column [6, 7]. A global damping of the flow was observed in the case of a vertical field aligned parallel to the main direction of the bubble motion. However, the application of a horizontal magnetic field causes intensive, non-steady and non-isotropic flow structures. This effect should be taken into account for a deliberate design of electromagnetic brakes for flow stabilisation.

A multitude of numerical studies have been carried out considering different magnetic field configurations [5, 8, 9] for the continuous steel casting, but the reliability of the numerical results is insufficiently confirmed by accompanying experimental activities. Experimental studies on industrial scale with hot metallic melts ($T \geq 600°C$) may require formidable effort and expense. The main drawback is the extremely limited availability of measuring techniques which are able to provide reliable quantitative data from the flow being relevant for numerical code validations. Cost-saving model experiments using low melting point metallic melts permit detailed investigations of the flow structure and related problems with a high grade of flexibility. The application of the Ultrasound Doppler Method enables for measurements of the flow field in opaque metallic liquids. Experiments at room temperature are possible using the ternary alloy GaInSn. That provides the possibility to avoid the usage of mercury for reasons of safety.

2 EXPERIMENTAL SETUP

Fig. 1 shows the small-scale setup, which is operated with the eutectic alloy GaInSn as model fluid. A stainless steel cylinder serves as the tundish which contains about 3.5 l of the GaInSn alloy. The melt is discharged through a Plexiglas tube as SEN with an inner diameter of 10 mm into the mould with a rectangular cross section of $140 \times 35\ \mathrm{mm}^2$ also made of Plexiglas. Two nozzle ports are situated about 80 mm below the free surface in the mould. From the mould the liquid metal flows through a U-bend channel into a storage vessel. The vertical position of the vessel inlet controls the free surface level in the mould. An electromagnetic pump conveys the melt from the vessel back into the tundish. The experiments presented here were performed in a discontinuous mode, i.e. after filling the tundish with the melt the stopper rod was lifted to drain the fluid into the mould. During this process the liquid level of both the tundish and the mould were monitored using a laser distance sensor. The liquid flow rate has been derived from the descent of the surface level in the tundish.

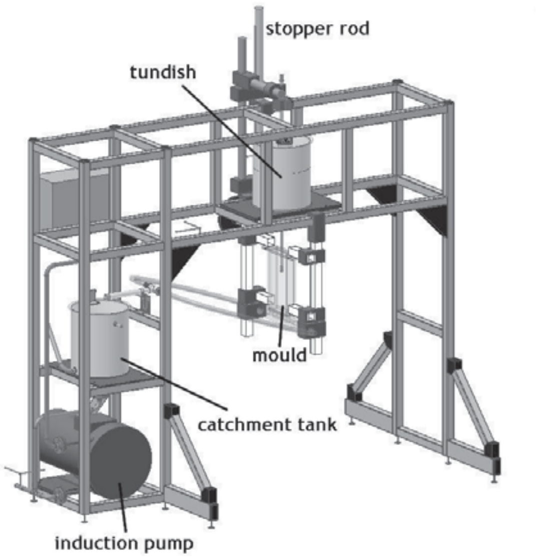

Figure 1: 3D-scheme of the small-scale GaInSn model.

A DC magnet supplies a transverse magnetic field. Measurements of the field strength have shown that the field is homogenous between the pole faces within a tolerance of about 5%. The pole faces of the magnet cover the wide side of the mould completely. The vertical extension of the pole shoes is 40 mm, whereas the position of the upper edge of the pole faces coincides with the nozzle outlet.

The Ultrasound Doppler Method was used for measuring the fluid velocity in the mould. This method is based on the pulse-echo technique and delivers instantaneous profiles of the local velocity along the ultrasonic beam and can be applied to attain experimental data from a bulk flow in opaque liquids [10]. In the last twenty years the ultrasound Doppler technique became an accepted method for flow investigations in various liquid metals (see for instance [6, 11, 12]). In the present study we have applied the DOP2000 velocimeter (model 2125, Signal Processing SA). A line array of ten 4MHz transducers (TR0405LS, acoustic active diameter 5 mm) was assembled with a distance of 10 mm between two adjacent sensors. As shown in Fig. 2, this array was vertically arranged at the outer wall of the mould aligned with the midsection of the narrow mould face. The internal multiplexer of the DOP2000 has been used for a sequential acquisition of data from all sensors with an overall scan rate of 5 Hz. The midpoint of the SEN at the height of the nozzle ports has been chosen as point of origin for our coordinate system.

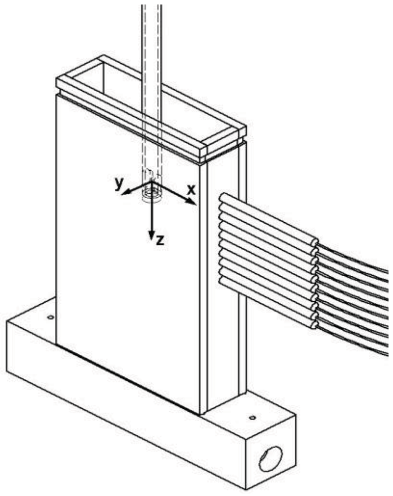

Figure 2: Mould with submerged entry nozzle (SEN) and the linear arrangement of 10 ultrasonic transducers for flow measurements along the vertical midsection.

3 RESULTS

3.1 Numerical calculations

The open source tool OpenFOAM® was used to simulate the fluid flow in the mould cavity. The Navier-Stokes equation was solved numerically in a steady state incompressible regime. The flow solver provides several turbulence models such as the SST-k - ω model, which was used in the calculations presented here. As boundary condition a turbulent velocity profile with a given flow rate value was imposed at the nozzle inlet. The liquid metal free surface in the mold was modeled as a stress-free interface with a zero vertical velocity component. The velocities measured by the Ultrasound Doppler method represent a mean value taken over the lateral extension of the ultrasonic beam. Therefore, for comparing the calculated velocity $u_x(x,z)$ with the experiment it was necessary to average the numerically obtained velocity profiles over a circular cross section with a diameter of 5 mm.

3.2 Flow measurements

The discharging flow from the nozzle ports impinges on the narrow face of the mould where it forms two vortices in the upper and lower mould region. Profiles of the horizontal velocity were recorded at the midsection along the wide side of the mould between the side wall and the submerged entry nozzle. The comparison between the results obtained from the numerical calculations and the flow measurements in Fig. 3 shows a very good agreement. The simulations provide an authentic reproduction of the location and extension of the emergent jet and the magnitude of the flow velocity as well.

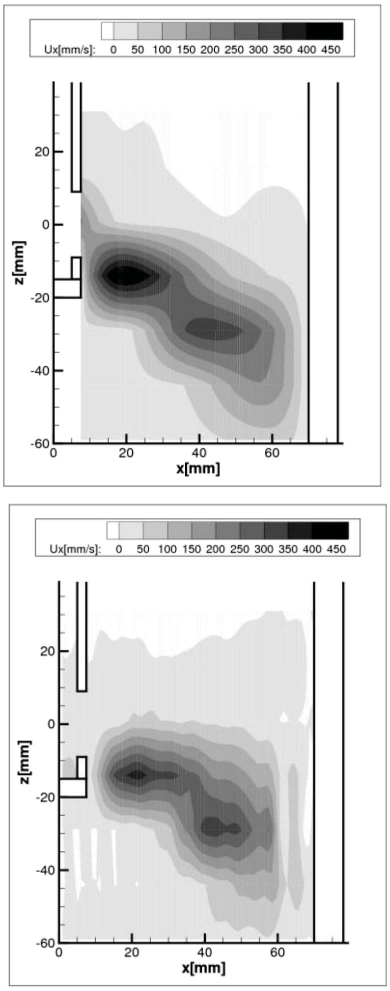

(a)

(b)

Figure 3: Time-averaged, horizontal flow at the nozzle outlet: (a) numerical results, (b) flow measurements.

Fig. 4 contains time-averaged plots showing the flow measurements of the horizontal velocity field for the case without magnetic field and a transverse field of 0.31 T, respectively. These two-dimensional plots were obtained by using the line array of ten transducers as described in section 2. The application of the magnetic field provokes the occurrence of a remarkable recirculating flow at the upper part of the nozzle outlet. The inclination angle of the jet becomes flat. The impingement point at the opposite side wall is shifted upwards by about 20 mm. However, the intensity of the velocity within the jet is only slightly reduced.

The arrangement of the ultrasonic transducers has been modified to measure the velocity distribution in the narrow cross section of the mould. Three transducers were positioned at the midsection (y = 0) and at a distance of 13 mm at either side of the central sensor. The vertical position corresponds to the bottom end of the SEN. Fig. 5(a) shows the situation without magnetic field. The maximum of the jet appears approximately at the central point of the measuring plane. Fig. 5(b) represents the case if a magnetic field of 310 mT was applied. Besides a slight reduction of the maximum velocities, the imposition of the magnetic field provokes a broadening of the jet width along the magnetic field lines.

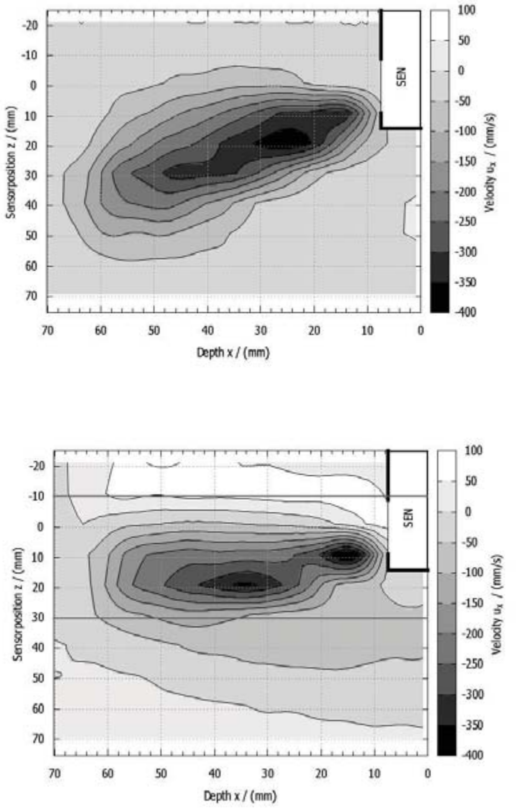

(a)

(b)

Figure 4: Flow measurements of the horizontal flow at the nozzle outlet (vertical arrangement of 10 transducers): (a) without magnetic field, (b) B = 0.31 T.

Fig. 6 displays time series of the velocity recorded at a position near the nozzle outlet. The sensor detects a turbulent flow with strong irregular velocity fluctuations if no magnetic field is applied. A slowdown of the velocity fluctuations due to the magnetic field effect cannot be observed. The measurements show large-scale oscillations of the local velocity which probably arise from an alternating up-and downturn of the jet flow.

4 SUMMARY

The application of tailored magnetic fields is the key issue for an effective optimisation of the continuous casting process, but it requires further investigations of the interplay between the mould flow and the magnetic field, in particular experimental data are needed to verify the electromagnetic braking effect and to prove respective numerical predictions.

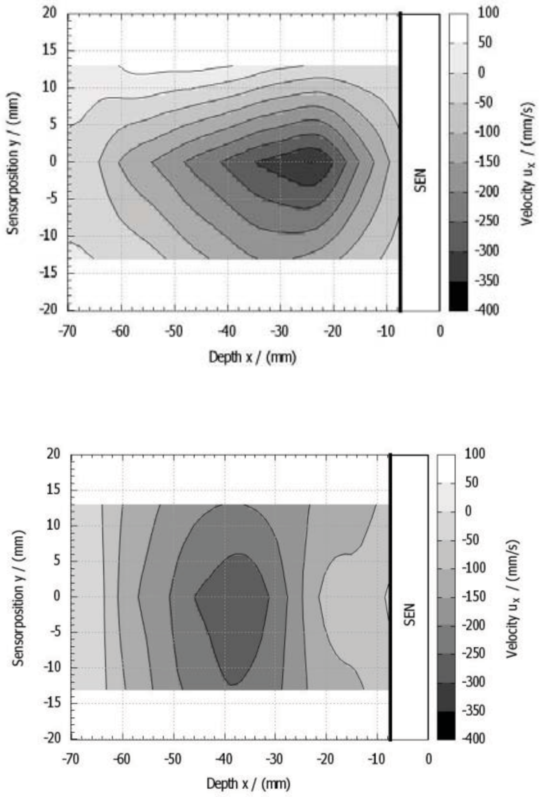

(a)

(b)

Figure 5: Horizontal flow at the nozzle outlet (horizontal arrangement of 3 transducers): (a) B = 0, (b) B = 0.31 T.

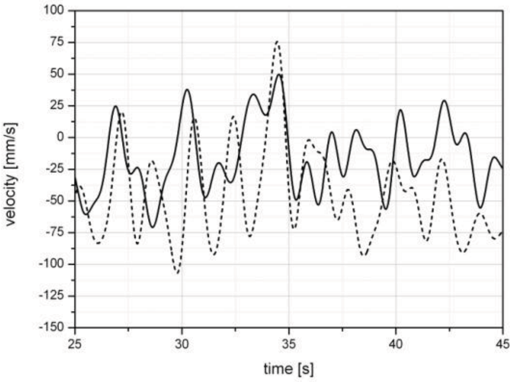

Figure 6: Time series of the horizontal velocity recorded at the position x = 24.5 mm and z = 49 mm for B = 0 (solid line) and B = 310 mT (dashed line).

The generic problem of an initially axisymmetric jet, which is affected by a uniform, transverse magnetic field, was considered by Davidson [13]. The imposed field causes regions of reverse flow on both sides of the central jet. Furthermore, an elongation of the jet cross-section parallel to the field lines occurs. These general features with respect to a reorganization of the flow pattern were also observed in our continuous casting model. An experimental study with respect to a bubble-driven liquid metal flow in a transverse magnetic field has been published recently [6, 7]. An outcome was the feature that a static magnetic field may give rise to non-steady, non-isotropic large-scale flow perturbations. Likewise, the flow measurements presented here did not confirm the expectation of a smooth reduction of the velocity fluctuations at the nozzle outlet due to the magnetic field. This problem requires further investigation, because the concept of an EMBR in the continuous casting process relies on a reliable damping effect of the applied magnetic field. The availability of liquid metal cold models appears as an important tool for an experimental investigation of such open questions. Moreover, these model experiments will provide valuable experimental data for the validation of numerical flow simulations.

Acknowledgement

The research is supported by the Deutsche Forschungsgemeinschaft (DFG) in form of the SFB 609 “Electromagnetic Flow Control in Metallurgy, Crystal Growth and Electrochemistry”.

REFERENCES

[1] Okazawa K, Toh T, Fukuda J, Kawase T, Toki M: Fluid flow in a continuous casting mold driven by linear induction motors, ISIJ Int. 41 (2001), 851-858.

[2] Takeuchi S, Kubota J, Miki Y, Okuda H, Shirayama A: Recent trend of molten steel flow control technology in a continuous casting mold by electromagnetic force, 4th Int. Conference on Electromagnetic Processing of Materials (2003), Lyon (France), 145-150.

[3] Toh T, Takeuchi E, Matsumiya T: Recent advances in MHD applications to steelmaking processes, 5th Int. Conference on Electromagnetic Processing of Materials (2006), Sendai (Japan), 21-25.

[4] Nagai J, Kojima S, Suzuki KI, Kollberg S: Steel flow control in a high-speed continuous slab caster using an electromagnetic brake, Iron Steel Eng. 61 (1984), 41-47.

[5] Bal D, Brockhoff J, Damen W, Peeters T: Numerical modeling of an FC-II mould in a vertical bending continuous caster, 5th Int. Conference on Electromagnetic Processing of Materials (2006), Sendai (Japan), 108-113.

[6] Zhang C, Eckert S, Gerbeth G: The flow structure of a bubble-driven liquid metal jet in a horizontal magnetic field, J. Fluid Mech. 575 (2007), 57-82.

[7] Zhang C, Eckert S, Gerbeth G: Modification of bubble-driven liquid metal flows under the influence of a DC magnetic field, ISIJ Int. 47 (2007), 795-801.

[8] Takatani K, Nakai K, Kasai N, Watanabe T, Nakajima H: Analysis of heat transfer and fluid flow in the continuous casting mold with electromagnetic brake, ISIJ Int. 29 (1989), 1063-1068.

[9] Cukierski K, Thomas BG: Flow control with local electromagnetic braking in continuous casting of steel slabs, Metall. Mater. Trans. 39B (2008), 94-107.

[10] Takeda Y: Development of an ultrasound velocity profile monitor, Nucl. Eng. Design 126 (1991), 277-284.

[11] Takeda Y, Kikura H: Flow mapping of the mercury flow, Exp. Fluids 32 (2002), 161-169.

[12] Eckert S, Gerbeth G, Melnikov VI: Velocity measurements at high temperatures by ultrasound Doppler velocimetry using an acoustic wave guide, Exp. Fluids 35 (2003), 381-388.

[13] Davidson PA: Magnetic damping of jets and vortices, J. Fluid Mech. 299 (1995), 153-186.

Posters

Transition to turbulence in a concentric annular pipe

Azuraien Jaafar[1,2], Marcel P. Escudier[2] and Robert J. Poole[2]
[1]Mechanical Engineering Department, Universiti Teknologi Petronas, 31750 Tronoh, Perak, Malaysia
[2]Department of Engineering, University of Liverpool, Brownlow Street, Liverpool, L69 3GH United Kingdom

In this study the pressure-drop, mean and rms axial velocity data are measured using a differential pressure transducer and a laser Doppler anemometer for the flow of Newtonian and non-Newtonian fluids in a concentric annular pipe (radius ratio κ=0.5) at various Reynolds numbers encompassing the laminar, transitional and turbulent regimes. Three different fluids are utilized; a semi-rigid shear-thinning polymer (a xanthan gum), a polymer known to exhibit a yield stress (carbopol) and a Newtonian fluid (glycerine-water mixture) as the reference fluid. A longer Reynolds number range for the transitional flow regime is observed for the more shear-thinning fluid as determined from the axial rms fluctuation level measured at fixed radial locations. Contrary to what is observed for the Newtonian fluid the higher shear stress on the inner wall compared to the outer wall does not lead to earlier transition for the shear thinning and the yield stress fluids, xanthan gum and carbopol, where more turbulent activity is observed in the time traces at the outer wall region. The mean axial velocity profiles show a slight shift (~5%) of the maximum velocity location towards the outer pipe wall within the transitional regime only for the Newtonian fluid.

Keywords: transition, annular flow, shear thinning fluid, yield-stress fluid

1 INTRODUCTION

The fundamental study of fluid flowing in an annulus within the laminar and turbulent regimes has been the subject of interest since the early work by Rothfus et. al. [1] due to its extensive engineering applications. However, very limited literature within the transitional flow regime especially for the non-Newtonian fluids are available. Velocity profile measurements of a Newtonian fluid were conducted by Rothfus et. al. [1] in a concentric annulus with varying radius ratios (κ=0.162 and 0.650 where $\kappa \equiv R_i/R_o$ with R_i and R_o being the inner and outer pipe radii) at moderate Reynolds number range covering the transitional regime ($1250 \leq Re \leq 21600$). The Reynolds number, $Re(\equiv \rho U_B D_H/\eta)$ is calculated based on the fluid density, ρ, bulk velocity, U_B, hydraulic diameter, $D_H(\equiv D_o - D_i)$ and the fluid viscosity, η. The position of maximum velocity, r_m is found to be the same for laminar and turbulent flow in both annuli. However, within the transitional regime the position is shifted towards the inner pipe. The extent of the transitional regime on the Reynolds number scale was found to be a function of the radius ratio and appeared longer than in circular pipes. Hanks and Bonner [2] performed a theoretical analysis on the stability of laminar Newtonian flow within a concentric annulus. The theory predicts that the inner flow region is the least stable and will undergo transition to turbulence while the flow in the outer region remains laminar. Consequently, the wall shear stress in the inner region will increase significantly due to the change in momentum transport mechanism to a turbulent mode. The increase in wall shear stress would then lead to a shift in r_m to a higher value, towards the outer wall. The r_m value will reach a maximum once the outer flow region undergoes transition to turbulence. Beyond this critical Reynolds number r_m will decrease to a value corresponding to that in turbulent flow. Amongst the limited literature on transitional non-Newtonian fluid flow, Escudier et. al. [3] monitored the axial turbulence intensity of Newtonian and non-Newtonian fluid (xanthan gum, carboxymethylcellulose (CMC) and laponite/CMC mixture) flows at the centre of the annular gap as a means to identify the onset of transitional flow. Although departure from the laminar flow regime was observed on the friction factor, f against the Reynolds number, Re plot, a sudden increase in the normalized axial turbulence intensity, u'/U_B, above the noise level was detected at a slightly lower Reynolds number than what is observed on the f-Re plot for all the fluids studied. The friction factor, f ($\equiv 2\tau_W/\rho U_B^2$) is calculated from the wall shear stress, τ_W and the Reynolds number, Re ($\equiv \rho U_B D_H/\eta_W$) is calculated using the viscosity at the wall, η_W. Despite the circumferential asymmetry highlighted by the authors, the mean axial velocity distribution for the Newtonian control case showed a slight shift of r_m towards the outer wall within the transitional regime, a trend which was absent for the non-Newtonian fluid flows.

2 EXPERIMENTAL ARRANGEMENT

A 5.81-m long annular-flow facility as shown in **Figure 1** was utilized. The test pipe comprised of four 1041-mm long, one 625-mm long and one 718-mm long precision-bore borosilicate glass tubes, with an average internal diameter of 100.4 mm. The inner centrebody was made of stainless steel thin walled tube with an outside diameter of 50.8 mm giving a radius ratio, κ=0.506. The fluid was driven from a 500-l capacity stainless-steel tank by a progressive cavity pump (Mono-type, E101). A Fischer and Porter MAG-SM Series 1000 electromagnetic flowmeter was also incorporated in the system. The pressure drop was measured by means of a differential pressure transducer, GE Druck (LPX9381) over a distance of 41.3D_H, starting 75.8D_H downstream of the inlet. Velocity profiles and turbulent fluctuation levels, performed at 104.7D_H downstream of the inlet of the test section, were determined using a Dantec Fibreflow laser Doppler anemometer (LDA) system supplied by Dantec Electronic Ltd, UK. The flowrates obtained from integration of the LDA mean velocity profiles were found to be within 1.5% of the value provided by the flowmeter. A vegetable based glycerine-water solution (40% w/w), supplied by Hays Chemical Ltd was utilized. It has a density of 1070 kg/m^3 and a shear viscosity, measured at 20°C, of 0.00386 Pa.s. The xanthan gum (XG) used in this study was obtained from the Kelco Co. (Ketrol TF) with the molecular weight reported by the supplier to be in excess of 10^6 g/mol while the Carbopol 980 (CB) was supplied by Noveon, France with a molecular weight of 4.00×10^6 g/mol. The carbopol solutions prepared in this research work is neutralized using laboratory grade 2N sodium hydroxide supplied by BDH Ltd, UK. Complete rheological characterizations of the polymers utilized in this study were conducted by Jaafar [4].

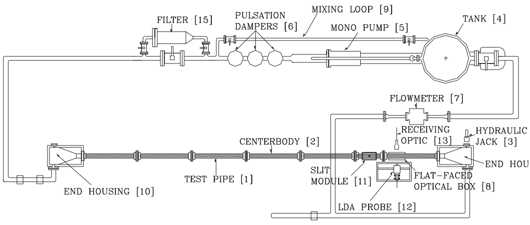

Figure 1: Schematic diagram of the flow loop

3 PRESSURE-DROP MEASUREMENTS AND TRANSITION IDENTIFICATION

In **Figure 2**, a plot of the Fanning friction factor, f against Reynolds number, Re for glycerine, good agreement is observed with the theoretical prediction given by Knudsen and Katz [5] for radius ratio κ=0.5 within the laminar regime. In the high Reynolds number turbulent flow regime, the data agrees well with the empirical predictions by Jones and Leung [6]

$$\frac{1}{\sqrt{f}} = 4\,log(1.343\,Re\,f^{1/2}) - 1.6 \quad \cdot \tag{1}$$

A method initially suggested by Zakin et. al. [7] was utilized in an attempt to detect transition from laminar to turbulent flow by plotting turbulent intensities measured at fixed radial locations against the Reynolds number. The axial rms fluctuation component is monitored at non-dimensional radial locations, ξ ($\equiv(r-R_i)/(R_o-R_i)$) of 0.1 and 0.9 with ξ=0.1 being closer to the inner wall while 0.9 is closer to the outer wall. In **Figure 2**, a plot of the axial rms fluctuation component normalized with the local mean velocity, U_{local} against Re for glycerine, a clear demarcation from the laminar regime can be detected where abrupt increases in the values are observed from 2% up to 22% of the local velocities. Two limits of transition could be seen, Re_1 and Re_2, with the first Reynolds number limit, Re_1, identifies the onset of transition seen as a noticeable change in the turbulent activity while the second Reynolds number, Re_2, represents the limit where the maximum value of turbulent intensity is reached. For glycerine, Re_1 is equal to 2100 for the inner and outer wall while the second limit is reached earlier for the inner wall at Re~2900 and for the outer wall Re_2 is about 3100.

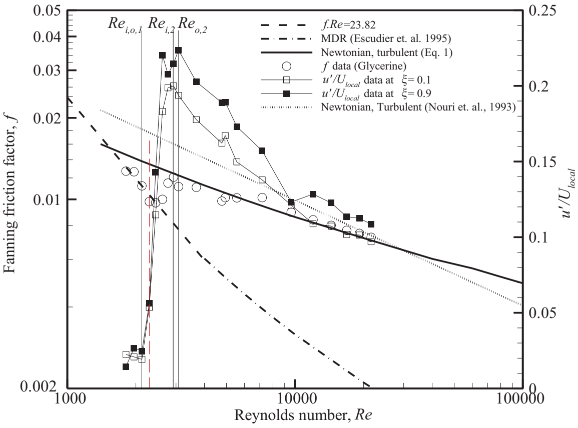

Figure 2: f-Re data for glycerine with u'/U_{local}-Re levels to monitor transition ($Re_{a,b}$ is the critical Reynolds number where a refers to the positions closer to the inner (i) or outer (o) walls while b refers to the transition stages with 1 refers to the onset of transition and 2 refers to the limit where maximum u'/U_{local}-Re is reached).

Figures 3 and **4** show the friction factor data for 0.07% and 0.15% xanthan gum solutions where within the flow loop operating range all three flow regimes; laminar, transition and turbulent; were clearly encountered. The f-Re and u'/U_{local}-Re data for 0.065% carbopol shown in **Figure 5** also comprises all three flow regimes. In **Figures 3-5**, Re_2 values were found to be higher for the more shear-thinning fluid indicating larger transitional regime on the Reynolds number scale. **Tab 1** lists all the Reynolds number limits as seen from the turbulent intensity activities and also the peak values for the fluids studied. It is interesting to note that these peak values decrease with increasing shear-thinning ability.

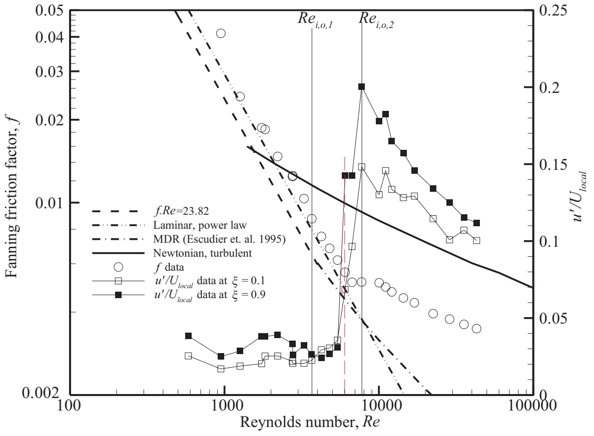

Figure 3: f-Re and u'/U_{local}-Re data for 0.07%XG

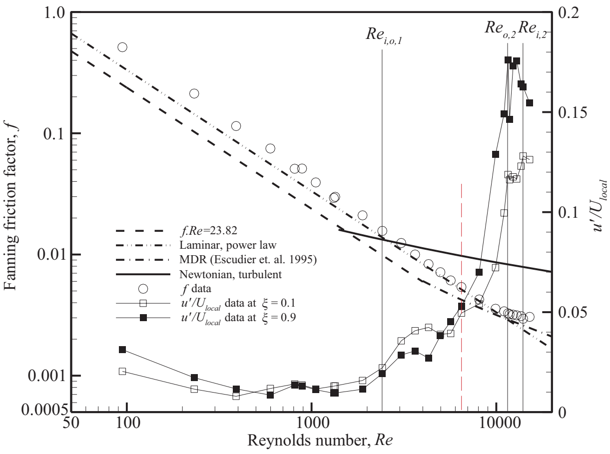

Figure 4: f-Re and u'/U_{local}-Re data for 0.15%XG

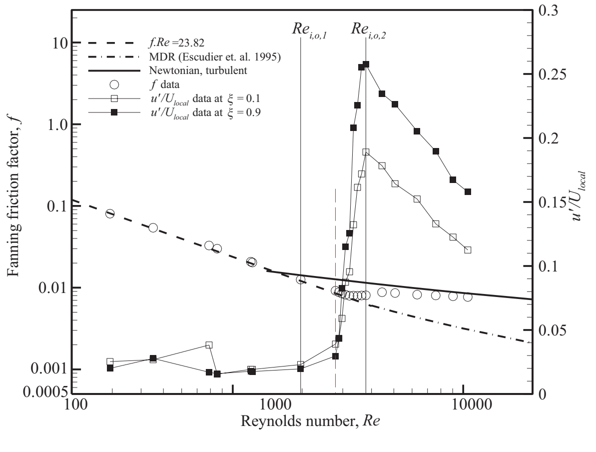

Figure 5: f-Re and u'/U_{local}-Re data for 0.065%CB

For the Newtonian and polymer flows time traces of the axial velocity at ξ of 0.1 and 0.9 for several Reynolds numbers were also monitored for 30 seconds up to a maximum of 90 seconds. Note that the time traces at these two locations were not measured simultaneously.

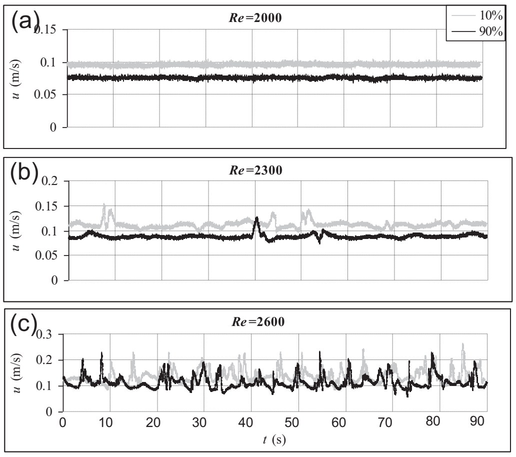

Figure 6: Time series of the axial velocity at ξ=0.1 and ξ=0.9 for glycerine

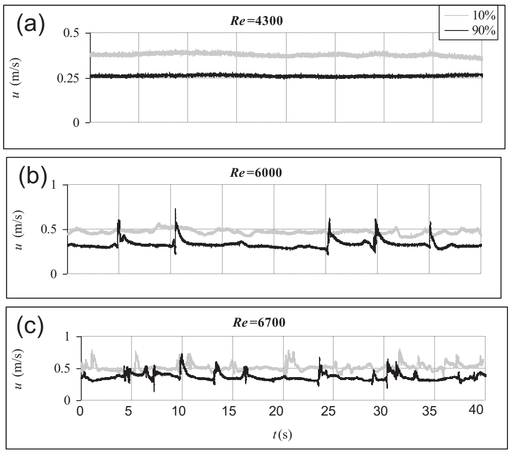

Figure 7: Time series of the axial velocity at ξ=0.1 and ξ=0.9 for 0.07%XG

Figure 6 shows the time traces for the Newtonian fluid, glycerine where the flow is completely laminar for Re=2000 and at Re=2300 spikes are detected at both positions closer to the inner and outer walls. In order to quantify the degree of turbulence at the onset of the transition region a method known as the $\bar{u}$ method [8] is utilized where a time ratio is defined such that:

$$\beta = \frac{\Delta t_{turbulent}}{\Delta t_{total}} \%. \qquad (2)$$

$\Delta t_{turbulent}$ is taken as the total time for the spikes. A spike is considered to have occurred within the time trace if the peak velocity is different by more than 15% of U_{local}. At the onset of transition for glycerine (Re=2300), the time ratio for the inner wall was found to be β=26% which is higher than that of the outer wall (β=11%). This observation is in agreement with the behaviour predicted by the theoretical stability analysis by Hanks and Bonner [2]. **Figure 7** shows the time trace for 0.07% xanthan gum at several Reynolds numbers. The velocity data at Re=4300 is essentially steady indicating laminar flow. At Re=6000, the flow close to the inner wall is clearly unsteady with no distinct spikes, however, high amplitude (>50% of local mean velocity) spikes could only be observed for the flow closer to the outer wall. The β values are 15% and 35% for the inner and the outer walls respectively indicating more turbulent activity near the outer wall. At the higher concentration of 0.15% xanthan gum (not shown) similar characteristics are observed with the first trace of turbulence found at Re=6500 with β values of 23% and 31% for the inner and outer walls respectively. The transitional flow study of the yield stress fluid, carbopol at a concentration of 0.065% (not shown) also revealed unsteady flow at Re=2800 with time ratio of 8% for the inner wall and 15% for the outer wall.

4 MEAN AXIAL VELOCITY MEASUREMENTS

Figure 8 shows the mean axial velocity profile for glycerine at several Reynolds number spanning the three flow regimes; laminar, transition and turbulent. The velocity profile within the laminar regime at Re=2000 is in good agreement with the theoretical profile given by Knudsen and Katz [5]. Deviations from the theoretical laminar profile are observed at Re=2600 where a slight shift towards the outer wall in r_m is also observed. As Re is further increased, the shape of the velocity profiles agrees with what would be expected of turbulent flow with a progressively flatter central region. The shift in r_m, however, is not detected and, if any, it is not significant for xanthan gum and carbopol solutions.

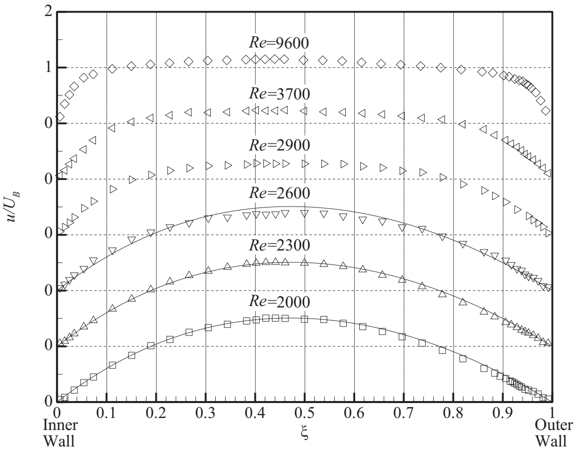

Figure 8: Velocity profiles for different Reynolds numbers including the analytical profile for laminar, Newtonian flow (continuous lines) for glycerine

5 CONCLUSIONS

In the transitional flow studies within the annular pipe larger Reynolds number range of the transitional flow regimes are observed for the more shear-thinning fluid by monitoring the axial rms fluctuation level at fixed radial locations close to the inner and outer walls (ξ=0.1 and 0.9). Time traces of the axial velocity at these radial locations provided further insight of the transitional flow within the annular pipe. The observations indicate that the higher shear stress on the inner wall compared to that on the outer wall does not lead to earlier transition for shear thinning and yield stress fluids as is observed for the Newtonian fluid, glycerine. The mean axial velocity component measured indicates a slightly different behaviour for the Newtonian and polymer flow in relation to the location of maximum velocity. A shift towards the outer wall from a location of ξ=0.44 could be seen within the transitional flow regime only for the glycerine-water mixture. The shift is a consequence of the flow adjusting to the change in momentum transport as suggested by Hanks and Bonner [2].

Table 1: Reynolds number limits and maximum axial rms fluctuation level

Fluid	Re_1		Re_2		u'_{max}/U_{local}	
ξ	**0.1**	**0.9**	**0.1**	**0.9**	**0.1**	**0.9**
Glycerine	2100	2100	2900	3100	0.20	0.22
0.07%XG (n=0.61)	3700	3700	7700	7700	0.15	0.20
0.15%XG (n=0.45)	2400	2400	14000	11600	0.13	0.18
0.065%CB (n=0.81)	2000	2000	3800	3800	0.19	0.26

REFERENCES

[1] Rothfus, R.R., Monrad, C.C., Senecal, V.E., 1950, “Velocity distribution and fluid friction in smooth concentric annuli”, Industrial and Engineering Chemistry, 42(12), 2511-2520.

[2] Hanks, R.W., Bonner, W.F., 1971, “Transitional flow phenomena in concentric annuli”, Industrial and Engineering Chemistry Fundamentals, 10(1), 105-113.

[3] Escudier, M.P., Gouldson, I.W., Jones, D.M., 1995, “Flow of shear-thinning fluids in a concentric annulus”, Experiments in Fluids, 18, 225-238.

[4] Jaafar, A., 2009, “Duct flow of polymer solutions”, PhD Thesis, University of Liverpool.

[5] Knudsen, J.G., Katz, D.L., 1958, “Fluid dynamics and heat transfer”, The McGraw-Hill Companies, ISBN 0882759175.

[6] Jones, O.C., Leung, J.C.M., 1981, “An improvement in the calculation of turbulent friction in smooth concentric annuli”, Journal of Fluids Engineering, 103, 615-623.

[7] Zakin, J.L., Ni, C.C., Hansen, R.J., 1977, “Laser Doppler velocimetry studies of early turbulence”, The Physics of Fluids, 20(10-2), 85-89.

[8] Zhang, D.H., Chew, Y.T., Winoto, S.H., 1996, “Investigation of intermittency measurement methods for transitional boundary layer flows”, Experimental Thermal and Fluid Sciences, 12, 433-443.

Laboratory-Scale Pipe Rheometry: A Study of a Microfibrillated Cellulose Suspension

Sanna Haavisto*, Martina Lille**, Johanna Liukkonen* and Juha Salmela*
Technical Research Centre of Finland, P.O. Box 1603, 40101 Jyväskylä, Finland
Addresses: * P.O. Box 1603, 40101 Jyväskylä, Finland. ** P.O. Box 1000, 02044 VTT, Finland
Email: forename.surname@vtt.fi

In this work a novel laboratory-scale pipe rheometer is utilized in rheological characterization of concentrated MFC and cellulose suspension. The method is based on a combination of pulsed ultrasound velocity profiling (UVP) and pressure difference measurement (PD). The rheological properties of the suspensions are described in terms of viscosity and pressure loss. The results are compared to rotational rheometer results. It is demonstrated that well controlled pipe flow environment together with UVP-PD technique is efficient in characterizing the rheological flow behavior of complex slurries.

Keywords: inline rheology, ultrasonic velocity profiling, microfibrillated cellulose

1 INTRODUCTION

Ultrasound velocity profiling (UVP) has been accepted as an important measuring technique in fluid dynamics and engineering applications. Furthermore, UVP is increasingly being used together with pressure difference measurement as a non-invasive rheological measuring technique commonly known as UVP-PD. This non-invasive method is capable of in-line rheological measurements for concentrated, opaque fluids in real-time [1-5].

Cellulose fibers generally form an opaque flocculated suspension with high viscosity already at very low mass concentrations. In many cases conventional rheometers fail to produce reliable information for these suspensions. Recently, both UVP and UVP-PD methods have been successfully applied in probing details of cellulose fiber suspension flows and their rheological properties [6-9].

Recent developments in cellulose fiber disintegration have facilitated production of micro- and nanofibrillated cellulose (MFC/NFC). The properties of these fibrils differ significantly from cellulose fibers, especially in specific surface area, aspect ratio, strength and flexibility [10]. Development of new materials and applications utilizing MFC/NFC requires understanding the rheology of them.

The aim of this work was to develop a laboratory-scale rheometer which has minimal restrictions in sample properties (consistency, particle dimensions) and which enables measurements in varying shear conditions. Tube flow geometry was selected due to its practical significance in process industry and effortless modification possibilities. The UVP-PD method was preferred to other ones due to its applicability for opaque fluids. Furthermore, UVP-PD is based on direct measurements and includes no assumptions concerning the flow pattern or boundary conditions.

The pipe rheometer was firstly applied for studying rheological properties of a commercial MFC and cellulose suspensions in high consistency. The rheological properties of the suspensions are described in terms of viscosity and pressure loss behavior. The viscosity results are compared to rotational rheometer results.

2 MATERIALS

Microfibrillated cellulose was a commercial product Celish® KY-100G (Daicel Chemical Industries, Japan) made from purified wood pulp. The average length and diameter of Celish® fibers reported by Tatsumi et al. [11] are 350 µm and 15 µm respectively.

As a reference for MFC, bleached birch cellulose was measured at similar conditions as MFC pulp. The approximate average fiber length and width are 0.9 mm and 20 µm, respectively.

Before measurements, the cellulose fibers were dispersed in deionised water and disintegrated. The mass consistency of the slurries was 1.5 % and temperature 20±0.5 °C.

3 METHODS

3.1 Laboratory-scale pipe rheometer

The schematic of the laboratory-scale pipe rheometer is shown in Fig 1. The pipe rheometer consists of two chambers connected by a replaceable vertical pipe section. The volume of each chamber is approx. 3 liters. The measurement pipe used in this study was a smooth acrylic tube with inner diameter of 16 mm.

The measurement is initiated by filling the sample fluid in the bottom chamber. The fluid is then pumped to the upper chamber. The desired filling level is determined by an ultrasound surface detector. The measurement is started by opening the valve downstream the measurement tube. The flow in the measurement tube can be driven by sole gravity or by overpressure in the upper chamber. The pressure driving the flow is controlled via a regulator and a pressure level sensor. Therefore the flow in the measurement tube is undisturbed by e.g. pulsations from pumps.

The mass flow rate of the fluid is determined with three weight sensors and the volume flow rate with the ultrasound surface detector. With these two independent measurements also the density of the fluid can be determined. The pressure difference in the measurement tube is measured over a distance of 0.99 m.

Rheological characterization of the fluid is carried out utilizing the UVP-PD method. Region of steady flow is determined from the measurement data and analyzed for mean pressure loss, mass rate and volumetric flow rate. The result is combined with the simultaneously measured mean velocity profile.

The operation of the pipe rheometer is fully automated starting from sample loading to execution of user-defined measurement scheme and sample removal. The measurement scheme can cover various processing conditions in the same measuring period.

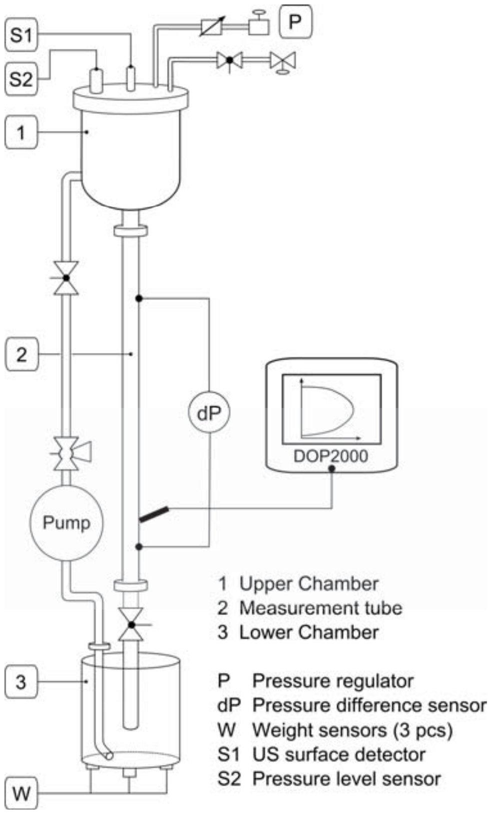

Figure 1: Schematic of the laboratory-scale pipe rheometer.

3.2 Ultrasound velocity profiling

The velocity profiles are measured using a pulsed UVP (DOP2000, Signal-Processing S.A., Switzerland). The settings used for the velocity measurements are summarized in Tab. 1. Depending on the flow speed 100 – 1000 individual profiles were recorded and analyzed for each measurement.

3.3 Reference measurements with a conventional rheometer

The viscosity of the MFC dispersion was measured at 20 °C with a stress controlled rotational rheometer (AR-G2, TA Instruments) equipped with the vane geometry. The diameter of the cylindrical sample cup was 30 mm and that of the vane 28 mm. The length of the vane was 42 mm.

After loading the sample to the measuring geometry, it was allowed to rest for 5 min before the measurement was started. The viscosity was measured in strain controlled mode with a gradually increasing shear rate in the range of 1E-4 - 100 s^{-1}. The reported viscosity at a certain shear rate was taken after a constant shear stress was reached or after a maximum time of 2 min.

3 RESULTS

3.1 Pipe rheometer

The experimental results acquired from the pipe rheometer can be analyzed using different approaches including implementations of rheological models as e.g. described by Wiklund et al. [4]. In this work the results are presented based on the direct measurements. Firstly, the results are analyzed utilizing only the pressure loss and volumetric flow rate data assuming laminar parabolic velocity profile. For a laminar Newtonian flow in a straight tube the apparent shear rate $\dot{\gamma}_a$ and shear stress τ_W at the tube wall are given by

$$\dot{\gamma}_a = \frac{4Q}{\pi R^3} \tag{1}$$

$$\tau_W = \frac{\Delta P R}{2L} \tag{2}$$

where Q is the volumetric flow rate, R is the radius of the tube and ΔP is the pressure difference over the length L of the tube. The shear viscosity is the ratio of shear stress to shear rate, $\eta_a = \tau_W / \dot{\gamma}_a$.

The first analysis corresponds to a conventional measurement of viscosity using e.g. capillary viscometer. In this analysis no corrections due to non-Newtonian profile of slip are applied. The result is referred as apparent viscosity.

The second analysis utilizes the experimental mean velocity profile and thereby gives viscosity measured locally in the flow. This method includes no assumptions concerning the flow profile or boundary condition. The local shear rate $\dot{\gamma}(r)$ is obtained directly from the velocity profile. As the shear stress at each distance from the tube wall is

$$\tau(r) = \tau_W (1 - r/R), \qquad (3)$$

the shear viscosity can be calculated locally. This result is referred as intrinsic viscosity $\eta(r) = \tau(r)/\dot{\gamma}(r)$.

The pressure drop as a function of mean flow velocity is shown in Fig. 2. For the birch cellulose suspension typical plug flow and lubrication layer regimes can be found as reported e.g. by Jäsberg [7]. Velocity profiles for selected flow rates are shown in Fig 3 (Roman numbers correspond to different flow rates).

In addition to the substantial difference in the pressure loss magnitude, the qualitative pressure loss behavior of MFC suspension differs clearly from that of cellulose suspension. Three different flow regimes can be identified by inspecting the pressure loss for increasing velocity. At low flow rates the pressure drop increases almost linearly and reaches a maximum value at velocity of approx. 0.4 m/s. After the maximum, the pressure loss decreases abruptly and then starts to increase linearly with velocity. All the velocity profiles (See Fig 4.) indicate clear slip at the wall. At low velocities, the shape of the profile is plug-like. As the velocity increases the plug starts to break down.

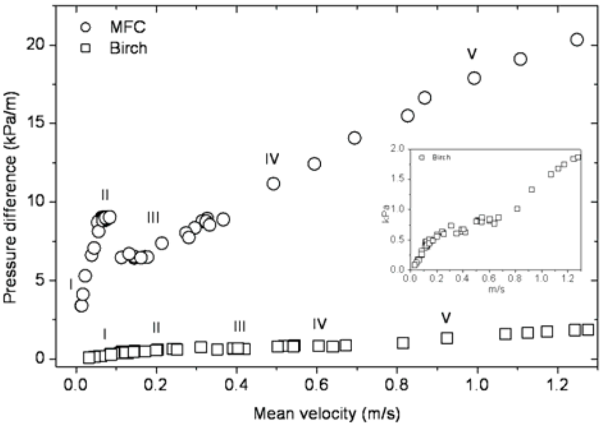

Figure 2: Pressure drop as a function of mean velocity. The roman numbers correspond to the velocity profiles in Figs 3 and 4.

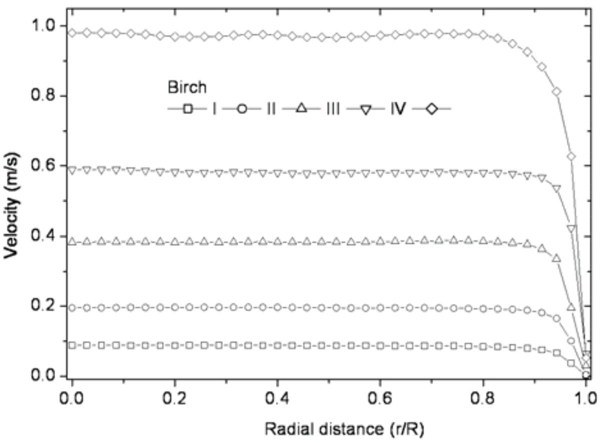

Figure 3: Mean velocity profiles for birch cellulose. The roman numbers for different profiles correspond to the pressure losses marked in Fig. 2.

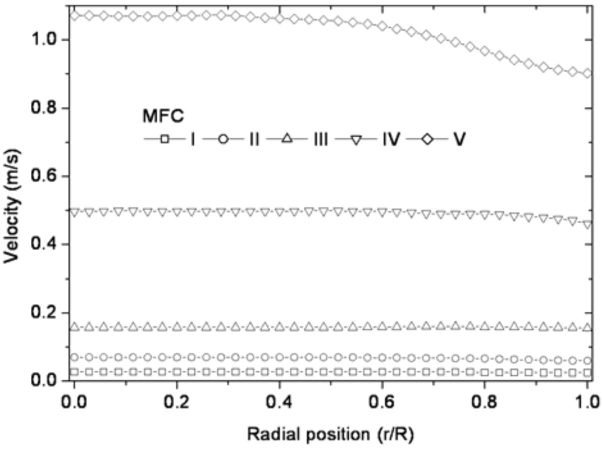

Figure 4: Mean velocity profiles for MFC. The roman numbers for different profiles correspond to the pressure losses marked in Fig. 2.

The viscosity results are presented in Fig. 5. As expected from the pressure loss results, the viscosity of MFC is clearly higher than that of birch cellulose. The results obtained from UVP-PD and rotational rheometer agree well. For both suspensions, the viscosity is strongly dependent on the shear rate in the measured range of shear rates. Also the apparent viscosity agrees qualitatively with the other results. Due to non parabolic velocity profile the average shear rate for apparent viscosity is too high, especially for low flow rates. The Reynolds number determined using the apparent viscosity values range from 1 to 150 for the MFC and from 30 to 1300 for the birch cellulose.

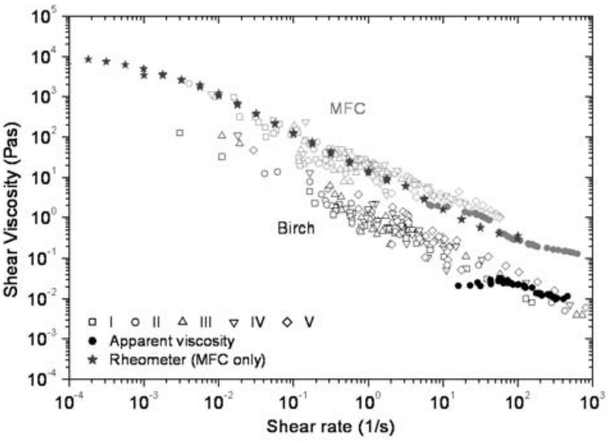

Figure 5: Intrinsic (open symbols) and apparent (solid symbols) shear viscosities for birch cellulose (black) and MFC (gray).

4 CONCLUSIONS

The pipe rheometer introduced in this study facilitates rheological studies for highly-concentrated, complex slurries in process like environment. The rheological measurements are based on the UVP-PD method. The results are highly consistent with the data from rotational rheometer.

Table 1: Main UVP settings

Setting	Value
Sensor base frequency	8 MHz
Sensor active diameter	5 mm
Doppler angle	80°
PRF	1–2.7 kHz
Burst length	4 cycles

REFERENCES

[1] Ouriev B, Windhab EJ: Rheological study of concentrated suspensions in pressure-driven shear flow using a novel in-line ultrasound Doppler method, Experiments in Fluids 32 (2002) 204-211.

[2] Brunn P, Wunderlich T, Müller M: Ultrasonic rheological studies of a body lotion, Flow Measurement and Instrumentation 15 (2004) 139-144.

[3] Pfund D, Greenwood MS, Bamberger JA, Pappas RA: Inline ultrasonic Rheometry by pulsed Doppler, Ultrasonics 44 (2006) e477-e482.

[4] Wiklund J, Shahram I, Stading M: Methodology for in-line Rheology by ultrasound Doppler velocity profiling and pressure difference techniques, Chemical Engineering Science. 62 (2007) 4277-4293.

[5] Birkhofer BH, Jeelani SAK, Windhab EJ, Ouriev B, Lisner K-J, Braun P, Zeng Y: Monitoring of fat crystallization process using UVP-PD technique, Flow Measurement and Instrumentation 19 (2008) 163-169.

[6] Xu H, Aidun CK: Characteristics of fiber suspension flow in a rectangular channel, International Journal of Multiphase Flow 31 (2005) 318-336.

[7] Jäsberg A: Flow behaviour of fibre suspensions in straight pipes: new experimental techniques and multiphase modelling, PhD thesis, University of Jyväskylä, Finland, 2007

[8] Wiklund J, Petterson AJ, Rasmuson A, Stading M: A comparative study of UVP and LDA techniques for pulp suspensions in pipe flow, A.I.Ch.E. Journal 52 (2006) 484-495.

[9] Wiklund J, Stading M: Application of in-line ultrasound Doppler-based UVP-PD Rheometry method to concentrated model and industrial suspensions, Flow Measurement and Instrumentation 19 (2008) 171-179.

[10] Pääkkö M, Ankerfors M, Kosonen H, Nykänen A, Ahola S, Österberg M, Ruokolainen J, Laine J, Larsson PT, Ikkala O, Lidström T: Enzymatic hydrolysis combined with mechanical shearing and high-pressure homogenization for nanoscale cellulose fibrils and strong gels, Biomacromolecules 6 (2007) 1934-1941.

[11] Tatsumi D, Ishioka S, Matsumoto, T: Effect of fiber concentration and axial ratio on the rheological properties of cellulose fiber suspensions, Journal of Society of Rheology 32 (2002) 27-32.

ISBN: 978-91-7290-292-3